Fall 12-16-2016

Development of CXCR4-Inhibiting Nanoparticles for the Treatment of Metastatic Cancer

Yan Wang
University of Nebraska Medical Center

Development of CXCR4-Inhibiting Nanoparticles for the Treatment of Metastatic Cancer

by

Yan Wang

A DISSERTATION

Presented to the Faculty of
the University of Nebraska Graduate College
in Partial Fulfillment of the Requirements
for the Degree of Doctor of Philosophy

Pharmaceutical Sciences
Graduate Program

Under the Supervision of Professor David Oupický

University of Nebraska Medical Center
Omaha, Nebraska

June, 2016

Supervisory Committee:

Tatiana Bronich, Ph.D.
Serguei Vinogradov, Ph.D.
Rakesh Singh, Ph.D.
Maneesh Jain, Ph.D.

Acknowledgments

I would like to express my sincere and profound gratitude to my mentor and advisor, Prof. David Oupický for the constant support, encouragement, appreciation, guidance and patience during the four years of my PhD study. His knowledge, passions, professional attitude, dedication and innovation in the field of pharmaceutical science and drug/gene delivery always have a huge inspiration in my professional life. He taught me countless qualities that are required for being a real scientist. I am lucky and proud to be his student.

I would also like to sincerely thank my committee members, Prof. Tatiana Bronich, Serguei Vinogradov, Rakesh Singh and Maneesh Jain, for their continuous guidance and valuable suggestions during my research at UNMC.

My thanks also goes to Dr. Surinder K. Batra and Dr. Sushil Kumar for the cooperation on the project “Polyplex-Mediated Inhibition of CXCR4 and NCOA3 Impedes Pancreatic Cancer Progression and Metastasis”. I would also like to thank Dr. Satyanarayana Rachagani for the help with orthotropic pancreatic cancer mice model and Dr. Michael D. Boska with the measurement of tumor perfusion by MRI. I especially thank all our former and current group members, for their help, suggestions and encouragement throughout the years. I would like thank Dr. Jing Li, who always give me continuous encouragements, talented suggestions, countless help and guidance. I thank Dr. Stuart T. Hazeldine, Dr. Zhengheng Peng and Fei Yu for helping me with the chemistry. I would thank Ying Xie with his help for flow cytometry. Special thanks goes to Suthida Boonsith and Yi Chen, who always support me in and out of the lab. I thank the Department of Pharmaceutical Sciences, University of Nebraska Medical Center for this great opportunity and study journey as a Ph.D. student.

I would like to thank my family and friends for their wonderful company, unlimited support, love and encouragement all the time. Finally, I appreciate everyone who has

constantly supported, encouraged and motivated me during my graduate studies. Thank you.

Abstract:

Development of CXCR4-Inhibiting Nanoparticles for the Treatment of Metastatic Cancer

Yan Wang, Ph.D.

University of Nebraska Medical Center, 2016

Supervisor: David Oupický, Ph.D.

Metastasis is the main cause of cancer mortality and morbidity, leading to several million deaths every year. Less than 20% of pancreatic cancer (PC) patients are candidates for surgery due to spread beyond the pancreas. Desmoplasia presents substantial barriers to perfusion, diffusion, and convection of antitumor therapeutics into the PC tissues. We focus on developing novel therapies that regulates tumor microenvironment, chemosensitizing tumor to therapeutics and preventing metastasis.

Gene therapy is emerging as a promising new therapeutic agents for cancer treatment. A targeted, systemic, effective and safe gene delivery system should be developed. CXCR4/SDF-1 axis plays a crucial role in the crosstalk between cancer cells and their microenvironment, and is involved in tumor progression, angiogenesis, metastasis and survival. We successfully designed dual-function polymeric CXCR4 inhibitors (PCX) as gene delivery vectors.

To enhance the CXCR4 antagonism, we reported synthesis of novel monocyclam monomers and their polymerization to PCX. In order to improve the physical properties and safety of PCX, it was modified by PEGylation. The negative effect of PEG on transfection activity of PEG-PCX polyplexes could be overcome by using polyplexes formulated with a mixture of PCX and PEG-PCX. Moreover, modification of PCX with cholesterol, the enzymatic stability against RNase and siRNA delivery efficiency were

enhanced dramatically. NCOA3 silencing can downregulate mucin expression and regulate tumor microenvironment. Using a series of PCX, we optimized formulation of PCX/siNCOA3 polyplexes to simultaneously target CXCR4 and NCOA3 in PC. Cholesterol-modified PCX showed maximum CXCR4 antagonism, NCOA3 silencing and inhibition of PC cell migration *in vitro*. The optimized PCX/siNCOA3 polyplexes were used in evaluating antitumor and antimetastatic activity in orthotopic mouse model of metastatic PC. The polyplexes displayed significant inhibition of primary tumor growth, which was accompanied by a decrease in tumor necrosis and increased tumor perfusion. These dual-function polyplexes also showed significant antimetastatic effect and effective suppression of metastasis to distant organs. Overall, dual-function PCX/siNCOA3 polyplexes can effectively regulate the tumor microenvironment to decrease progression and dissemination of PC.

Table of Contents

List of Schemes

List of Figures

List of Tables

List of Abbreviations

PC - pancreatic cancer

CXCR4 - C-X-C chemokine receptor type 4

PCX - polymeric CXCR4 antagonist

SDF-1 - sromal cell-derived factor 1

CMC - critical micelle concentration

NMR - nuclear magnetic resonance spectroscopy

DLS - dynamic light scattering

RNAi - RNA interference

siRNA - small interfering RNAs

ECM - extracellular matrix

Hh - hedgehog

EMT - epithelial to mesenchymal transition

TGF- transforming growth factor

CAFs - cancer-associated fibroblasts

PDGF - platelet-derived growth factor

MMPs - matrix metalloproteinases

HIFs - hypoxia-inducible factors

VEGF - vascular endothelial growth factor

EtBr - ethidium bromide

DLS - dynamic light scattering

MRI - magnetic resonance imaging

PBLs - peripheral blood leukocytes

RES - reticulo-endothelial systems

HCS - high content screening

PanIN - pancreatic intraepithelial neoplasia

NCOA3 - nuclear receptor coactivator-3

Chapter 1. Introduction

Please note that part of this chapter was taken from a review titled "Potential of CXCR4/CXCL12 Chemokine Axis in Cancer Drug Delivery" published in Drug Delivery [1]. The authors of the book chapter include Ying Xie, Prof. David Oupický and me. I wrote the draft of manuscript, Ying gave me suggestions, Dr. David Oupický revised it and made it published. All the authors agreed with including their contributions in this dissertation.

1.1 Cancer metastasis

Metastasis is the major reason for the failure of cancer therapy and accounts for approximately 90% mortality of cancer patients [2]. It requires several successive steps for cancer cells spreading from the primary site and continuous growth into secondary tumors in distant organs. Metastasis is a complex process that begins with invasion into local stroma, followed by intravasation of cancer cells into blood and lymphatic vessels, movement of cancer cells through the lymphatic system or blood circulation, extravasation into the parenchyma of distant tissues, adaption to a new environment at secondary site, formation of micrometastases, and finally the growth into macroscopic tumors [3, 4]. During the process of intravasation, cancer cells should be survival without adhesion and escape from recognition by the host immune system [5]. The complex molecular mechanism of metastasis includes the alteration of multistep, multistage and multigene. However, cancer cells tightly interact with their surrounding microenvironment during each step, which plays a critical part in the cancer metastasis [6].

Tumor microenvironment consists of the extracellular matrix (ECM) and stromal cells, involving endothelial cells, fibroblasts, immune cells, bone marrow-derived cells, progenitor cells and stem cells. Clarification of the relationship between the tumor

microenvironment and metastasis will suggest a key point to prevent cancer metastasis and improve the life quality of patients [7]. Stromal cells interact with cancer cells directly and indirectly to influence the progress of tumorigenesis and development. There are two complementary strategies facilitate cancer cells take advantage of the primary tumor microenvironment to initiate metastasis [2]. First, cancer cells alter their gene expression pattern to utilize the signals from tumor stroma and migrate to a different site. Second, stromal cells will be vigorously recruited to primary tumor site to promote metastasis. In another words, cancer cells gain metastatic potential at the primary tumor site, which is supported by the comparability in the investigations that gene expressions of metastases and the corresponding primary tumor are similar in various cancers, such as breast, colorectal, prostate and pancreatic cancer [8-10].

1.1.1 Epithelial to mesenchymal transition (EMT)

EMT is a key developmental program and often activated in the initiating steps of primary tumor invasion. Tumor cells lose epithelial markers, acquire mesenchymal traits, express stem cell markers and obtain a migratory phenotype [11]. In a normal tissue, epithelial cells connect tightly with each other by epithelial adherens junctions with the aid of protein E-cadherin and their migratory capacity is prohibited. However, in the first step of cancer metastasis, cancer cells have to break the ECM. Epithelial cells are separated from multiple layers of stroma by ECM [2]. In EMT, the expression of E-cadherin is suppressed, resulting in the detachment of cancer cells from epithelial sheets [12]. Moreover, the mesenchymal state is related with the ability of cancer cells to subsequently differentiate into multiple cell types during the initiation and development of metastasis.

Researchers reported that the stroma plays an critical role in the phenotypic transitions in cancer by the expression of transforming growth factor β (TGF-β) [12]. Labelle et al. investigated that platelet-tumor cell interactions were sufficient to prime

tumor cells for subsequent metastasis. The TGF-β/Smad and NF-κB pathways were synergistically activated in cancer cells by the interaction of platelet-derived TGF-β and direct platelet-tumor cell, leading to the transition to an invasive mesenchymal-like phenotype and increased metastasis *in vivo*. However, inhibition of NF-κB signaling pathway or the expression of TGF-β1 alone in platelets prevents lung metastasis *in vivo* [13]. Bonde et al. found that tumor associated macrophages regulated EMT intratumorally through TGF-β signaling and activation of the β-catenin pathway [14]. Long term exposure of teratocarcinoma cells to macrophage-conditioned medium resulted in reduced expression of E-cadherin, activation of the EMT-mediating β-catenin signaling pathway, enhanced mesenchymal marker and an invasive phenotype [14]. Moreover, it was proved that intratumor macrophage densities, EMT markers and TGF-β levels have a positive correlation by an immunohistochemical study of a series of non-small cell lung cancer patients' samples.

1.1.2 Recruitment of immune and stromal cells

In order to alter tumor microenvironment to a metastasis-promoting position, stromal cells will be transformed to support cancer cells invasion or metastasis-promoting stromal cells will be recruited to remodel the microenvironment [2]. Researchers revealed that direct communication between macrophages and tumor cells in the microenvironment resulted in invasion and intravasation of tumor cells into the blood or lymphatic vessels. Macrophages promote the angiogenesis, facilitate ECM breakdown/remodeling and enhance the motility of cancer cells, suggesting a potential target for anticancer drugs [15]. Recruited immature myeloid cells can facilitate cancer cells evade the host immune response through inhibiting the differentiation of antigen-presenting DCs after accumulation in cancer microenvironment. In the normal conditions, myeloid cells are the most abundant nucleated hematopoietic cells and terminally differentiated into three

groups, including macrophages, dendritic cells and granulocytes, which are necessary for the innate and adaptive immune systems. However, in the tumor microenvironment, myeloid cells would be changed into effect immunosuppressive cells and support tumor immune evasion [16]. Van Zijl et al. found that myofibroblasts or cancer-associated fibroblasts (CAFs) induced invasion of hepatocellular carcinoma was through TGF-β and platelet-derived growth factor (PDGF) signaling pathway using a collagen gel-based three dimensional hepatocellular carcinoma model *in vitro*. Thus, TGF-β/PDGF axis is very important during hepatic tumor-stroma crosstalk to regulate tumor growth and progression [17]. Moreover, CAFs keeps continuously activated in tumors. The long-term activation of fibroblasts contributes to the perpetual secretion of activating cytokines, such as SDF-1, VEGF, PDGF and HGF [18, 19]. Orimo et al. demonstrated that CAFs within invasive breast carcinomas secreted SDF-1, which promoted the recruitment of endothelial cells and contributed to tumor promotion by acting the cognate receptor CXCR4 expressed by carcinoma cells [20].

1.1.3 ECM remodeling

Proteolysis and breakdown of ECM is an essential component of microenvironment remodeling and important in the early step of local invasion of cancer cells into adjacent tissue. During the process of ECM remodeling, matrix metalloproteinases (MMPs) are crucial effectors [21]. For instance, tumor-associated fibroblasts differentiate into myofibroblasts and promote tumor progression by protease-catalysed remodeling of the stroma using MMP9 [22]. MMP9 is recruited to the cell surface of fibroblasts by lysyl hydroxylase via fibronectin-like domain and facilitate the differentiation of tumor-associated fibroblasts.

1.1.4 Hypoxia

Due to the rapid proliferation of primary cancer cells, the concentration of oxygen is much lower in the region of tumor cells than in the normal tissues. Hypoxia-inducible factors (HIFs) are the most critical transcription factors, which response to hypoxia, induce the formation of angiogenesis and promote the survival of cancer cells. Cancer cells alter their intrinsic gene expression and adapt to the hypoxic environment by the HIF signaling pathway [23]. Moreover, hypoxia is also a main driving force for recruiting stromal cells to tumors. Chouaid et al. reported that hypoxia contributed to the tumor tolerance to immune surveillance through the recruitment of regulatory T cells and myeloid derived suppressor cells by activating HIF-1 and vascular endothelial growth factor (VEGF) pathways [24]. After stromal cell recruitment medicated by hypoxia, cancer invasion is promoted at the edge of tumor periphery. Simultaneously, hypoxia provides an aggressive selection pressure for cancer stem cells migrate to the tumor periphery to facilitate cancer cell escape. Therefore, hypoxia and stromal cells work together to promote cancer metastasis [6].

1.1.5 Intravasation and selection at distant site

The possibility of cancer metastasis to a specific organ is determined by various reasons, including routes of blood circulation, the ability of cancer cell intravasation into vasculature and modulating tumorigenesis at secondary organs. During this process, cancer cells also need to deal with the microenvironments. Macrophages localizing to blood vessels facilitate cancer cells intravasate into the circulation [25]. Platelets play an important role in the enemy microenvironment of the vasculature and support tumor metastasis by directly interacting with cancer cells. In circulation, platelets can form protective clusters with cancer cells, impacting NK cell-mediated cytotoxicity, preventing the recognition by immune cells, promoting the arrest at the endothelium and supporting the establishment of secondary lesions [26]. However, most disseminated cancer cells die

at the secondary site and only 0.01% of cancer cells intravasating into circulation are able to form detectable metastasis [27]. The metastatic outgrowth is affected by the microenvironment factors in the secondary organs [28]. After cancer cells initially reach distant organs, the microenvironment may suppress metastatic cancer growth by inhibitory stromal factors. For instance, immune cells (cytotoxic T cells or natural killer cells) of adaptive and innate immune system form a critical barrier for the survival and proliferation of cancer cells. Stroma cells from the secondary sites release apoptotic signals (Fas-L and Trail), which inhibit the cancer cell proliferation and cause elimination. However, cancer cells can induce alternation of stroma and regulation of microenvironment to support cancer growth and metastasis. For example, cancer-associated fibroblasts secrete various cytokines and growth factors, such as SDF-1, PDGF, VEGF and HGF. Modified ECM and secreted growth factors can reactivate metastatic cancer cells from dormancy, inducing angiogenesis and enhance the survival as well as multi-functionality of metastatic cancer cells. Furthermore, the recruitment of macrophages, myeloid progenitors and mesenchymal cells establish an inflammatory environment and secrete various signals to enhance the metastatic cancer growth.

1.2 Pancreatic Cancer

In 2016, it is expected to have 53,070 new cases and 41,780 deaths of pancreatic cancer (PC) in the US. From 2000 to 2012, the incidence rate enhanced by 1.2% per year and since 2000, the death rate increased slightly by 0.4% per year. PC is predicted to become the second leading cause of cancer-related mortalities by 2030 [29]. The patients usually do not feel the symptoms until the disease has progressed, including weight loss, abdominal discomfort and occasionally the development of diabetes. Diagnosis at an early stage is difficult for PC, except that tumor develops near the common bile duct and cause jaundice. Until now, there is no reliable method for the early detection of PC. PC patients

at advanced stage may have nausea, vomiting and severe abdominal pain. Smoking cigarette is one of the significant risk factors of PC (~2 fold vs. nonsmokers). About one-fifth of PC patients are because of smoking. Also, family history of PC, history of chronic pancreatitis, obesity, diabetes and genetic syndromes (BRCA1&2 mutation) can cause high risk of PC.

The main treatment options for PC are surgery, radiation therapy, and chemotherapy to extend survival or relieve symptoms, however, seldom produce a cure. The one-year and five-year survival rates remain consistently low (~29% and ~7% respectively), which are due to late diagnosis, early metastasis, and complex microenvironment in PC. PC microenvironment contributes to inherent resistance to available therapies and severely limits drug delivery [30-32]. More than half (53%) of patients are diagnosed at a distant stage, for which the 1- and 5-year survival is 15% and 2%, respectively. Less than 20% of patients are candidates for surgery because PC is usually detected after it has spread beyond the pancreas. Thus, there is a urgent need to develop better therapeutic strategies for the treatment of PC [33].

1.3 Desmoplasia and Treatment Strategies

PC is unique among solid tumors due to the extremely dense desmoplastic reaction which wraps the cancer cells. The emergence of desmoplasia in PC is becoming a problem which presents substantial barriers to perfusion, diffusion, and convection of antitumor therapeutics into the PC tissues and leads to acquired resistance [34]. Desmoplasia contains extracellular matrix (ECM) proteins, myofibroblastic pancreatic stellate cells (PaSCs), and immune cells, which modulate the growth of PC by providing a scaffold for the cancer cells to grow as well as growth factors and immune modulators (**Scheme 1)** [35]. Researchers reported that extensive fibroblastic cell proliferation in PC relates to poor disease outcomes [36]. The prominence of desmoplastic reaction has

caught researchers' eyes as one of the major factors responsible for the severe and malignant biologic behavior of PC. Tumor local environment plays any important role in cancer initiation, progression, metastasis and resistance [37, 38]. Desmoplastic PC microenvironment shows high interstitial pressure and a dense stroma with vascular dysfuction, which results from the proliferation of fibroblasts and increased stromal fibrosis [39, 40]. The key regulatory pathways to regulate desmoplasia include Hyaluroran-CD44 and Hedgehog (Hh), which are aberrantly overexpressed in PC [39, 41, 42].

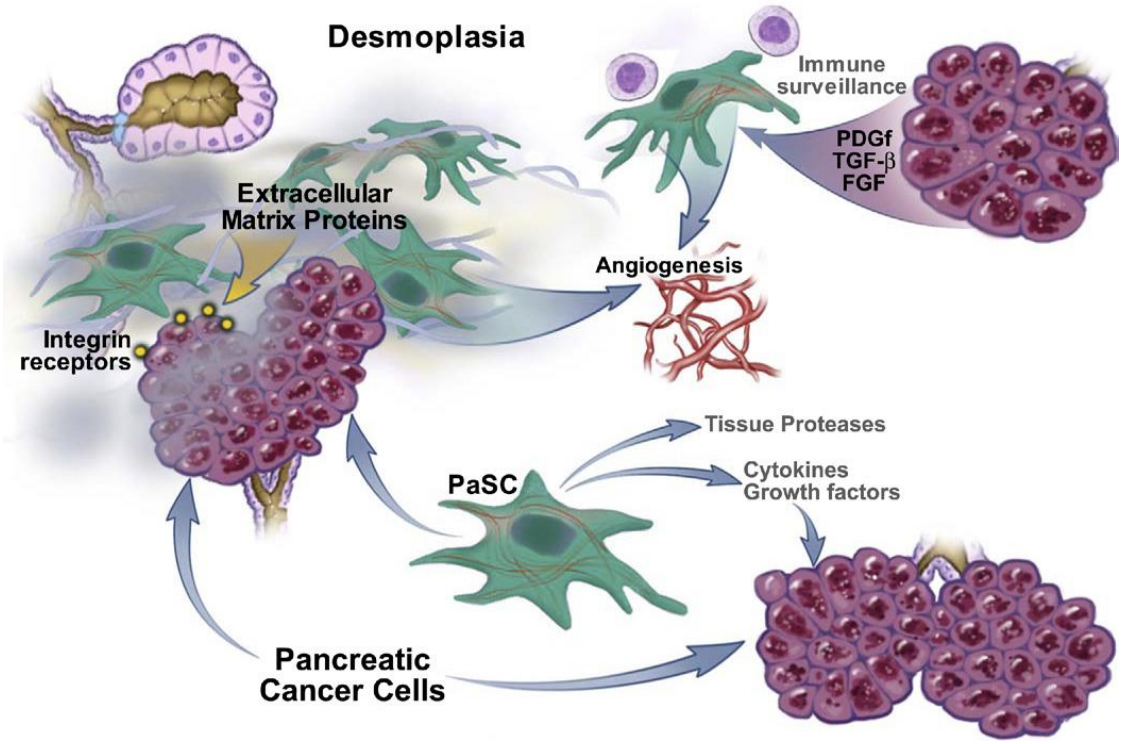

Scheme 1. Components of desmoplasia in PC. Pancreatic cancer cells and pancreatic duct cells promote each other's growth and proliferation and together regulate processes of ECM deposition, angiogenesis, and disordered immune surveillance (Adapted from [35]).

1.3.1 Hyaluronan-CD44 pathway

One strategy to overcome the dense stromal barrier is to target the ECM component. In the desmoplastic reaction, a key role of fibroblasts is hyaluronan synthesis and its interaction with CD44. CD44 has been associated with malignant transformation of pancreatic tumors. It is an integral cell-surface glycoprotein and overexpresses in its variant forms, which is driven by IFN-γ [43]. Meanwhile, CD44 is also the major cell surface receptor for hyaluronan as well as matrix metalloproteinases, playing a critical role in pancreatic carcinogenesis. Hyaluronan is a non-sulphated glycosaminoglycan. In response to factors released from tumor cells, such as lactate, or by direct cell-cell contact, hyaluronan is produced by activated fibroblasts [44]. Hyaluronan-rich stroma is associated with poor prognosis in many epithelial cancers including pancreatic and together with CD44 promotes tumor cell growth, migration, and metastases [42]. Hyaluronan-CD44 interaction reorganizes the desmoplasmic barrier and enhances its integrity, so that the drug is impeded from entering into the PC tissue and causes the failure of therapy [42].

Researchers have taken a lot of efforts to design novel strategies to minimize desmoplasia and improve the delivery of therapeutics to PC tissues. Disruption of hyaluronan-CD44 interaction would be a critical method to prevent drug resistance in PC. Provenzano et al. reported that systemic administration of PEGPH20, a PEGylated human recombinant PH20 hyaluronidase, could ablate stromal HA from autochthonous murine PC, normalize interstitial fluid pressure and re-expand the microvasculature. Combination of PEGPH20 with gemcitabine treatment resulted a near doubling of overall survival [45]. 37]. 4-Methylumbelliferone (4-MU) is a hyaluronan synthesis inhibitor, which has been shown to slow down the development of human PC cell lines both *in vitro* and *in vivo* as well as inhibit cancer cell migration, proliferation and invasion [46, 47]. 4-MU also prolonged the survival time of nude mice bearing abdominally transplanted pancreatic

cancer cells and enhanced the efficacy of gemcitabine, suggesting that its potential usage in patients with end-stage pancreatic cancer [48]. Diop-Frimpong et al. found that angiotensin receptor inhibitor losartan led to a dose-dependent reduction in stromal collagen and hyaluronan production in desmoplastic models of human breast, pancreatic, and skin tumors in mice, thus enhanced the efficacy of chemotherapy [49].

1.3.2 Hedgehog pathway

Hh signaling pathway is genetically changed and aberrantly activated in most of PC, which causes tumor initiation, progression, and metastatic spread. Moreover, it has been involved in the initiation and maintenance of desmoplastic reaction **Scheme 2** [50]. Hh pathway consists of Sonic (Shh), Indian (IHh), patched (PTCH) and smoothened (SMO), which are almost undetectable in normal human pancreas, however, become prominently visible during PC [41]. Myofibroblast differentiation and stroma-derived growth promoting molecules are induced by Hh signaling pathway, which promote tumorigenesis. Moreover, Hh ligands intensify desmoplastic reaction and fibrosis by stimulating the interaction with TGF-β1 and MMPs [51]. This pathway is activated when Shh bind to the PTCH receptor relieving the inhibitory effects of SMO receptor from PTCH and thus activating the glioma-associated oncogene (GLI) family of transcription factors [52]. Activated GLI induces the expression of the Hedgehog genes such as PTCH, epidermal-derived, platelet-derived, and vascular-endothelial growth factors, cyclins B, D, and E and GLI1, which promotes the tumor progression and desmoplastic reaction [53].

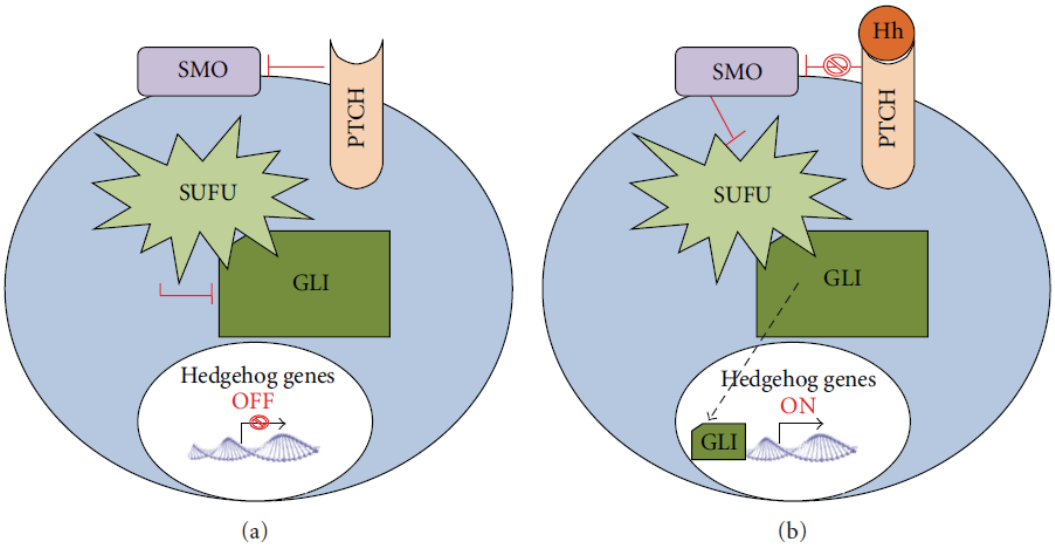

Scheme 2. The Hedgehog pathway (Adapted from [54]).

Inefficient drug delivery may be an important contributor to chemoresistance in PC. Inhibition of Hh signaling pathway is a promising strategy to overcome the desmoplastic reaction in PC and thus increase the delivery of anticancer therapeutics into tumors. Olive et al. reported that the efficacy of gemcitabine in the mice could be improved by co-administration of a small molecule inhibitor of Hh pathway (IPI-926). The combination treatment depleted tumor-associated stromal tissue and produced a transient increase in intratumoral vascular density, resulting in improved intratumoral concentration of gemcitabine and transient stabilization of disease [55]. Kumar et al. designed a self-assembled copolymer to simultaneously encapsulate Hh inhibitor GDC-0449 and complex tumor suppressor miR-let7b into micelles to treat athymic nude mice bearing ectopic pancreatic tumor, resulting decreased tumor proliferation and enhanced apoptosis [56]. Feldmann et al. investigated that blocking the Hh pathway with the small molecule cyclopamine, which is a naturally occurring inhibitor of SMO receptor, resulted in prevention of PC metastases and enhancement in chemo-delivery to tumors [57].

The survival rate of PC patients has not been significantly improved during the past 30 years. Due to PC is highly resistant to the currently available chemotherapy and radiotherapy, the new effective patterns for the treatment are urgently needed. In recent a few years, gene engineering technology is becoming a rapidly and potentially developing area of modern medicine to treat tumor with the promising progress of modern biology and nanomedicine. Therefore, the treatment of patients who are not curable by current therapies will be improved by gene modification [58].

1.4 Gene Therapy

Gene therapy is an experimental technique that uses genes to treat or prevent disease by inserting a gene into patients' nidus instead of using drug or surgery. Gene therapy aims at delivering genetic material into target cells or tissue and to express it with

the intention to gain a therapeutic effect. There are several approaches for gene therapy, including replacing a mutated gene that causes disease with a healthy copy of the gene, or inactivating a mutated gene that is functioning improperly, or introducing a new gene into the body to help against a disease.

In 1989, the US Food and Drug Administration (FDA) approved the first gene therapy protocol. A marker gene was *ex vivo* transduced into the tumor infiltrating lymphocytes, which were collected from advanced melanoma patients. The transduced cells were expanded *in vitro* and re-infused to the patients. In the following year, tumor infiltrating lymphocytes were genetically modified *ex vivo* to express tumor necrosis factor and used to treat patients with advanced melanoma, which was the first clinical trial on cancer using gene therapy with an therapeutic intend [59]. Significant progresses in gene therapy have been obtained since the first clinical trial in 1990. It was reported that two patients with metastatic melanoma were received a successful immunogene therapy. Until June 2012, the entries for 1843 trials undertaken in 31 countries were reported and most of which were focused on cancer treatment [60]. Jones et al. performed a comprehensive genetic analysis of 24 pancreatic cancers and determined the sequences of 23,219 transcripts, as well as representing 20,661 protein-coding genes. After they searched for homozygous deletions and amplifications in the tumor DNA by using microarrays containing probes for about 10^6 single-nucleotide polymorphisms, an average of 63 genetic alterations were found in pancreatic cancers, the majority of which were point mutations. These alterations defined a core set of 12 cellular signaling pathways and processes that were each genetically altered in 67 to 100% of the tumors [61]. Therefore, genes in these cellular pathways would be potential targets for PC gene therapy. However, the highly efficient gene therapy is based on selection of efficient targets, effective gene delivery, tumor targeted therapy and low toxicity.

1.4.1 Vector systems for gene delivery

An ideal gene delivery system is the foundation of gene therapy, which should have the properties, such as non-invasive mode of administration, tumor-specific targeting, including primary lesion and distant metastatic lesion, sustained gene expression, and high insertion capacity, bio-safety, stability and easy preparation [58]. Vector systems are divided as viral and non-viral methods. The advantages of viral vector system includes higher transfection efficiency and long-term gene expression. However, viral method may cause toxicity, immunogenicity, high cost and inability to transfer large size genes, which can be avoided by non-viral delivery systems. Non-viral methods have the advantages of easy preparation and modification with ligands for tissue and cell specific targeting [62].

In gene delivery systems, viral vectors are the most commonly studied and applied. More than two-thirds of clinical trials used viral vectors, including adenovirus (AdV), retrovirus (RV), adeno-associated virus (AAV), lentivirus, herpes simplex virus (HSV), influenza virus, Newcastle disease virus, pox virus, and Epstein-Barr virus (EBV). Viruses can take advantage of the innate mechanism of infection to enter and transfer DNA molecules into cells without any physical or chemical processing. Then the therapeutic gene would be expressed after entering the nucleus and integrating into the host gene pool [63].

Non-viral vectors consist of physical methods, biological vectors, and chemical vectors to introduce naked DNA (plasmid DNA), RNA molecules, or oligonucleotides into cells. Microinjection, microparticle bombardment and electroporation are most commonly used in physical delivery. Even though physical techniques can achieve high transfection efficiency, they are laborious, impractical, invasion and difficult to apply in a clinical setting [62]. Both bacteria and mammalian cells (hematological cells or mesenchymal stem cells) can be used as biological vectors for gene therapy. Bacteria is engineered to express

therapeutic genes and deliver both therapeutic gene and protein product to recipient cells. For instance, a bacterial cancer vaccine was prepared using a live attenuated Listeria strain of bacteria to express mesothelin and demonstrated antitumor effect in an early-phase clinical trial [64]. The commonly used chemical vectors can be divided into two types based on the materials, cationic lipids (liposomes) and cationic polymers. Cationic lipids consist of an aqueous compartment enclosed in a phospholipid bilayer and bind with nucleic acids based on the electrostatic interaction. After fusion with target cell membrane and endocytosis, nucleic acid will be delivered into cytoplasm. Cationic polymers include a wide range of chemical compounds, such as chitosan, polyamidoamine, polypeptides and so on. They form nanosized particles with negatively charged nucleic acids through electrostatic interaction. Cationic polymers increase cellular uptake by endocytosis, protects nucleic acids from nuclease degradation and facilitate endosome escape. Then, nucleic acids would be released into cytoplasm and regulate gene expression [58]. The combination system of lipid/polymer/DNA has been developed to exhibit further condensation, protection and increase circulating half-life *in vivo* [62]. Furthermore, ligands or peptides can be conjugated to polymer to improve cell/tissue specificity by receptor-directed gene delivery.

1.4.2 Nucleic acids

Plasmid is a double stranded circular DNA with transgene to encode for specific protein. Besides the transgene, plasmid DNA consists other regulatory signals such as the promoter, enhancer sequences, splicing and polyadenylation sites to regulate gene expression [65]. The size of plasmid ranges from hundreds of to several thousand base pairs. Engineering the plasmid with tissue or tumor specific promoters would improve the efficiency of initiating the transcription process by recognizing the RNA polymerase. The commonly used promoters are derived from viral origins such as cytomegalovirus (CMV)

and roux sarcoma virus. Enhancers locate in either upstream or downstream of the promoter region, which are the binding sites for proteins to enhance the initiation of gene transcription [66]. Splicing and polyadenylation sites are responsible for the correction of mRNA obtained from transcription.

Antisense Oligonucleotide (AON) is a short single-stranded segments (18-21 base pairs) of DNA or RNA artificially synthesized *in vitro*. It has a complementary sequence to the target mRNA to inhibit gene expression by different mechanisms, including translational arrest by steric hindrance of ribosomal activity and the induction of RNase H endonuclease activity [67]. RNase H enzyme cleaves the mRNA in the RNA-DNA heteroduplex and leaves AON intact. AON can also inhibit gene expression by interfering with mRNA maturation or destabilizing the pre-mRNA in the nucleus [68]. Therefore, AON can be used to treat diseases which are associated with dysregulated gene expression.

RNA interference (RNAi) is emerging as a novel way for the treatment of PC. The sequence-specific small interfering RNAs (siRNAs) are a length of 20–25 base pairs, which mediate the degradation of the homologous mRNA and consequently regulate the expression of the targeted gene [69, 70]. siRNAs can be artificially synthesized *in vitro* and directly delivered into target cells. siRNAs also can be produced in the genetically modified target cells, in which a gene encoding siRNA is introduced via appropriate vectors with the help of endogenous RNAase [58]. After releasing into cytoplasm, siRNAs bind to ribozyme compunds and form RNA-induced silencing complexes (RISCs). RISCs bind to the target mRNA and induce the degradation of mRNA. RNAi takes more advantages in comparison with other gene blockade technologies, such as high degree of specificity to mRNAs, non-immunogenic property and high resistance to ribonucleases. RNAi has turned into one of the most promising method for gene therapy. Yang et al. developed a biodegradable charged polyester-based vector for K-ras siRNA delivery to

MiaPaCa-2 PC cells and initiated a cascade gene regulation of downstream proteins, which significantly reduced the growth, migration and invasion of MiaPaCa-2 cells were as well as promoted the apoptosis [71]. Owing to high expression of hypoxia-inducible factor 1α (HIF1α) increasing the resistance of gemcitabine for PC, Zhao et al employed biocompatible lipid-polymer hybrid nanoparticles to co-deliver siHIF1α and gemcitabine for PC treatment [72]. This nanoparticle absorbed negatively charged siHIF1α on the surface and encapsulated gemcitabine to the hydrophobic core to prevented siRNA degradation in serum as well as gemcitabine leakage, which exhibited significant synergistic antitumor effects and inhibited metastasis in orthotopic PC model. To investigate the efficiently systemic delivery of siRNA, Pittella et al. reported an efficient and biocompatible nanocarrier comprising poly(ethylene glycol)-block-charge-conversional polymer (PEG-CCP)/calcium phosphate (CaP) hybrid micelles for systemic delivery of siRNA to spontaneous PC model in transgenic mice [73]. All these results have shown great potential towards a breakthrough in siRNA therapy for PC.

1.5 Nuclear Receptor Coactivator-3

Nuclear receptor coactivator (NCOA) belongs to the p160/steroid receptor coactivator (SRC) family, which consists of SRC-1, TIF-2 (GRIP1) and AIB1 (ACTR/RAC3/TRAM-1/SRC-3/NCOA3) [74-77]. NCOA3 plays an important role in hormone-sensitive tumors, such as breast cancer, ovarian cancer, prostate cancer, and meningioma [78-80]. NOCA3 is the rate limiting step in estrogen-mediated growth signaling, such as insulin-like growth factor I and epidermal growth factor, and increases the transcriptional activity of many steroid nuclear receptors and growth factors, suggesting that transcriptional activation medicated by estrogen receptor might provide a growth advantage to cancer cells. For instance, Reiter et al reported that NCOA3

overexpressed in breast cancers and strongly improved epidermal growth factor-medicated transcription in squamous cell carcinoma cells [81].

NCOA3 is one of the frequently mutated genes in PC [82]. High-level amplification of NCOA3 has been found in four of nine pancreatic cancer cell lines and >37% of archival PC tissues [83, 84]. Henke et al reported that NCOA3 did not show in normal pancreatic tissue, however, high expressed in pancreatic adenocarcinoma and high-grade pancreatic intraepithelial neoplasia (PanIN) lesions [84]. Detectable levels of NCOA3 mRNA or protein were rarely detected in normal pancreas ducts (<6% of sample positive). There was an increase of NCOA3 expression in pancreatitis and low-grade intraepithelial neoplasia with >14 and >23% of samples positive, respectively ($P<0.01$, vs. normal tissues). The highest frequency of NCOA3 expression at mRNA or protein levels was with > 65% of samples positive, which were found in adenocarcinoma as well as high-grade PanIN ($P<0.0001$ vs. the other groups). Moreover, NCOA3 is also elevated in lung, lymph and liver metastatic lesions [85]. Therefore, NCOA3 can serve as an important diagnostic indicator due to its overexpression in pancreatic adenocarcinoma and its precursor lesions.

In 2014, Kumar et al. found that NCOA3 worked as a chromatin remodeling enzyme and modulated the expression of mucins via transcriptional and post-translational changes in the development of PC [85]. Mucins, such as Muc1, Muc4, Muc5ac and Muc16, aberrantly express early in PanIN and enhance with the PC progression, promoting the processes of metastasis and chemoresistance [86-92]. In PC, constitutive active mutations of K-ras initiate the cellular signaling to create pro-inflammatory microenvironment, which caused the development of dense stroma and *de novo* expression of mucins. Mucins promote PC tumorigenicity via the interaction of their cytoplasmic tails with intracellular signaling, such as enhancement of EGFR signaling pathway and activation of focal adhesion kinases to increase cancer motility [90, 93-97].

De novo expression of mucins would require chromatin modifications at transcription level. NCOA3 interacts with nuclear receptors and transcription factors and remodels chromatin for active transcription due to its intrinsic histone-acetyltransferase activity [98]. Silencing of NCOA3 expression in PC cell lines led to significant reduction in transcripts and proteins of both Muc4 and Muc1 [85].

In addition to regulation of mucin expression, NCOA3 also plays a critical role in regulation of PC microenvironment. It upregulates the expression of multiple chemokines that are responsible for the recruitment of immune cells to pancreatic tumors, and perpetuation of pro-inflammatory conditions. Activated pancreatic stellate cells secret collagen and other extracellular matrix proteins in the tumor microenvironment, which were crosslinked by lysyl oxidases (LOX). NCOA3 may involve in the development of ECM by upregulating the expression of lysyl oxidase-like-2 (LOXL2). LOXL2 is associated with the aggressiveness of PC [99]. It participates in fibroblast activation and results in hardening of desmoplasia and subsequent collapse of the blood vessels, poor tumor perfusion, increased interstitial pressure, extreme hypoxia, and poor delivery of therapeutics [99]. Therefore, NCOA3 will be a novel target for PC diagnosis and therapy.

1.6 C-X-C chemokine receptor type 4

Chemokines are signaling proteins secreted by various stromal and epithelial cells capable of inducing concentration gradient-driven chemotactic migration of cells through interaction with their respective chemokine receptors [100]. Based on the number and spacing of N-terminal cysteines, chemokine receptors are divided into four groups (CXC, CX3C, CC and CX) [101]. There are 19 different chemokine receptors that all belong to the seven-transmembrane G-protein-coupled receptor family. In tumors, a complex network of chemokines and chemokine receptors controls cell trafficking into and out of the tumor microenvironment and thus mediate crucial parts of the metastatic spread of

tumor cells [102]. The corresponding chemokines expressed at the site of metastasis provide chemo-attractive signaling that guides trafficking of tumor cells to distant organ sites. Even though cells from different types of cancer may have different expression profiles of chemokine receptors, CXC receptor 4 (CXCR4) is the most widely expressed chemokine receptor in human cancers, which makes it among the most-promising targets within the chemokine network for cancer therapy.

1.6.1 CXCR4/CXCL12 signaling

CXCL12 binding to CXCR4 initiates multiple downstream signaling pathways and results in various responses, such as increasing intracellular calcium flux, gene transcription, chemotaxis, cell survival, and proliferation [103]. The heterotrimeric G protein is activated and dissociated into GTP-bound α and βγ subunits [104]. Gβγ subunits activate two major enzymes, phospholipase C-β (PLC-β) and a phosphatidylinositol-3-OH kinase (PI3K). Phosphatidylinositol (4, 5)-bisphosphate is cleaved by PLC-β into two secondary messengers, inositol (1, 4, 5)-trisphosphate (IP3) and diacylglycerol (DAG). IP3 causes the release of Ca^{2+} from intracellular stores and DAG activates protein kinase C and mitogen-activated protein kinase (MAPK) in conjunction with Ca^{2+}, thus contributing to cell migration [105]. Gα or Gβγ subunits activate PI3K leading to tyrosine phosphorylation of components of focal adhesions, including the related adhesion focal tyrosine kinase (RAFTK), the adaptor molecule p130 Cas, and the cytoskeletal protein paxillin, thus contributing to reorganization of the actin cytoskeleton and changes necessary for cell migration [106]. Transcription and gene expression are regulated by Gαi signaling through the PI3K-AKT-NF-κB, MEK1/2, and ERK1/2 axes [107]. The activated AKT can regulate the survival of cells. Dimerization of CXCR4 leads to G protein independent signaling via JAK/STAT pathway, which promotes cell morphology changes and chemotactic responses [108].

1.6.2 The role of CXCR4 in cancer and cancer metastasis

CXCR4 overexpression has been reported in more than 20 human tumor types, including mammary, ovarian, prostate, esophageal, pancreatic, melanoma, and renal cell carcinoma [109]. The upregulation of CXCR4 is associated with changes in multiple growth factors, transcription factors, and hypoxia-inducible factors [110-112]. Many preclinical and clinical studies observed significant correlation between CXCR4 expression and metastasis and found that CXCR4 expression is associated with poor survival and aggressive type of cancers. CXCR4 overexpression has been identified as a poor prognostic biomarker. For instance, a microarray study of 2,000 invasive breast carcinomas and 214 pre-invasive breast samples revealed the critical role of CXCR4 in cancer progression [113]. Elevated levels of CXCR4 in primary tumors were associated with a higher risk of developing bone metastasis [114]. Another clinical studies showed that CXCR4 promotes metastasis through the lymphatic system [115]. Elevated levels of CXCR4 in cancer cells have also correlated with increasing risk of cancer recurrence [116].

By activating intracellular signaling pathways, such as PI3K, MAPK and Erk1/2, CXCR4 plays a critical role in cancer cell survival, proliferation, invasion and migration [117-120]. The influence of CXCR4-induced activation of focal adhesion complexes and matrix metalloproteinases mediates degradation of extracellular matrix and contributes to invasion of cancer cells. CXCL12 expression levels are elevated in brain, bone marrow, lungs, and liver. The CXCL12 concentration gradients then drive movement of CXCR4-positive tumor cells in circulation and are responsible for the process of extravasation and organ-specific metastasis [121].

Among various chemokine pathways associated with the pathology of PC, the CXCR4/SDF1 axis plays critical role in the invasion and metastasis of PC [122-124]. The stromal cells produce abundant SDF-1, which activates CXCR4 in PC cells and results in

enhanced chemotaxis, transendothelial migration, and invasion [125]. CXCR4 upregulation can also augment the Sonic Hedgehog pathway, promotes stem-cell-like phenotype, enhanced desmoplasia, chemoresistance, and invasiveness of PC [126]. Multiple retrospective clinical studies have directly linked the expression of CXCR4 with poor survival and metastasis in PC patients [127, 128].

CXCR4/CXCL12 axis is an important emerging target for developing novel delivery strategies for improved cancer therapies [129, 130]. In addition to utilizing CXCR4 overexpression as a simple target for improved ligand-mediated delivery of drugs to tumors, blocking CXCR4/CXCL12 interaction using CXCR4 antagonists or silencing CXCR4 expression by siRNA has potential to prevent primary tumor growth and reduce metastasis, especially when combined with chemotherapy and radiotherapy. This review focuses on the role of CXCR4 in cancer metastasis and its potential in drug delivery systems for cancer therapy. Multiple targeting ligands and CXCR4 antagonists have been developed, including peptides, antibodies and small organic molecules. The main uses of CXCR4 in drug delivery for cancer therapy are summarized in **Scheme 3** and representative examples that explore CXCR4 in drug delivery are summarized in **Table 1**.

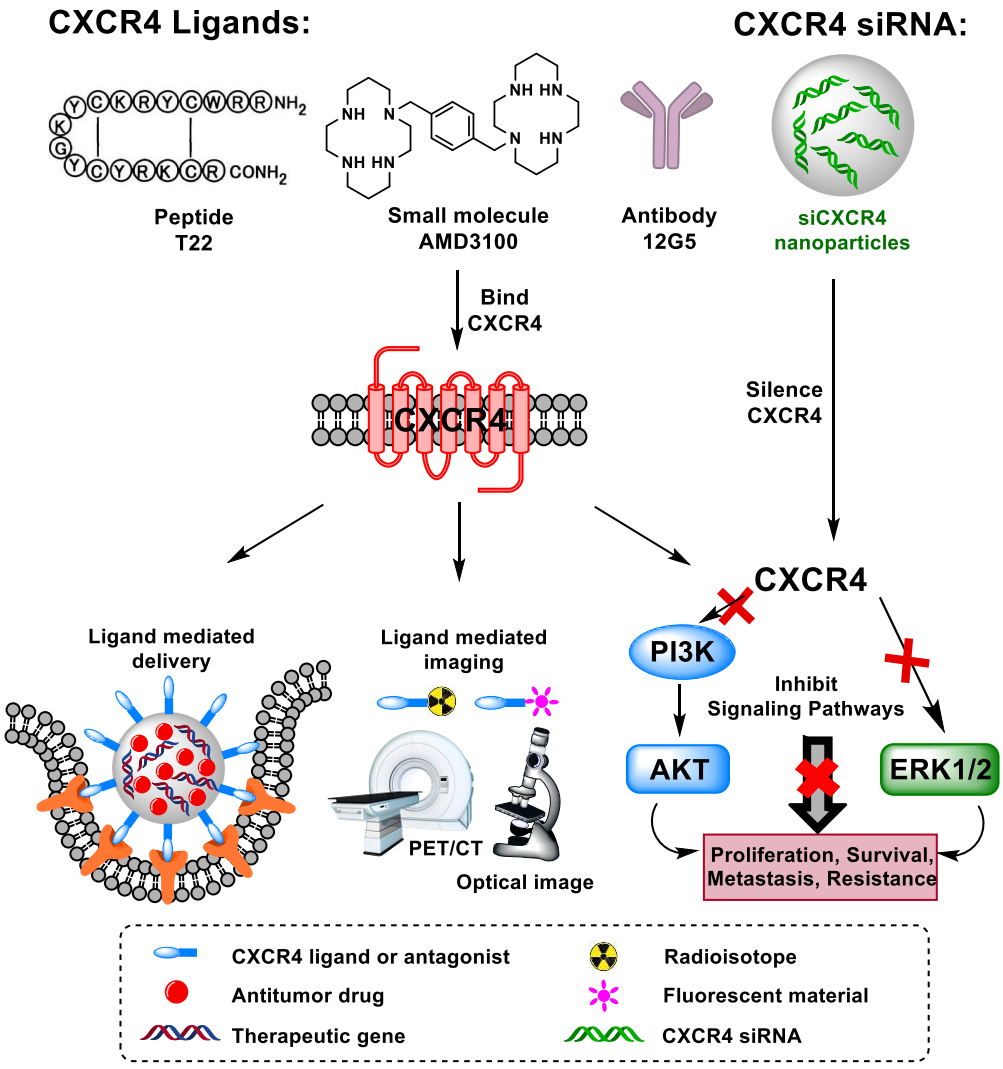

Scheme 3. Summary of the main approaches utilizing CXCR4 in cancer drug delivery

Table 1. Examples of CXCR4-targeted drug delivery systems

Targeting moiety	Delivery system	Delivered cargo	Application	References
T22 peptide	Fused fluorescent protein nanoparticle	Green fluorescent protein	Increase nanoparticle delivery to colorectal cancer (*in vivo*)	[131]
LFC131 peptide	Chitosan and PLGA nanoparticles	Docetaxel and doxorubicin	Increase anticancer drug delivery in lung cancer (*in vitro*)	[132, 133]
DV3 peptide	Cationic peptide transduction domain (PTD)	Anticancer peptides	Increase targeting and killing of CXCR4-positive lymphoma cells	[134]
Azide-containing T22 analogue peptide	Mesoporous silica nanoparticles	Doxorubicin	Increase anticancer drug delivery in lymphoma cells (*in vitro*)	[135]
N-terminal sequence of CXCL12	Polyplexes	Reporter plasmid DNA	Increase gene delivery to CXCR-positive human glioblastoma and cervical carcinoma cells	[136, 137]
Peptide analog 4F-benzoyl-TE14011	Lipoplexes	Reporter plasmid DNA	Increase gene delivery to rat glioma cells	[138]
Ac-TZ14011 peptide	Radiopharmaceutical	^{111}In	Image CXCR4 expression in metastatic pancreatic tumors *in vivo*	[139]
Ac-TZ14011 peptide	Dendrimers	^{111}In and Cy5.5 dye	Image CXCR4 expression in breast cancer *in vivo*	[140, 141]
X4-2-6 peptide	Self-assembled peptide nanoparticles	Anticancer drug HKH-40A	Inhibit breast tumor metastasis *in vivo*	[142]
Anti-CXCR4 antibody	Liposomes	Doxorubicin	Increase delivery and efficacy of anticancer drug in breast cancer (*in vitro*)	[143]
Anti-CXCR4 antibody	Liposomes	Anti-lipocalin-2 siRNA	Inhibit both the CXCR4 and Lcn2 mediated migratory pathways in metastatic breast cancer (*in vitro*)	[144]

Anti-CXCR4 antibody	Radiopharmaceutical	^{111}In	Image brain tumor by SPECT/CT (*in vivo*)	[145]
AMD3100	Lipoplexes and polyplexes	Reporter plasmid DNA	Increase gene transfection in CXCR4-positive human lymphoma Jurkat cells	[146]
AMD3100	PLGA nanoparticles	siRNA (anti-GFP)	Increase uptake, suppress CXCR4 signaling and deliver siRNA in triple negative breast cancer and metastatic breast cancer (*in vitro*)	[147]
AMD3100	PLGA nanoparticles	Sorafenib	Target malignant hepatocellular carcinoma and improve anticancer effect with sorafenib (*in vivo*)	[148]
AMD3100	Polyplexes	siRNA (siPLK1)	Simultaneously deliver gene and block CXCR4 to inhibit metastasis (*in vivo, in vitro*)	[149-152]
AMD3100 derivatives	Polyplexes	Reporter plasmid DNA	Simultaneously deliver gene and block CXCR4 to inhibit cell invasion (*in vitro*)	[153]
Viologen dendrimers	Dendrimer polyplexes	TNFα plasmid DNA	Simultaneously prevent CXCR4-mediated cancer cell invasion and facilitate TNFα-mediated cancer cell killing (*in vitro*)	[154]
AMD3100	Radiopharmaceutical	^{64}Cu	Image lung metastasis derived from human breast cancer by PET (*in vivo*)	[155]
AMD3465	Radiopharmaceutical	^{64}Cu	Image brain tumor and colon tumor by PET/CT (*in vivo*)	[156]

1.6.3 CXCR4 as target for ligand-mediated delivery and imaging

Multiple reports explored the use of CXCR4-binding ligands as a way of improving drug delivery to CXCR4-overexpressing tumors. The most popular ligands are based on short CXCR4-binding peptides, but small organic molecules and antibodies have also been explored and are discussed in this section.

1.6.3.1 CXCR4-binding peptides

Peptide ligands that bind CXCR4 has been widely used to direct drug delivery systems to CXCR4 overexpressing tumor cells with the goal of improving intracellular delivery of antitumor agents by receptor-medicated cellular uptake. Among the most successful has been a peptide T22 derived from horseshoe crab polyphemusin II. The T22 peptide binds CXCR4 and efficiently penetrates target cells via a rapid receptor-specific endosomal route. When conjugated to nanoparticles, T22 mediates delivery and accumulation of the nanoparticles in the perinuclear region of the target cells both in cell culture and in metastatic cancer models *in vivo*. The T22 peptide has been used for intracellular delivery of proteins, nanoparticles, and imaging agents [131]. Torre et al. have described a CXCR4-targeted delivery system using mesoporous silica nanoparticles that were loaded with doxorubicin and capped with an azide-containing modified T22 peptide by a click reaction [135]. Residues Tyr^5, Lys^7, and Tyr^{12} dramatically enhanced the affinity of the T22 peptide for the CXCR4 receptor overexpressed in B-cell non-Hodgkin's lymphoma cells. The peptide capped the pores in the porous nanoparticles to block the release of doxorubicin and facilitated uptake via the CXCR4 receptor. In lysosomes, proteolytic enzymes degraded the T22 peptide and allowed intracellular doxorubicin release.

Wang et al. have investigated a low-molecular-weight CXCR4 peptide antagonist LFC131 (Tyr-Arg-Arg-Nal-Gly). The authors conjugated the LFC131 peptide to O-

carboxymethyl chitosan nanoparticles and poly(lactide-*co*-glycolide) (PLGA) nanoparticles for enhanced targeted delivery of docetaxel and doxorubicin to CXCR4 overexpressing lung cancer cells [132, 133].

To enhance the targeting and killing of tumor cells, Snyder et al. linked another CXCR4 ligand, DV3, to two transducible anticancer peptides: a p53-activating peptide (DV3-TATp53C') and a cyclin-dependent kinase 2 antagonist peptide (DV3-TAT-RxL). Treatment with either of the targeted peptides resulted in an enhancement of tumor cell killing compared with treatment with non-targeted parent peptides [134].

CXCR4-binding peptides have also been successfully used to improve nucleic acid delivery with cationic peptides and cationic polymers. Egorova et al. have developed chemokine-derived peptides as carriers for gene delivery [136]. The authors used three synthetic peptides for CXCR4 receptor targeting: two derived from N-terminal sequence of CXCL12 and one from viral macrophage inflammatory protein (vMIP)-II. One of the peptides (KPVSLSYRSPSRFFESH-K9-biotin) derived from CXCL12, consisting of an N-terminal sequence of CXCL12 (KPVSLSYR) and an RFFESH motif (residues 12–17), was able to specifically target cells overexpressing CXCR4 and to exhibit high transfection efficacy. In a follow-up study, the authors found that the use of the oligolysine (K9) as the DNA-binding moiety compromised the gene delivery due to instability in physiological conditions and lack of endosomolytic properties. To circumvent these problems, the authors developed a gene delivery system using CXCL12-derived cross-linking peptides and demonstrated that a modular peptide KPVSLSYRSPSRFFESH-Ahx-Ahx-CHRRRRRRHC could be used as efficient gene delivery carrier. The flanking cysteines formed intermolecular disulfide bonds to stabilize the particles and tightly condense DNA. Subsequent internalization and intracellular disulfide breakage resulted in enhanced gene expression when compared with the K9-based peptides, in part also because of the

buffering capacity and membrane activity of the peptide containing histidine and arginine residues [137].

Feasibility of CXCR4 targeting using lipoplexes containing peptide analog 4F-benzoyl-TE14011 was also demonstrated [138]. The peptide ligand (4-fluorobenzoyl-RR-Nal-CY-Cit-KEPYR-Cit-CR) binds CXCR4 with high affinity (K_d 1.5 nM) and when covalently linked to a phospholipid used in lipoplex formulation resulted in CXCR4-targeted gene delivery.

1.6.3.2 CXCR4-binding small molecule organic ligands

Synthetic small molecule organic molecules that bind CXCR4 have been among the most successful CXCR4 antagonists. In fact, the only currently FDA-approved CXCR4 antagonist is a cyclam derivative AMD3100 (Plerixafor). AMD3100 has been shown to bind and block CXCR4 signaling in multiple animal models as well as in clinical trials [157, 158]. Several reports exist on the use of drug and gene delivery systems conjugated with small molecule ligands like AMD3100. Probably the first report described a nonviral carrier in which AMD3100 was covalently attached to polyethylenimine (PEI) and cationic lipids [146]. The study showed that the CXCR4-targeted polyplexes could effectively deliver genes into CXCR4-positive Jurkat cells. The role of CXCR4 in the uptake of the polyplexes was clearly demonstrated when nonspecific internalization pathways were minimized or when phorbolmyristate acetate (PMA) was used to enhance CXCR4 receptor endocytosis. AMD3100 has also been successfully used to target multicompartment PLGA nanoparticles to CXCR4-overexpressing breast cancer cells [147]. In this case, AMD3100 was conjugated to the surface of the nanoparticles by using PLGA with terminal acrylate groups that were reacted with AMD3100 amines via Michael addition. The targeted nanoparticles were then selectively taken up by CXCR4-overexpressing breast cancer cells and they also effectively blocked CXCR4 signaling. When loaded with siRNA, the

AMD3100-PLGA nanoparticles allowed for more effective gene silencing *in vitro* than their corresponding nontargeted nanoparticles.

1.6.3.3 Anti-CXCR4 antibodies

Multiple anti-CXCR4 antibodies have been developed and applied as experimental treatments in animal models of cancer metastasis [159, 160]. Such antibodies can be also used as ligands to facilitate improved delivery of drug carriers, similar to the peptide and small molecule ligands discussed above [143, 144]. For example, liposomes targeted with anti-CXCR4 antibody were used to improve doxorubicin activity in CXCR4-overexpressing breast cancer cells [143]. The liposomes were prepared by the extrusion using 1,2-dioleoyl-sn-glycero-3-phosphoethanolamine-N-dodecanoyl (N-dod-PE) and 1,2-dioleoyl-sn-glycero-3-phosphocholine (DOPC), followed by conjugation of mouse anti-human CXCR4 monoclonal antibody via N-dod-PE anchor by EDC/NHS chemistry. Overexpression of CXCR4 was observed in HCC1500 and MDA-MB-175VII breast cancer cells relative to normal control cells MCF10As. Expression levels of CXCR4 in the breast cancer cells directly correlated with increased liposome binding and enhanced drug activity. Based on this study, the knowledge of the levels of CXCR4 expression may be used to predict the efficacy of CXCR4-targeted drug delivery systems.

1.6.3.4 Imaging agents that target CXCR4

Due to the established role of CXCR4 in cancer metastasis, there is a growing interest and potential in using CXCR4-binding ligands for imaging of primary and metastatic tumors. CXCR4-binding imaging agents have been developed based on peptide and small molecule organic ligands. For example, using systematic structure-activity relationship study, Hanaoka et al. have developed a radiopharmaceutical for the imaging of CXCR4-expressing tumors *in vivo* based on the T22 peptide [139]. The authors designed a peptidic CXCR4 ligand named Ac-TZ14011 (Ac-RR-Nal-CY-Cit-RKPYR-Cit-

CR). The ligand contains four residues (Arg^2, Nal^3, Tyr^5, and Arg^{14}) that formed the intrinsic pharmacophore and were necessary for the CXCR4 inhibition. ^{111}In was then used as radionuclide for radiolabeling of the peptide containing diethylenetriaminepentaacetic acid (DTPA) attached to the side chain of $D\text{-}Lys^8$. The resulting ^{111}In-DTPA-Ac-TZ14011 inhibited the binding of CXCL12 to CXCR4 in a concentration-dependent manner with an IC50 of 7.9 nM. Biodistribution studies in athymic nude mice bearing subcutaneous CXCR4-overexpressing pancreatic carcinoma cells showed preferential accumulation of ^{111}In-DTPA-Ac-TZ14011 in the tumor. Similarly, Kuil et al. have developed peptide-conjugated dendrimers using Ac-TZ14011 peptide to obtain constructs capable of multimodal imaging. The constructs consisted of a Cy5.5-like fluorophore and a DTPA chelating group for ^{111}In labeling and were used to image CXCR4 expression in breast cancer animal model using both SPECT/CT and fluorescence imaging [140, 141].

The cyclam-based CXCR4 antagonists like AMD3100 constitute a diverse class of compounds with common ability to chelate transition metals in the cyclam macrocycle. These compounds have been used in multiple studies to chelate PET-positive radioisotope ^{64}Cu for imaging of CXCR4-expressing tumors. For example, Nimmagadda et al. have reported the development and evaluation of [^{64}Cu]-AMD3100 to image lung metastasis derived from human MDA-MB-231 breast cancer by PET [155]. Another cyclam-containing CXCR4 ligand, AMD3465, was also used for imaging CXCR4 expression. De Silva et al. reported that [^{64}Cu]-AMD3465 was capable of detecting tumor lesions using dynamic and whole-body PET/CT in a CXCR4 dependent fashion with high target selectivity in both U87 brain tumor and HT-29 colon tumor animal models [156].

Anti-CXCR4 antibodies are commonly used for fluorescence microscopy imaging but they also showed potential in SPECT/CT imaging in vivo. Using ^{125}I-labeled anti-CXCR4 monoclonal antibody (12G5), the results of a recent study showed successful

SPECT/CT imaging of CXCR4-positive U87 brain tumors [145]. Compared with isotype control, the tumor-to-tissue uptake ratio for ^{125}I-12G5 was 2.5-fold higher at 48 h after injection, indicating the feasibility of antibody-targeted tumor imaging.

1.6.4 Inhibition of CXCR4 in anticancer therapies

Due to its significant role in multiple steps involved in cancer progression, inhibition of CXCR4 has been explored in various drug delivery systems with the goal of reducing cancer cell proliferation and metastasis. Several strategies have been employed to either directly silence expression of CXCR4 gene in malignant cells using siRNA or to codeliver small-molecule CXCR4 antagonists with other antitumor therapeutics to achieve enhanced anticancer effect.

1.6.4.1 Silencing of CXCR4 gene

Specific targeting and silencing of CXCR4 expression with siRNAs has been proposed to slow down cancer cell growth and metastasis both *in vitro* and *in vivo*. CXCR4 expression was significantly downregulated in liver metastasis of colorectal cancer when anti-CXCR4 siRNA was delivered by nanoparticles based on spermine-modified dextran [161, 162]. In the study, spermine was conjugated to oxidized dextran by reductive amination process to obtain cationic dextran and the results showed that CXCR4 silencing decreased the extent of cancer cell and lymphocyte infiltrationin in the liver of treated animals. In a study of the effect of CXCR4 silencing on metastasis of breast cancer, a fusion protein based on HER2-scFv and arginine nonamer peptide (e23sFv-9R) was developed and tested as siRNA carrier [163]. Delivery of anti-CXCR4 siRNA by the e23sFv-9R carrier resulted in decreased CXCR4 expression and subsequent reduction in proliferation and metastasis in HER2-positive breast cancer BT-474 cell line *in vitro*. Importantly, systemic delivery of the anti-CXCR4 siRNA by the fusion protein was able to

suppress tumor growth, reduce metastasis, and prolong survival in mice bearing HER2-positive xenografts.

Tumor progression is associated with intratumoral hypoxia and an abnormal vascular architecture, which provides heterogeneous perfusion within the tumor tissue [164]. Hypoxia regulates the expression of multiple genes involved in angiogenesis, epithelial-mesenchymal transition, extracellular matrix degradation, and chemotaxis [165]. CXCR4 is a potential target in the events associated with hypoxia because of its hypoxia-triggered upregulation. Romain et al. have demonstrated that hypoxia upregulated CXCR4 expression in colon cancer cells and that CXCR4 expression remained elevated for up to 48 h even when the cancer cells were returned to normoxic conditions [166]. As a result of the CXCR4 upregulation, the migration of the colon cancer SW480 cells increased up to 6-fold in hypoxia when compared with normoxic conditions. Importantly, the increased invasiveness of the cancer cells could be reduced significantly by CXCR4 gene silencing.

1.6.4.2 Inhibition of CXCR4 in cancer metastasis

In addition to offering a simple targeting to CXCR4-overexpressing cancer cells, many of the existing CXCR4-binding ligands also function as receptor antagonists and thus inhibit CXCR4/CXCL12 signaling. The inhibition of the CXCR4 signaling can utilized to achieve additional antitumor and antimetastatic benefits, especially when combined with other simultaneously delivered drugs. There has been a growing number of successful examples of drug and gene delivery vectors that combine delivery function with a pharmacological CXCR4-inhibiting activity and they will be discussed in this section.

Multiple innovative drug delivery systems that combine CXCR4 inhibition and drug delivery have been reported in recent years. Taking advantage of the structural plasticity of transmembrane peptides, biologically active nanoparticles that effectively inhibit tumor metastasis *in vivo* have been developed based on a 24-amino acid peptide X4-2-6 which

corresponds to the second transmembrane helix of the CXCR4. The peptide self-assembled into nanoparticles that inhibited CXCR4 function *in vitro* and prevented CXCR4-dependent tumor metastasis in MDA-MB-231 breast cancer xenograft model [142]. These nanoparticles could additionally encapsulate hydrophobic antitumor drugs, thus providing an effective combination delivery system. The peptides were capable of assembling into a variety of structures including spherical, fibrous, tubular and discoid shapes [167]. The ability to control the morphology of the assemblies may allow improved delivery of such peptide particles as it was found that stronger intermolecular interactions observed in nanospheres than in fibrils resulted in slower rates of particle disassembly and in improved protection against proteolytic degradation.

As part of our long-term efforts to develop dually functioning polycations for combination drug/gene delivery, we have designed polycations (PAMD) based on the cyclam CXCR4 antagonist AMD3100. The PAMD polymers showed dual functionality as efficient nucleic acid (gene and siRNA) delivery vectors and CXCR4 antagonists that inhibited invasion of cancer cells *in vitro* and decreased metastasis in several tumor models *in vivo* [149, 150]. Modification of PAMD with PEG was used to improve the *in vivo* applicability [151]. Modification with cholesterol was used as a way of enhancing siRNA delivery efficacy of PAMD, while preserving the CXCR4-inhibiting activity of the polymers [152]. Although based on an approved drug and easy to synthesize, PAMD synthesis resulted in the formation of highly branched polymers and in a relatively low CXCR4 antagonistic activity when compared with the original AMD3100. Based on the knowledge of the AMD3100 pharmacophore, we developed a second generation of CXCR4-inhibiting polycations based on a series of linear poly(amido amine)s using Michael-type polyaddition of novel monocyclam monomers. The use of monocyclam monomers allowed preparation of polymers with well-defined architecture and the CXCR4-binding moieties

present in the sidechain of the polymers, which resulted in improved presentation and accessibility for CXCR4 binding, resulting in greatly increased CXCR4 antagonism [153].

In addition to naturally derived peptides and lipids and polymers based on existing small molecule CXCR4 inhibitors, dendrimers based on viologen (dialkylated 4, 4'-bipyridinium salts) have been found to exhibit potent antagonistic activity against CXCR4 [168]. Viologen dendrimers (VGD) were also recently used as a promising class of gene delivery vectors when they demonstrated promising synergistic anticancer activity when used to deliver TNFα plasmid DNA [154].

Similar to the other types of CXCR4 inhibitors, anti-CXCR4 antibodies have been used both for their drug targeting ability to CXCR4-overexpressing cancers as well as for their ability to block the CXCR4/CXCL12 signaling in antimetastatic approaches. For example, pH-responsive CXCR4-targeted liposomes were prepared to achieve combined inhibition of CXCR4 and siRNA silencing of lipocalin-2 (Lcn2) [144]. The liposomes were composed of a mixture of DOPC, 1, 2-dioleoyl-3-dimethylammoniumpropane (DODAP) and N-dod-PE and were modified with anti-CXCR4 antibody to target metastatic breast cancer cells and block cell migration. Liposomes incorporating DODAP responded to the acidic endosomal environment by increasing the cationic character, fusing with the endosomal membrane, and delivering siRNA into the cytoplasm. The combined liposomes significantly reduced migration in triple negative human breast cancer cells (88% for MDA-MB-436 and 92% for MDA-MB-231) when compared with inhibition of the CXCR4 or Lcn2 pathways alone.

1.6.4.3 Inhibition of CXCR4 as a chemosensitizing approach

Drug resistance remains a serious problem in cancer chemotherapy. Anticancer potency can be greatly improved by combining chemotherapy with a chemosensitizing effect of CXCR4 inhibition. For example, a multikinase inhibitor sorafenib is an anti-

angiogenic agent used in the treatment of advanced hepatocellular carcinoma (HCC) and its use results in a significant increase in overall patient survival. However, prolonged sorafenib treatment increases tumor hypoxia due to decreased neovasculature, which in turn upregulates the expression of CXCR4. This causes HCC to acquire more invasive phenotype and to rapidly develop resistance to antiangiogenic therapy with sorafenib [169-171]. AMD3100 can sensitize HCC to sorafenib treatment by inhibiting CXCR4 axis-induced cancer cell proliferation and polarization of the tumor-promoting microenvironment [171]. To take advantage of the chemosensitizing ability of AMD3100, Gao et al. encapsulated sorafenib in lipid-coated PLGA nanoparticles. The surface of the nanoparticles was modified with AMD3100 to allow systemic delivery of the sorafenib/AMD3100 combination into HCC [148]. The results of the study demonstrated that the nanoparticles could efficiently deliver sorafenib and AMD3100 in HCC and that the combined treatment showed improved anti-angiogenic effect and decreased infiltration of tumor-associated macrophages *in vivo*. The combined nanoparticle treatment significantly inhibited primary HCC growth and distal metastasis and thus increased overall survival *in vivo*, indicating clinical potential of CXCR4 inhibition in overcoming acquired drug resistance in HCC.

1.6.5 CXCR4 and PC

CXCR4/SDF-1 axis plays an important role in PC pathology, involving in metastasis, invasion, angiogenesis, and proliferation [123, 124]. Clinical data indicates that CXCR4 has been directly linked to poor survival of PC patients [127, 128, 172]. CXCR4 expression is overexpressed in majority of PC tissues and precancerous lesions, suggesting its role in PC pathogenesis [173]. The stromal cells produce abundant CXCL12, which activates CXCR4-expressing PC cells and results in enhanced chemotaxis, transendothelial migration and invasion [125]. PC cells are easily mediated by CXCR4

activation and migrate towards the gradient of SDF-1 in distant organs, such as lymph nodes, lung and liver [174]. Furthermore, activation of CXCR4/SDF-1 signaling confers drug resistance to pancreatic cancer cells by potentiating survival. Singh et al. reported that gemcitabine induced chemoresistance was partly mediated by the activation of Akt and Erk signaling pathways [175]. However, a small-molecule antagonist AMD3100 against CXCR4 could effectively abrogate the survival signals and resensitise the PC cells to gemcitabine cytotoxicity. Moreover, CXCR4/SDF-1 signaling confers chemoresistance not only by directly impacting the tumor cells but also indirectly through SHH-induced pancreatic fibrosis, suggesting the potential of the CXCL12-CXCR4 pathway as a therapeutic target in PC [176].

Chapter 2. Statement of the Problem and Hypothesis

Metastasis is the one of the major reasons for cancer mortality and morbidity. Each year, several million patients died from cancer metastasis. Existing therapeutic approaches rarely reverse or stop metastatic progression. Late diagnosis, early metastasis, and complex microenvironment caused extremely low survival rate of PC. The one-year and five-year survival rates are ~29% and ~7% respectively. Complicated PC microenvironment contributes to inherent resistance to available therapies and severely limits drug delivery [30-32]. Gemcitabine is the first-line treatment for metastatic pancreatic cancer. However, the objective response is less than 10%. Thus, there is an urgent need to develop novel therapies for the treatment of PC [33, 177].

PC is unique among solid tumors because of the extremely dense desmoplstic reaction which wraps the cancer cells. It forms a barrier to chemotherapy penetration due to the growth of dense, collagen rich, extracellular matrix and stroma with high interstitial pressure around PC tumors. Desmoplastic reaction creates a unique microenvironment that paradoxically promotes both tumor growth and metastatic spread. Furthermore, mucins, such as Muc1, Muc4, Muc5ac and Muc16, aberrantly express early in PanIN and enhance with the PC progression, promoting the processes of metastasis and chemoresistance [86-92].

NCOA3 is one of the frequently mutated genes in PC [82]. High-level amplification of NCOA3 has been found not only in PC cell lines, but also in PC tissues and metastatic lesions [83, 84]. It works as a chromatin remodeling enzyme and modulates the expression of mucins via transcriptional and post-translational changes in the development of PC [85]. In addition to regulation of mucin expression, NCOA3 may involve in the development of ECM by upregulating the LOXL2. LOXL2 participates in fibroblast

activation and results in hardening of desmoplasia, which is associated with the aggressiveness of PC [99].

CXCR4/SDF-1 axis plays a critical role in PC metastasis, invasion, angiogenesis, and proliferation [123, 124]. Abundant SDF-1 is produced by PC stromal cells and activates CXCR4 expression in PC cells, which also augments Shh pathway to elevate desmoplasia, enhance chemoresistance as well as promote invasion in PC [125, 126]. Gemcitabine induced chemoresistance was medicated by activation of CXCR4/SDF-1 signaling pathway [175]. However, a small-molecule CXCR4 inhibitor AMD3100 could effectively abrogate the survival signals and resensitize the PC cells to gemcitabine cytotoxicity. Multiple retrospective clinical studies have directly linked the expression of CXCR4 with poor survival and metastasis in PC patients [127, 128].

Targeting components of the tumor stroma that contribute to the desmoplastic reaction is a promising new platform of investigation. Most strategies aim to enhance chemotherapeutic and even radiotherapeutic efficacy, by increasing tumor accumulation, penetration, and drug-distribution and targeting signaling pathways, which are directly implicated in the formation of desmoplastic reaction. Changes in the tumor microenvironment that decrease desmoplasia can improve access of drugs to the tumor but they may also inadvertently promote metastasis. PC metastasizes readily and early in its progression.

Based on the critical role of NCOA3 and CXCR4 as well as the therapeutic challenges of PC, we designed novel treatment that relies on delivery of NCOA3-silencing siRNA using polyplexes formed by polymeric CXCR4 inhibitors (PCX). We hypothesized that the ability of the developed polyplexes to simultaneously downregulate mucin expression *via* NCOA3 silencing and inhibition of CXCR4 will lead to improved antitumor

and antimetastatic activity. The use of PCX to deliver siNCOA3 is in part selected to minimize the chances of increased metastasis.

The working hypothesis for this dissertation is that PCX will not only exhibit CXCR4 antagonism but will also effectively deliver siRNA to inhibit NCOA3. The hypothesis is supported by successful synthesis of PCX and the demonstration of PCX's ability to deliver multiple types of nucleic acids (DNA, siRNA). Development of functional poly(amido amine) CXCR4 antagonists with increased CXCR4 inhibitory activity is explored in the results and discussion part of **4.1**. Part **4.2** focuses on modification of PCX with PEGylation to enhance colloidal stability and safety for gene therapy in cancer. In **4.3** we investigate cholesterol modification of PCX to improve siRNA delivery for combined anticancer therapies. The combination of NCOA3 silencing and CXCR4 inhibition by PCX nanoparticles to improve antitumor and antimetastasis in PC is described in **4.4**. The central **hypothesis** is that the combination of NCOA3 gene silencing and CXCR4 antagonism by PCX will decrease mucin expression, regulate tumor microenvironment, reduce metastasis, and chemosensitize PC to improve the treatment. We will pursue the following specific aims.

Aim 1. Develop and modify PCX polymers to inhibit CXCR4 and deliver nucleic acids to cancer cells.

Aim 2. Screen PCX capable of efficient delivery of siRNA to inhibit NCOA3 in PC.

Aim 3. Determine if combination of NCOA3 silencing and CXCR4 inhibition by PCX nanoparticles improves antitumor and antimetastatic activity in orthotopic PC model.

Chapter 3 - Materials and Methods

3.1 Materials

N,N'-hexamethylenebisacrylamide (HMBA) was purchased from Polysciences, Inc. (Warrington, PA). Cyclam (1,4,8,11-tetraazacyclotetradecane) was from Alfa Aesar (Ward Hill, MA). Cholesteryl chloroformate and branched polyethylenimine (PEI, 25 kDa) was obtained from Sigma-Aldrich (St. Louis, MO). mPEG-Acrylamide (2 kDa) was from Creative PEGworks (Winston-Salem, NC). *N,N*-diisopropylethylamine (DIPEA) was from Acros Organics (New Jersey, US). Trifluoroacetic acid (TFA) and 4-amino-1-butanol (ABOL) were purchased from ACROS Organics (Fair Lawn, NJ). AMD3100 (base form) was from Biochempartner (Shanghai, China). Plasmid DNA, gWiz high-expression luciferase (gWiz-Luc), containing luciferase reporter gene was from Aldevron (Fargo, ND). Dulbecco's modified Eagle medium (DMEM), Dulbecco's phosphate buffered saline (PBS), and fetal bovine serum (FBS) were from Thermo Scientific (Waltham, MA). Cell culture inserts (for 24-well plates, 8.0 μm pores, Translucent PET Membrane, cat# 353097) and BD Matrigel™ Basement Membrane Matrix (cat# 354234) were purchased from BD Biosciences (Billerica, MA). Human SDF-1α was from Shenandoah Biotechnology, Inc. (Warwick, PA). Non-targeting siRNA control (siScr, 5'-UUCUCCGAACGUGUCACGUUU-3'), siGENOME human polo-like kinase 1 (PLK1) siRNA Smartpool (siPLK1) and stability enhanced NCOA3 siRNA (siNCOA3, 5'-GACAGGCACUUGAAUUGAAUU-3') were purchased from GE Healthcare Dharmacon, Inc. (Lafayette, CO). Succinimidyl ester of Alexa Fluor® 647 carboxylic acid was from Life Technologies (Eugene, OR). Rotor-Gene SYBR Green RT-PCR Kit was from QIAGEN (Hilden, Germany). TRIzol® reagent, human CXCR4 primers (F 5'-GCATGACGGACAAGTACAGGCT-3', R 5'-AAAGTACCAGTTTGCCACGGC-3'), and primers of gWiz Luciferase (F 5'-GAAGAGCTGTTTCTGAGG, R 5'-CGAAGAAGGAGAATAGGGT) were purchased from

Life Technologies (Carlsbad, CA). Allophycocyanin (APC) mouse anti-human CXCR4 antibody and APC mouse IgG2a, κ isotype controls were from BD Biosciences (San Jose, CA). Anti-CXCR4 antibody [UMB2] was purchased from Abcam (ab124824, Cambridge, MA). Anti-NCOA3 antibody was purchased from Santa Cruz Biotechnologies (sc25742, Dallas, TX). The MUC4 monoclonal antibody (8G7) used in this study was developed by Dr. Batra group [178]. All other reagents were from Fisher Scientific and used as received unless otherwise noted.

3.2 Synthesis of monocyclam-based monomers

*Tri-tert-butyl-1,4,8,11-tetraazacyclotetradecane-1,4,8-tricarboxylate (**2**):* A solution of Boc_2O (3.27 g, 15.0 mmol) in CH_2Cl_2 (75 mL) was added dropwise over a period of 2 h to a solution of **1** (1.00 g, 5.0 mmol) in CH_2Cl_2 (200 mL) at 0°C. The mixture was allowed to warm to room temperature and stirred overnight. The mixture was concentrated and purified by chromatography (AcOEt→10:1 AcOEt:CH_3OH) to first give tetra-Boc cyclam as a white foam and then tri-Boc cyclam (compound **2**, 2.10 g, 84%) as a white set foam: ^{1}H NMR (400 MHz, $CDCl_3$, δ) 1.46 (s, 27H), 1.65–1.76 (m, 2H), 1.80–2.00 (m, 2H), 2.62 (bt, *J* = 5.6 Hz, 2H), 2.79 (t, *J* = 4.8 Hz, 2H), 3.31 (t, *J* = 6.4 Hz, 8H), 3.34–3.47 (m, 4H).

*Tri-tert-butyl-11-(4-(chloromethyl)benzyl)-1,4,8,11-tetraazacyclotetradecane-1,4,8-tricarboxylate (**3**):* to a solution α,α'-dichloro-*p*-xylene (7.44 g, 41.6 mmol) in CH_3CN (100 mL), anhydrous K_2CO_3 (1.44 g, 10.4 mmol) was added followed by **2** (4.17 g, 8.33 mmol) dissolved in CH_3CN (50 mL). The mixture was refluxed for 6 h before filtering and washing the solid with acetone. The filtrate was concentrated to give a white solid that was heated with 2:1 hexanes:AcOEt and concentrated to a small volume to allow the excess dichloroxylene to crystallize out. The filtrate was then further purified by chromatography (2:1→1:1 hexanes:AcOEt) to first give more excess dichloroxylene and then the desired mono-cyclam product (compound **3**, 4.31 g, 81%) as a white set foam: ^{1}H NMR (400 MHz,

$CDCl_3$, δ) 1.44 (s, 18H), 1.47 (s, 9H), 1.68 (bs, 2H), 1.90 (bs, 2H), 2.30–2.47 (m, 2H), 2.50–2.70 (m, 2H), 3.15–3.48 (m, 12H), 3.52 (s, 2H), 7.23 (d, *J* = 8.0 Hz, 2H), 7.32 (d, *J* = 7.2 Hz, 2H).

*Tri-tert-butyl-11-(4-((2-hydroxyethylamino)methyl)benzyl)-1,4,8,11-tetraaza cyclotetradecane-1,4,8-tricarboxylate (**4a**):* To a mixture of **3** (2.17 g, 3.39 mmol) and anhydrous K_2CO_3 (0.70 g, 5.1 mmol) in CH_3CN (15 mL), ethanolamine (2.1 mL, 2.1 g, 34 mmol) was added and the mixture stirred overnight. The formed solid was filtered and washed with AcOEt (50 mL). The filtrate was washed with water (2 × 10 mL), saturated NaCl (10 mL), then dried ($MgSO_4$) and concentrated to give a viscous liquid, which was purified by chromatography (10:1 CH_2Cl_2:CH_3OH, adding 0.5% NH_3 later) to give the amino alcohol as a white foam (compound **4a**, 2.08 g, 92%): ^{1}H NMR (400 MHz, $CDCl_3$, δ) 1.44 (s, 18H), 1.47 (s, 9H), 1.67 (bs, 2H), 1.90 (bs, 2H), 2.20–2.46 (m, 4H), 2.52–2.70 (m, 2H), 2.80 (t, *J* = 6.0 Hz, 2H), 3.18–3.44 (m, 12H), 3.50 (s, 2H), 3.67 (t, *J* = 5.2 Hz, 2H), 3.80 (s, 2H), 7.19–7.26 (m, 4H).

*Tri-tert-butyl-11-(4-((3-hydroxypropylamino)methyl)benzyl)-1,4,8,11-tetraazacyclo tetradecane-1,4,8-tricarboxylate (**4b**):* To a solution of **3** (2.14 g, 3.35 mmol) and anhydrous K_2CO_3 (0.69 g, 5.0 mmol) in CH_3CN (15 mL), 3-amino-1-propanol (2.6 mL, 2.55 g, 33.5 mmol) was added and the mixture stirred overnight. The formed solid was filtered and washed with AcOEt (50 mL). The filtrate was washed with water (2 × 10 mL), saturated NaCl (10 mL), dried ($MgSO_4$) and concentrated to give a viscous liquid, which was then purified by chromatography (10:1 CH_2Cl_2:CH_3OH, adding 0.5% NH_3 later) to give the amino alcohol as a white foam (compound **4b**, 2.16 g, 95%): ^{1}H NMR (400 MHz, $CDCl_3$, δ) 1.44 (s, 18H), 1.47 (s, 9H), 1.67 (bs, 2H), 1.74 (quintet, *J* = 5.6 Hz, 2H), 1.90 (bs, 2H), 2.36 (bs, 2H), 2.52–2.68 (m, 2H), 2.91 (t, *J* = 5.6 Hz, 2H), 3.18–3.44 (m, 12H), 3.51 (s, 2H), 3.79 (s, 2H), 3.81 (t, *J* = 5.2 Hz, 2H), 7.22 (s, 4H).

*Tri-tert-butyl-11-(4-((tert-butoxycarbonyl(2-hydroxyethyl)amino) methyl)benzyl)-1,4,8,11-tetraazacyclotetradecane-1,4,8-tricarboxylate (**5a**):* To a solution of **4a** (1.67 g, 2.52 mmol) in CH_2Cl_2 (25 mL), Boc_2O (0.82 g, 3.8 mmol) in CH_2Cl_2 (5 mL) was added and the mixture stirred overnight. It was concentrated to give a light yellow liquid and purified by chromatography (1:1 hexanes:AcOEt) to give the Boc protected amino alcohol as a white set foam (compound **5s**, 1.90 g, 99%): ^{1}H NMR (400 MHz, $CDCl_3$, δ) 1.44 (s, 18H), 1.47 (s, 18H), 1.67 (bs, 2H), 1.90 (bs, 2H), 2.36 (bs, 2H), 2.53–2.68 (m, 2H), 3.18–3.44 (m, 14H), 3.51 (bs, 2H), 3.68 (bs, 2H), 4.40–4.54 (m, 2H), 7.12–7.25 (m, 4H).

*Tri-tert-butyl-11-(4-((tert-butoxycarbonyl(3-hydroxypropyl)amino)methyl)benzyl)-1,4,8,11-tetraazacyclotetra decane-1,4,8-tricarboxylate (**5b**):* To a solution of **4b** (2.16 g, 3.18 mmol) in CH_2Cl_2 (30 mL), Boc_2O (1.08 g, 4.77 mmol) in CH_2Cl_2 (5 mL) was added and the mixture stirred overnight. It was concentrated to give a light yellow liquid and purified by chromatography (1:1 hexanes:AcOEt) to give the Boc protected amino alcohol as a white set foam (compound **5b**, 2.24 g, 91%): ^{1}H NMR (400 MHz, $CDCl_3$, δ) 1.44 (s, 18H), 1.47 (s, 18H), 1.57–1.78 (m, 4H), 1.91 (bs, 2H), 2.36 (bs, 2H), 2.51–2.70 (m, 2H), 3.18–3.44 (m, 14H), 3.47–3.59 (m, 4H), 3.82 (bs, 2H), 4.35 (bs, 2H), 7.11–7.25 (m, 4H).

*Tri-tert-butyl-11-(4-((tert-butoxycarbonyl(2-(1,3-dioxoisoindolin-2-yl)ethyl)amino)methyl) benzyl)-1,4,8,11-tetraazacyclotetradecane-1,4,8-tricarboxylate (**6a**):* A mixture of **5a** (1.41 g, 1.85 mmol), PPh_3 (0.98 g, 3.7 mmol), phthalimide (0.29 g, 1.93 mmol) and anhydrous THF (20 mL) was heated under N_2 until all the solid dissolved. The mixture was cooled to 0°C and diethyl azodicarboxylate (DEAD) (0.60 mL, 0.67 g, 3.7 mmol) was added dropwise and the mixture warmed to room temperature, after which it was concentrated to give a white solid. The solid was heated with 2:1 hexanes:AcOEt until all the solid dissolved and filtered through silica gel, collecting the fractions that contained product. These fractions where concentrated to a small volume and any solid that

crystallized out was removed by filtration. The filtrate was further purified by chromatography (2:1 hexanes:AcOEt) to give the phthalimide as a white set foam (compound **6a**, 1.65 g, 100%): ^{1}H NMR (400 MHz, $CDCl_3$, δ) 1.43 (s, 18H), 1.47 (s, 18H), 1.66 (bs, 2H), 1.89 (bs, 2H), 2.35 (bs, 2H), 2.58 (bs, 2H), 3.14–3.40 (m, 12H), 3.40–3.48 (m, 3H), 3.51 (t, *J* = 5.2 Hz, 1H), 3.81 (t, *J* = 5.6 Hz, 1H), 3.86 (t, *J* = 5.2 Hz, 1H), 4.41 (s, 1H), 4.47 (s, 1H), 7.17 (s, 4H), 7.65–7.75 (m, 2H), 7.80–7.86 (m, 2H).

*Tri-tert-butyl-11-(4-((tert-butoxycarbonyl(3-(1,3-dioxoisoindolin-2-yl)propyl)amino) methyl) benzyl)- 1,4,8,11-tetraazacyclo tetradecane-1,4,8-tricarboxylate (**6b**):* A mixture of **5b** (0.89 g, 1.14 mmol), PPh_3 (0.61 g, 2.3 mmol), phthalimide (0.19 g, 1.3 mmol) and anhydrous THF (15 mL) was heated under N_2 until all the solid dissolved, before it was cooled to 0°C. DEAD (0.37 mL, 0.41 g, 2.3 mmol) was added dropwise and the mixture warmed to room temperature, after which it was concentrated to give a white solid. This was heated with 2:1 hexanes:AcOEt until all the solid dissolved and filtered through silica gel, collecting the fractions that contained product. These fractions where concentrated to a small volume and any solid that crystallized out was removed by filtration. The filtrate was further purified by chromatography (2:1 hexanes:AcOEt) to give the phthalimide as a white set foam (compound **6b**, 1.03 g, 100%): ^{1}H NMR (400 MHz, $CDCl_3$, δ) 1.44 (s, 27H), 1.47 (s, 9H), 1.67 (bs, 2H), 1.88 (bs, 4H), 2.36 (bs, 2H), 2.61 (bs, 2H), 3.12–3.45 (m, 12H), 3.50 (s, 2H), 3.65 (bs, 2H), 4.18–4.25 (m, 2H), 4.43 (bs, 2H), 7.10–7.20 (m, 4H), 7.69–7.75 (m, 2H), 7.81–7.86 (m, 2H).

*Tri-tert-butyl-11-(4-(((2-aminoethyl)(tert-butoxycarbonyl)amino)methyl)benzyl)- 1,4,8,11-tetraazacyclotetrade cane-1,4,8-tricarboxylate (**7a**).* To a solution of **6a** (1.54 g, 1.7 mmol) in CH_3OH (20 mL), NH_2NH_2 (0.54 mL, 0.55 g, 17 mmol) was added and the mixture stirred overnight. It was concentrated to give a white solid that was mixed with CH_2Cl_2 and filtered. This was repeated until no more amine was extracted from the solid.

The combined filtrates were concentrated to give a white foam (compound **7a**, 1.31 g, 100%). This was further purified by chromatography (10:1 CH_2Cl_2:CH_3OH, adding 0.5% NH_3 latter). ^{1}H NMR (400 MHz, $CDCl_3$, δ) 1.44 (s, 18H), 1.47 (s, 18H), 1.67 (bs, 2H), 1.91 (bs, 2H), 2.06 (bs, 2H), 2.36 (bs, 2H), 2.62 (bs, 2H), 2.79 (bs, 2H), 3.13–3.45 (m, 14H), 3.51 (s, 2H), 4.43 (bs, 2H), 7.11–7.24 (m, 4H).

*Tri-tert-butyl-11-(4-(((3-aminopropyl)(tert-butoxycarbonyl)amino)methyl)benzyl)-1,4,8,11-tetraazacyclotetradecane-1,4,8-tricarboxylate (**7b**):* To a solution of **6b** (1.03 g, 1.1 mmol) in CH_3OH (20 mL), NH_2NH_2 (0.36 mL, 0.36 g, 11 mmol) was added and the mixture stirred overnight. It was concentrated to give a white solid that was mixed with CH_2Cl_2 and filtered. This was repeated until no more amine was extracted from the solid. The combined filtrates were concentrated and purified by chromatography (10:1 CH_2Cl_2:CH_3OH, adding 0.5% NH_3 latter) to give a white foam (compound **7b**, 0.66 g, 75%). ^{1}H NMR (400 MHz, $CDCl_3$, δ) 1.44 (s, 18H), 1.47 (s, 18H), 1.66 (bs, 4H), 1.91 (bs, 2H), 2.17 (bs, 2H), 2.36 (bs, 2H), 2.52–2.78 (m, 4H), 3.13–3.44 (m, 14H), 3.51 (s, 2H), 4.33–4.47 (m, 2H), 7.09–7.23 (m, 4H).

3.3 Polymer synthesis

3.3.1 Synthesis of PCX^{G1}

Polymeric Plerixafor PCX^{G1} was synthesized by Michael-type polyaddition of equal molar ratio of HMBA and a corresponding cyclam monomer AMD3100. Typically, each reactant was dissolved at a concentration at 80 mg/mL in a glass vial containing MeOH/water (7/3 v/v) mixture. Polymerization was carried out under nitrogen atmosphere and in dark at 37 °C for 4 days. Then, additional 10% of AMD3100 was added and the reaction mixture was stirred for further one day to consume all residual acrylamide groups. PCX^{G1} was isolated by double precipitation in diethyl ether, collected by centrifugation, and dried in vacuum for further modification. The final PCX^{G1} was obtained by adjustment

of pH to 4 using 1 M HCl and dialysis against deionized water (membrane molecular weight cut-off 3.5 kDa) with yield higher than 80%.

3.3.2 Synthesis of PCX^{G2}

Polymeric CXCR4 antagonists PCX^{G2} based on the monocyclam monomers were synthesized by Michael-type addition copolymerization of HMBA with a mixture of **7a** or **7b** and different amount of ABOL. In a typical polymerization reaction, **7a** (76.3 mg, 0.1 mmol), ABOL (8.9 mg, 0.1 mmol) and HMBA (44.8 mg, 0.2 mmol) were dissolved in 0.65 mL of MeOH/water (7/3 v/v). Polymerization was carried out for 14 days at 50 °C in dark under nitrogen. Then, in order to remove any residual acrylamide groups, excess of cyclam (4 mg, 0.02 mmol) was added and the reaction mixture was stirred for additional 2 days. The resultant Boc-protected polymers were isolated by evaporating solvent using oil vacuum pump. The protecting Boc groups were then removed by dissolving the obtained polymers in TFA at concentration of 20 mg/mL and stirring for 15 h at room temperature. The product was dried under oil vacuum pump and dissolved in acidified water (pH 4). The product was then dialyzed against acidified water (pH 4) with molecular weight cut-off of 3.5 kDa. Final product was obtained by lyophilization as hydrochloride salt. The typical yield after dialysis was 58-63%. Control polymer PABOL without cyclam moiety was synthesized as hydrochloride salt using the same conditions described as above by copolymerization of equal molar ratio of ABOL (89.1 mg, 1 mmol) and HMBA (224.2 mg, 1 mmol) with yield of 30.4% after dialysis.

3.3.3 PEGylation of PCX^{G1}

The PEGylation of PCX^{G1} was carried out by Michael addition between the secondary amines in the cyclam groups of PCX^{G1} and acrylamide group of mPEG-acrylamide. PCX^{G1} (72.3, 66.4 or 69.7 mg) and mPEG-acrylamide (8.0 mg, 35.8 mg or 69.7 mg) were dissolved in MeOH/water mixture (7/3 v/v) at a total concentration of 120

mg/mL and the solution was stirred for 2 days at 37 °C, followed by 1 day at 50 °C. The reaction was cooled to room temperature and the pH was adjusted to 4 using 1 M HCl. The resulting copolymers (PEG-PCX^{G1}) were isolated by precipitation in diethyl ether, centrifugation, and drying in vacuum, and finally dialyzed against deionized water (pH 4, membrane molecular weight cut-off 3.5 kDa). Typical yield was 70-80%.

3.3.4 Cholesterol modification of PCX^{G1}

In order to synthesize Chol-PCX^{G1} with various degrees of cholesterol substitution, PCX^{G1} was first dissolved in a mixture of anhydrous methylene chloride and DIPEA. Different calculated amounts of cholesteryl chloroformate (15.4 mg, 32 mg or 55.62 mg) in anhydrous methylene chloride were added drop wise to the ice-cold PCX^{G1} (83.4 mg, 86.3 mg or 90 mg) solution over 1 h. The reaction was continued under stirring for another 24 h. The product was isolated by evaporating the solvent and washing with diethyl ether three times to remove unreacted cholesteryl chloroformate. The product was further dissolved in ethanol/water (v/v 1/1) mixture, followed by adjusting the pH to 4.0 using 1 M HCl. The polymers were then obtained by lyophilization after extensive dialysis against ethanol/water mixture (v/v 1/1) for 2 days and distilled water for another day (membrane molecular weight cut-off 3.5 kDa). Typical yield of Chol-PCX^{G1} ranged from 61% to 88%.

3.4 Polymer characterization

The molar mass of PCX was analyzed by gel permeation chromatography (GPC) operated in 0.3 M sodium acetate buffer (pH 5) using Agilent 1260 Infinity LC system equipped with a miniDAWN TREOS multi-angle light scattering (MALS) detector and a Optilab T-rEX refractive index detector from Wyatt Technology (Santa Barbara, CA). GPC data were analyzed using Astra 6.1 software from Wyatt Technology. The content of PEG or cholesterol in modified PCX^{G1} was determined using ^{1}H-NMR on Varian INOVA (500 MHz). The molecular weights of PEG-PCX^{G1} or Chol-PCX^{G1} were calculated on the basis

of the determined molar mass of PCX^{G1} by GPC and the known PEG or cholesterol substitution degree determined by ^{1}H-NMR.

3.5 Critical Micelle Concentration (CMC)

Fluorescence spectroscopy was used to determine CMC of Chol-PCX^{G1} polymers using pyrene as a hydrophobic fluorescent probe. Different concentrations of Chol-PCX^{G1} in water were allowed to equilibrate with 600 nM pyrene overnight at room temperature after 1 h sonication. Each fluorescence intensity index ratio at $335_{ex}/384_{em}$ nm (I_3) vs. $335_{ex}/373_{em}$ nm (I_1) (I_3/I_1) was measured, and plotted against the logarithmic concentration of the polymer. The concentration at the inflection point was determined as CMC [179].

3.6 DNA condensation by ethidium bromide exclusion assay

The ability of the synthesized polymers to condense DNA was determined by ethidium bromide (EtBr) exclusion assay by measuring the changes in EtBr/DNA fluorescence. 1 mL of DNA solution (20 µg/mL) was prepared in 10 mM HEPES buffer (pH 7.4) and mixed with EtBr (1 µg/mL). Raw fluorescence intensity was measured and set to 100% using an excitation wavelength of 540 nm and an emission wavelength of 590 nm. The fluorescence of ethidium bromide only in HEPES buffer was defined as background and set as 0%. Fluorescence readings were recorded following a stepwise addition of polymer solution and condensation curves (relative fluorescent intensity % vs. w/w ratio) were constructed.

3.7 Preparation and characterization of DNA polyplexes

Plasmid DNA solution at a concentration of 20 µg/mL was prepared in 10 mM HEPES buffer (pH 7.4). Polyplexes were formed by adding predetermined volume of a polymer to achieve desired polymer/DNA w/w ratio. The mixture was vigorously vortexed for 10 s and then stablized at room temperature for 30 min before further analysis. To

prepare mixed polyplexes, solutions of PCX^{G1} and PEG-PCX^{G1} were initially mixed at desired ratios and then added to the DNA solution. Hydrodynamic diameter and zeta potential of the polyplexes were determined by dynamic light scattering (DLS) using a ZEN3600 Zetasizer Nano-ZS (Malvern Instruments Ltd., Worcestershire, UK). The results were expressed as mean ± standard deviation (SD) of three measurements.

3.8 Preparation and characterization of siRNA polyplexes

siRNA polyplexes were formed by mixing equal solution volumes of siRNA (20 μg/mL) and polymer by pipetting, followed by incubation at room temperature for 20 min before further use. Complexation of siRNA by polymers was examined by agarose gel electrophoresis. PCX/siRNA polyplexes were prepared at various polymer/siRNA w/w ratios, loaded onto a 2% agarose gel containing 0.5 μg/mL ethidium bromide. Gels were run at 75 V in 0.5x Tris/Borate/EDTA (TBE) buffer for 30 min and then imaged under UV. Hydrodynamic diameter and zeta potential of the polyplexes in 10 mM HEPES buffer (pH 7.4) were determined by DLS. The results were expressed as mean ± standard deviation (SD) of three measurements.

3.9 Colloidal stability

Polypelxes were prepared accordingly as described above. To evaluate colloidal stability of the polyplexes, 10x phosphate-buffered saline (PBS) was added to the polyplexes to obtain a final 1x PBS solution (pH 7.4) with the following composition: 137 mM NaCl, 2.7 mM KCl, 10 mM Na_2HPO_4, 1.8 mM KH_2PO_4. The hydrodynamic diameter was then measured using DLS after 15 min, 1 h, and 12 h incubation at 25 °C. Results were expressed as mean ± standard deviation (SD) of three measurements.

3.10 Enzymatic stability

To study the resistance of PCX/siRNA polyplexes to RNase I, polyplexes containing a total amount of 0.2 µg siRNA were incubated with 2.5 units of RNase I at 37 °C for 30 min, followed by incubation at 90°C for 30 min to inactivate the enzyme. Heparin (200 µg/mL) was added to the samples and the mixture was incubated for additional 30 min to release the siRNA. Gel electrophoresis was then used to determine siRNA integrity.

3.11 Cell culture

Human hepatocellular carcinoma, HepG2 cells were purchased from ATCC (Manassas, VA) and cultured in MEM supplemented with 10% FBS. Human epithelial osteosarcoma U2OS cells stably expressing functional EGFP-CXCR4 fusion protein were purchased from Fisher Scientific and cultured in DMEM supplemented with 2 mM L-glutamine, 1% Pen-Strep, 0.5 mg/ml G418 and 10% FBS. Mouse melanoma B16F10 cells were a kind gift from Dr. Rakesh Singh (UNMC) and maintained in DMEM supplemented with 10% FBS. Mouse mammary carcinoma 4T1 cell line was from ATCC (Manassas, VA) and cultured in RPMI supplemented with 10% FBS. Human PC cell line CD18/HPAF was originally derived from the parental heterogeneous HPAF pancreatic tumor cell line by a limiting dilution technique [180]. Luciferase-expressing CD18/HPAF (CD18/HPAF.luc) cell line was obtained by transfecting CD18/HPAF cells with pbabe.puro-Fluci vector as described previously [181]. The cell line was cultured in DMEM with 1% Pen-Strep and 10% FBS. All cells were maintained in an incubator at 37 °C and 5% CO_2.

3.12 Cytotoxicity

Cytotoxicity of the synthesized polycations was evaluated by CellTiter 96®AQueous Non-Radioactive Cell Proliferation Assay or CellTiter-Blue Cell Viability Assay (Promega, Madison, WI). Single cell suspension was seeded in 96-well plates and incubated overnight. Culture medium was then replaced by 150 µL of serial dilutions of a

polymer in serum-supplemented medium. Cells were incubated at 37 °C for 24 h, and the medium was replaced with a mixture of 100 µL medium and 20 µL of assay reagent. After 1 h incubation, the absorbance [A] or fluorescence intensity [I] was measured using SpectraMax®M5e Multi-Mode Microplate Reader (Molecular Devices, CA) at a wavelength of 490 nm or at $\lambda_{ex}/\lambda_{em}$ 560/590 nm.. The relative cell viability (%) was calculated as $[A]_{sample}/[A]_{untreated} \times 100\%$ or $[I]_{sample}/[I]_{untreated} \times 100\%$. The IC_{50} were calculated in GraphPad Prism using a built-in dose-response analysis as the polymer concentration that causes 50% decrease in cell viability relative to untreated cells.

3.13 CXCR4 antagonism

CXCR4 antagonism of the polycations and polyplexes was measured by CXCR4 redistribution assay using a high-contant fluorescence microscopy analysis. U2OS cells stably expressing functional EGFP-CXCR4 fusion protein were seeded at a density of 8,000 cells/well in 96-well black plates with optical bottom 24 h before the experiment. On the day of the assay, cells were washed twice with 100 µL assay buffer (DMEM supplemented with 2 mM L-glutamine, 1% FBS, 1% Pen-Strep, and 10 mM HEPES) and incubated with different concentrations of the polycations, polyplexes, or AMD3100 in the assay buffer containing 0.25% DMSO at 37 °C for 30 min. Then, 10 nM SDF-1 was added to each well and the cells were incubated at 37 °C for 1 h. Cells were fixed with 4% paraformaldehyde at room temperature for 20 min, washed 4 times with PBS and stained in 1 µM Hoechst 33258 solution for 30 min before imaging (EVOS fl microscope). Cellomics ArrayScan V^{T1} High Content Analysis Reader (Thermo Scientific) was then used to quantify the internalization of the CXCR4 receptors, and the images were analyzed by SpotDetectorV3 BioApplication software. CXCR4 antagonism was determined based on % CXCR4 internalization inhibition calculated relative to the positive (AMD3100, 100%) and negative (SDF-1 only, 0%) controls, and the results were expressed as mean % inhibition

± SD (n = 3 or 4). EC_{50} values (polymer concentrations that cause 50% CXCR4 inhibition) were determined in Prism Graghpad software using a three-parameter inhibitor dose-response analysis method.

3.14 Cell invasion

Transwell cell culture inserts were coated with 40 µL ice-cold Matrigel which was diluted 1:3 (v/v) with serum-free medium. The 24-well plates with coated inserts were then placed in 37 °C incubator for 2 h. U2OS cells were harvested and resuspended with PCX polymers or polyplexes before adding to the inserts at a final concentration of 50,000 cells in 300 µL serum-free medium per insert. 20 nM SDF-1 in serum-free medium was added as the chemoattractant to the lower chamber of the wells. After 19 h, the non-invaded cells on the top surface of the insert membrane were removed by cotton swabs and the invaded cells on the bottom surface were fixed in 100% methanol and stained with 0.2% Crystal Violet solution for 10 min at room temperature. The number of invaded cells was counted under microscope set to 20× magnification. The results were expressed as average number of cells/imaging area ± SD (n = 5-10 random imaging areas).

3.15 Cell uptake DNA polyplexes by flow cytometry

Fluorescent gWiz-Luc DNA was prepared by using Label IT-TrackerTM CX-Rhodamine Kit (Mirus, Madison, WI) according to manufacturer's protocol. B16F10 and U2OS cells were seeded in 24-well plate at density of 200,000 and 100,000 cells/well 24 h prior to transfection. On the next day, cells were incubated with PCX^{G2}/DNA polyplexes containing 0.8 µg labeled DNA per well at w/w 5 in 300 µl of medium with or without 10% FBS. After incubation for 4 h, polyplexes were removed, and cells were washed with PBS, detached and resuspended for flow cytometry. The results were processed using flow cytometry data analysis software Flowjo (Tree Star Inc., Ashland, OR) and expressed as mean relative fluorescence intensity (n=3). To detect the possibility of CXCR4 receptors

involving into the process of cellular uptake of PCX^{G2} polyplexes, U2OS cells were pretreated with 0.3 μM AMD3100 in serum-free medium for 1 h before adding PCX^{G2}/DNA polyplexes (n=2).

3.16 DNA transfection activity

The transfection experiments were carried out in 48-well cell culture plates with cells at logarithmic growth phase. B16F10 (40,000 cells/well) and U2OS (20,000 cells/well) cells were seeded 24 h prior to transfection. On the day of transfection, culture medium in each well was removed and replaced with 150 μL of antibiotic-free medium with or without 10% FBS before adding 20 μL of polyplexes (DNA dose 0.4 μg/well). After 4 h incubation, polyplexes were completely removed and the cells were cultured in complete culture medium for 24 h prior to measuring luciferase expression. The medium was discarded and the cells were lysed in 100 μL of 0.5x cell culture lysis reagent buffer (Promega, Madison, WI) for 30 min. To measure the luciferase content, 100 μL of 0.5 mM luciferin solution was automatically injected into each well of 20 μL of cell lysate and the luminescence was integrated over 10 s using GloMax 96 Microplate Luminometer (Promega). Total cellular protein in the cell lysate was determined by the bicinchoninic acid protein assay using calibration curve constructed with standard bovine serum albumin solutions (Pierce, Rockford, IL). Transfection activity was expressed as relative light units (RLU)/mg cellular protein ± SD (n=3).

3.17 Mobilization of peripheral blood leukocytes (PBL)

6 weeks old female BALB/c mice were purchased from Charles River Laboratories and housed under controlled temperature, humidity and lighting conditions in facilities accredited by the American Association for Accreditation of Laboratory Animal Care, operating in accordance with standards set by the Guide for the Care and Use of Laboratory Animals (The National Academies Press, 1996). All procedures were approved

by the University of Nebraska Medical Center Institutional Animal Care and Use Committee. For cell mobilization studies, mice were randomized into three groups (n=5). Mice in the experiment group were administered intravenously with PCX^{G2}-4 at 1.25 mg kg^{-1} in 100 µL PBS. Positive control group was administered subcutaneously with AMD3100 at the dose of 5 mg/kg in 100 µL PBS. Negative control mice received matched subcutaneous injection of 100 µL PBS. Whole blood samples were collected into heparinized tubes after 1 h of injection and PBL were counted with an automatic hematology analyzer HEMAVET 950FS (Drew Scientific Inc., Dallas, TX).

3.18 siRNA transfection of siPLK1 polyplexes

siRNA transfection efficiency of the polyplexes was evaluated in U2OS cells using human siPLK1 as a therapeutic siRNA. Cells were seeded at a density of 2,500 cells/well in 96-well plates 24 h prior to the experiment. On the next day, culture medium was carefully removed and replaced with 50 µL medium with or without 10% FBS and 12.5 µL polyplexes (siRNA dose: 5 pmol per well). After 4 h of incubation, polyplexes were removed and cells were maintained in 200 µL fresh culture medium for another 44 h. CellTiter-Blue Cell Viability Assay (Promega) was used to measure % cell viability. Activity was expressed as % cell death induced by PLK1 gene silencing compared with scrambled siRNA (n=3 or 4).

3.19 Cellular uptake and intracellular distribution of polyplexes by confocal microscropy

Chol-PCX^{G1} polymers were fluorescently labelled with AlexaFluor 647 following manufacturer's instructions and purified by dialysis against distilled water to remove unreacted dye. Fluorescently labelled siRNA (Block-iT™ Alexa Fluor® Red) was purchased from Invitrogen (Carlsbad, CA). 100,000 of U2OS cells were seeded in a 23 mm glass-bottom dish (Nioptechs Inc. Cat# 0420041500C) one day before the experiment.

Cells were then incubated with Chol-PCX^{G1}/siRNA polyplexes (containing 25 nM siRNA) for 1 h, washed twice with PBS, fixed with 4% paraformaldehyde, washed with PBS for additional 4 times and stained in 1 μM Hoechst 33258 solution. All the images were taken using Zeiss 710 confocal laser scanning microscope equipped with a 63x oil objective and 4 lasers (Blue Diode 405 nm, Argon 458/488/514 nm, DPSS 561 nm and He-Ne 633 nm).

3.20 DNA biodistribution in mice

6 weeks old female BALB/c mice were purchased from Charles River Laboratories and housed under controlled temperature, humidity and lighting conditions in facilities accredited by the American Association for Accreditation of Laboratory Animal Care, operating in accordance with standards set by the Guide for the Care and Use of Laboratory Animals (The National Academies Press, 1996). All procedures were approved by the University of Nebraska Medical Center Institutional Animal Care and Use Committee. The mice were inoculated with 5 ×10^5 4T1 cells in left hind flank zone. After two weeks, mice were sacrificed 1 h after tail-vein injection of polyplexes (15 μg DNA/mice, w/w 3 in 200 μL HEPES-buffered glucose (20 mM HEPES, 5% Glucose, pH 7.4; HBG)) and organs were harvested. The samples were suspended in PCR lysis buffer (0.5 mg/ml Proteinase K, 2 mg/ml poly-L-aspartic acid) at a concentration of 50 mg of tissue per milliliter and homogenized using TissueLyser II (Qiagen, Hilden, Germany). After homogenization, 2 μl of homogenized solution was mixed with 25 μl PCR lysis buffer and incubated in 37°C for 12 h. The luciferase DNA contents in different organs were analyzed by RT-PCR. The PCR cycle was 2 min at 50°C, 10 min at 95°C, 40 cycles for 15 s at 95°C, and 1 min at 60°C. A series of luciferase plasmid DNA dilution solutions (20 μg/ml, 2 μg/ml, 200 ng/ml, 20 ng/ml, 2 ng/ml, and 0.2 ng/ml) were used to construct the calibration curve.

3.21 NCOA3 knockdown

The efficiency of the PCX to deliver siNCOA3 and to downregulate NCOA3 gene was evaluated in CD18/HPAF.luc cells. Cells were seeded at a density of 100,000 cells/well in 12-well plates one day before experiment. On the next day, culture medium was carefully removed and replaced with 800 µL medium and 200 µL polyplexes. The PCX polyplexes were prepared at w/w ratio of 2 using either siNCOA3 or a negative control siRNA (siScr). PEI/siRNA polyplexes prepared at w/w of 1.5 were used as controls. After 4 h of incubation, polyplexes were removed and cells were maintained in 2 mL fresh culture medium for another 72 h. Cells were washed with PBS twice and prepared for western blot. NCOA3 silencing at protein level was compared with that of scrambled siRNA.

3.22 CXCR4 expression by flow cytometry

CD18/HPAF.luc cells were seeded in 6-well plates in DMEM with 10% FBS overnight. On the day of experiment, fresh DMEM with or without 10 µM gemcitabine was added. After 24 h of incubation, cells were washed with PBS twice, detached using enzyme-free PBS-based cell dissociation buffer (Gibco by Life Technologies, Grand Island, NY), and resuspended in PBS. After centrifugation at 800 rpm for 5 min, the supernatant was removed and the cells were resuspended in FACS buffer (1% BSA, 0.1% NaN_3 in PBS) to obtain final cell concentration of 5 x 10^6/mL. The cell suspension (100 µL) was mixed with 20 µL of APC mouse anti-human CXCR4 antibody or the corresponding isotype control. After incubation at room temperature for 30 min, the cells were washed three times with FACS buffer to remove free antibody and resuspended in 500 µL of FACS buffer for the measurement by flow cytometry. The data were processed and analyzed using FlowJo software (Tree Star Inc., Ashland, OR) and expressed as percentage of CXCR4-positive cells.

3.23 Western blotting

Whole-cell lysate was prepared in Pierce® RIPA lysis buffer (Thermo Scientific, Rockford, IL) supplemented with 1x protease and phosphatase inhibitor cocktail. Total protein content was quantified using BCA assay, and samples were normalized by dilution with RIPA buffer to obtain equal protein concentration. Equal volume of 2x Laemmli sample buffer (BIO-RAD, Hercules, CA) was added, followed by boiling in water for 5 min. Equal amounts of total protein (20-40 µg) were loaded to SDS-polyacrylamide electrophoresis gel, run first at 80 V for 30 min and then at 120 V for 2 h. The protein contents were transferred to polyvinylidene difluoride (PVDF) membrane, and the membrane was blocked with 5% skim milk at room temperature for 1 h, and incubated overnight with the primary antibodies at 4 °C. Next day, the blot was washed three times with TBST buffer (20 mM Tris, 500 mM NaCl, 0.1% Tween 20, pH 7.5) and incubated with horseradish peroxidase-conjugated secondary antibody for 1 h at room temperature. The protein signals were visualized by Pierce® ECL Western blotting substrate (Thermo Scientific, Rockford, IL). The band intensity was evaluated using ImageJ software.

3.24 RNA isolation and Real Time PCR analysis

The total RNA from the cells was isolated using TRIzol® reagent and the RNA from tissues was isolated using mirVana miRNA isolation kit according to the protocols from Life Technologies. Cells were washed with PBS and lysed in the TRIzol® Reagent. The homogenized samples were incubated at room temperature for 5 min to complete dissociation of the nucleoprotein complex. Chloroform was added and the samples were centrifuged. RNA was precipitated by addition of 0.5 mL of isopropanol to the aqueous phase. RNA pellet was resuspended in RNase-free water and stored at -80 °C. For isolation of RNA from tissues, tumor tissues were homogenized in liquid nitrogen and lysed in the lysis/binding buffer. miRNA Homogenate Additive was added to the tissue lysates and acid-phenol: chloroform was added and vortexed for 1 min. The aqueous

phase was collected, mixed with equal volume of ethanol, and the mixture was passed through a filter cartridge. The RNA isolated from cells and tissues was reverse-transcribed to cDNA using High-Capacity cDNA Reverse Transcription Kits (Applied Biosystems, Foster City, CA) using a thermal cycler in Rotor-Gene Q RT-PCR (Qiagen, Hilden, Germany). The thermal cycling conditions used were 25 °C for 10 min, 37 °C for 120 min, and 85 °C for 5 min. The expression pattern of the gene of interest was analyzed and the fold change in gene expression was calculated using the $2^{-\Delta\Delta CT}$ method. Results were expressed as mean expression compared with untreated cells ± SD (n=3)

3.25 Cell migration

CD18/HAPF.luc cells were pretreated with 10 μM gemcitabine for 24 h, trypsinized, and resuspended with 1 μg/mL PCX in serum-free medium for 15 min. The cell suspension with PCX was then added to transwell inserts at a final cell density of 200,000 cells in 300 μL medium per insert. DMEM with 10% of FBS was added as the chemoattractant in the companion plate. After 24 h, the non-invaded cells on the upper surface of the insert membrane were removed by cotton swabs. The invaded cells on the bottom surface were fixed in 100% methanol and stained with 0.2% Crystal Violet solution for 10 min at room temperature. The migrated cells were counted at 10× magnification. The results were expressed as percentage of migrated cells relative to untreated cells/imaging area ± SD (n = 4 random imaging areas of triplicate samples).

3.26 Orthotopic implantation of tumor cells and analysis of anticancer activity

Female athymic nude mice (6 weeks old) were purchased from Harlan Laboratories and housed under controlled humidity, temperature and lighting conditions in facilities accredited by the American Association for Accreditation of Laboratory Animal Care, operating in accordance with standards set by the Guide for the Care and Use of Laboratory Animals (The National Academies Press, 1996). All procedures were approved

by the University of Nebraska Medical Center Institutional Animal Care and Use Committee. Orthotopic implantation of pancreatic cancer cells was performed as described previously [182]. Briefly, CD18/HPAF.luc cells were trypsinized, washed and resuspended in sterile PBS. Prior to surgery, mice were anesthetized with 350 µL of intraperitoneal injection of a 4:1 mixture of ketamine (100 mg/mL) and xylazine (20 mg/mL) diluted 10 times in sterile water. The surgical site was sterilized with 70% ethanol wipe and a 1-cm incision was made in the peritoneum at the mid-abdomen region below the sternum by scissors. 2.5 x 10^5 of CD18/HPAF.luc cells were injected into the head of pancreas without causing injury and torsion. The abdomen was closed using a 2-layer suture with 5-0 chromic catgut and soft staple. The skin staples were removed 10 days after surgery. The animals inoculated with tumor cells were housed in the animal facilities. After 10 days of growth, the luciferase-expressing tumors were imaged by IVIS and the mice were randomly assigned into three groups: saline (n=7), negative siRNA control polyplexes (Chol17-PCX^{G1}/siScr, n=7) and combination polyplexes (Chol17-PCX ^{G1}/siNCOA3, n=6) group. The PCX/siRNA polyplexes were prepared at w/w 2 and administered three times per week through tail vein (40 µg siRNA/mouse). The mice were observed and weighed every other day. Tumor growth and total tumor burden were monitored by palpation and whole-body IVIS bioluminescence imaging. Magnetic resonance imaging (MRI), a non–invasive approach, was used to assess tumor perfusion in the above mouse model of PC before sacrifice. Mice were sacrificed after 39 days of tumor growth. Changes in tumor growth and sites of metastasis were evaluated in each experimental group. Pancreatic tumors from different experimental groups were collected for immunohistochemistry (IHC) analysis.

3.27 Immunohistochemistry analysis (IHC)

To analyze the histopathology, the tumor tissues were fixed in 10% formalin for 72 h and stored in 75% ethanol. The tissues were embedded in paraffin and 5 µm sections were cut and stained with haematoxylin & eosin (H&E) as well as requisite antibodies as described previously [85]. Typically, tissue slides were baked at 58 °C overnight. Next day, tissues were deparaffinized, hydrated and antigens were recovered by boiling in citrate buffer. Tissue sections were blocked with 2.5% horse serum and incubated with indicated primary antibody (8G7) overnight at 4 °C. Tissues were washed and incubated with HRP-conjugated secondary antibody. Subsequently, tissues slides were washed and developed using 3.3'-diaminobenzidine kit (Vector Laboratories, Burlingame, CA) for colorimetric detection and counterstained with hematoxylin. Tissues were dehydrated, dried and mounted with Permount and evaluated by a pathologist.

3.28 Tumor perfusion analysis

Mice were evaluated at the end of the treatment before euthanasia by magnetic resonance imaging (MRI) to assess tumor vascular function using perfusion imaging, after acquiring a reference T_2-weighted image set to visualize the tumor location. For these procedures, all equipment that direct contacted with animals were treated with disinfectant and animals were handled as described below. Mice were anesthetized by inhalation anesthesia (1.5% isoflurane). The anesthetized mice were positioned in a Plexiglas holder and placed in an RF coil for imaging. The anesthetized animal was secured in place to a support platform upon which the animal's body rested horizontally for MRI acquisition. The breathing rate and temperature of the anesthetized animals were monitored continuously with this holder design using an SA Instruments (Stony Brook, NY) model 1025 small animal monitoring and gating system. During image acquisition, animals were maintained on 0.5-1.5% isoflurane, in oxygen with an output of 1 L/min with gases continuously vacuumed from the opposite side of the chamber using the facility vacuum line regulated

at a flow rate of 1 L/min. Animals were monitored during the procedure and respiration rates were maintained at 40-60 bpm by adjusting isoflurane during examinations. The holder with the mouse was inserted into a birdcage quadrature transmit/receive coil and mounted at the magnet center. Studies began with a localizer to center the head in the magnet and coil. After localization and system shimming, T_2-weighted high-resolution anatomical image was obtained for each animal, followed by the acquisition of perfusion maps. Perfusion maps were acquired and analyzed using Flow Sensitive Alternating Inversion Recovery (FAIR) [183]. Perfusion maps were generated with a Rapid Acquisition with Relaxation Enhancement (RARE) readout. Images were acquired with a RARE factor of 16, 16 inversion recovery times ranging from 30-2300 ms, 1 mm slice thickness, selective inversion slab thickness of 4 mm, 30 mm x 30 mm field of view, 128 x 128 matrix. Total imaging time for MRI was 0.5-1 hour per animal.

3.29 Statistical analysis

Statistical analyses were performed using GraphPad InStat 3 software. Student's t-test was used to determine the statistical significance between groups and statistical differences among multiple groups were analyzed using non-parametric ANOVA with Tukey-Kramer multiple comparisons test. Fisher's exact test was used to compare the incidence of metastasis between groups. $P<0.05$ was considered as significant difference.

Chapter 4 - Results and Discussion

4.1 Development of Functional Poly(amido amine) CXCR4 Antagonists with Increased CXCR4 Inhibitory Activity to Deliver Therapeutic Nucleic Acids

Please note that the data of this part was from the paper published in the Advanced Healthcare Materials [153]. The authors include Dr. Stuart Hazeldine, Dr. Jing Li, Dr. David Oupický and me. Dr. Hazeldine proposed and developed synthetic strategy for the novel cyclam monomers and copolymers. As the first author, I performed all the other experiments to characterize the copolymers in vitro and in vivo. I collected all the data, participated in their analysis, and wrote early draft of the manuscript. Drs. Li and Oupický analyzed data, wrote the manuscript, and handled its submission and publication. All the authors agreed with including their work in this dissertation.

Scientists have undertaken extensive researches to control cancer over half a century. For early stage cancer patients, surgical intervention is a potential treatment. However, most of the cancer patients are diagnosed with advanced stage due to scarce symptoms until the disease has progressed and the treatment is limited to chemotherapy or radiation [184]. The vast amount of chemodrugs used in clinic are low molecular-weight compounds, which lack of selectivity and cause high toxicity *in vivo*. Small molecular-weight chemodrugs distribute fast and uniformly into healthy tissues, exhibit a short half-life and a rapid clearance in the systemic circulation. The frequent severe systemic side effects include neurotoxicity, cardiotoxicity, nephrotoxicity, bone marrow toxicity, mucositis and gastrointestinal toxicity [185].

Polymer therapeutics are becoming popular in recent years to treat cancer, which are a class of delivery systems, including polymeric drugs, polymer conjugates of proteins,

drugs and aptamers, block copolymers micelles, as well as multicomponent non-viral vectors with covalent linkages [186]. The pathophysiological properties of solid tumor have been utilized to design polymer therapeutics to improve the drug efficiency *in vivo*. Tumor tissues exhibited enhanced extravasation and retention of macromolecules from tumor blood vessels, which is not observed in normal vasculature and termed as “enhanced permeability and retention (EPR) effect” [187, 188]. Macromolecular drugs can more easily extravasate through the leaky tumor endothelium and get trapped in the poorly developed lymphatic system of the tumor, leading to prolonged circulation time. In comparison with conventional chemodrugs, polymer therapeutics enhance the selectivity of cancer targeting, improve the anti-cancer efficiency and diminish the side effects [189, 190].

In contrast to drug delivery systems containing non-covalently therapeutic agents, the complex and multicomponent constructs of polymer therapeutics work as actual drugs and macromolecular prodrugs. Polymeric drug Copaxone has been successfully developed as a treatment for multiple sclerosis and progressed to market, which is a random copolymer of three amino acids (Glu, Ala and Tyr) [191]. The Oral polymeric sequestrants Renagel binds phosphate and is used to treat chronic kidney disease [192]. SMANCS is a polymer-protein conjugate consisting of the anticancer protein neocarcinostatin and a synthetic copolymer of styrene and a maleic acid anhydride drug, which has been approved for the treatment of hepatocellular cancer in Japan [189].

In tumors, a complex network of chemokines and chemokine receptors controls cell trafficking into and out of the tumor microenvironment [193]. Cells from different cancer types have different expression profiles of chemokine receptors. However, CXCR4 is the most widely expressed chemokine receptor in human cancers, which makes it and its ligand SDF-1 the most-promising targets within the chemokine network. CXCR4/SDF-1 axis regulates survival, proliferation, migration and invasion of cancer cells by activating

various intracellular signaling transduction pathways that affect cell survival and migration. Those pathways include phosphatidylinositol-3-kinase (PI3K) and the mitogen-activated protein kinase pathways. CXCR4 also activates Erk1/2, which phosphorylates transcription factors including Elk-1 to promote cancer cell proliferation and survival [117]. CXCR4/SDF-1 is also involved in activating focal adhesion complexes and promoting adhesion through integrins. All this, combined with increasing secretion of matrix metalloproteinases that mediate degradation of extracellular matrix, contributes to invasion of cancer cells [118-120]. Clinical evidence shows that certain anticancer therapies increase CXCR4 expression and inadvertently enhance the metastatic potential of tumors [194]. Animal studies of several types of cancer show that CXCR4 antagonists inhibit macrophage infiltration, induce tumor growth arrest and apoptosis, and prevent metastatic spread.

Our lab has developed the first generation of polymeric antagonists of the CXCR4 chemokine receptor (PCX^{G1}) based on a commercial CXCR4 antagonist AMD3100 (Plerixafor) (**Figure 1a**), which was approved by FDA in 2008 for mobilization of hematopoietic stem cells in bone marrow transplantation procedures [195]. PCX^{G1} worked as a dual-function polymeric drug suitable for simultaneous delivery of nucleic acids and inhibition of cancer metastasis [149, 150, 196]. Based on the proof-of-principle studies, it is difficult to control the polymerization due to the presence of six reactive secondary amines in AMD3100, which contributed to the generation of poorly defined highly branched polymers. The highly branched PCX^{G1} also showed compromised the CXCR4 antagonistic activity when compared with the original AMD3100. Therefore, we designed the second generation of polymeric CXCR4 antagonists (PCX^{G2}) based on novel monocyclam monomers with improved presentation of CXCR4-binding moieties and

better-controlled polymerization (**Figure 1b**). The novel linear PCX^{G2} were able to function dually as gene delivery vectors and inhibitors of cancer cell invasion (**Figure 1c**).

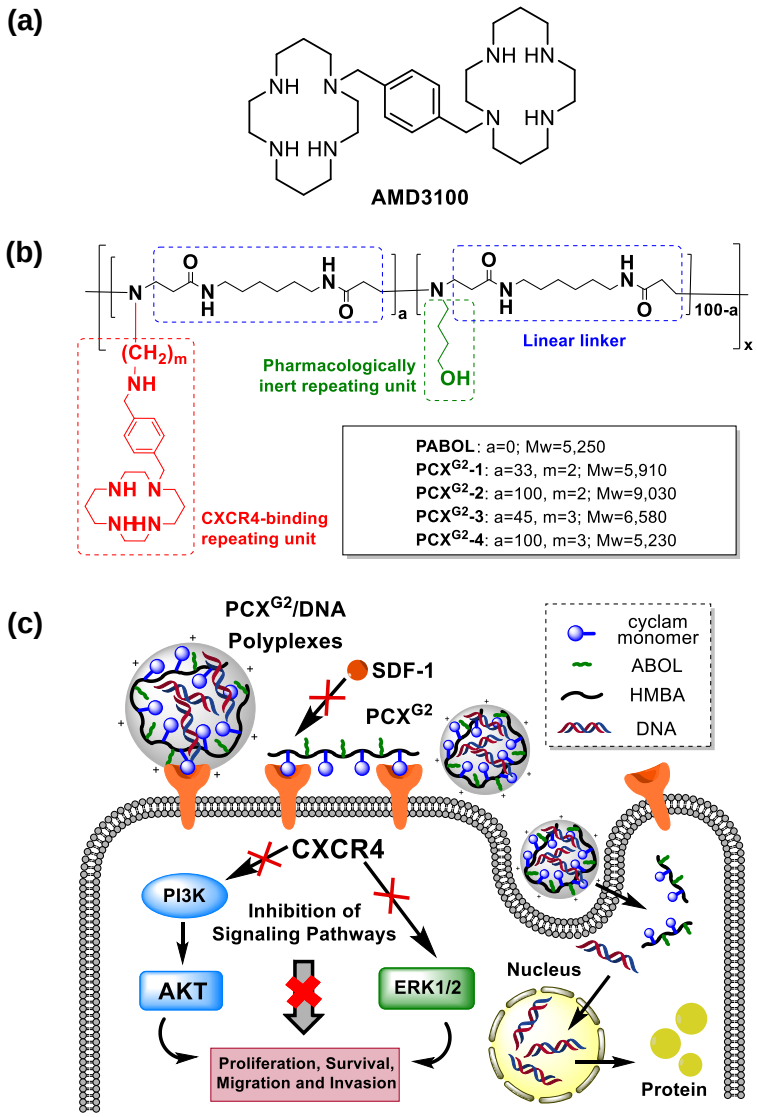

Figure 1. (a) Chemical structure of AMD3100 (Plerixafor). (b) Chemical structure of PCX^{G2}. (c) Mechanism of action of polymeric CXCR4 antagonists (PCX^{G2}) and PCX ^{G2} polyplexes.

4.1.1 Synthesis of monocyclam monomers

By sequential replacement or deletion of the amino groups within the azamacrocyclic ring systems of AMD3100, Bridger et al reported that all eight amino groups are not required for CXCR4 inhibition. This approach results in the design of several single ring azamacrocyclic analogues with high potency as AMD3100 [197]. Two novel monocyclam monomers were developed and synthesized according to the AMD3100 pharmacophore. The synthesis scheme was summarized in **Figure 2**. Three of the four secondary amines in cyclam (**1**) were protected by Boc to gain compound **2** with yield of 84%. Chloro-compund **3** was achieved by reaction of excess dichloroxylene or dibromoxylene with unprotected amine in compound **2**. Amino-alcohols were added to obtain compound **4** with secondary amine and terminal hydroxyl group. The secondary amine of **4** was also protected by Boc and the terminal hydroxyl was converted into primary amine by Mitsunobu reaction using phthalimide, triphenylphosphine (PPh_3) and diethylazodicarboxylate (DEAD) to obtain protected amine **6**. Hydrazine was added to get the final monocyclam monomers (**7a** and **7b**) with ethylene and propylene spacer respectively.

4.1.2 Synthesis and characterization of polymeric CXCR4 antagonists (PCX^{G2})

We hypothesized that when compared with PCX^{G1}, well-defined liner PCX^{G2} would improve the CXCR4 antagonism due to better presentation of CXCR4 binding moiety in the polymer side chain and easier accessibility to CXCR4 receptor. In order to conduct side-by-side comparison and study the influence of cyclam content and spacer length on the physicochemical characterizations and pharmacological activity of PCXG2, a series of PCX^{G2} were synthesized by Michael-type polyaddition (**Figure 1b**). The reaction of equimolar amount of HMBA and Boc-protected monomer **7a** or **7b** resulted in homopolymers PCX^{G2}-2 and PCX^{G2}-4. Copolymers PCX^{G2}-1 and PCX^{G2}-3 were obtained

by polymerization of equimolar amounts of HMBA with a mixture of 4-amino-1-butanol (ABOL) and **7a** or **7b**. Negative control polymer (PABOL) without CXCR4 antagonism was obtained by polymerization of HMBA and ABOL. To achieve desirable molecular weights, the polymerization conditions of PCX^{G2} were more rigorous than that of PCX^{G1}. The bulky Boc-protected monocyclam monomers were polymerized at enhanced temperature (50 °C) and extended reaction time (2 weeks) to get PCX^{G2}. Excess amount of cyclam was added and reacted for another two days to consume the unreacted acrylamide residues to terminate the polymerization. As show in **Figure 3**, the disappearance of HMBA acrylamide bonds (5.76 and 6.21 ppm) in ^{1}H-NMR confirmed the completion of the polymerization. Additional larger amount of cyclam was added to quench all acrylamide bond residues of PCX^{G2}-2. The content of monocyclam in the PCX^{G2}-1 and PCX^{G2}-3 was calculated from integral intensities of the phenylene protons (7.3-7.7 ppm) in **7a** and **7b** and of the methylene protons ($C\underline{H}_2CH_2OH$) in ABOL (3.65 ppm). Due to the steric hindrance of the bulky Boc-protected cyclam, the incorporation of the monocyclam monomers into the copolymers was lower than in feed ratio, suggesting weaker reactivity of the primary amines in **7a** and **7b** in comparison with the amine in ABOL. Based on the analysis of GPC in **Table 2**, the molecular weight of PCX^{G2} ranged from 5.2 to 9.0 kDa with low polydispersity, indicating the linear structure of the polymers.

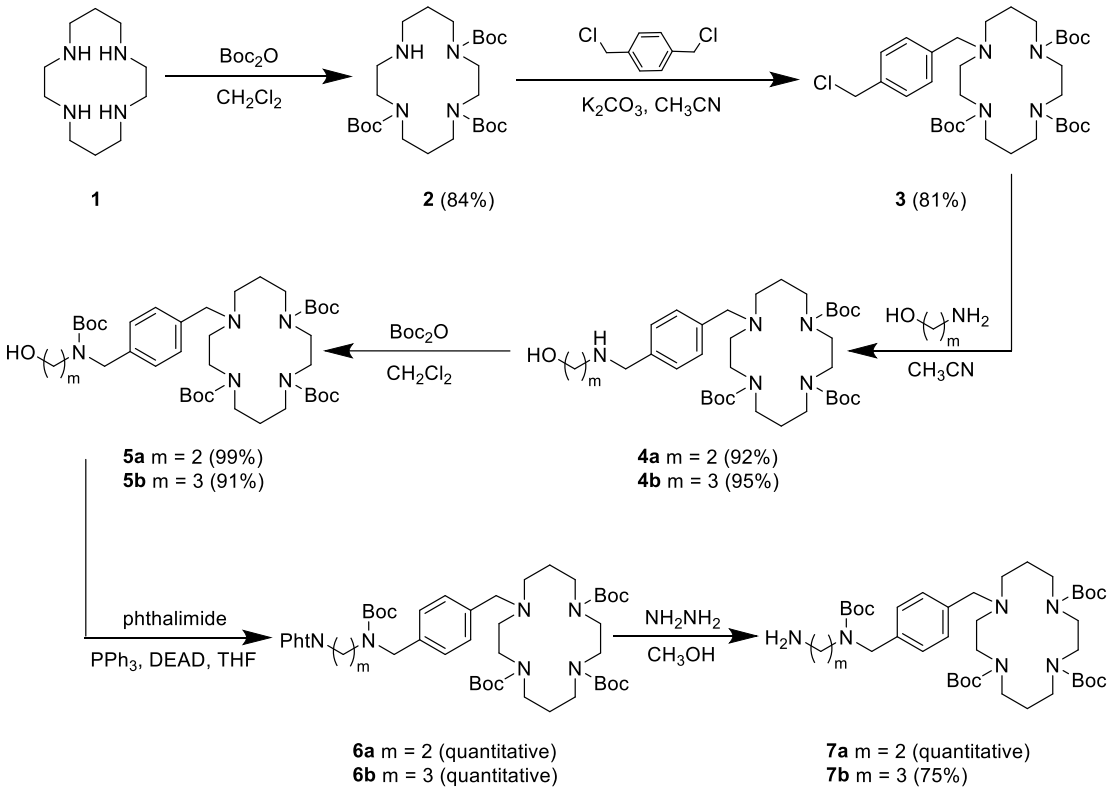

Figure 2. Synthesis of monocyclam monomers.

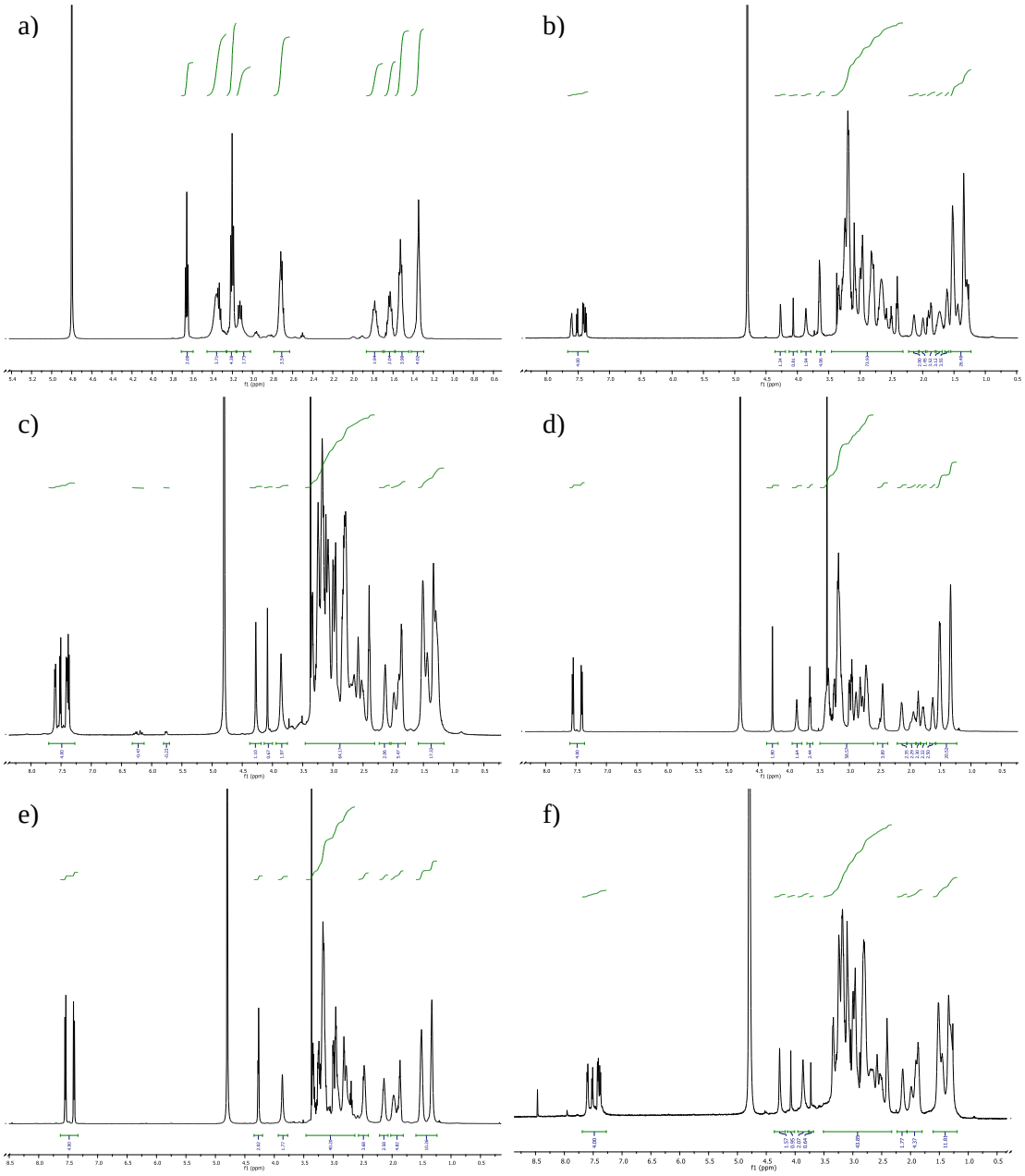

Figure 3. ^{1}H-NMR of PCX^{G2} in D2O (a. PABOL, b. PCX^{G2}-1, c. PCX^{G2}-2, d. PCX^{G2}-3, e. PCX^{G2}-4 and f. PCX^{G2}-2 after consuming all of the acrylamide bonds).

Table 2. Characterization of polymers

Polymer	Cyclam monomer	In feed (mol %)		In polymer (mol %)[a]	M_w	M_w/M_n
		ABOL	Cyclam monomer			
PABOL	--	100	0	0	5,250	1.26
PCX^{G2}-1	7a	50	50	33	5,910	1.11
PCX^{G2}-2	7a	0	100	100	9,030	1.11
PCX^{G2}-3	7b	50	50	45	6,580	1.29
PCX^{G2}-4	7b	0	100	100	5,230	1.27

[a] Content of the cyclam monomer units determined from ^{1}H-NMR.

4.1.3 Cytotoxicity of PCX^{G2}

Safety is the major challenge of synthetic polycations to apply nucleic acid therapeutics to patients. Cytotoxicity study will help with design and selection of safer polycationic vectors for clinical gene therapy [198]. Hepatocellular carcinoma HepG2 was widely used for prediction of the potential liver toxicity and human osteosarcoma U2OS cells was used to define the safe dosing window of PCX^{G2} for further studies about CXCR4 antagonism and gene transfection [199]. Typically high molecular weight and high charge density typically related with high cytotoxicity of polycations, which corresponds with the cytotoxicity result of PCX^{G2}-2 [198]. **Figure 4** showed that PCX^{G2}-2 with the highest molecular weight and highest charge density due to highest contant of cyclam exhibited the highest cytotoxicity among all PCX^{G2}. However, PCX^{G2}-1 with lowest cyclam content exhibited the lowest toxicity. Moreover, all of PCX^{G2} had dramatically less toxic than the commercial control PEI, indicating the potential usage of PCX^{G2} *in vivo*.

4.1.4 CXCR4 antagonism of PCX^{G2}

High content screening (HCS) analysis was used to study the CXCR4 antagonist activity of monocyclam monomers and PCX^{G2} polymers by monitoring the degree of inhibition of SDF-1 triggered internalization of membrane-localized EGFP-CXCR4 fusion protein to endosomes in human osteosarcoma cell line U2OS. HCS is a phenotypic assay that in this case uses automatic image analysis to quantify the extent of EGFP-CXCR4 internalization into the cells. As shown in **Figure 5a**, the untreated cells display punctate fluorescence documented by EGFP-CXCR4 internalization into endosomes. However, the control small-molecule CXCR4 antagonist AMD3100 inhibits EGFP-CXCR4 internalization, as indicated by the diffuse pattern of fluorescence. The usage of propylene linker in **7b** led to 2.6-fold higher activity than that of ethylene linker in **7a** (EC_{50} = 41.2 vs. 105.5 ng/mL ~ 69 vs. 180 nM). After removal of Boc-groups, the CXCR4 antagonism of

all PCX^{G2} was calculated and compared with the activity of corresponding monomers (**Figure 5b**). Control polymer PABOL exhibited no CXCR4 antagonism. Homopolymer PCX^{G2}-4 exhibited higher CXCR4 inhibitory activity than PCX^{G2}-2, which corresponded with less potent of **7a** than **7b** (EC_{50} = 21.4 vs. 28.2 ng/mL). Copolymers (PCX^{G2}-1 and PCX^{G2}-3) showed decreased CXCR4 potency due to less content of the CXCR4 binding moieties by incorporation of ABOL. Therefore, the polymerization of the monocyclam monomers improved the CXCR4 antagonism dramatically. To determine the influence of polymerization on CXCR4 antagonism of the repeating monocyclam unit, the potency was calculated based on the activity per cyclam in polymers. As shown in **Figure 5b**, polymerization increased activity of **7a** more than 5-fold and the activity of **7b** increased about 3-fold after incorporation into the polymer chain of PCX^{G2}. Moreover, decreasing the content of the monocyclam monomers in PCX^{G2} did not impact the activity of the repeating units. However, polymerization of AMD3100 caused a significantly decrease in CXCR4 inhibitory activity per repeating units in the first generation of PCX (PCX^{G1}) (2 vs. 139.1 ng/mL). The activity of PCX^{G2} was significantly higher than that of PCX^{G1}, indicating that better presentation of the CXCR4-binding moieties in polymeric CXCR4 antagonists is important for improving the CXCR4 potent activity. In order to investigate the duration of CXCR4 inhibition of PCX, U2OS cells were incubated with AMD3100 (0.15 μg/mL) or the most potent PCX^{G2} (PCX^{G2}-4, 1.5 μg/mL) respectively for 30 min and the extent of CXCR4 inhibition was quantified at different time points (**Figure 5c**). AMD3100 has a high affinity to CXCR4 receptors and results in long lasting inhibitory effect [200]. In comparison with AMD3100, there was no significant differences in the duration of CXCR4 inhibition between AMD3100 and PCX^{G2}-4. We noticed that both treatments maintained CXCR4 inhibition above 80% for at least 36 h and about 50% until 48 h, suggesting the long lasting antagonist effect and high affinity of PCX^{G2}.

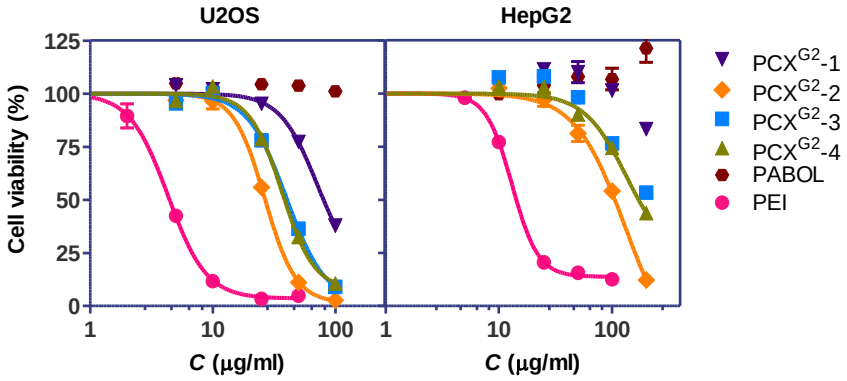

Polymer	IC_{50} [µg/mL]	
	U2OS	HepG2
PCX^{G2}-1	79.8±1.6[a),b)]	> 200[a),b)]
PCX^{G2}-2	26.7±0.4[a),d)]	105.7±1.9[a),d)]
PCX^{G2}-3	40.4±0.8[a),c)]	> 200[a)]
PCX^{G2}-4	38.5±0.1[a)]	171.4±1.3[a)]
PABOL	> 200[a)]	> 200[a)]
PEI	4.4±0.1	14.3±0.5

Figure 4. Cytotoxicity of PCX^{G2} in U2OS and HepG2 cells. The IC_{50} curves were constructed using mean cell viability ± SD (n=3). One-way ANOVA with Tukey-Kramer multiple comparisons test ([a)](P<0.001 vs. PEI); [b)](P<0.001 vs. PCX^{G2}-2); [c)](P>0.05 vs. PCX^{G2}-4); [d)] (P<0.001 vs. PCX^{G2}-4)).

(a)

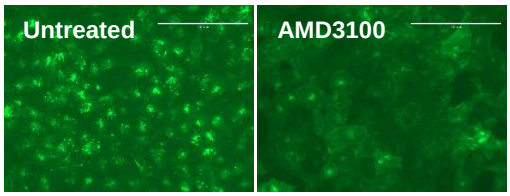

(b)

Sample	CXCR4 antagonism	
	EC_{50} [ng/mL]	EC_{50} per antagonist moiety [ng/mL]
PCX^{G2}-1	56.8	19.9
PCX^{G2}-2	28.2	19.5
PCX^{G2}-3	29.9	13.3
PCX^{G2}-4	21.3	14.9
7a	105.5	105.5
7b	41.2	41.2
PCX^{G1}	103.0	76.5
AMD3100	2.0	2.0

(c)

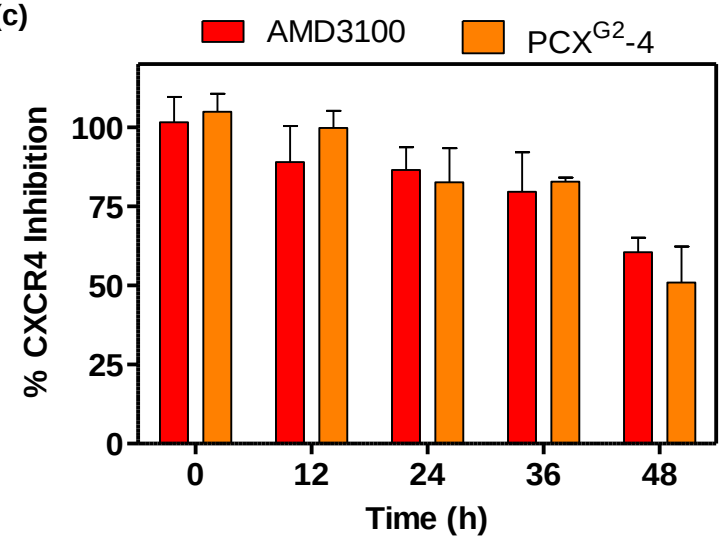

Figure 5. CXCR4 antagonism of PCX^{G2}. (a) Effect of AMD3100 on redistribution of EGFP-CXCR4 receptor in U2OS cells. (b) Effect of monomer type and content on CXCR4 antagonism. EC_{50} values determined from receptor redistribution assay in U2OS cells (n=3). (c) Duration of CXCR4 antagonism (n=3).

4.1.5 Inhibition of cancer cell invasion by PCX^{G2}

The activity of CXCR4 induced by SDF-1 contributes to migration and invasion of a series of cancers, which can be inhibited by CXCR4 antagonists like AMD3100. To investigate if the CXCR4 antagonism of the synthesized PCX^{G2} polymers was also manifested by inhibition of cancer cell invasion, a Boyden chamber method was used. Treatment of CXCR4+ U2OS cells with control AMD3100 resulted in maximum 83% of cancer cells from invading and migrating through the layer of Matrigel (**Figure 6**). All PCX^{G2} exhibited effective inhibition of invasion ranging from 62 to 82% at concentrations relevant for subsequent transfection experiments. And the ability of PCX^{G2} to prevent cancer cell invasion increased with the higher content of the incorporated monocyclam units. PCX^{G2}-4 was the most potent CXCR4 antagonist and showed the highest inhibition of cancer cell invasion (82%), which was fully comparable to AMD3100. However, the negative control PABOL was unable to inhibit cell invasion due to no CXCR4 potency.

4.1.6 Transient mobilization of peripheral blood leukocytes (PBLs)

CXCR4 contributes to tethering leukocytes and hematopoietic stem and progenitor cells to the bone marrow and the leukocytosis associated with CXCR4 inhibition has been used as an indicator of the mobilization of hematopoietic stem and progenitor cells. Small molecule CXCR4 antagonists such as AMD3100 induce a transient leukocytosis in humans, dogs, mice and rats. An increase in PBL is normally observed within 1 h after administration of AMD3100 both in humans and animals [201]. We evaluated if the CXCR4 antagonism of PCX^{G2} observed *in vitro* will be manifested also by leukocytosis and thus indirectly assessed the PCX^{G2} ability to mobilize hematopoietic stem and progenitor cells. We selected the best performing PCX^{G2}-4 with the highest CXCR4 antagonism *in vitro* and administered it intravenously to BALB/c mice.

Before we started the experiment, the maximum tolerated dose of PCX^{G2} was tested in Balb/c mice. PCX^{G2}-4 showed the lowest toxicity *in vivo* with MTD of 5 mg/Kg by i.v. injection (**Figure 7a**). We selected a relatively low dose of PCX^{G2}-4 (1.25 mg/kg) to avoid any possible side effect related to potential polycation toxicity. Positive control AMD3100 was given subcutaneously at 5 mg/kg according to a standard protocol. A widely used polycation PEI was also injected as a negative control, which was with no known CXCR4 activity. As shown in **Figure 7b**, the total number of PBL was compared after administration for 1 h. PCX^{G2}-4 induced 1.6-fold increase in the total number of PBL when compared with PBS-treated group, which was fully comparable with the effect of AMD3100 ($P>0.05$). Different populations of PBL were also analyzed to identify any possible differences among the tested samples. Administration of both PCX^{G2}-4 and AMD3100 resulted in a significant increase in the number of lymphocytes and monocytes, while no significant effect was observed for eosinophils, neutrophils and basophiles. No statistically significant differences were observed in the ability of PCX^{G2}-4 and AMD3100 to mobilize different PBL populations. We did not observe leukocytosis in the PEI control group, indicating that the increase in the number of PBL by administration of PCX^{G2}-4 was indeed due to the inhibition of CXCR4 and not related to any nonspecific polycation-related toxicity. It is our first time to show that the polymeric CXCR4 antagonists can rapidly and efficiently mobilize PBL and thus possibly have the potential to mobilize hematopoietic stem and progenitor cells as AMD3100 used in clinics.

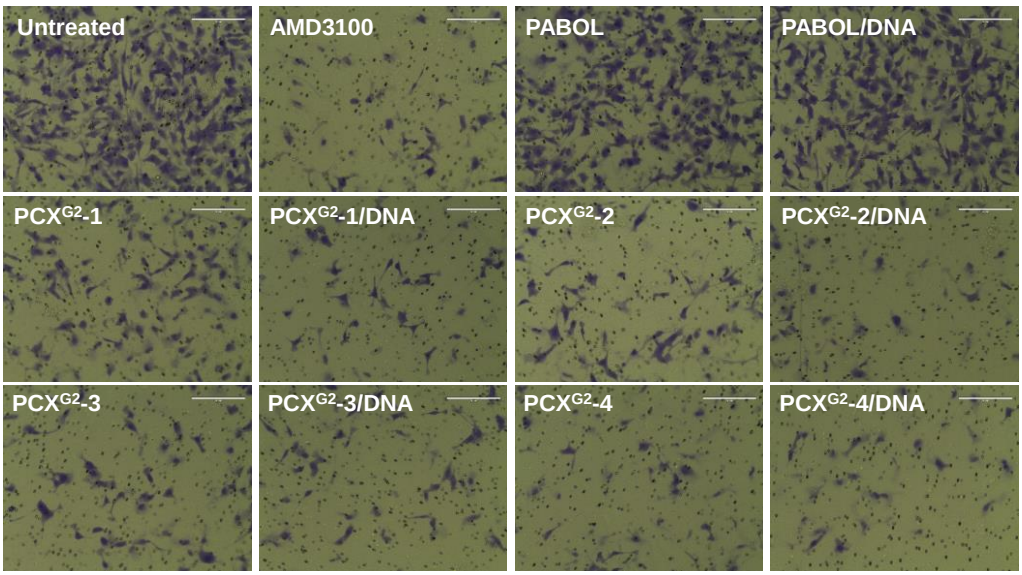

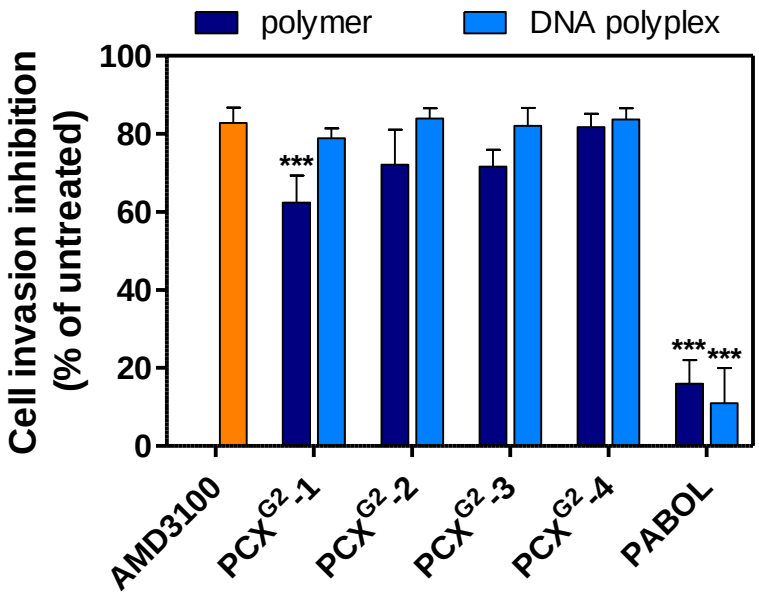

Figure 6. Inhibition of cancer cell invasion by PCX^{G2} (2 µg mL^{-1}) and polyplexes (w/w = 5, total polymer = 2.5 µg mL^{-1}). Statistical comparisons were done using the One-way ANOVA with Tukey-Kramer Multiple Comparisons Test (***P<0.001 compared with AMD3100 treated cells).

(a)

Polymer	MTD (mg/Kg) in Balb/c mice
PCX^{G2}-1	< 5
PCX^{G2}-2	< 5
PCX^{G2}-3	4
PCX^{G2}-4	5

(b)

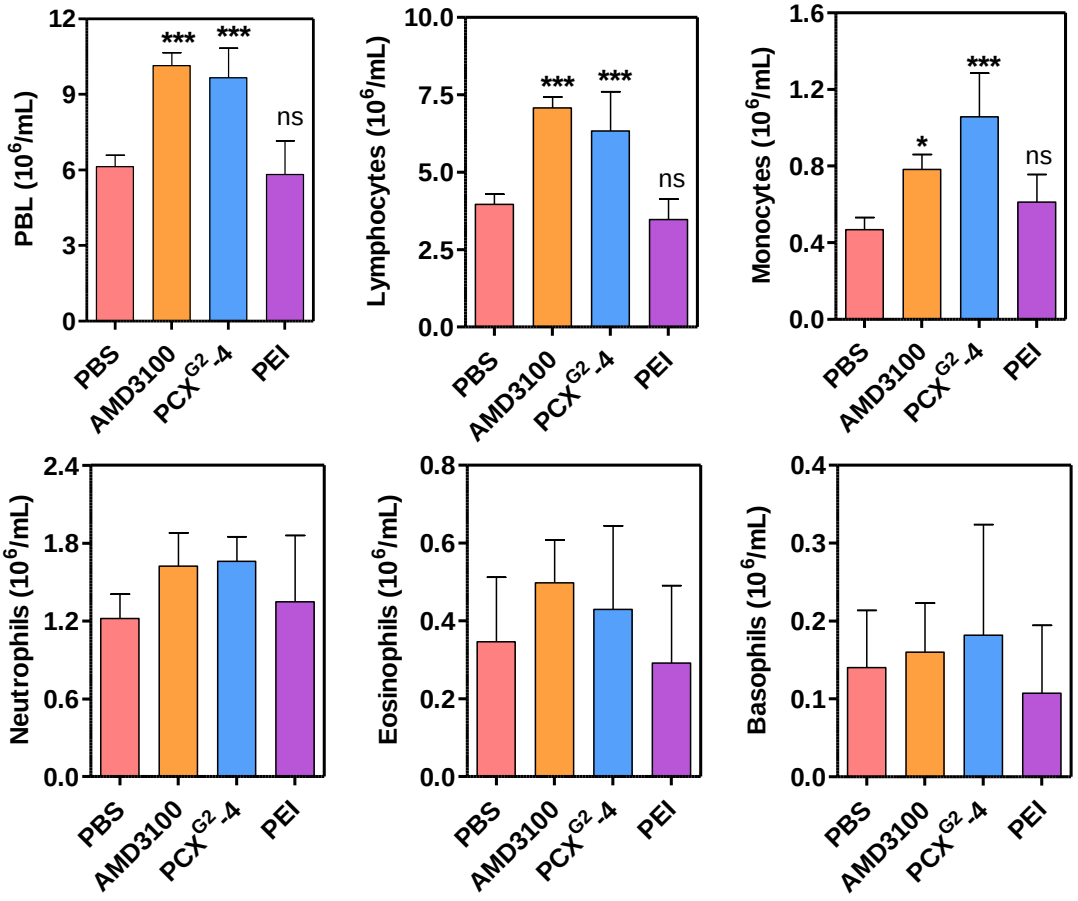

Figure 7. (a) MTD of PCX^{G2}-3 and -4 in Balb/c mice. (b) Mobilization ability of PCX^{G2}-4 polymer. Results are expressed as mean PBL numbers ± SD (n=5 mice per group). Statistical comparisons were done using the One-way ANOVA with Tukey-Kramer Multiple Comparisons Test ($^{*}P<0.05$, $^{**}P<0.01$, $^{***}P<0.001$ compared with PBS treated mice; AMD3100 vs. PCX^{G2}-4, ns, $P>0.05$).

4.1.7 DNA condensation and transfection activity by PCX^{G2}

After evaluation of PCX^{G2} CXCR4 antagonism and ability to inhibit cancer cell invasion, we have investigated the capability of PCX^{G2} to function as gene delivery vectors. First, the ability of all PCX^{G2} to condense DNA and form polyplexes was confirmed using ethidium bromide (EtBr) exclusion assay. **Figure 8** showed that the DNA condensation ability increased with increasing content of the cyclam monomers in PCX^{G2}. In agreement with previous reports [202, 203], the ability of PABOL to condense DNA was poor in the studied range of polymer/DNA w/w ratios. The length of spacer in the cyclam monomers had no discernible effect on DNA condensation ability. Hydrodynamic size and zeta potential of PCX/DNA polyplexes were determined by dynamic light scattering at polymer/DNA w/w ratio of 5, which corresponded to about 3-fold excess of PCX^{G2} relative to the minimum amount required to fully condense DNA. The sizes of PCX^{G2}/DNA polyplexes ranged from 56 to 122 nm and the polyplexes were all positively charged with zeta potential 17 to 31 mV (**Table 3**). Control PABOL cannot condense full condense DNA at w/w ratio of 5, which was reflected by a large hydrodynamic size and slightly negative zeta potential. Moreover, PCX^{G2}/DNA polyplexes prepared at w/w 5 were also evaluated for their ability to inhibit CXCR4-mediated cancer cell invasion. All the PCX^{G2} polyplexes (polymer concentration 2.5 μg/mL) showed effective inhibition of cancer cell invasion that was fully comparable to AMD3100 (**Figure 6**).

In vitro transfection activity of PCX^{G2}/DNA polyplexes at varying polycation/DNA (w/w) ratios was evaluated in U2OS and B16F10 cells both in the presence and absence of 10% FBS (**Figure 8**). PEI/DNA polyplexes at w/w ratio of 1.2 was used as a control. A single DNA dose of 2.35 μg/mL was used in all transfection experiments. The transfection activity of PCX/DNA polyplexes in U2OS was almost independent of the type and content of cyclam monomer at the lowest tested w/w ratio of 5. There was a marked decrease in

serum-free transfection with increased cyclam content at higher w/w ratios because of the polymer toxicity. In contrast, no such effect was observed in the presence of 10% serum as the transfection increased 7-fold when increasing the cyclam content (PCX^{G2}-2 vs. PCX^{G2}-1). Transfection in B16F10 was much less sensitive to PCX^{G2} toxicity and cyclam content, although weak tendency for transfection to increase with increasing cyclam content was observed. The type of cyclam monomer had no discernible effect on transfection. Overall, transfection of PCX^{G2} polyplexes was several orders of magnitude higher than transfection of PABOL polyplexes and comparable to transfection of PEI polyplexes. The low dependence of transfection on cyclam content suggests that using PCX^{G2} with lower cyclam content could be beneficial because of the lower toxicity.

4.1.8 Cell uptake of PCX^{G2}/DNA polyplexes

We developed PCX^{G2} with the goal of combining CXCR4 antagonism with the ability to deliver therapeutic nucleic acids. Successful nucleic acid therapies require efficient internalization into cells and delivery to the appropriate intracellular organelles. Since PCX^{G2} inhibit internalization of CXCR4 receptor, it was important to determine if the PCX^{G2} antagonism negatively impacts the intracellular uptake of DNA polyplexes, which could compromise transfection activity. DNA was labeled with CX-Rhodamine and used to prepare PCX/DNA polyplexes. We first measured cell uptake of the fluorescently labeled PCX^{G2}/DNA polyplexes in two cancer cell lines (U2OS and B16F10) by using flow cytometry (**Figure 10**). Based on the results, the cell uptake properties of PCX^{G2}/DNA polyplexes were highly cell line dependent. In U2OS cells, higher cyclam led to lower uptake. The cellular uptake of PCX^{G2}/DNA polyplexes in U2OS cells was much higher than PEI control. PCX^{G2}-1 complex with lower content of cyclam monomer had higher fluorescence than PCX^{G2}-2, and PCX^{G2}-3 complex showed a little higher cellular uptake than PCX^{G2}-4. However, the opposite behavior was observed in B16F10 cells with lower

CXCR4 levels, there was no so much difference between PCX^{G2} and control PEI. Moreover, PCX^{G2}-3 and PCX^{G2}-4 showed a little better cellular uptake than PCX-1 and PCX-2 in serum free conditions. The overall cellular uptake of PCX^{G2} polyplexes was several folds higher than that of PABOL polyplexes. Under the consideration that higher CXCR4 expression in U2OS cells compared with B16F10 cells, we investigated whether CXCR4 receptors was involved in the process of cellular uptake of PCX polyplexes. U2OS cells were pretreated with CXCR4 antagonism AMD3100 for 1 h before adding PCX^{G2} polyplex (**Figure 10c**). The relative fluorescence intensity of PCX^{G2} polyplexes did not show decrease in U2OS cells pretreated with AMD3100 in comparison with untreated one, suggesting that CXCR4 receptor did not affect the cellular uptake of the CXCR4-inhibiting polyplexes.

4.1.9 Summary

The above studies described the successful design and development of polymeric drugs PCX^{G2} with a dual function to simultaneously inhibit CXCR4 chemokine receptor and deliver genes. Polymerization improved the CXCR4 inhibitory activity of the synthesized monocyclam monomers significantly after incorporation into the polymer chains. And CXCR4 antagonism of the second generation of PCX was much higher when compared with the first generation, confirming the importance of a proper presentation of the ligands within synthetic polymers. We first reported that intravenous administration of PCX^{G2} resulted in mobilization of leukocytes from bone marrow into peripheral blood, which might work as synthetic polymeric mobilizers for blood stem cells or progenitor cells. Furthermore, PCX^{G2} inhibited cancer cell invasion in either formation of free polymers or polyplexes to a level fully comparable with AMD3100. And the gene transfection results indicated the ability of PCX^{G2} to efficiently deliver genes to cancer cells. Therefore, PCX^{G2} have the potential to become a new class of polymeric drugs for cancer treatment with a

promising dual functionality that synergistically combine CXCR4 antagonism to inhibit cancer metastasis with anti-cancer therapeutic effect of the delivered nucleic acids [204].

Polypelxes have received significant attention as promising gene delivery vectors due to multiple potential advantages when compared with viral vectors, including minimal immunogenicity, lower toxicity, and easier manufacturing and functional modifications [205, 206]. Safety and stability are still the major concerns to apply dual-functional polycationic nanoparticles *in vivo*. Positively charged polyplexes attached to negatively charged heparan sulfate proteoglycans on the cell surface to facilitate uptake into cells via adsorptive endocytosis [207]. During endocytosis, the decreasing pH confers "proton sponge effect", which causes enhanced protonation of polycations, influx of anions and high internal osmotic pressure, leading to burst of endosome membrane, escape of complexes from endosomes and high transfection efficiency *in vitro* [208]. However, high density of positive charges damages negatively charged cell membranes and contributes to cytotoxicity of polyplexes [209]. Positively charged polyplexes are colloidally stabilized by electrostatic repulsion and frequently aggregate under physiological salt conditions. The positive aggregation was rapidly eliminated from circulation by reticulo-endothelial systems (RES) [210-212].

In the next part of **4.2**, the goal is to improve the *in vivo* applicability of PCX polyplexes by chemical modification. PCX^{G1} was used as the model cationic polymer. Nonionic polymer poly(ethylene glycol) (PEG) was applied to modify PCX^{G1} to shield the surface charges and improve colloidal stability by steric stabilization [213-216]. PEGylation typically prolongs circulation by increasing stability of polyplexes in physiological fluid and reduces the interaction of polyplexes with extracellular membrane surface to decrease *iv vivo* toxicity [217, 218].

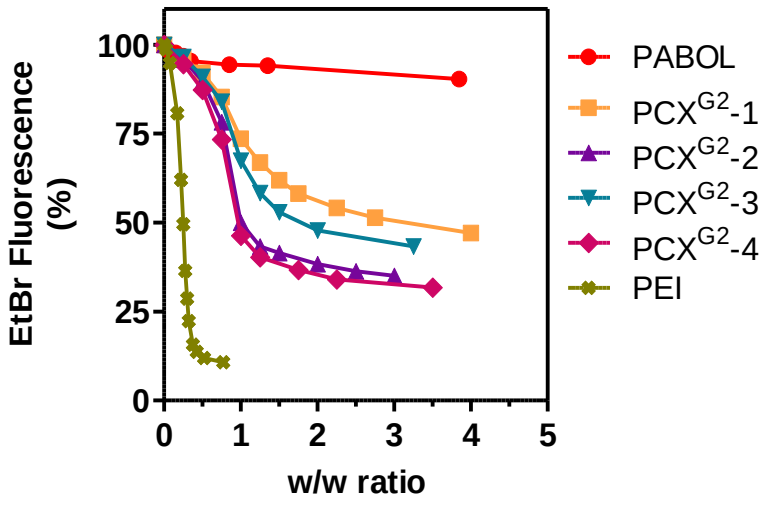

Figure 8. DNA condensation ability of PCX^{G2}.

Table 3. Hydrodynamic size and zeta potential of DNA polyplexes

	w/w 5		w/w 10		w/w 15	
Polyplex	Size (nm)	δ potential (mV)	Size (nm)	δ potential (mV)	Size (nm)	δ potential (mV)
PABOL	870.9 ± 7.5	-2.3 ± 0.9	796.9 ± 5.9	4.0 ± 0.2	650.1 ± 8.6	6.7 ± 0.1
PCX^{G2}-1	121.7 ± 2.5	24.4 ± 0.5	90.4 ± 2.0	29.6 ± 0.4	87.1 ± 2.1	30.5 ± 0.7
PCX^{G2}-2	59.9 ± 1.1	22.0 ± 0.9	56.3 ± 2.6	17.3 ± 0.5	64.9 ± 0.9	20.6 ± 1.0
PCX^{G2}-3	84.6 ± 2.5	29.9 ± 0.9	70.3 ± 0.1	29.1 ± 0.8	65.1 ± 0.3	27.8 ± 1.5
PCX^{G2}-4	75.0 ± 0.8	30.5 ± 0.5	65.1 ± 0.4	28.6 ± 1.0	64.0 ± 1.6	25.6 ± 0.3
PEI (N/P 10)	52.4 ± 5.5	20.8 ± 1.2				

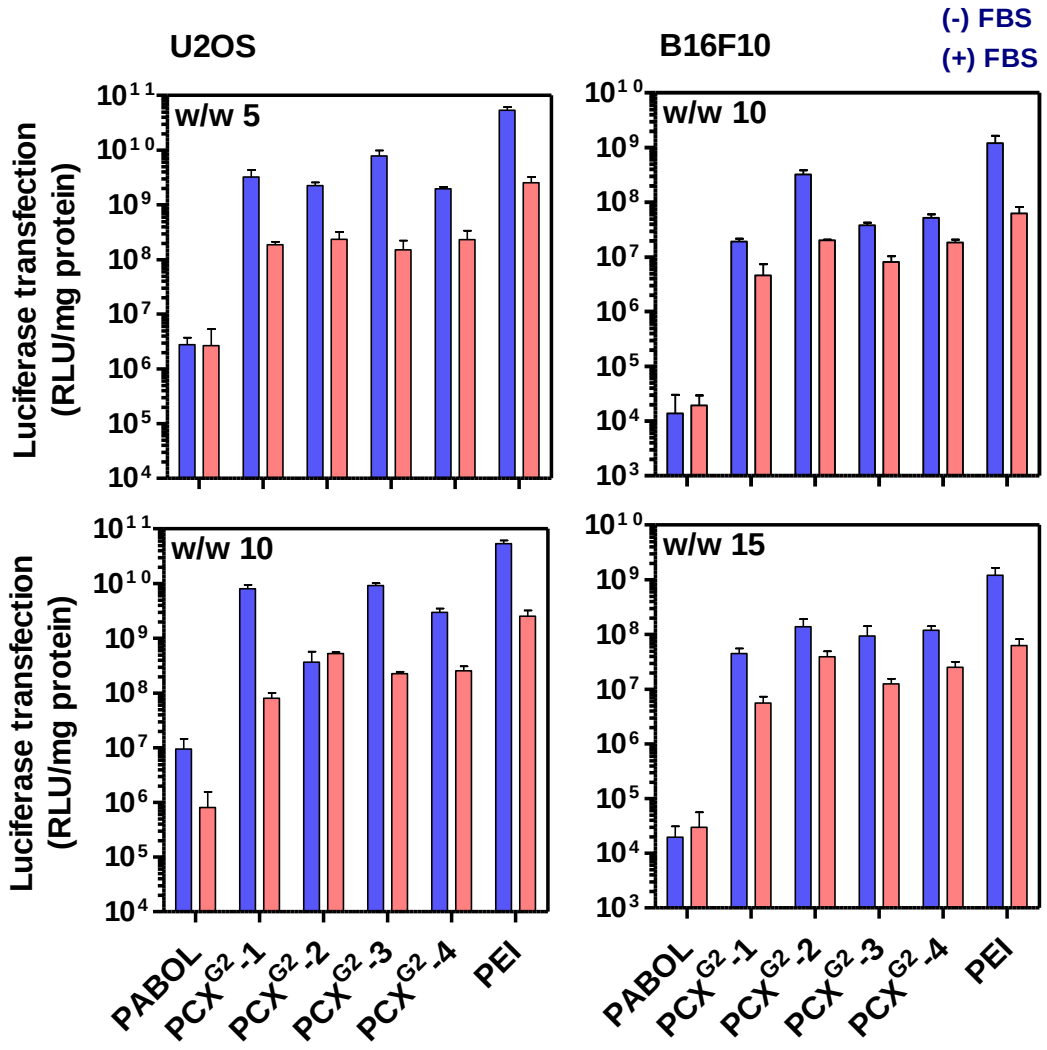

Figure 9. Transfection activity of PCX^{G2}/DNA polyplexes in U2OS and B16F10 cells. The transfections were conducted in the absence and presence of 10% FBS and the results are expressed as luciferase expression in RLU/mg protein ± SD (n=3).

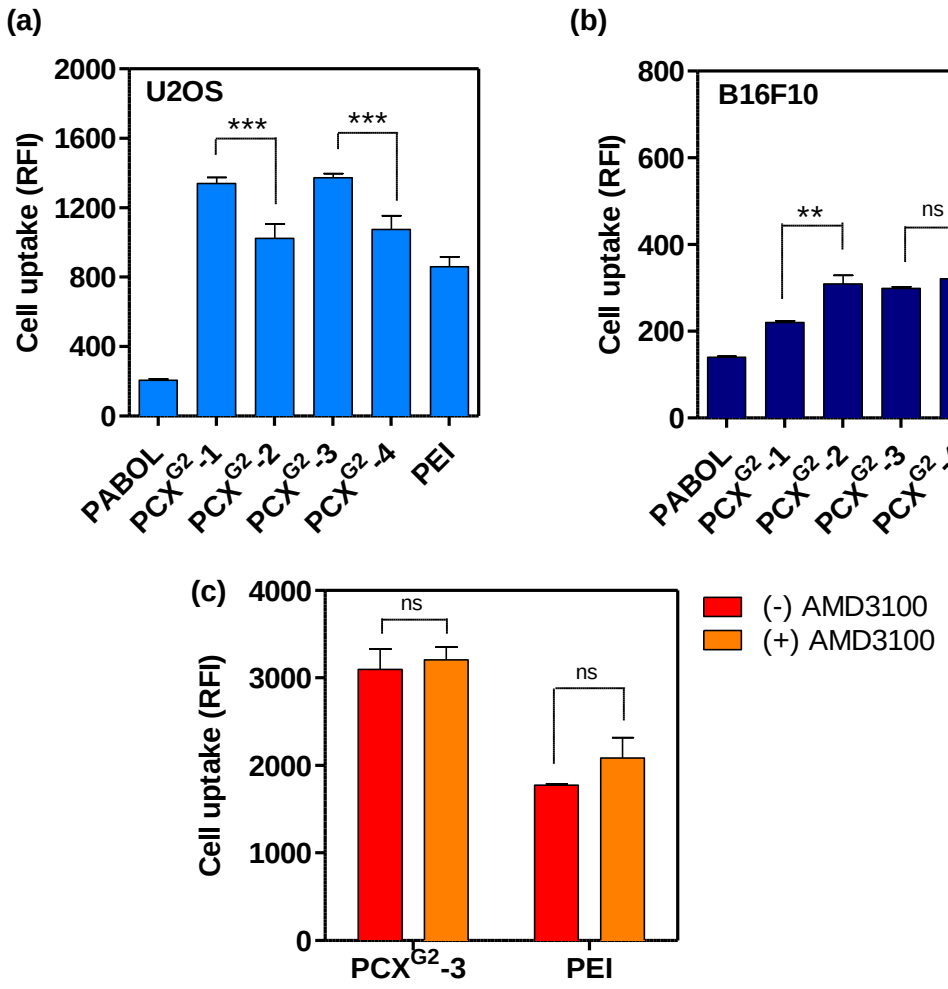

Figure 10. Cell uptake of PCX^{G2}/DNA polyplexes in (a) U2OS and (b) B16F10 cells. Polyplexes were prepared with fluorescently labeled DNA at w/w ratio of 5 and incubated with cells in the presence of 10% FBS. Results were shown as mean fluorescence intensity (RFI) ± SD (n=3). (c) Effect of AMD3100 on cell uptake of PCX^{G2}-3/DNA polyplexes in U2OS cells (n=2). ($^{*}P<0.05$, $^{**}P<0.01$, $^{***}P<0.001$ and "ns" for $P>0.05$).

4.2 PEGylation of Poly(amido amine) CXCR4 Antagonists to Enhance Safety and Colloidal Stability for Gene Therapy in Cancer

Please note that the data of this part was from the paper published in the Pharmaceutical Research [151]. The authors include Dr. Jing Li, Dr. David Oupický and me. As the first author, I performed all the experiments, analyzed data and wrote the draft of manuscript. Dr. Jing Li and Dr. Oupický helped to revise it and made it publishable. All the authors agreed with including their work in this dissertation.

The goal of PEGylation was to improve physical properties and safety of polycationic PCX^{G1}. However, it would decrease the transfection activity due to minimizing cellular association, cell uptake, endosomal escape, and gene release [219, 220]. To optimize the physicochemical characteristics and biological activities, proper PEG content should be carefully balanced. In the following studies, how the presence of PEG affects colloidal stability, safety, CXCR4 antagonism, inhibition of cancer cell invasion, and transfection activity of the polymers and their polyplexes would be evaluated. We would develop proper polyplex formulations that retain CXCR4 antagonism of PCX^{G1}, while exhibiting enhanced colloidal stability, decreased cytotoxicity, but improved transfection activity under physiologic conditions (**Scheme 4**).

4.2.1 Synthesis and characterization of PEG-PCX^{G1}

PCX^{G1} was synthesized in the form of a poly(amido amine) by Michael polyadditon of secondary amines present in AMD3100 with bisacrylamide monomer HMBA (**Figure 11**). Plerixafor functions as a hexafunctional monomer in the Michael polyaddition and leads to insoluble crosslinked PCX^{G1} at high temperature and high monomer concentrations [221, 222]. A more gentle condition resulted in a soluble PCX^{G1} with

weight-average molecular weight (Mw) of 10.6 kDa and unimodal distribution of molecular weights (**Figure 12**). Owing to excess and high reactive secondary amines in the AMD3100 structure, PEG chain could be introduced into the polymer by the reaction of mPEG-acrylamide with the secondary amines of PCX^{G1} (**Figure 11**). In contrast to common amide coupling, using Michael addition for the PEGylation allowed us to conserve the overall number of protonizable amines in PCX^{G1}. Three copolymers with increasing content of PEG were synthesized and named according to their PEG content as described in **Table 4**. The copolymers were isolated by precipitation in diethyl ether and collected as hydrochloride salts after extensive dialysis. The content of PEG in the copolymers was calculated from ^{1}H-NMR integral intensity of the PEG methylene protons at 3.7 ppm and aromatic protons of AMD3100 at 7.4-7.8 ppm (**Figure 13**). As shown in **Table 4**, a slight higher content of PEG was gained in comparison with original feed composition, which could be explained by the preferential removal of lower molecular weight polymer fraction by precipitation process in organic solvent and removal of the low molecular weight polymer fractions rich in PCX^{G1} during dialysis. The successful synthesis of PEGylated polymer and absence of unreacted mPEG-acrylamide can also reflect from GPC trace (**Figure 13**) of starting material PEG-acrylamide and those polymers. The PEGylated polymers with higher PEG composition showed earlier elution time, suggesting higher molecular weight. The polydispersity index (PDI) of the polymers ranged from 1.1 to 1.4, suggesting a good control of the polymerization. Therefore, the direct PEG modification of PCX^{G1} with a range of conformed substitution was developed, and the effects of PEGylation on PCX^{G1} in respect to DNA condensation, polyplexes stability, toxicity, transfection as well as CXCR4 antagonism would be studied comprehensively.

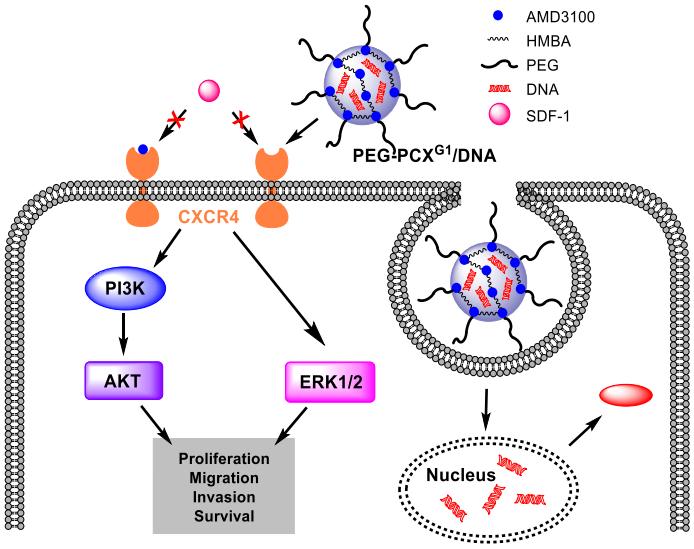

Scheme 4. Mechanism of dual-function PEG-PCX^{G1} as gene delivery vector and CXCR4 antagonist inhibiting cancer cell invasion.

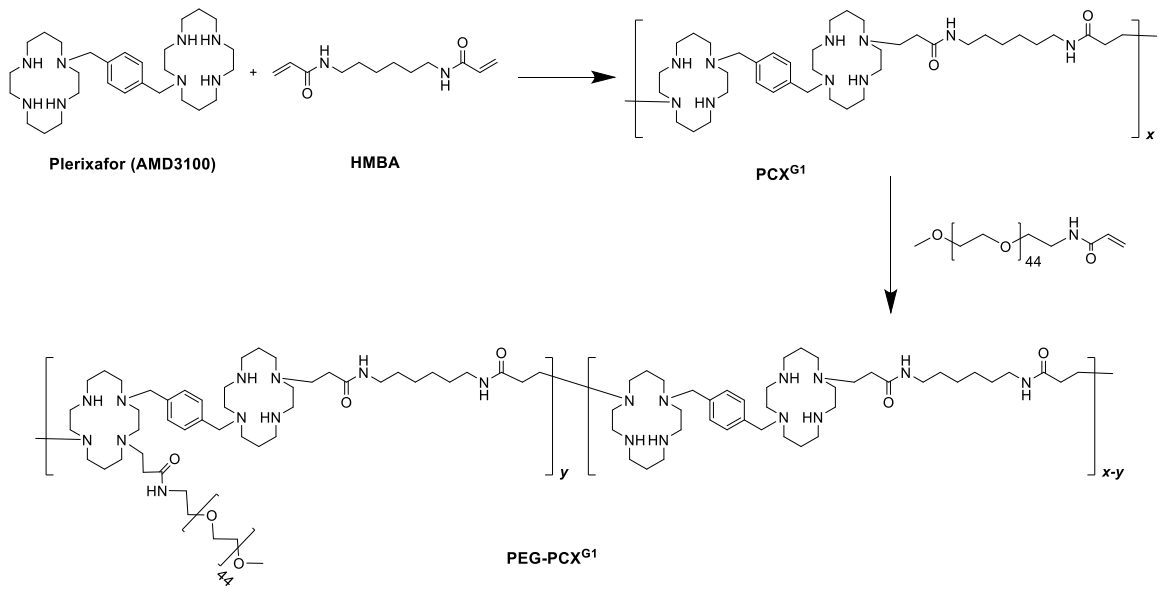

Figure 11. Synthesis of PCX^{G1} and PEG-PCX^{G1}.

Table 4. PEG content in PEG-PCX^{G1} determined by ^{1}H-NMR.

Polymer	PEG content (wt %)	
	in feed	in copolymer
PCX^{G1}	0	0
PEG12-PCX^{G1}	10	12
PEG41-PCX^{G1}	35	41
PEG52-PCX^{G1}	50	52

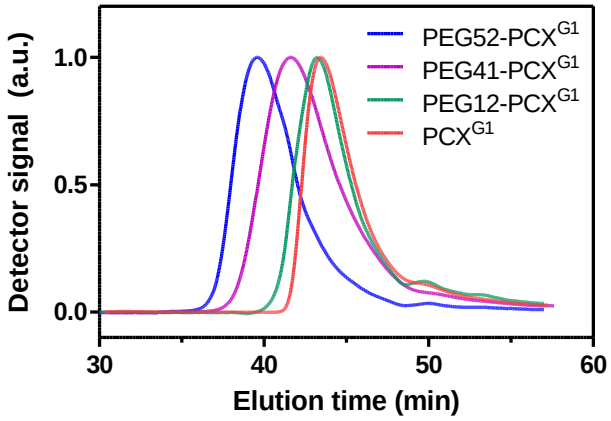

Figure 12. Gel permeation chromatograms of PCX^{G1} and $PEG\text{-}PCX^{G1}$.

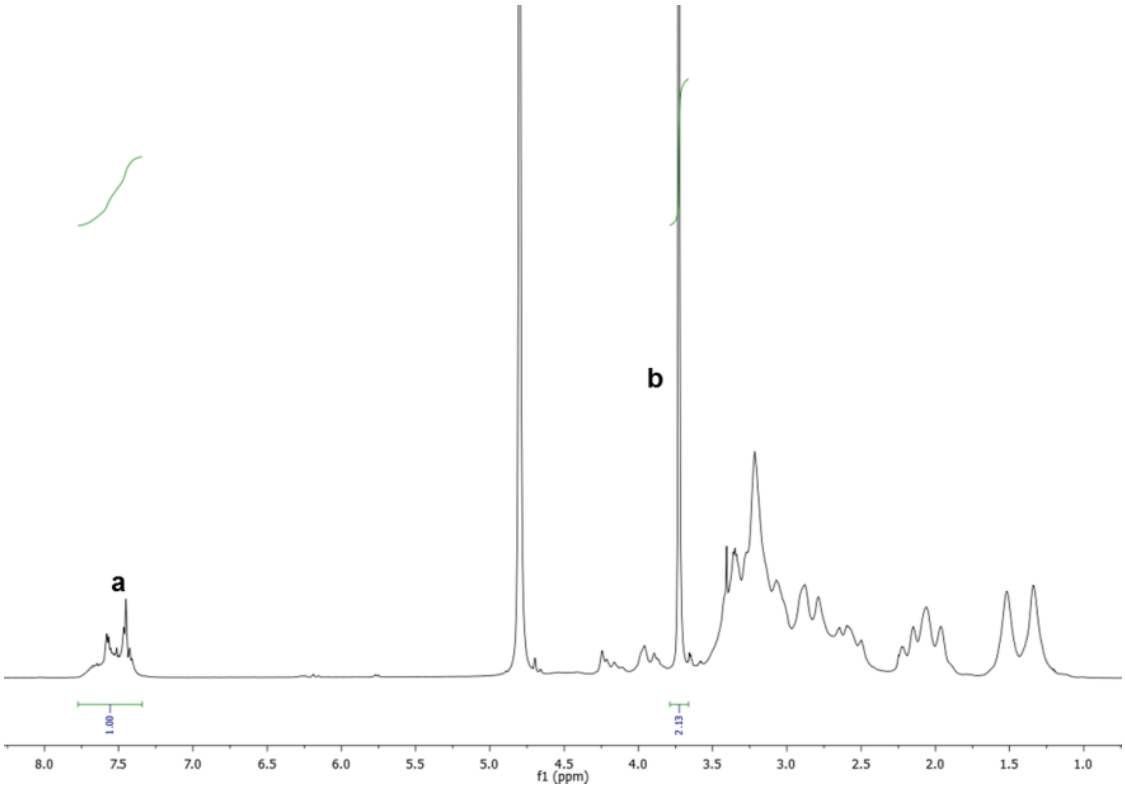

Figure 13. Typical ^{1}H-NMR spectrum of PEG-PCX^{G1} (PEG12-PCX^{G1} in D_2O) used in the determination of the PEG content (**a** – aromatic phenylene protons of AMD3100, **b** – methylene protons of PEG).

4.2.2 Preparation and characterization of PEG- PCX^{G1} polyplexes

The effect of PEGylation on DNA condensation ability of PCX^{G1} was investigated by EtBr exclusion assay as shown in **Figure 14.** All the PEG-PCX^{G1} exhibited similar condensation curves with a typical sigmoidal shape and were able to condense plasmid DNA to the same extent as PCX^{G1} as indicated by the same residual fluorescence at the highest polymer/DNA ratios. With increasing PEG content**,** the DNA condensation curves shifted to higher w/w ratios. However, if we only considered the polycation part and transformed PEG-PCX^{G1} into equivalent content of PCX^{G1}, the DNA condensation curves almost overlaid, suggesting that DNA binding properties of PCX^{G1} part in the copolymer are not affected by the presence of PEG chain. A similar finding was recently reported by Fitzsimmons and Uludağ [223].

One of the key motivations for PEGylation is to shield the positive surface charge of polyplexes by neutral PEG chains. The influence of PEGylation on polyplex surface charge was investigated. Our results confirmed that the use of PEG-PCX^{G1} significantly decreases surface charge of the polyplexes as documented by the decrease in the measured zeta potential (**Figure 15**). The PEGylated polyplexes showed almost neutral surface charge (3.3-5 mV) in 10 mM HEPES buffer, pH 7.4. However, unPEGylated PCX^{G1}/DNA showed zeta potential of + 20 mV. PEGylation significantly reduced polyplex surface charge, which is consistent with other researches on influence of PEGylated polyplexes [224-226].

The positive surface charge provides electrostatic stabilization to the polyplex nanoparticles at low concentration buffers. However, physiological ionic conditions would cause aggregation and destabilization of polyplexes by non-specific interactions [227, 228]. Steric stabilization by PEG can typically overcome the problem of low colloidal stability of polyplexes [229]. We have prepared PEG-PCX^{G1} and PCX^{G1} polyplexes in 10

mM HEPES buffer (pH 7.4) at polymer/DNA (w/w) ratio of 5 and measured their hydrodynamic diameter. Then polyplexes were incubated in phosphate-buffered saline (PBS) (pH 7.4) to mimic the physiologic ionic conditions and observed changes in polyplex size during the following period of 12 h were monitored by DLS (**Figure 16**). The results showed that PCX^{G1} polyplexes displayed an immediate aggregation after PBS addition as documented by the increase of their size from ~60 nm to ~430 nm in the span of only 15 min. The size of PCX^{G1} polyplexes increased to nearly 1 µm within 1 h of PBS addition. In contrast, polyplexes prepared with PEG-PCX^{G1} exhibited markedly improved colloidal stability. Polyplex containing 12% PEG showed an improved stability up to 1 h in PBS, but it was ineffective in long-term evaluation as documented by the increase in size from 58 nm to 690 nm within 12 h of PBS addition. In contrast, polyplexes containing 41% and 52% PEG totally prevented aggregation up to 12 h with stable size lower than 200 nm. Modification with PEG chain is an efficient method to stabilize particles against physiological salts. PEG chains formed a hydrophilic corona surrounding the particle core and protected them from aggregation through electrostatic interaction between polyplexes and physiological ionic components [225, 230].

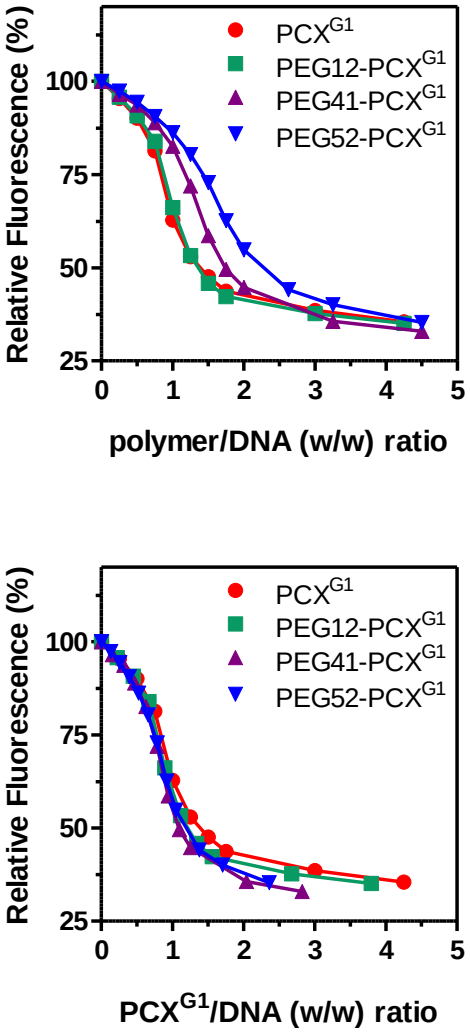

Figure 14. DNA condensation ability of PCX^{G1} and PEG-PCX^{G1} determined by ethidium bromide exclusion assay.

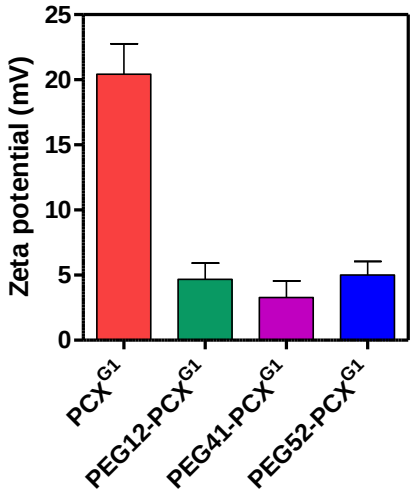

Figure 15. Zeta potential of DNA polyplexes prepared at polymer/DNA (w/w) ratio of 5 and measured in 10 mM HEPES (pH 7.4) (mean ± SD, n = 3).

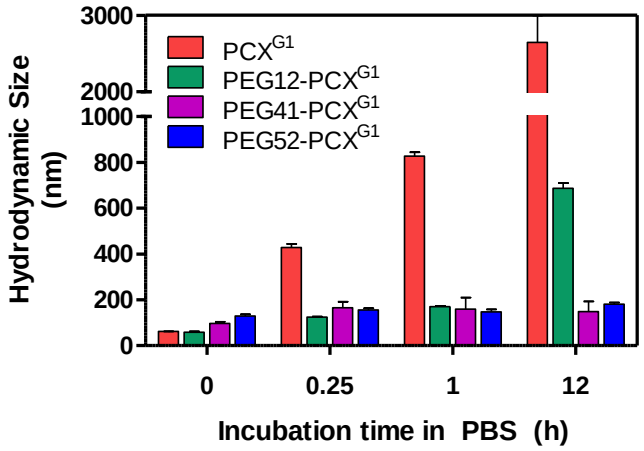

Figure 16. Effect of PEG on colloidal stability of PCX^{G1} polyplexes (w/w 5) in phosphate-buffered saline (PBS). Results are shown as mean ± SD (n=3).

4.2.3 Cytotoxicity of PEG-PCX^{G1}

Usually, cationic polymers display cytotoxicity by disturbing cell membrane such as high density of positive charge mediated membrane damage and phospholipids reshuffling [209]. PEGylation could produce a hydrophilic shell on the particle surface to efficiently decrease the charge density and block intermolecular interaction, avoiding extracellular mechanism of cytotoxicity. Cytotoxicity of PEGylated polymers and control PEI was evaluated by MTS assay in HepG2 and U2OS cells (**Figure 17**). HepG cells are widely used for prediction of liver toxicity [199]. The PEGylated polymers showed lower toxicity than the unPEGylated polymer as expected [219, 231, 232]. Importantly, similar trend was observed also when only the polycation part of the copolymers was considered in calculating IC_{50}. The measured IC_{50} value for PCX^{G1} was 72 µg/mL. The IC_{50} values of PEG-PCX^{G1} were calculated considering only the PCX^{G1} polycation content. In such case, the cytotoxicity of PEG12-PCX^{G1} was similar to that of PCX^{G1} (77 µg/mL). The two copolymers with higher PEG content exhibited significantly decreased cytotoxicity with their IC_{50} values above the maximum tested polycation concentration of 100 µg/mL. In order to establish a safe, nontoxic working concentration range of PCX^{G1}, we tested U2OS cells which were then used throughout this study in evaluating CXCR4 antagonism, cell invasion inhibition, and transfection of PCX^{G1}. IC_{50} values for PCX^{G1} and PEG12-PCX^{G1} were indistinguishable at ~17 µg/mL but they increased to 25 µg/mL and 41 µg/mL in case of PEG41-PCX^{G1} and PEG52-PCX^{G1} respectively, which were all higher than control PEI (22.0 µg/mL). In conclusion, the cell viability study proved that PEGylation effectively decreased the cytotoxicity profile of polycations not only by simply reducing the cationic content in polymers but also by decreasing the interactions of the toxic part with cellular membranes and vital intracellular proteins, which are unlike existing reports [223, 232].

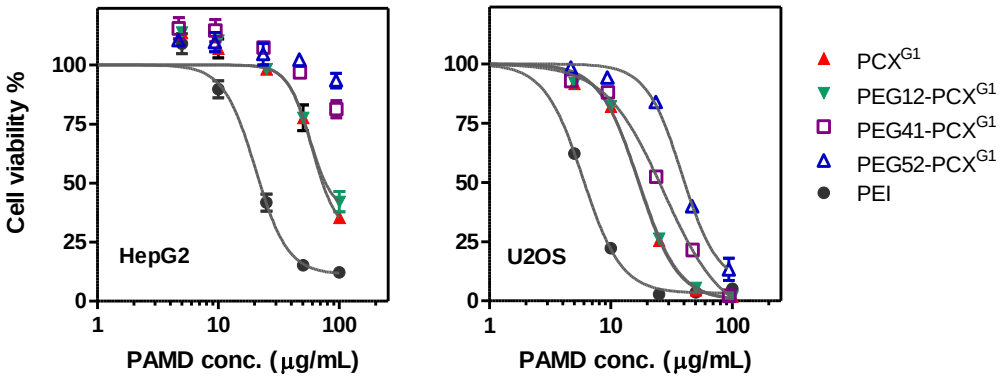

Figure 17. Effect of PEG on cytotoxicity of PCX^{G1} in HepG2 and U2OS cells. Cell viability was measured by MTS assay after 24 h incubation with increasing concentrations of polymers. Polymer concentration for PEG-PCX^{G1} copolymers is expressed as PCX^{G1} concentration only (i.e., excluding PEG). Results are expressed as mean ± SD (n=3).

4.2.4 CXCR4 antagonism of PEG-PCX^{G1}

Binding of PCX^{G1} to CXCR4 receptor is required for the copolymers to exhibit CXCR4 inhibitory activity. However, steric barrier created by PEGylation might cause the negative effect on binding of polymers to receptors. Therefore, CXCR4 redistribution assay was used to evaluate the influence of PEGylation on CXCR4 antagonism of PCX^{G1} polymer and PCX^{G1}/DNA polyplexes. This assay is based on monitoring the degree of inhibition of SDF-1 triggered endocytosis of membrane-localized EGFP-tagged CXCR4 receptor using HCS analysis. **Figure 18a** showed the difference in the fluorescence pattern of EGFP-CXCR4 between untreated cells (punctate fluorescence) and cells treated with CXCR4 inhibitor (diffuse pattern of fluorescence). The CXCR4 inhibitory activity of PEG-PCX^{G1} was tested at equal concentrations of the polycationic (PCX^{G1}) content and expressed as % CXCR4 antagonism relative to the control AMD3100 (**Figure 18b**). The CXCR4 antagonism of PEG-PCX^{G1} at the lowest tested concentration (0.05 µg/mL) ranged from 57-77% of AMD3100 activity, which had no statistically significant in a one-way ANOVA analysis in comparison with PCX^{G1}. At two higher tested concentrations of 0.15 µg/mL and 0.5 µg/mL, all PEG-PCX^{G1} and PCX^{G1} exhibited comparable CXCR4 inhibitory activity to the control AMD3100, indicating that PEG did not affect the binding properties of polymers with CXCR4 receptors. We also tested whether PEG-PCX^{G1} polyplexes prepared at two different w/w ratios (1.5 and 5) retained the CXCR4 inhibitory functionality of the free polymers under practically relevant experimental conditions employed in transfection assays (**Figure 18c**). Both polyplex formulations achieved nearly 100% CXCR4 inhibition According to the EtBr exclusion assay, polymers were just used to fully condense DNA and little amount of free polymers were present in polyplexes at w/w of 1.5, indicating the ability of polyplexes to inhibit CXCR4. At w/w of 5, the observed CXCR4 antagonism came from the free polymer in the formulation. The

cyclam ring of AMD3100 was totally 2+ charged at physiological pH and formed a stable *trans*-III *R,R,S,S*-type conformation regarding to the four nitrogen atoms, which permitted AMD3100 to bind tightly with CXCR4 receptor by hydrogen bond interactions with carboxylic acid group [233]. PEGylation does not negatively affect pharmacologic activity of PCX^{G1} to fully inhibit CXCR4 even in polyplex formulations. The possible reason might be that PEG chain did not decrease the overall charge profiles of cyclam rings and maintained their binding ability with Asp262, Glu318 or Asp 171 to fit into the main ligand-binding pocket of CXCR4 receptors [234].

4.2.5 Inhibition of cancer cell invasion by PEG-PCX^{G1}

As we know, CXCR4/SDF-1 axis plays a significant role in regulation of stem cell trafficking, neovascularization as well as cancer migration [235-241]. However, CXCR4 antagonists like AMD3100 can inhibit invasion of those cancer cells towards SDF-1 concentration gradient. In this study, Boyden chamber method was used to evaluate the effect of PEGylation on the ability of PCX^{G1} polyplexes to inhibit invasion of cancer cells. As shown in **Figure 19**, all PEG-PCX^{G1} polyplexes prepared at equivalent PCX^{G1}/DNA w/w ratio 5 effectively prevented 77.1-79.8% cancer cells from invading and migrating through Matrigel, which was comparable to that of AMD3100 (81.3%). Therefore, the ability of PCX^{G1} polyplexes to inhibit cancer cell invasion was not negatively impacted by PEGylation, suggesting that PEG-PCX^{G1} could be well-suited for applications in the treatment that aim at preventing or delaying metastasis. To apply the PEG-PCX^{G1} for gene therapy, the gene transfection efficiency would be tested and formulation studied would be discussed.

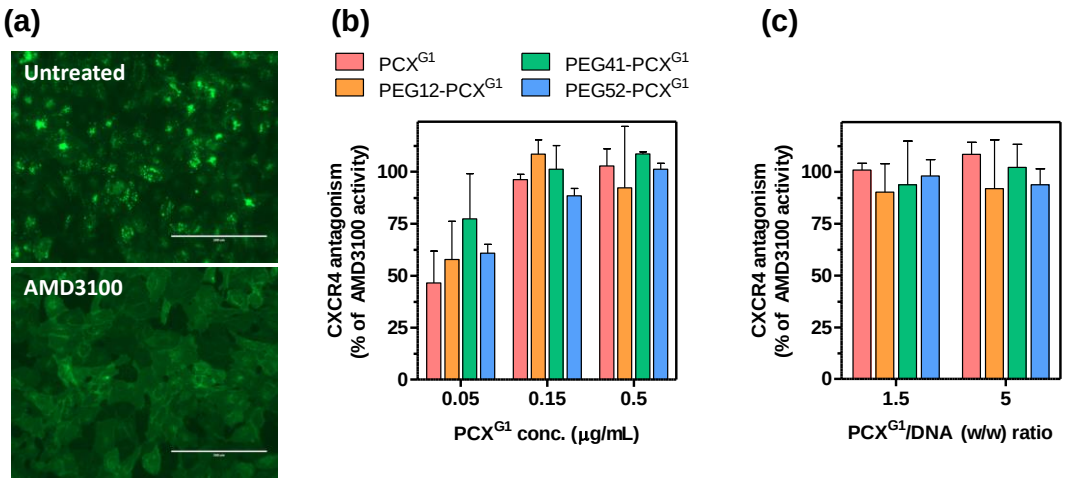

Figure 18. CXCR4 antagonism of PEG-PCX^{G1} polycations and polyplexes. (a) Effect of AMD3100 on redistribution of EGFP-CXCR4 receptor in U2OS cells. CXCR4 antagonism of PCX^{G1} and PEG-PCX^{G1} (b) and their polyplexes (c). The results are shown as mean % CXCR4 inhibition relative to AMD3100 ± SD (n=3).

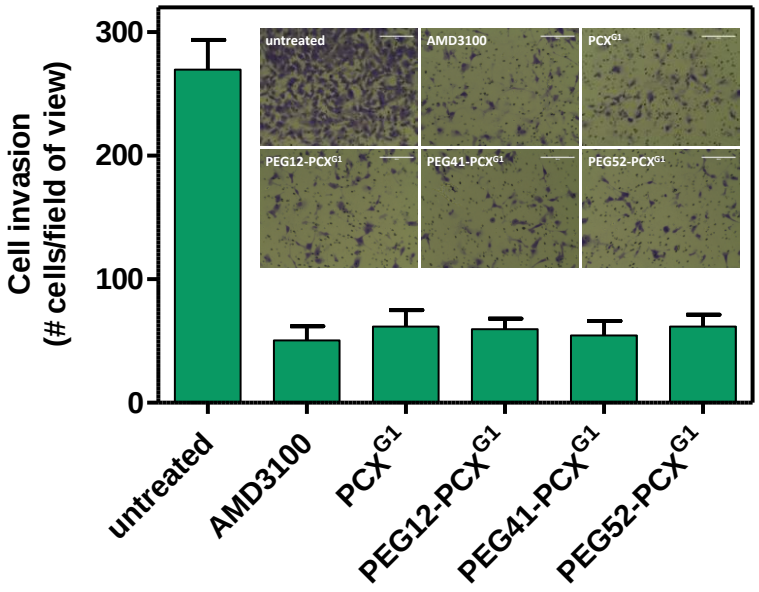

Figure 19. Inhibition of cancer cell invasion by PEG-PCX^{G1} polyplexes. Polyplexes were prepared at w/w ratio of 5 (total PCX^{G1} concentration 2.5 µg/mL). Cells were allowed to invade through a layer of Matrigel toward SDF-1 concentration gradient for 19 h before fixation and imaging. Average numbers of invaded cells were counted in randomly selected 5-10 imaging areas at 20x magnification (Scale bar = 200 µm).

4.2.6 Transfection activity of PEG-PCX^{G1} polyplexes

To study the effect of PEGylation on gene transfection activity, B16F10 and U2OS cell lines were incubated for 4 h with PEG-PCX^{G1} polyplexes formed with luciferase reporter plasmid in the absence or presence of 10% of FBS and continuously cultured in fresh medium for another 24 h (**Figure 20**). PCX^{G1} and PEG12-PCX^{G1} polyplexes displayed fully comparable transfection efficiency, however, the transfection decreased dramatically for polyplexes containing higher amount of PEG in either absence or presence of FBS. The possible reasons of reduced gene transfection of PEGylated polyplexes are that decreasing surface charge decreased cellular association and internalization, leading to a low transfection activity [219, 230]. DNA unpackaging from PEGylated polyplexes decreased, which might be another reason for poor luciferase expression. Unmodified polyplexes may escape more easily from endosome because aggregated particles filled intracellular vesicles and distort the membrane, however, the vesicles with PEGylated particles had more smooth appearance and would restrict the endosome escape [230]. In conclusion, the effect of PEGylation on transfection activity of polyplexes are due to restricted interaction with cellular membranes, resulting in decreased cellular uptake and compromised endosomal escape of polyplexes [219, 229].

4.2.7 Mixture formulation of PCX^{G1} and PEG-PCX^{G1}

With the increasing content of PEG in the polyplexes, the colloidal stability enhanced but transfection activity reduced correspondingly. As discussed above, several strategies have been developed to overcome the negative effect of PEGylation on transfection activity. In an attempt to solve the problems and easily control the amount of PEG, we have utilized a mixed polyplex strategy to prepare polyplexes with acceptable colloidal stability, near-neutral zeta potential, and high transfection activity. The mixed polyplex strategy depends on using a mixture of non-PEGylated and PEGylated

polycations. The mechanism is that the non-PEGylated polycation provides effective DNA condensation and facilitates endosomal escape of the polyplexes, while the PEGylated polycation equips the polyplexes with favorable surface properties and colloidal stability. This strategy has been successfully utilized with several different types of polycations [242-244]. We optimized PEG/polycation amounts by mixing PCX^{G1} and its PEGylated counterpart PEG52-PCX^{G1} to obtain largest range of PEG composition (**Figure 21**).

As shown in **Figure 21a**, with increasing PEG content, the DNA condensation curves of the mixed formulations shifted to higher w/w ratios. However, the condensation efficiency of PCX^{G1} part in the formulation was not affected because the curves overlaid when re-plotted as relative fluorescence vs. PCX^{G1}/DNA ratio (not shown). Using a mixture consisting of 80% PCX^{G1} and 20% PEG52-PCX^{G1} leads to positively charged polyplexes and rapid increase in size and aggregation in PBS (**Figure 21b**). However, increasing the content of PEG52-PCX^{G1} in the mixture to 40 and 70% resulted in decreased zeta potential and formulation of colloidally stable polyplexes.

In order to investigate the influence of mixture formulation on gene transfection, we tested the polyplexes above in both U2OS and B16F10 cells in the absence or presence of 10% FBS (**Figure 21c**). The transfection results showed that even polyplexes formed with 70% PEG52-PCX^{G1} retained transfection activity that was similar to that of non-PEGylated PCX^{G1} polyplexe, confirming that the mixed polyplex strategy is a suitable approach to prepare polyplexes with low surface charge, good colloidal stability as well as high transfection activity.

CXCR4 antagonism and the ability to inhibit cancer cell invasion are required for the mixed polyplexes. We also confirmed them in the CXCR4+ U2OS cells as displayed in **Figure 22** and **23**. All of the mixed polymers and polyplexes exhibited comparable CXCR4 inhibitory activity at all tested concentrations and w/w ratios. Similarly, mixed

formulation retained the ability to prevent cancer cell invasion, which was fully comparable with AMD3100. Those results indicated that mixed PCX^{G1} and PEG52-PCX^{G1} can be well-suited for applications in treatment that aim at combining gene therapy with preventing cancer metastasis.

4.2.8 DNA biodistribution *in vivo*

The ability of mixed PCX^{G1} and PEG-PCX^{G1} to deliver intact DNA *in vivo* was detected in 4T1 mice model. Linear PEI was used as positive control. Before the experiment, the size and zeta potential of DNA polyplexes prepared in HBG buffer were investigated. As shown in **Figure 24**, using a mixture consisting of 60% PCX^{G1} and 40% PEG52-PCX^{G1} leads to the smallest size with near-neutral zeta potential. This formulation was administrated in 4T1 mice and RT-PCR was used to study the biodistribution of intact DNA delivered to different organs. **Figure 25** revealed that the large amount of DNA was delivered to liver and spleen, which caused the sever off-target effect. However, in comparison with positive control PEI, PCX^{G1} and the mixed PEGylated formulation reduced the off-target effect as well as improved the ability to deliver DNA to tumors with 5.8-fold and 10.8-fold increase, respectively. Therefore, mixed PCX^{G1} and PEG52-PCX^{G1} would be a good option to target tumors and deliver nucleic acid for gene therapy.

4.2.9 Conclusion

To conclude, polymeric CXCR4 antagonism is a potential dual-fucntion vector, which are capable to inhibit cancer cell invasion and deliver efficient gene transfection. In order to perform colloidal stability, retain CXCR4 antagonism and exhibit high transfection activity, combination of PEGylation of PCX^{G1} with using a mixed polyplex approach is a viable strategy. The ability of PCX^{G1} to deliver DNA has been comprehensively studied, however, the siRNA delivery by the dual-funtional PCX still need to be further investigated.

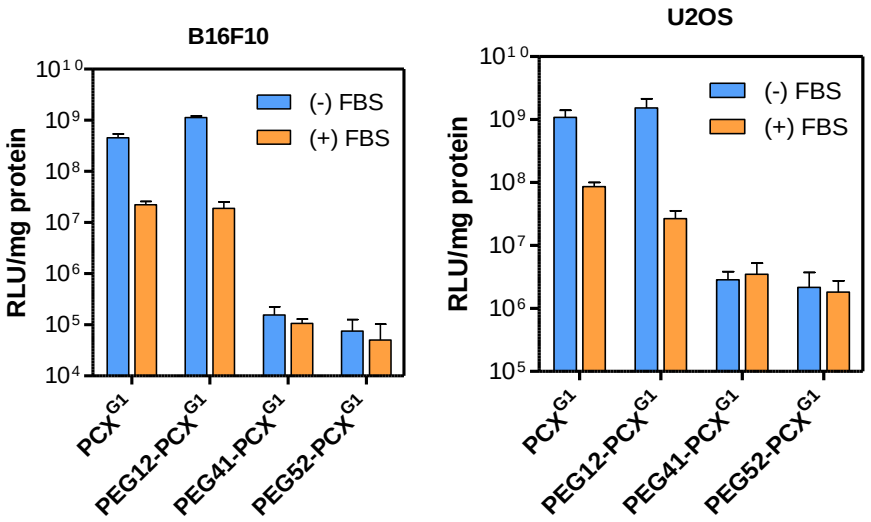

Figure 20. Transfection activity of PEG-PCX^{G1} polyplexes in B16F10 and U2OS cells. Polyplexes were prepared at PCX^{G1}/DNA (w/w) ratio 10 in B16F10 transfections and 5 in U2OS transfections. Results are expressed as luciferase expression in RLU/mg protein ± SD (n=3).

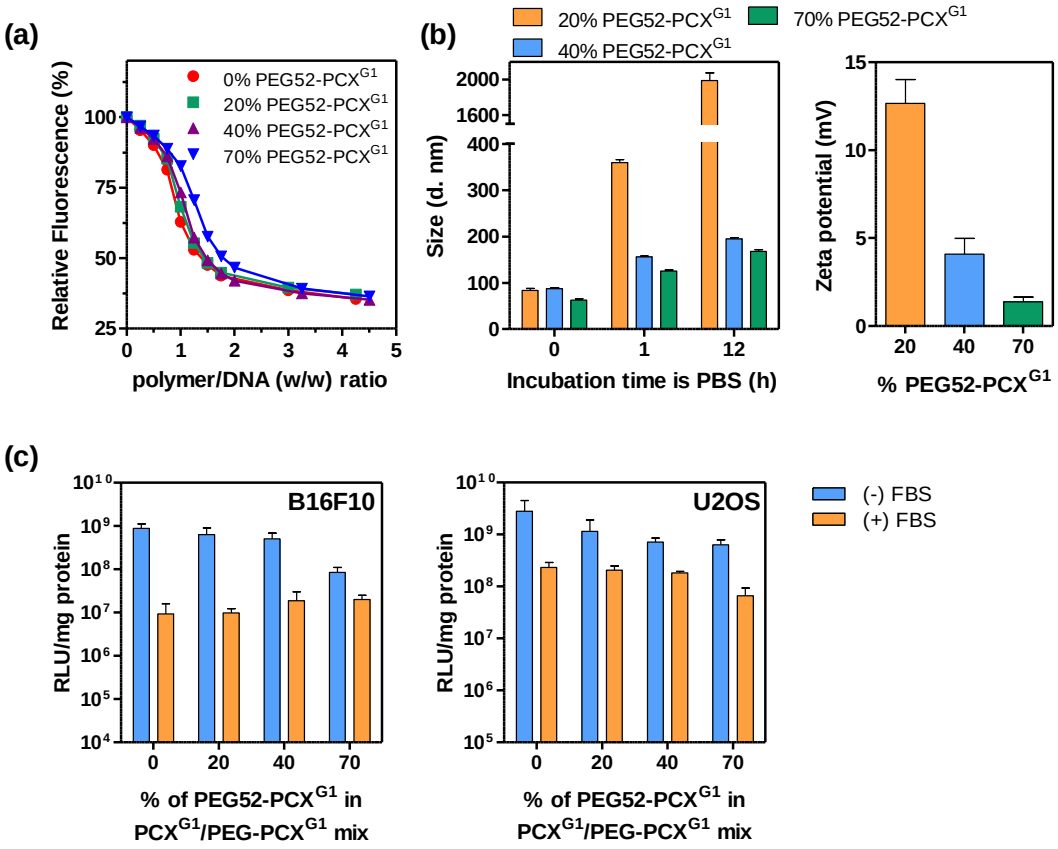

Figure 21. Properties of mixed PCX^{G1}/PEG-PCX^{G1} polyplexes. (a) DNA condensation ability of the PCX^{G1}/PEG-PCX^{G1} mixture determined by ethidium bromide exclusion assay. (b) Colloidal stability (left) and zeta potential (right) of polyplexes (w/w 5) prepared with increasing content of PEG52-PCX^{G1} in a mixture with PCX^{G1}. (c) Transfection activity of the mixed polyplexes.

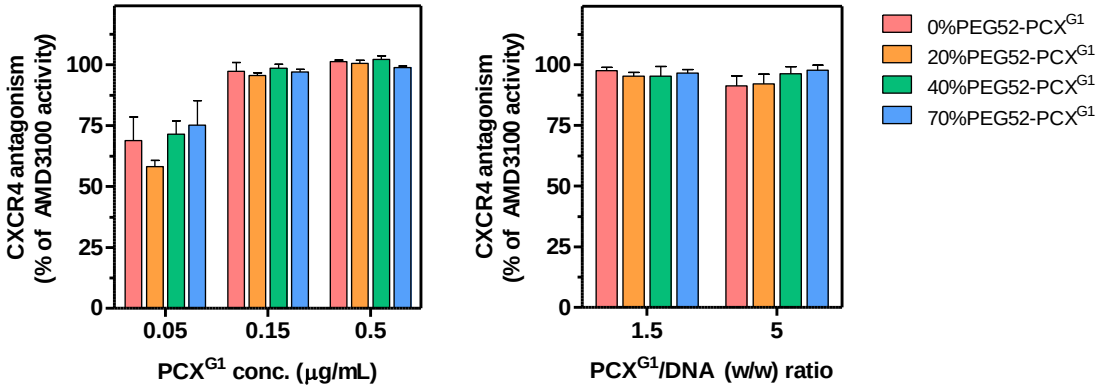

Figure 22. CXCR4 antagonism of mixed PCX^{G1}/PEG-PCX^{G1} polymer and polyplexes in U2OS cells. The results are shown as mean % CXCR4 inhibition relative to AMD3100 ± SD (n=3).

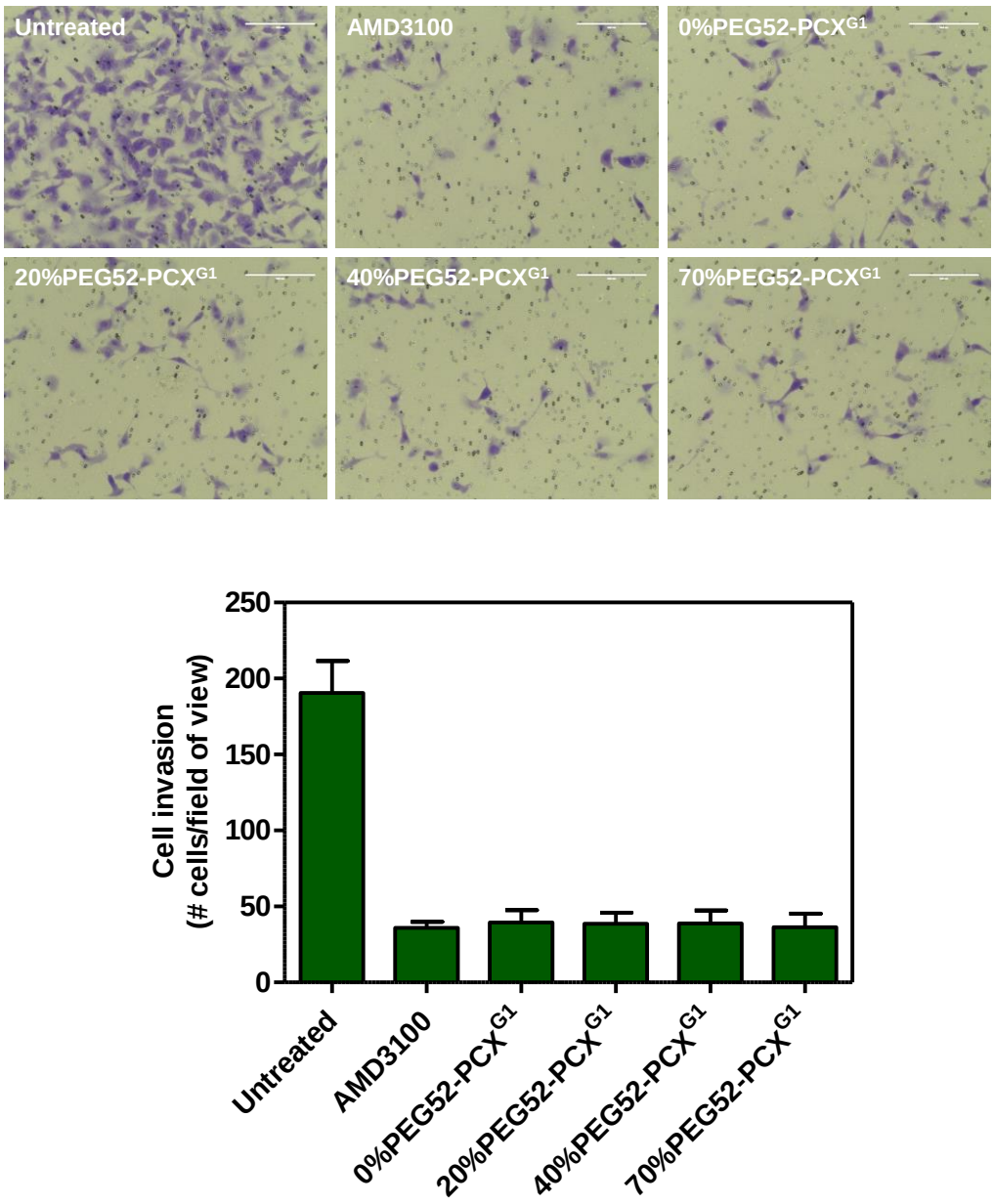

Figure 23. Inhibition of cancer cell invasion by mixed PCX^{G1}/PEG-PCX^{G1} polyplexes. Polyplexes were prepared at equivalent PCX^{G1}/DNA w/w ratio of 5 (total equivalent PCX^{G1} concentration 2.5 μg/mL). Cells were allowed to invade through a layer of Matrigel toward SDF-1 concentration gradient for 19 h before fixation and imaging. Average numbers of invaded cells were counted in randomly selected 5-10 imaging areas at 20x magnification (Scale bar = 200 μm).

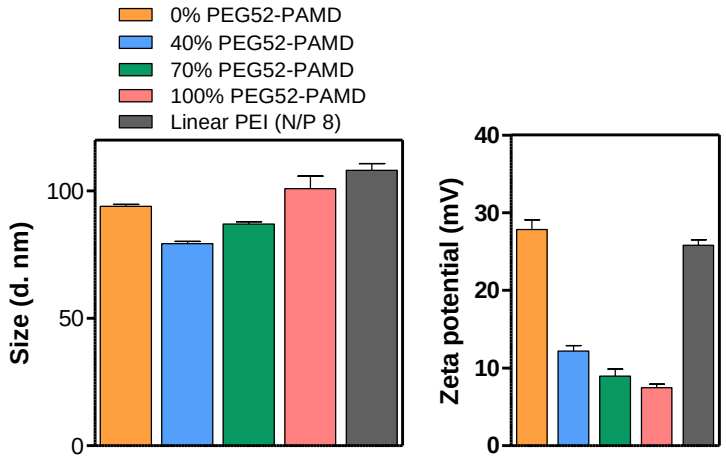

Figure 24. Size (left) and zeta potential (right) of mixed PCX^{G1}/PEG-PCX^{G1} polyplexes at equivalent PCX^{G1}/DNA w/w 3 in HBG buffer. Results are shown as mean ± SD (n=3).

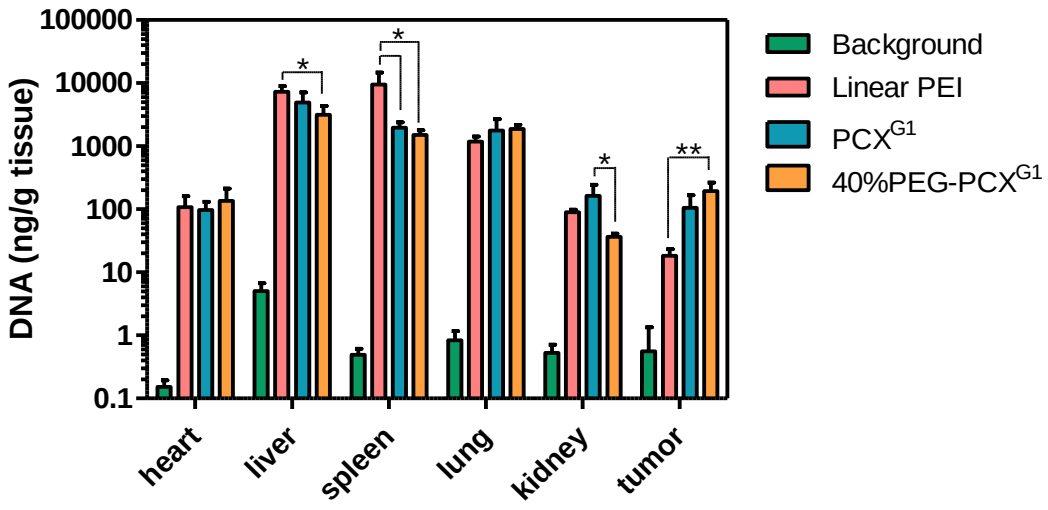

Figure 25. DNA biodistribution by polyplexes in BALB/c mice. Results are expressed as luciferase DNA ng/g tissue ± SD (duplicate of two mice). Statistical comparisons were done using the One-way ANOVA with Tukey-Kramer Multiple Comparisons Test ($^{*}P<0.05$ and $^{**}P<0.01$).

4.3 Cholesterol Modification of Poly(amido amine) CXCR4 Antagonists to Improve siRNA Delivery for Combined Anticancer Therapies

Please note that the data of this part was from the paper published in the Biomaterials Science with permission from The Royal Society of Chemistry [152]. The authors include Dr. Jing Li, Yi Chen and Dr. David Oupický and me. As the first author, I performed all the experiments, analyzed data and wrote the draft of manuscript. Dr. Jing Li and Dr. Oupický revised it and made it publishable. All the authors agreed with including their work in this dissertation.

Therapy with nucleic acids has potential in a broad range of disease. For instance, small interfering RNA (siRNA) was capable to achieve sequence-specific gene silencing effect in mammalian cells, and emerging as one of the most potential agents for the treatment of various diseases, such as viral infections, gene disorders as well as cancers [245-247]. Polyelectrolyte complexes of nucleic acids with polycations have been under development as delivery vectors for over two decades and received significant attention for multiple potential advantages, including lower toxicity, minimal immunogenicity, easier manufacturing and functional modifications [205, 206]. However, low bioavailability of siRNA has hampered its therapeutic application in clinical. Enzymatic degradation, accumulation in non-targeted tissues, insufficient cellular uptake, endosomal/lysosomal escape, and dissociation of siRNA from gene carriers must be circumvented when developing safe and efficient siRNA delivery vectors [248-250].

In comparison with lipid based delivery methods, the use of siRNA polyplexes remains hindered by a relatively low efficacy [249, 250]. And polyplex formulations

optimized for delivery of large DNA often perform poorly when delivering siRNA [251]. Many efforts have been made to develop various types of siRNA-loaded nanoparticles to overcome biological hurdles of siRNA delivery in recent years [252, 253]. Modification of polycations with hydrophobic moieties (e.g., cholesterol) have been among the most successful approaches [254, 255]. Cholesterol is a naturally occurring lipid and metabolized in the body. It also plays an important role in self-assembly of lipopolymer into miclelles or nanoparticles in biological environment, reducing cytotoxicity and facilitating endocytosis [256-258]. For example, water-soluble lipopolymers based on polyethylenimine and cholesterol exhibited high serum compatibility, enhanced cellular uptake, and better gene delivery than commercially available PEI, which were due to favourable interactions between cholesterol moiety and cell membrane [259]. In another example, a series of bio-reducible cholesterol-grafted poly(amidoamines) were synthesized and able to self-assemble into cationic nanoparticles in aqueous solution, which possessed high cell uptake, offered effective VEGF gene silencing *in vitro* as well as exhibited effective inhibition of tumor growth *in vivo* [260].

In this section of study, we focus on further development of PCX^{G1} as siRNA delivery vectors to achieve combined antimetastatic and antitumor effect by inhibiting CXCR4 activity. Based on available evidence, we proposed that modification of PCX^{G1} with cholesterol will improve overall stability and improve cell uptake and intracellular trafficking of siRNA polyplexes. We would synthesize a series of copolymers with different cholesterol grafting degress. The influence of cholesterol modification on siRNA complexation, colloidal and enzymatic stability of polyplexes, and the ability to inhibit CXCR4 and deliver anticancer siRNA against PLK1 will be investigated (**Scheme 5**).

4.3.1. Synthesis and characterization of Chol-PCX^{G1}

The synthesized PCX^{G1} was described before by Michael-type polyaddition of sencondary amines present in AMD3100 and acryloyl group of bisacrylamide HMBA at equal molar ratio. AMD3100 functions as a hexafunctional monomers and HMBA reacted randomly with one of the six amines, resulting in a branched water-soluble polymer when the reaction was performed at relatively low temperature and monomer conentrations [221, 222]. The weight-average molecular weight of PCX^{G1} was 13.9 kg/mol with a polydispersity of 1.9 as determined by gel permeation chromatography. As shown in **Figure 26**, the Chol-PCX^{G1} copolymers were synthesized by amidation reaction between the cholesteryl chloroformate and the remaining secondary amines in PCX^{G1}. The content of cholesterol moiety in the copolymers could be tuned by changing the feed ratio of cholesteryl chloroformate to PCX^{G1} in the reaction. Three copolymers with increasing content of cholesterol were synthesized and named according to their cholesterol content (**Table 5**). The content of cholesterol in the copolymers was determined from ^{1}H-NMR integral intensity of the methyl group **b** directly linked to the cyclic hydrocarbon at chemical shift of 0.65 ppm in cholesterol and aromatic protons **a** of AMD3100 at 7.1-7.5 ppm (**Figure 27**). The weight-average molecular weight of each synthesized Chol-PCX^{G1} was calculated based on the Mw of PCX^{G1} and the cholesterol grafting degree as estimated by ^{1}H-NMR.

4.3.2 Critical Micelle Concentration of Chol-PCX^{G1}

Hydrophobic cholesterol moieties were linked to the hydrophilic PCX^{G1}, which made copolymers amphiphilic and be possible to self-assemble into micelles in aqueous media. This potential self-assembly into micelles could change the nature and dynamic of the complexation with siRNA, which depended on whether the copolymers bind the nucleic acid as a unimer or as assembled micelles. Fluorescence spectroscopy was used to estimate the CMC values of these copolymers in distilled water with pyrene as a

hydrophobic fluorescent probe [179, 260-262]. Above CMC (in the presence of micelles), pyrene could be incorporated into the hydrophobic core in the micelles, leading to the increase in the ratio of two fluorescence intensity peaks (I_3/I_1). CMC of each Chol-PCX^{G1} could be determined by plotting the ratio of I_3/I_1 against the polymer concentration. The CMC values decreased from 63.1 µg/mL for Chol17-PCX^{G1} to 89.1 µg/mL for Chol25-PCX^{G1} (**Figure 28**), indicating that the increasing cholesterol modification could reduce CMC values of those copolymers.

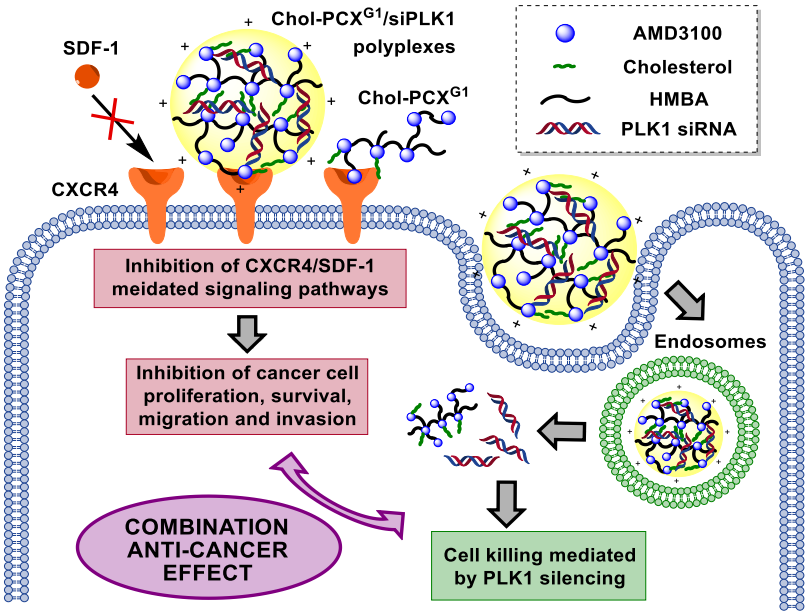

Scheme 5. Proposed mechanism of action of the dual-function Chol-PCX^{G1} as polymeric CXCR4 antagonists and siRNA (PLK1) delivery vectors.

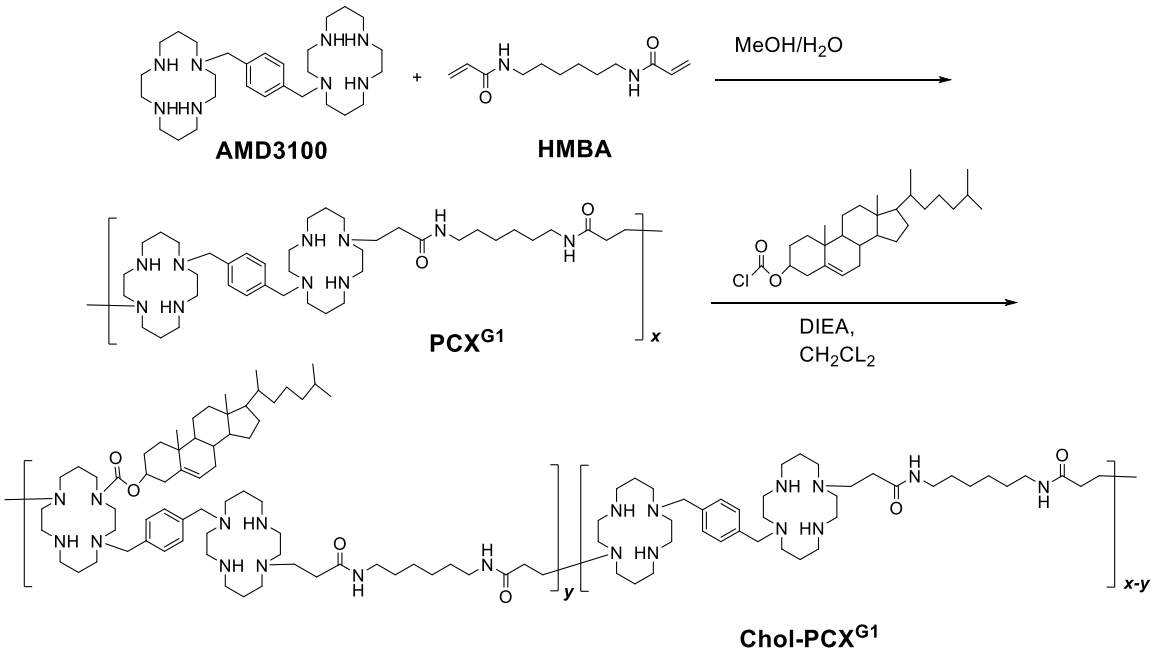

Figure 26. Synthesis of Chol-PCX^{G1}.

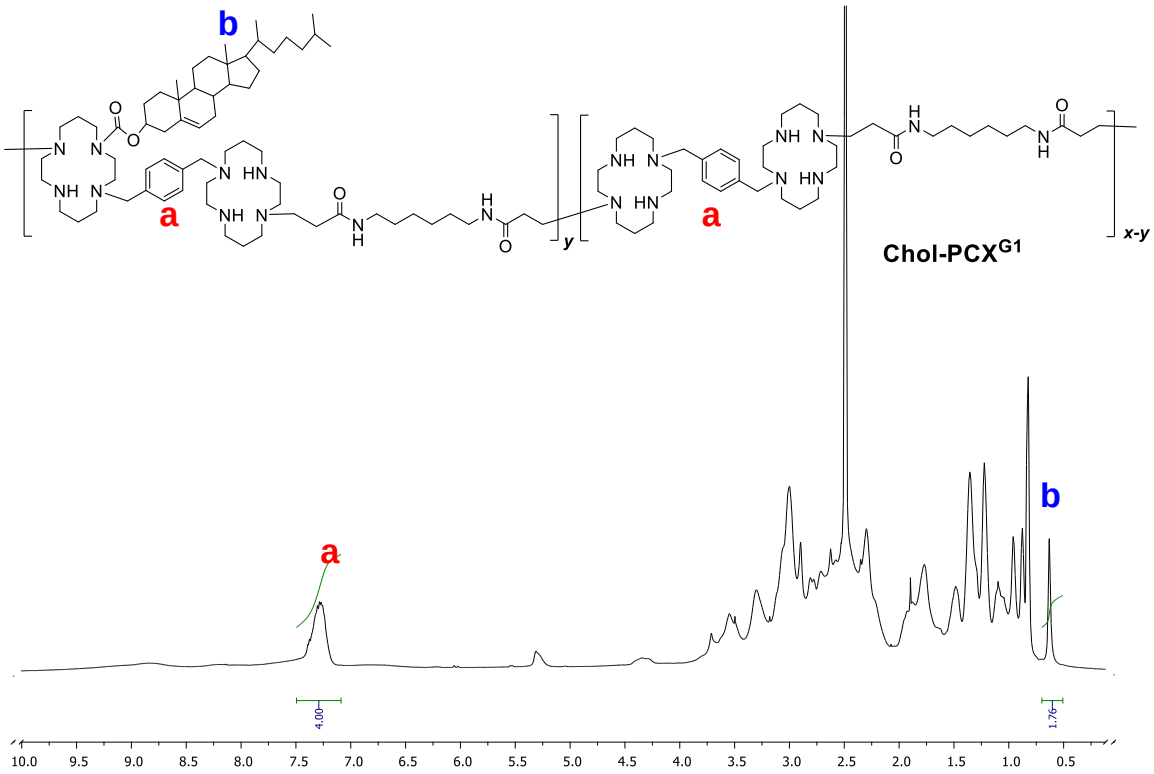

Figure 27 Typical ^{1}H-NMR spectrum of Chol-PCX^{G1} used in the determination of the cholesterol content (spectrum of Chol25-PCX^{G1} in DMSO shown).

Table 5. Characterization of Chol-PCX^{G1} copolymers.

Polymer	Cholesterol content (wt %)		M_w (kg/mol)
	In Feed	In copolymer[a]	
PCX^{G1}	0	0	13.9[b]
Chol17-PCX^{G1}	15	17	16.7[c]
Chol25-PCX^{G1}	25	25	18.5[c]
Chol34-PCX^{G1}	36	34	21.1[c]

[a] From ^{1}H-NMR.
[b] From GPC.
[c] Calculated from the M_w of PCX^{G1} and cholesterol content.

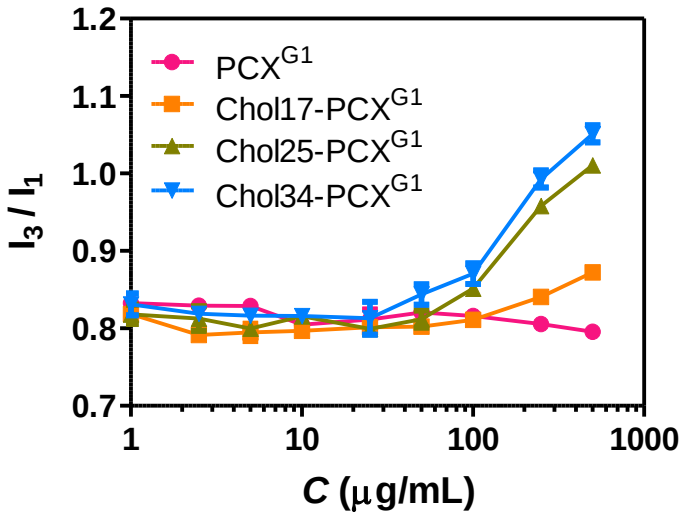

Figure 28. Critical micelle concentration (CMC) of Chol-PCX^{G1} determined by fluorescence spectroscopy. CMC was determined as the concentration at the inflection point of the curve where I_3/I_1 was plotted against Chol-PCX^{G1} concentration (n=3).

4.3.3 Preparation and characterization of Chol-PCX^{G1}/siRNA polyplexes

Agarose gel electrophoresis assay was used to investigate the influence of cholesterol grafting on the ability of PCX^{G1} to complex siRNA into polyplexes (**Figure 29a**). The complete retardation of siRNA mobility was achieved for all complexes at equivalent PCX^{G1}/siRNA w/w ratio of 1. The siRNA binding ability of the parent PCX^{G1}was slightly better than that of cholesterol modified copolymers as shown by the minimum siRNA releasing from complexes at w/w ratio 0.5. The better complexation ability of PCX^{G1} is likely due to that cholesterol conjugation caused a decreased number of protonated amines in Chol-PCX^{G1}. The w/w ratios in this study were expressed as equivalent PCX^{G1}/siRNA ratios, not taking cholesterol content into account. In all of the following studies, all siRNA polyplexes were prepared above w/w of 1 to maintain complete siRNA complexation.

The hydrodynamic size and zeta potential of Chol-PCX^{G1}/siRNA polyplexes prepared in 10 mM HEPES buffer (pH 7.4) at various equivalent PCX^{G1}/siRNA w/w ratios were measured by dynamic light scattering (**Figure 29b**). The polyplexes were stabilized for 20 min at room temperature before measurement. Except for Chol34-PCX^{G1}/siRNA prepared at lower w/w ratios, all the other polyplexes displayed small particle size ranging from 56 to 121 nm. All the Chol-PCX^{G1}/siRNA polyplexes prepared at higher w/w ratios showed significantly smaller sizes than polyplexes prepared at lower w/w ratios, perhaps suggesting tighter binding. At w/w ratios above 2, Chol17-PCX^{G1} with the lowest cholesterol content exhibited the smallest sizes compared with other Chol-PCX^{G1}/siRNA polyplexes, which is possibly due to that the proper content of cholesterol in copolymers allowed tighter hydrophobic interaction between cholesterol molecules. All Chol-PCX^{G1}/siRNA polyplexes exhibited positive surface charge indicated by zeta potentials ranging from 18 to 31 mV.

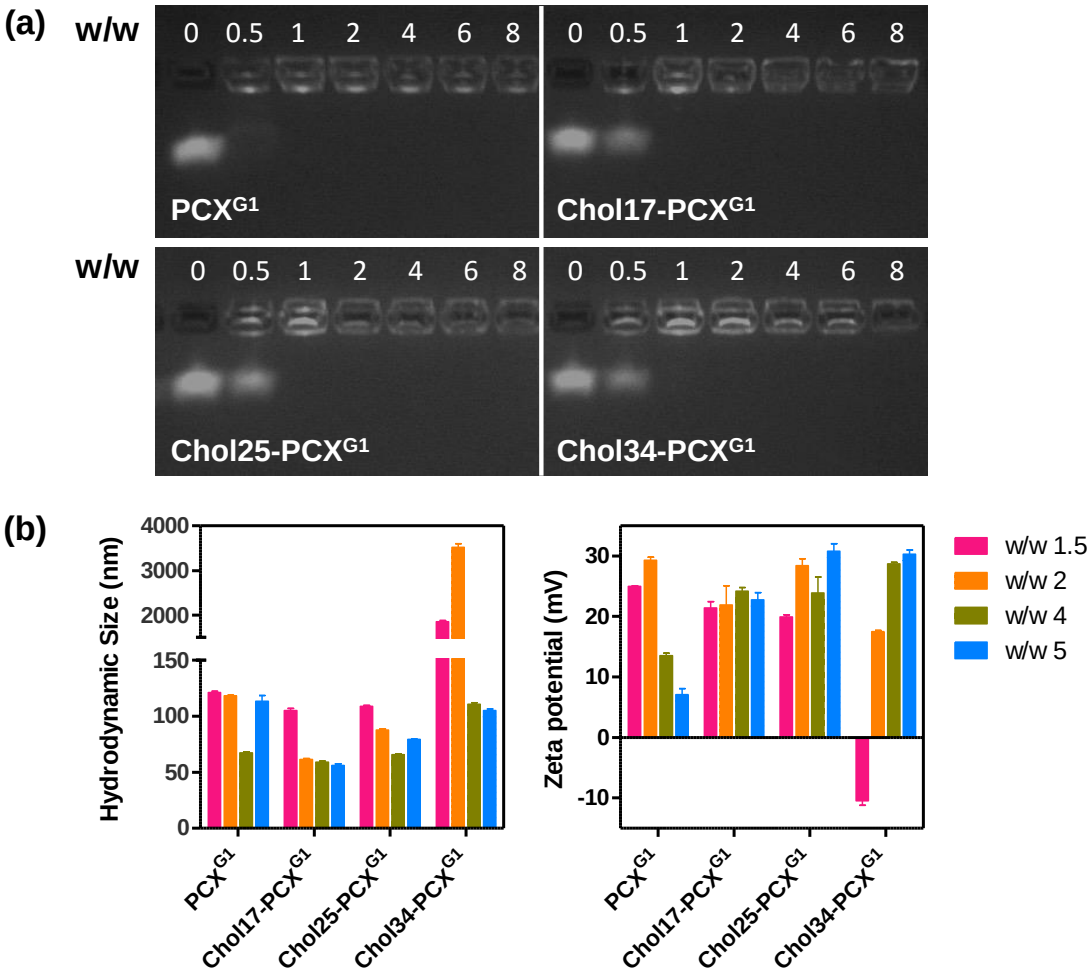

Figure 29. siRNA complexation and physicochemical characterization of siRNA polyplexes. (a) siRNA binding ability of the Chol-PCX^{G1} copolymers. (b) Hydrodynamic size and zeta potential of Chol-PCX^{G1}/siRNA polyplexes at various w/w ratios (equivalent PCX^{G1}/siRNA). Results are shown as mean ± SD of three measurements.

4.3.4 Colloidal and enzymatic stability of Chol-PCX^{G1}/siRNA polyplexes

For simulating physiologic conditions, the Chol-PCX^{G1}/siRNA polyplexes were analysed for their colloidal and enzymatic stability, which are important prerequisites for successful application. In low concentration buffers (e.g., 10 mM HEPES, pH 7.4), PCX^{G1}/siRNA polyplexes retained stable size like other polycation/siRNA polyplexes. However, addition of salts to reach physiologically relevant levels, polyplexes would aggregate into large molecules (**Figure 29b** vs. **30**). Aggregation of polyplexes depends on various parameters, including the chemical structure, molar mass and hydrophobicity of the used polycations [263]. We prepared Chol-PCX^{G1}/siRNA polyplexes at two different equivalent w/w ratios (2 and 5) and incubated them in PBS. And the changes in polyplex size during the following period of 12 h incubation were monitored by DLS (**Figure 30**). At w/w ratio of 2, all the Chol-PCX^{G1}/siRNA polyplexes aggregated and reached sizes ranging from ~690 nm to ~2 µm within 15 min of incubation in PBS. siRNA polyplexes with higher cholesterol content (Chol25-PCX^{G1} and 34) showed significantly faster rate of aggregation than that of Chol-PCX^{G1} with low (Chol17-PCX^{G1}) or no (PCX^{G1}) cholesterol. However, all of the siRNA polyplexes prepared with Chol-PCX^{G1} copolymers at w/w ratio 5 exhibited markedly improved colloidal stability with nearly constant size (< 150 nm) displayed for the duration of the experiment (12 h). In contrast, siRNA polyplexes prepared with the parent PCX^{G1} showed similar aggregation behavior as polyplexes prepared at w/w ratio of 2 and rapidly formed large aggregates. This similar findings were also reported in DNA polyplexes where increasing the amount of cholesterol resulted in polyplexes with enhanced colloidal stability [264]. For the reasons of maintaining good colloidal stability at w/w 5, we propose that as the surface positive charge of polyplexes is reduced at physiological salt concentrations, more Chol-PCX^{G1} can bind to the particle surface via hydrophobic interactions and increase colloidal stability by forming an additional shell of a

polycation. Moreover, even the Chol-PCX^{G1} concentrations were below their CMC in all of the above experiments. The concentration of the local copolymer within each polyplex particle was possibly significantly higher than CMC, which provided another contribution to improve the stability.

Enzymatic degradation is one of the main factors, which hampered effective siRNA delivery *in vivo*. Therefore, we evaluated the stability of those Chol-PCX^{G1}/siRNA polyplexes against RNase I degradatin. siRNA polyplexes were formed at at various equivalent w/w ratios ranging from 1 to 5, and followed by the incubation with 0.5 U RNase I for 30 min. In order to evaluate siRNA integrity, the samples were incubated with 200 µg/mL of heparin for another 30 min to dissociate polyplexes. Gel electrophoresis was used to examine the siRNA integrity and the intensity of each band was quantified and normalized to free siRNA. As shown in **Figure 31**, naked siRNA was not stable and completely degraded after half hour in the presence of RNase I. All the polymers, including parent PCX^{G1}, were able to provide protection of the siRNA against RNase I. PCX^{G1} with lower cholesterol modification (Chol17-PCX^{G1} and 25) displayed improved ability to protect siRNA when compared with the parent PCX^{G1} at the same equivalent w/w ratio, which might be due to the proper hydrophobic interaction of cholesterol molecules. Similar to PCX^{G1}, Chol17-PCX^{G1} and Chol25-PCX^{G1} also exhibited improved resistance to RNase I with increasing w/w ratios, indicating important role of excess polycations in properties of polyplexes. At w/w of 4, Chol25-PCX^{G1}/siRNA polyplexes prepared demonstrated the best protection against RNase I degradation with ~80% siRNA remaining intact after exposure. However, Chol34-PCX^{G1} with the highest cholesterol content remained only 50% siRNA intact when the polyplexes were prepared at w/w 1.5 and displayed decreasing ability to protect siRNA above w/w 2, indicating that proper content of cholesterol were needed to take into consideration.

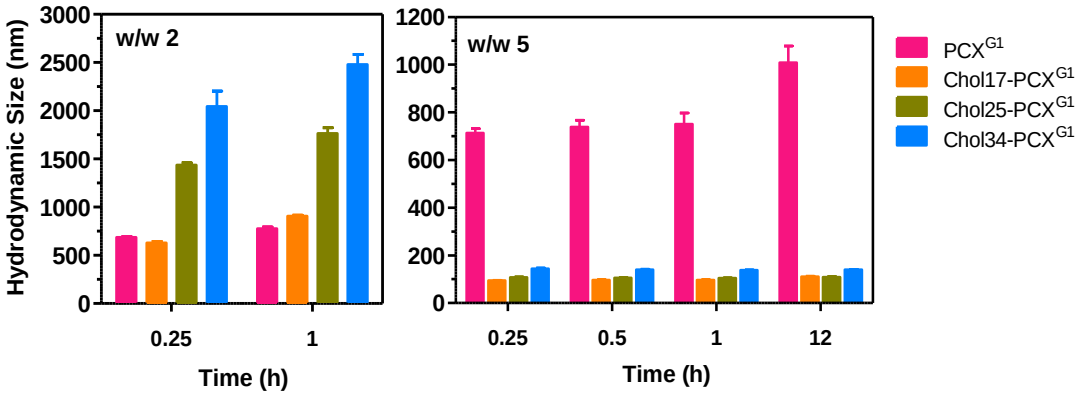

Figure 30 Colloidal stability of Chol-PCX^{G1}/siRNA polyplexes in PBS up to 12 h. Results are shown as mean ± SD of three measurements.

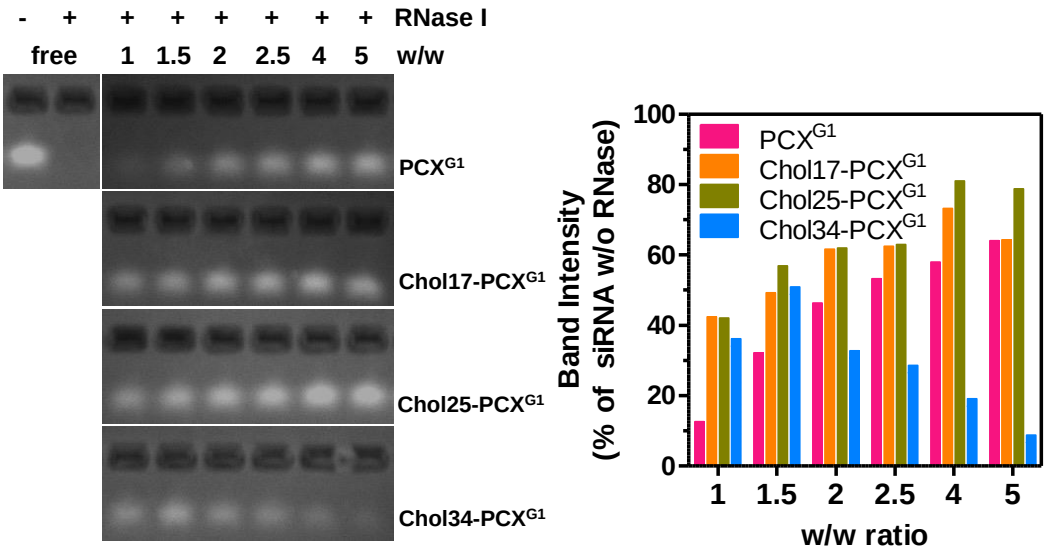

Figure 31. Stability of Chol-PCX^{G1}/siRNA polyplexes against RNase I. Polyplexes prepared at various w/w were exposed to RNase I, followed by incubation with heparin to release the siRNA for agarose gel electrophoresis. siRNA band intensity was quantified to calculate % siRNA remaining compared with untreated free siRNA.

4.3.5 Cytotoxicity of Chol-PCX^{G1}

Cytotoxicity is a major concern for application of polycations in clinical. Several key factors relate with cytotoxicity of polycation-based gene delivery systems, such as molar mass of the polycations, polymer structure, charge density and biodegradability [265-267]. The influence of hydrophobic modification on polycations has been reported with both positive and negative effects [255]. For instance, some hydrophobic moieties are common endogenous physiological molecules, so that the conjugated polycation should be non-cytotoxic. However, in some cases, high content of hydrophobic chains could cause cell membrane disruption and result in cell death [268]. Thus it was important to evaluate how cholesterol affects toxicity of PCX^{G1} to avoid or minimize any undesired toxic side effects. Cytotoxicity of Chol-PCX^{G1} was investigated in human osteosarcoma U2OS cell line by MTS assay (**Figure 32**). U2OS cells would be used to determine the safe dosing window to study the biological activity of the Chol-PCX^{G1}/siRNA polyplexes. The cute 24 h toxicity of those polymers was assessed, which could be mostly attributed by the polycation character of the polymers. In order to directly evaluate the effect of cholesterol modification on the toxicity of the polycation, Chol-PCX^{G1} concentrations were expressed as PCX^{G1} concentration only and the IC_{50} values were calculated based on the PCX^{G1} content. The benchmark 25 kDa branched PEI was used here as a control with IC_{50} of 4.2 μg/mL. Parent PCX^{G1} showed IC_{50} 12.8 μg/mL, which was significantly higher than PEI control. Chol-PCX^{G1} was slightly more toxic than PCX^{G1} with IC_{50} 10.3 μg/mL. However, for the polycations with higher content of cholesterol (Chol25-PCX^{G1} and Chol34-PCX^{G1}), the IC_{50} values increased to 16.7 μg/mL and 33.4 μg/mL, respectively. The formation of amido bonds after cholesterol modification decreased the protonable amine group in PCX^{G1} available for interaction with cell membranes, which possibly induced the decreased cytotoxicity in polycations with higher content of cholesterol.

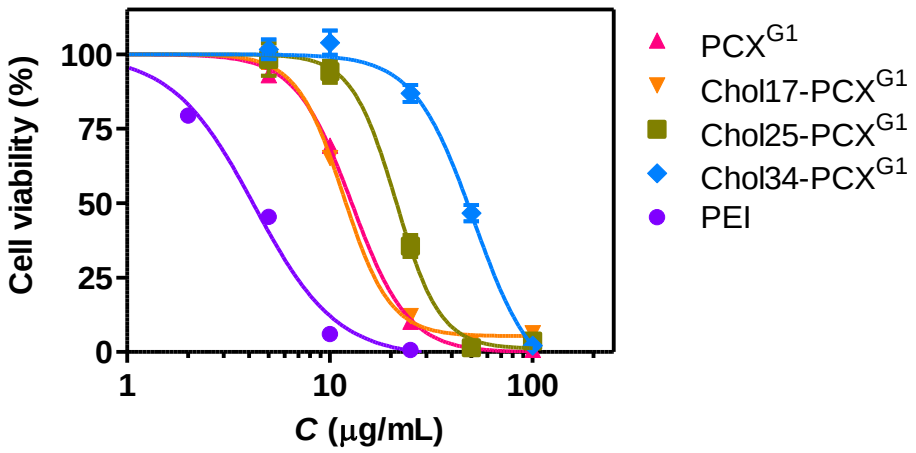

Figure 32. Cytotoxicity of Chol-PCX^{G1}. Cell viability was measured by MTS assay after 24 h incubation with increasing concentrations of polymers. Chol-PCX^{G1} concentrations are expressed as PCX^{G1} concentration only (i.e., excluding cholesterol). Results are expressed as mean cell viability ± SD (n=3).

4.3.6 CXCR4 antagonism of Chol-PCX^{G1} and Chol-PCX^{G1}/siRNA

Binding of PCX^{G1} to CXCR4 receptor is required for the pharmacologic activity of the polymers and polyplexes. The accessibility of the receptor-binding cyclam moieties in the polycation structure is necessary for PCX^{G1} binding with CXCR4 to exhibit inhibitory activity. Not all of the eight amino groups in the AMD3100 are required for CXCR4 binding and inhibition [197]. However, binding of polymers to receptors on the cell surface can be negatively affected by the configuration alternation created by cholesterol. Therefore, it is important to investigate the influence of cholesterol on CXCR4 antagonism and confirm that the proposed dual functionality of the vector is preserved. We evaluated the CXCR4 inhibition of SDF1-triggered endocytosis of EGFP-CXCR4 receptors in U2OS osteosarcoma cells by CXCR4 receptor redistribution assay, as described before. The different fluorescence patterns of EGFP-CXCR4 between untreated and AMD3100 treated cells are illustrated in **Figure 33a**.

In order to permit direct evaluation of the effect of cholesterol moieties on CXCR4 antagonism of PCX^{G1}, we have tested activity of the synthesized copolymers at equal concentrations of the polycationic (PCX^{G1}) part of the copolymers. Activity of PAMD-Ch was analyzed and expressed as % CXCR4 antagonism relative to the control AMD3100 (300 nM) (**Figure 33b**). We tested Chol-PCX^{G1} at two different concentrations (0.6 and 2 µg/mL) and evaluated Chol-PCX^{G1}/siRNA polyplexes prepared at w/w ratios (1.5 and 5). The selected w/w ratios allowed us to achieve the same polymer concentrations as in the experiment with free copolymers. CXCR4 antagonism of Chol-PCX^{G1} copolymers and their siRNA polyplexes exhibited similar concentration-dependent behavior. When compared with the free polymer at the same concentration, Chol-PCX^{G1} polyplexes showed slightly decreased CXCR4 inhibition, which might be due to a result of sequestration of a portion of the copolymers in the core of the siRNA polyplexes. A

decrease in CXCR4 antagonism showed up with the increasing content of cholesterol grafting degree. Chol34-PCX^{G1} with the highest cholesterol content displayed the lowest CXCR4 antagonism among all the tested polymers. However, at a low w/w ratio of 1.5, Chol17-PCX^{G1}/siRNA polyplexes achieved nearly 100% CXCR4 inhibition. And Chol25-PCX^{G1}/siRNA polyplexes achieve similar levels of CXCR4 antagonism at w/w 5. Those results indicated that there is a fine balance between the hydrophobicity caused by cholesterol moiety and CXCR4 binding.

4.3.7 Delivery of anti-PLK1 siRNA (siPLK1) by Chol-PCX^{G1}

PLK1 expression is elevated in multiple types of human cancers, which is a key mitotic regulator in mammalian cells, has prognostic value for predicting aggressiveness of cancer as well as target values for cancer treatment [269-271]. Inhibition of PLK1 could be achieved by small molecule inhibitors or using PLK1 gene silencing with siRNA. Both of them caused cell apoptosis and inhibition of tumor growth *in vivo* [272-274].

We proposed that combination of antimetastatic effect by Chol-PCX^{G1} and antitumor activity by PLK1 silencing would be promising for cancer treatment. Therefore, the investigated the ability of Chol-PCX^{G1} to deliver siPLK1 in U2OS osteosarcoma cells. PEI/siPLK1 polyplexes prepared at w/w 1.5 were used as a positive control. Scrambled siRNA (siScr) was used in control experiments to assess toxicity of the studied polyplexes. As shown in **Figure 34a** (left), in serum-free conditions, the safety of the selected polyplex formulations were evaluated with acceptable cell viability above 85%. The anticancer activity of Chol-PCX^{G1}/siPLK1 polyplexes was determined from their ability to induce cancer cell death as a result of PLK1 gene silencing. Different anticancer activities were shown with different grafting degrees of cholesterol in PCX^{G1} polymers. Chol17-PCX^{G1} and Chol25-PCX^{G1} polyplexes polyplexes exhibited better anticancer activity than unmodified PCX^{G1} at equivalent PCX^{G1}/siRNA w/w ratios. The best performing Chol17-

PCX^{G1}/siPLK1 polyplexes showed cell killing activity (48-62%) fully comparable to the PEI/siPLK1 control. Although grafting degree of cholesterol reached 34% in Chol-PCX^{G1} polymer, the siPLK1 induced cell killing was not further improved, indicating that it was necessary to optimize cholesterol content in the preparation of copolymers and investigated the best percentage.

In order to investigate the practical application of Chol-PCX^{G1}/siRNA polyplexes, we also evaluated the anticancer activity in the presence of 10% serum (**Figure 34b**). In the presence of serum, the safety of the tested polyplex formulations was improved, as indicated by the negligible effect on cell viability by Chol-PCX^{G1}/siScr polyplexes. Serum compromised the the ability of most of the tested polyplexes to deliver siPLK1 as indicated by nearly-background levels of cell killing. For instance, both PCX^{G1}/siPLK1 and PEI/siPLK1 lost nearly all their anticancer activity when compared with the serum-free conditions. However, Chol17-PCX^{G1} and Chol25-PCX^{G1} achieved optimal activity at w/w 1.5 and 2. Especially, Chol17-PCX^{G1}/siPLK1 polyplexes maintained the significant cell killing activity at w/w 2, which was comparable to the activity in serum-free conditions. While in the case of Chol34-PCX^{G1}, the highest activity was obtained at w/w 2.5. These findings suggest that cholesterol modified copolymers can protect siRNA from degradation in serum and facilitate efficient siRNA delivery, but the content of cholesterol and proper ratio of polymer/siRNA have to be optimized to achieve maximum anticancer activity.

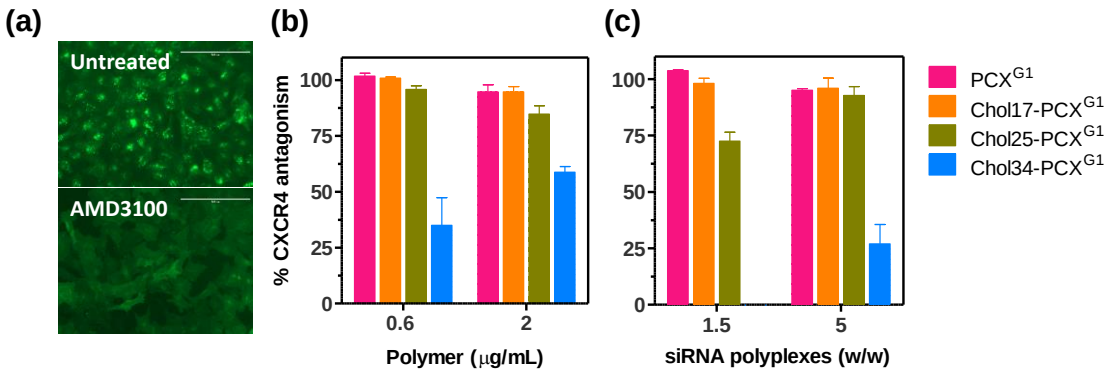

Figure 33. CXCR4 antagonism of Chol-PCX^{G1} and Chol-PCX^{G1}/siRNA polyplexes. (a) Illustration of EGFP-CXCR4 receptor redistribution assay: untreated cells (0% CXCR4 antagonism) and cells treated with 300 nM AMD3100 (100% CXCR4 antagonism). (b) CXCR4 antagonism of Chol-PCX^{G1} and their siRNA polyplexes. The results are shown as mean % CXCR4 inhibition relative to positive control 300 nM AMD3100 ± SD (n=3).

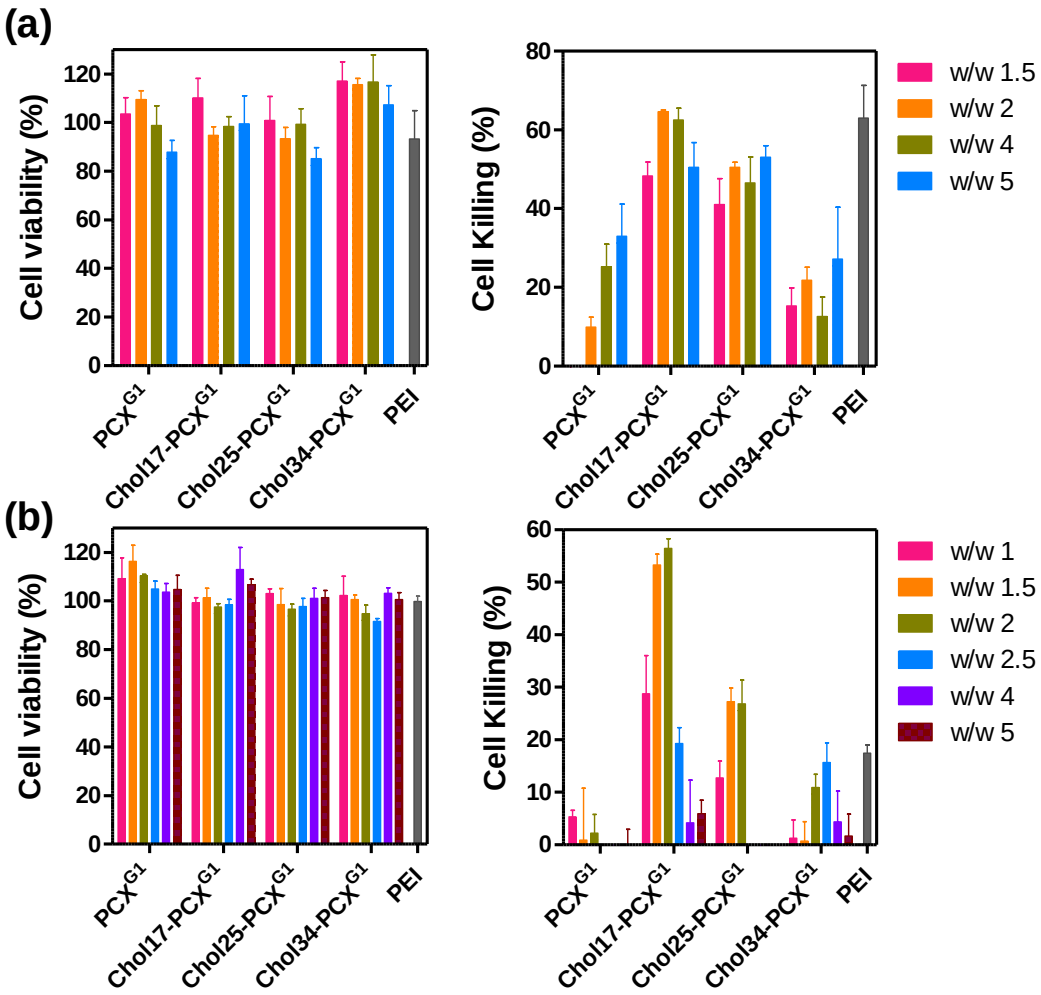

Figure 34. siRNA delivery by Chol-PCX^{G1} in U2OS cells. Transfections were conducted either in the absence (a) or the presence of 10% serum (b). Polyplexes were prepared with control siScr (left) or siPLK1 (right) at various equivalent PCX^{G1}/siRNA w/w ratios and cell killing mediated by PLK1 knockdown was measured (n=4).

4.3.8 Intracellular distribution of Chol-PCX^{G1}/siRNA polyplexes

To gain the expected therapeutic effect, siRNA has to be protected in the polyplexes, internalized by the cells and released in the cytoplasm. Proper intracellular trafficking is significant for successful delivery of functional siRNA by polyplexes. It was reported that introducing hydrophobic moiety like cholesterol into polycations showed positive effects on enhancing nucleic acid delivery [255, 260]. Hydrophobic moiety can promote cell membrane adsorption, alleviate serum inhibition and facilitate nucleic acid dissociation from polycations. In order to visualize both components of the polyplexes, copolymers were lablelled with AlexaFluor 647 and form polyplexes with commercially available siRNA labelled with AlexaFluor 555. Side-by-side comparison was conducted between the best performing Chol17-PCX^{G1}/siRNA polyplexes and parent PCX^{G1}/siRNA polyplexes (**Figure 35**). Confocal microscopy was used to investigate the influence of cholesterol modification on the cellular uptake and intracellular distribution of the Chol-PCX^{G1}/siRNA polyplexes.

Cellular uptake is one of the main factors determining the success of siRNA delivery by the dual-function PCX^{G1} polyplexes. As shown in **Figure 35**, polyplexes that exhibited high transfection activity also exhibited high levels of cellular internalization. Serum contains large amount of anionic proteins that can bind to cationic polyplexes and impact the extent and mechanism of cell uptake and intracellular trafficking [275]. The effect of serum on the polyplex uptake and intracellular distribution was evaluated. The severe adverse effect of serum on the cellular uptake of PCX^{G1}/siRNA polyplexes was observed. PCX^{G1}/siRNA polyplexes prepared at w/w 2 exhibited considerably much lower cellular uptake and distribution to the cytoplasm than that of Chol17-PCX^{G1}/siRNA polyplexes, which correlated to the previous reports that hydrophobic modification of polycations can enhance serum compatibility [276, 277]. Moreover, less co-localization of

the Chol17-PCX^{G1} and siRNA signal (bright pink) were shown when compared with PCX^{G1}/siRNA where nearly all siRNA was associated with the polycation. The reduced co-localized points were due to enhanced intracellular dissociation of the polyplexes and release of free siRNA. Incorporating hydrophobic moieties have been reported to facilitate intracellular polyplex dissociation [278, 279].

We have demonstrated that the internalization of PCX^{G1}/DNA polyplexes was independent of the CXCR4 trafficking pathway. However, the interaction mechanism of polyplexes with cell membranes and membrane receptors might be altered by cholesterol modification. Therefore, it was necessary to investigate if the CXCR4 trafficking was involved in the intracellular distribution of siRNA polyplexes. EGFP-CXCR4 expressing U2OS cells were treated with fluorescently labelled Chol17-PCX^{G1}/siRNA polyplexes (w/w 5) and 10 nM SDF-1 for 1 h, which allowed Chol17-PCX^{G1} polyplexes to directly compete with the chemokine ligand for binding with CXCR4. As shown in the confocal microscopy pictures (**Figure 36**), Chol17-PCX^{G1}/siRNA polyplexes can efficiently inhibit CXCR4 as indicated by the diffuse pattern of EGFP-CXCR4 fluorescence. And there were only a small amount of internalized receptors as shown by the discrete green puncta. A fraction of the Chol-PCX^{G1}/siRNA polyplexes overlapped with the CXCR4 trafficking as demonstrated by the colocalization of siRNA and CXCR4 (yellow) as well as the Chol17-PCX^{G1} and CXCR4 (bright blue), indicating that cholesterol modification might change the interaction of polyplexes with CXCR4 and facilitate siRNA internalization. However, more details of this mechanism have to be further studied.

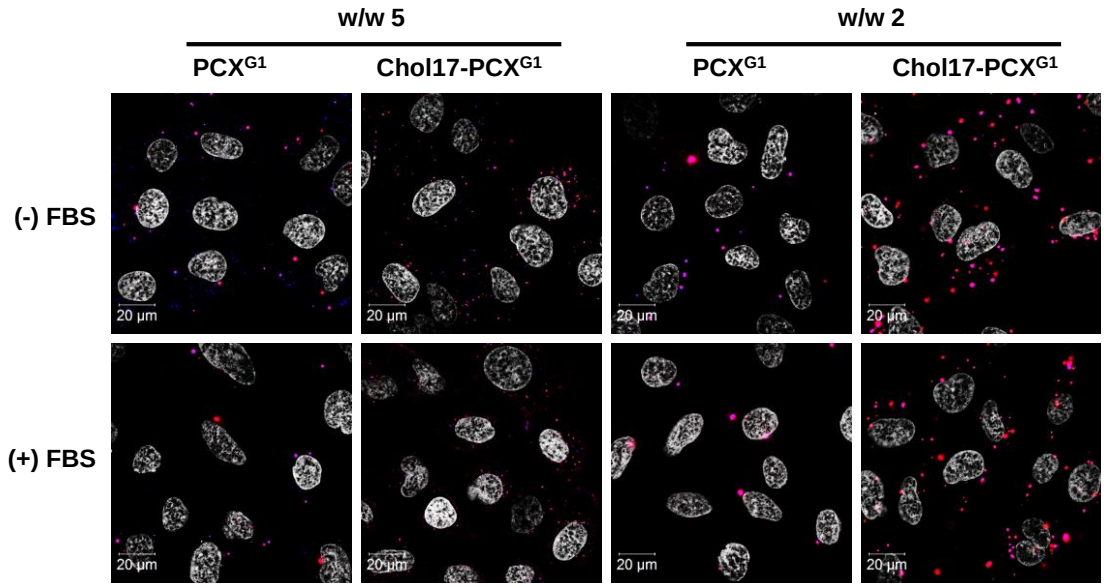

Figure 35. Intracellular distribution of PCX^{G1}/siRNA and Chol17-PCX^{G1}/siRNA polyplexes in U2OS cells using siRNA labelled with AlexaFluor 555 (red) and polymers labelled with AlexaFluor 647 (blue) (cell nuclei stained with Hoechst 33258 (shown as white)).

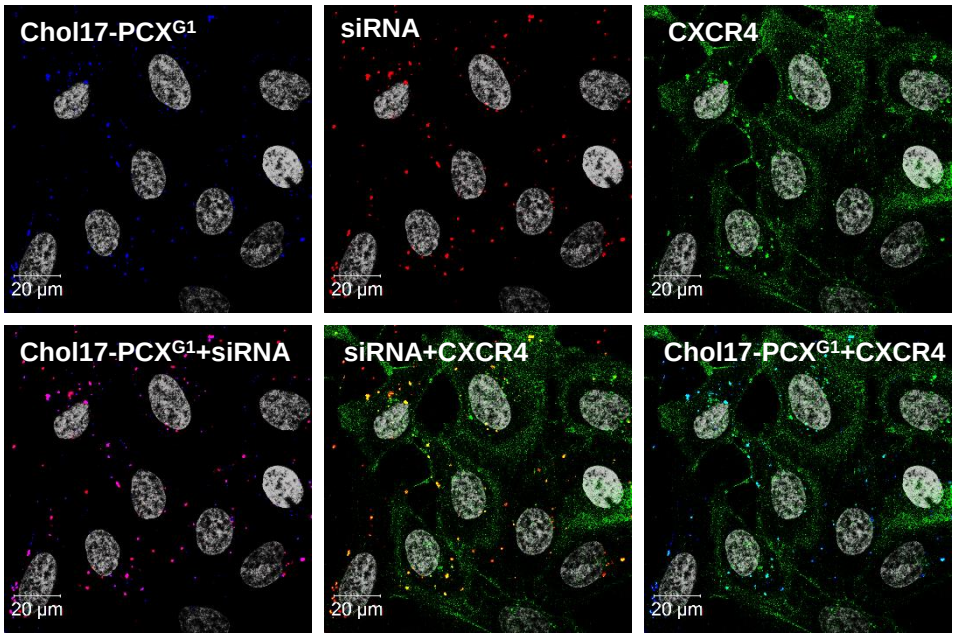

Figure 36. Intracellular distribution of fluorescently labelled Chol17-PCX^{G1}/siRNA polyplexes in U2OS cells expressing EGFP-CXCR4 receptors. Cells were incubated with polyplexes and 10 nM SDF-1 for 1 h and imaged using a confocal microscope: siRNA (red), Chol17-PCX^{G1} (blue), EGFP-CXCR4 (green), cell nuclei (white).

4.3.9 Conclusion

PCX^{G1} was modified with different contents of cholesterol and developed for siRNA delivery vector. The above findings showed that proper cholesterol modification provided the Chol-PCX^{G1}/siRNA polyplexes with increased colloidal stability, improved enzymatic stability against RNase, and greatly enhanced siRNA transfection in the presence of serum, while retaining strong CXCR4 antagonism. Furthermore, investigation of combining Chol-PCX^{G1} with therapeutic siPLK1 showed promising cell killing effects in cancer cells. Therefore, Chol-PCX^{G1}/siRNA polyplexes would be a novel and potential dual-functional strategy to treat metastatic cancer.

As we know, cancer metastasis caused nearly 90% death of cancer patients, which is the main reason for the failure of cancer treatment [2]. For instance, less than 20% of PC patients are candidates for surgery because it has spread beyond the pancreas at the time of diagnosis. Late diagnosis, complex microenvironment and early metastasis in PC contributes to the extremely low five-year survival rate (~7%) [30-32]. Better therapeutic strategies are needed to be designed to treat PC. Dual-functional PCX nanoparticles will be further investigated for PC treatment by combining prevention of cancer metastasis by inhibiting CXCR4/SDF-1 axis and ability to deliver therapeutic nucleic acids to tumors.

4.4 Polyplex-Mediated Inhibition of CXCR4 and NCOA3 Impedes Pancreatic Cancer Progression and Metastasis

Please note that the data presented in this chapter were published in Biomaterials [280]. The authors include Dr. Sushil Kumar, Dr. Satyanarayana Rachagani, Dr. Balasrinivasa R. Sajja, Ying Xie, Yu Hang, Dr. Maneesh Jain, Dr. Jing Li, Dr. Michael D. Boska, Dr. Surinder K. Batra, Dr. David Oupický and me. I contributed equally with Dr. Sushil Kumar to this paper. I prepared polyplexes, characterized their physicochemical properties, toxicity, and in vitro activity. I helped to analyze data and wrote early draft of the manuscript. Dr. Sushil Kumar designed the in vivo experimental plan and analyzed NCOA3 expression in primary tumors by RT-PCR, analyzed primary tumor necrotic area and Muc4 expression by immnuohistochemistry staining. Ying Xie helped me with the operation of flow cytometry to measure CXCR4 expression. The animal surgery, tumor implantation, and IVIS measurements were done by Dr. Satyanarayana Rachagani with my help. Perfusion measurement by MRI and data analysis were performed by Dr. Boska and Dr. Sajja. Drs. Li, Kumar, Jain, Batra, and Oupicky wrote and revised the manuscript and made it published. All the authors agreed with including their work in this dissertation.

PC is one of the worst prognoses of all cancer with a prediction of 53,070 new cases and 41,780 deaths in US of 2016 [281]. By 2030, PC might become the second leading cause of cancer-related mortalities [29]. PC is unique among solid tumors due to the extremely dense desmoplstic reaction, which presents substantial barriers to perfusion, diffusion, and convection of antitumor therapeutics into the PC tissues, resulting in acquired resistance [34]. Desmoplasia contains extracellular matrix (ECM) proteins, myofibroblastic pancreatic stellate cells, and immune cells, which provide growth factors and immune modulators to support PC growth [35]. The proliferation of fibroblasts and

increased stromal fibrosis induces desmoplastic PC microenvironment with high interstitial pressure, dense stroma and vascular dysfuction [39, 40]. Aberrant expression of mucins has been found as one of the characteristic features of PC and increases with PC progression [93, 94, 282-284]. Mucins induce PC progression, metastasis and chemoresistance by interaction with receptor tyrosine kinase, extracellular matrix and signal via the cytoplasmic tails [85, 285]. NCOA3 is a crucial regulator of mucin expression at both transcriptional and post-translational levels [85]. Furthermore, NCOA3 also promote the expression of chemokines in PC microenvironment, which involve in the recruitment of immune cells, activation of pancreatic stellate cells and maintenance of proinflammatory conditions [286]. Chemokine pathway CXCR4/SDF-1 axis has been significantly studied for its role in PC invasion, angiogenesis and proliferation [123, 124]. Abundant SDF-1 is produced by PC stromal cells and activates CXCR4 expression in PC cells, which also augments Shh pathway to elevate desmoplasia, enhance chemoresistance as well as promote invasion in PC [125, 126]. Multiple retrospective clinical studies have directly linked the expression of CXCR4 with poor survival and metastasis in PC patients [127, 128]. Given the critical role of NCOA3 and CXCR4 in the progress of PC, we can develop novel treatment by delivery of NCOA3-silencing siRNA using PCX. Our hypothesis is that combination of NCOA3 gene silencing and CXCR4 inhibition will reduce mucin expression, regulate tumor microenvironment, decrease desmoplasia, prevent metastasis, chemosensitize tumor cells and improve the overall anticancer activity in PC treatment (**Scheme 6**).

4.4.1 PCX selection

All of the PCX polymers were obtained by Michael-type polyaddition of cyclam-based CXCR4 antagonists as described in **4.1-4.3** [149, 152, 287]. However, the ability of the polymers to condense and deliver siRNA in PC cells was never compared

simultaneously. In order to select PCX polymers with the most optimized properties, we chose two unmodified PCX as shown in **Figure 37**: branched PCX^{G1} synthesized from a commercial CXCR4 antagonist AMD3100 and linear PCX^{G2} synthesized from a monocyclam monomers with CXCR4 antagonism. We also chose cholesterol modified PCX^{G1} (Chol17-PCX^{G1} and Chol25-PCX^{G1}) with high enzymatic stability again RNase and improved siRNA delivery. Then, PEGylated PCX^{G1} in the mixed formation was selected to prepared polyplexes with decreased positive surface charge and acceptable colloidal stability. All of the above PCX polymers would be screened simultaneously in a series of experiments, such as cytotoxicity, siRNA condensation, CXCR4 antagonism, NCOA3 gene silencing and inhibition of PC cell migration to obtain the most favorable formulation for *in vivo* studies.

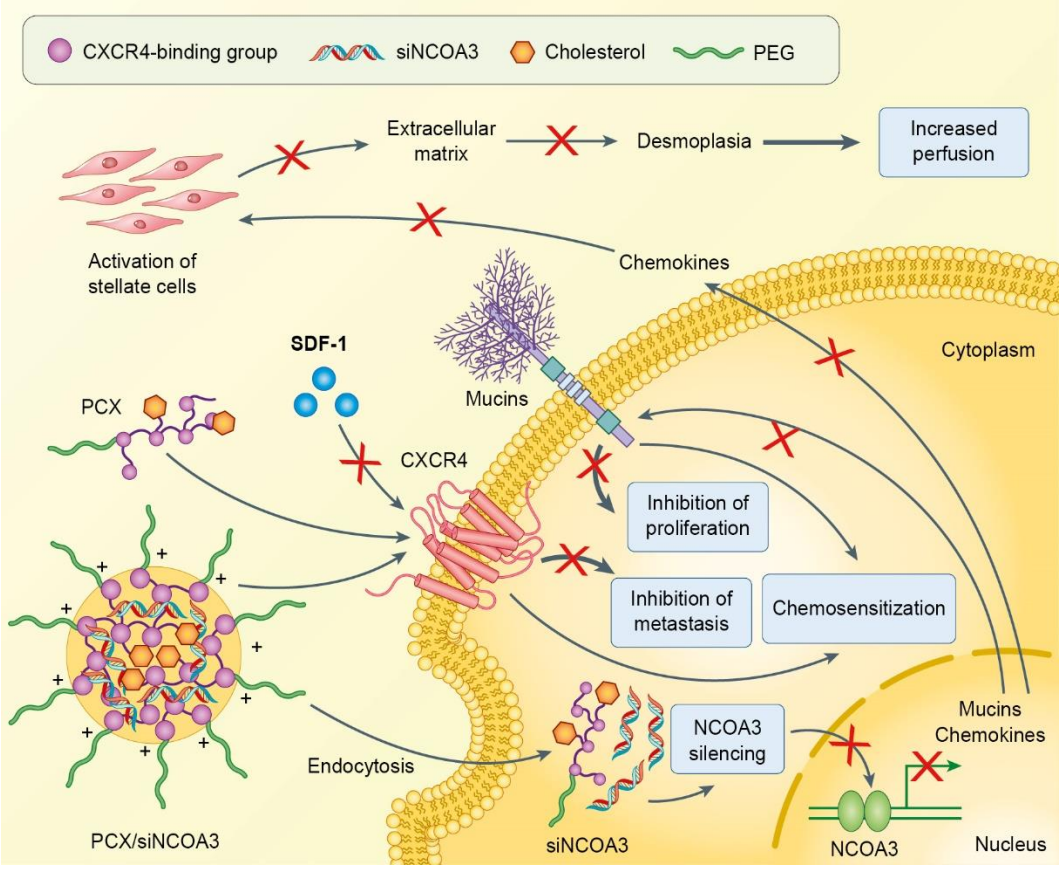

Scheme 6. Proposed mechanism of action of PCX/siNCOA3 polyplexes.

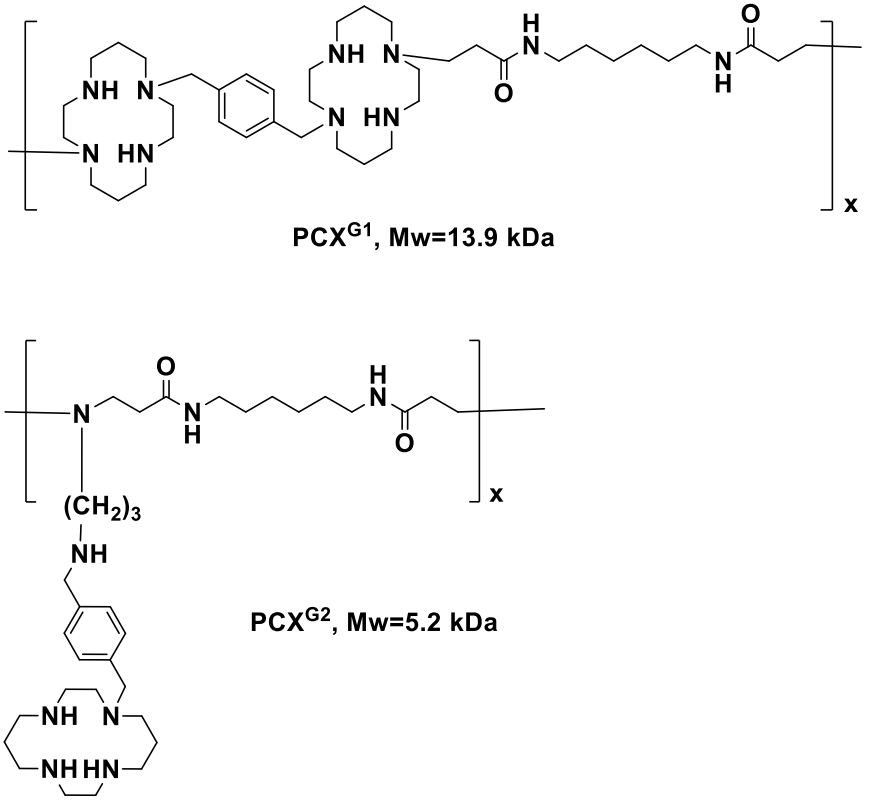

Figure 37. Chemical structures of polymeric CXCR4 inhibitors PCX^{G1} and PCX^{G2}.

4.4.2 Cytotoxicity

Before the *in vitro* experiments, toxicity of polycations have to be investigated to predict their application for delivery nucleic acid. HepG2 cells were utilized to evaluate the possible toxicity of novel compounds in liver. A shown in **Figure 38a**, all PCX exhibited significantly less toxic in comparison with benchmark commercial control PEI. Linear PCX^{G2} had lower molecular weight as well as charge density than the branched PCX^{G1} and displayed the least toxic of all the tested polymers. PEG-PCX^{G1} showed the lowest toxicity of the polymers on the basis of PCX^{G1} due to the steric hindrance of PEG that prevents interaction of the polycations with cell membranes and vital intracellular proteins [198, 288]. Cholesterol modification of PCXG1 did not impact the cytotoxicity in HepG2 cells, indicating that proper content of hydrophobic moieties would not cause cell death induced by cell membrane disruption. PC cell line CD18/HPAF.luc was used to determine the cytotoxicity of PCX and establish safe concentration for the subsequent optimization studies *in vitro*. As shown in the table of **Figure 38**, all of the PCX polymers displayed less toxicity than control PEI. However, the sensitivity of PC cells to PCX increased and the differences of IC_{50} values between PCX and PEI reduced. The preferred cytotoxicity and sensitivity of PC cells to PCX may have the potential to improve anticancer activity of PCX delivery system. More studies need to conduct to explain the phenomenon.

4.4.3 Preparation of PCX/siNCOA3 polyplexes

The ability of PCX to form polyplexes with siNCOA3 was first investigated by agarose gel electrophoresis (**Figure 38b**). All w/w ratios in this study are expressed as equivalent PCX/siRNA ratios without taking cholesterol or PEG content into consideration. The polyplexes were prepared at increasing PCX-to-siNCOA3 w/w ratios and incubated at room temperature for 20 min before use. All PCX were able to fully complex siNCOA3 at or above w/w ratio 2. The siNCOA3 binding ability of PEG-PCX was slightly weaker

than the other PCX at w/w 1, as suggested by a stronger smear of siNCOA3 releasing from loading well. The weaker complexation ability of PEG-PCX is likely due to interference of the interaction between polymer and siRNA by the long PEG chains. Therefore, all siNCOA3 polyplexes used in the following studies were prepared at w/w 2 to assure complete siRNA complexation.

4.4.4 Characterization of PCX/siNCOA3 polyplexes

Hydrodynamic size and zeta potential of PCX/siNCOA3 polyplexes were evaluated by dynamic light scattering (**Figure 38c**). Polyplexes were prepared in HBG buffer at equivalent w/w ratio of 2 and were allowed to stabilize for 20 min at room temperature before measurement. Except for PCX^{G2}/siNCOA3, all the other polyplexes displayed small particle ranging from 88 to 125 nm. All PCX/siNCOA3 polyplexes exhibited positive surface charge indicated by zeta potentials ranging from 5 to 23 mV. Cholesterol or PEG modified siNCOA3 polyplexes showed smaller sizes than PCX^{G1}/siNCOA3, perhaps suggesting tighter binding at w/w ratio of 2. However, PEGylated PCX exhibited nearly neutral zeta potential because that PEGylation shielded the positive surface charge of polyplexes [288].

4.4.5 CXCR4 antagonism of PCX/siRNA polyplexes

The CXCR4 inhibitory activity is significant for the proposed mechanism of polyplexes to inhibit cancer metastasis. CXCR4 redistribution assay was used to conduct this experiment and HCS analysis was used to quantify the extent of EGFP-CXCR4 internalization into the cells as described before [287]. In order to avoid any potential confounding effects from NCOA3 silencing, negative control siRNA (siScr) was utilized to prepare polyplexes with PCX. As shown in **Figure 39**, all PCX polyplexes displayed nearly complete CXCR4 inhibition at w/w ratio of 2, which were comparable to positive control AMD3100. Cholesterol modification induced a slight decrease in CXCR4 inhibitory activity

of the polyplexes. Chol17-PCX^{G1}/siScr and Chol25-PCX^{G1}/siScr showed 96% and 91% CXCR4 inhibition, respectively. PCX^{G1}, PCX^{G2} and PEG-PCX^{G1} were more effective than Chol17-PCX^{G1}. Polycation PEI worked as a negative control and did not display CXCR4 antagonism, indicating that the observed effect is due to the specific binding of PCX to the CXCR4 receptor, but not due to the polycationic character. After confirming the complete CXCR4 inhibitory activity of PCX, the ability of PCX to inhibit PC cell metastasis would be evaluated.

4.4.6 CXCR4 expression in PC cell line

CXCR4 overexpression increases PC cell motility and invasion, leading to enhanced metastasis [122, 289, 290]. And a growing experimental and clinical evidence shows that anticancer therapies can promote hypoxic environment and increase CXCR4 expression, which may inadvertently enhance the metastatic potential of the tumors [291-293]. It is also reported that CXCR4/SDF-1 signaling plays an important role in gemcitabine resistance of PC cells. Gemcitabine up-regulates CXCR4 expression in PC cells (Colo357 and MiaPaCa) and promotes their invasiveness, indicating that some current chemodrug administration may cause aggressive phenoty of PC [294]. Here, we used CD18/HPAF.luc cells as PC model in the study. To detect the CXCR4 expression after gemcitabine treatment in CD18/HPAF.luc cells, the changes of CXCR4 expression on cell membrane were determined by flow cytometry and changers at total protein level were analyzed by western blot. As shown in **Figure 40**, the population of CXCR4-positive CD18/HAPF.luc cells enhanced from 11.3% to 18% after treatment with 10 μM gemcitabine for 24 h. Similarly, western blot analysis corroborated this finding, as there was a noticeable increase in CXCR4 expression in CD18/HPAF.luc cells (1.75-fold and 1.7-fold) at both 1 and 10 μM gemcitabine concentrations. Therefore, we will test the ability of PCX to prevent CXCR4-mediated migration of PC cells in the following study.

(a) Cytotoxicity of PCX (IC50 in µg/mL)

Cell line	PCX^{G1}	Chol17 -PCX^{G1}	Chol25 -PCX^{G1}	PCX^{G2}	PEG-PCX^{G1}	PEI
CD18/HPAF.luc	16.3	25.8	44.5	25.4	22.2	11.1
HepG2	52.3	47.9	59.6	185	144	25.1

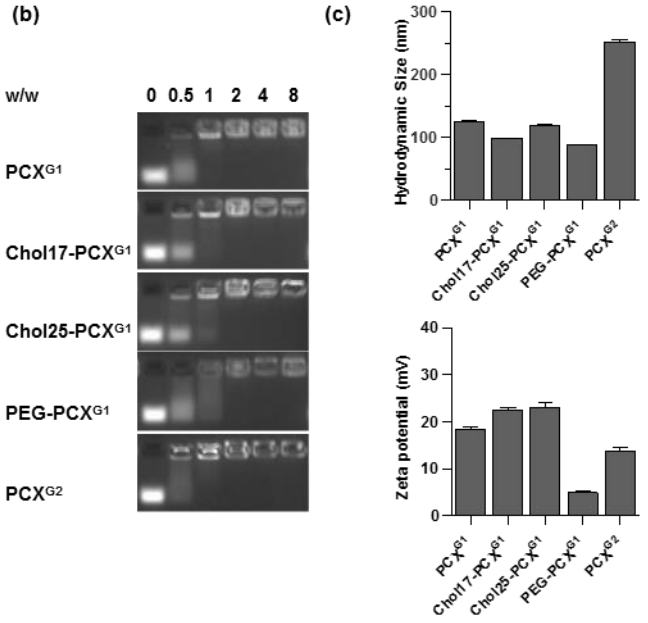

Figure 38. Characterization of PCX and PCX/siNCOA3 polyplexes. (a) Cytotoxicity of PCX in HepG2 and CD18/HPAF.luc cells. IC_{50} (in µg/mL) were calculated as the polymer concentration that achieves 50% decrease in cell viability relative to untreated cells (n = 3). (b) Ability of PCX to form polyplexes with siNCOA3 evaluated by agarose gel retardation assay at increasing PCX/siNCOA3 w/w ratios. (c) Hydrodynamic size and zeta potential of PCX/siNCOA3 polyplexes prepared at w/w 2 (mean ± SD, n = 3). All polyplexes were prepared in HBG at siNCOA3 concentration of 20 µg/mL.

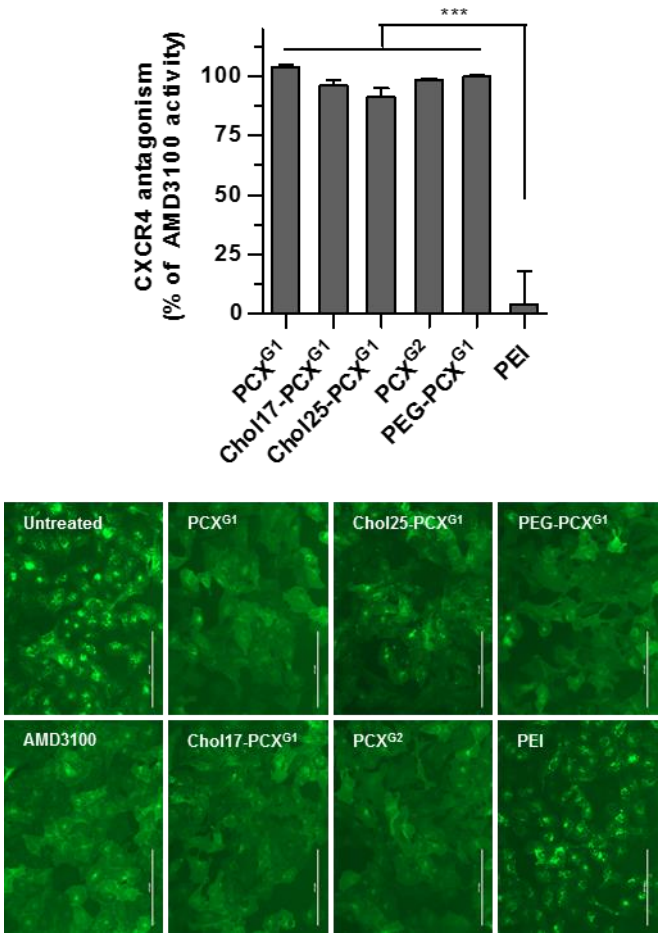

Figure 39. CXCR4 antagonism of PCX/siScr polyplexes (polymer = 1 µg/mL, w/w 2) in U2OS cells. (a) The results are shown as mean % CXCR4 inhibition relative to AMD3100 ± SD (n=4). One-way ANOVA with Tukey-Kramer multiple comparisons test (***P<0.001 vs. PEI). (b) Representative images of EGFP-CXCR4 distribution in cells treated with different polymers. The scale bar = 200 µm.

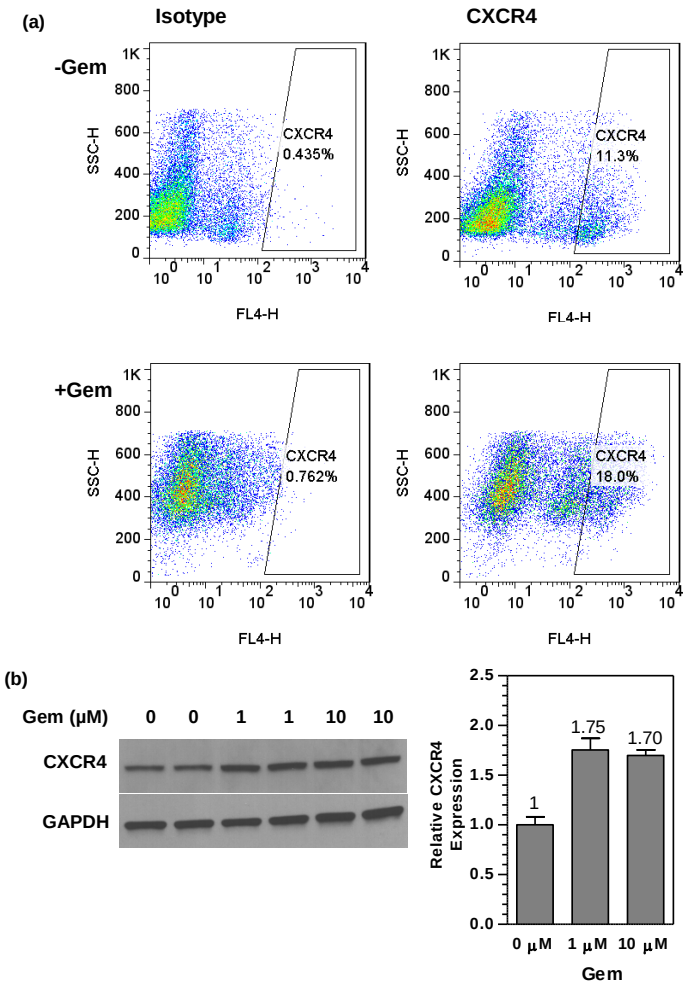

Figure 40 Effect of gemcitabine (Gem) on the CXCR4 expression in CD18/HPAF.luc PC cells. (a) Cell surface CXCR4 expression in CD18/HPAF.luc cells by flow cytometry before and after gemcitabine treatment. (b) Total cellular CXCR4 expression by Western blot (n=2). Results are expressed as ratio of a mean relative CXCR4 expression vs. cells not treated with gemcitabine (n=2).

4.4.7 Inhibition of PC cell migration by PCX

As we confirmed, CXCR4 expression was enhanced by gemcitabine treatment in CD18/HPAF.luc cells. We studied the migration of gemcitabine-treated CD18/HPAF.luc cells in a Boyden chamber using 10% serum as the chemotactic signal. PC cells were pretreated with 10 µM gemcitabine for 24 h and 10^5 cells were loaded into each insert on the next day. As shown in **Figure 41**, without gemcitabine treatment, seldom cells migrated through the membrane. However, gemcitabine promoted the aggressiveness of PC cells and increased their metastasis. CXCR4 antagonists can inhibit migration of cancer cells that are based on the CXCR4/SDF1 axis. We have shown that PCX and their polyplexes inhibited CXCR4-mediated migration and invasion in human osteosarcoma and cholangiocarcinoma cells [152, 287, 295]. Here, we would like to investigate the ability of PCX to prevent CXCR4-medicated migration in CD18/HPAF.luc cells (**Figure 42**). After pretreated with 10 µM gemcitabine for 24 h, $2x10^5$ cells were loaded into each insert. Untreated cells migrated significantly toward the chemotactic gradient. Small-molecule CXCR4 antagonist AMD3100 was able to reduce the number of migrated cells by 29.5%. However, all tested PCX PCX were capable to effectively inhibit cell migration at 1 µg/mL, ranging from 38% for Chol25-PCX^{G1} to 43% for PCX^{G2}, which was more efficient than conventional CXCR4 inhibitors. In contrast, polycation control PEI was not observed any inhibitory effect on cell migration, suggesting that PCX would be well-suited for applications in treatment of PC that aim at preventing or delaying metastasis.

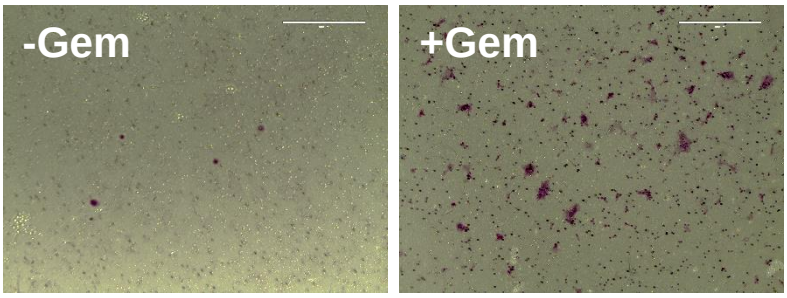

Figure 41. Migration of PC cell enhanced after gemcitabine treatment. CD18/HPAF.luc were pretreated with or without 10 µM gemcitabine for 24 h. 10^5 cells were loaded into the insert and culture medium containing 10% FBS was used as chemoattractant. Images were taken at 10x magnification (scale bar = 400 µm).

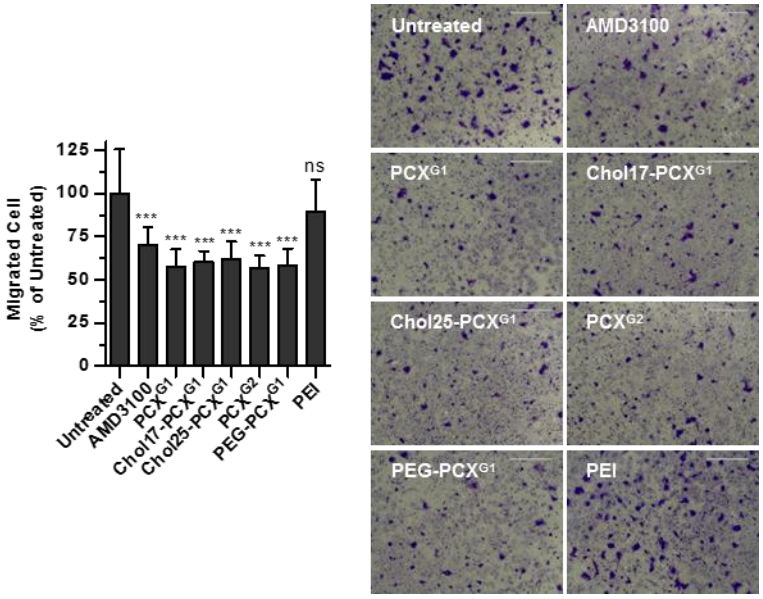

Figure 42. Inhibition of PC cell migration by PCX (1 µg/µL). CD18/HPAF.luc cells were treated with 10 µM gemcitabine for 24 h before the migration study. $2x10^5$ cells were loaded into the insert. Migrated cells were counted in 4 randomly selected imaging areas at 10x magnification of triplicate samples (scale bar = 400 µm). One-way ANOVA with Tukey-Kramer multiple comparisons test (***P<0.001, vs. untreated cells).

4.4.8 NCOA3 silencing by PCX/siNCOA3 polyplexes

After evaluating the ability of PCXs to form polyplexes with NCOA3 siRNA and inhibit the migration of PC cells, we have studied the capacity to deliver siNCOA3 and downregulate NCOA3 in PC cells. The NCOA3 silencing by PCX polyplexes at protein level was analysed by western blot. PCX polyplexes were formulated at w/w of 2 using either siNCOA3 or a negative control siRNA (siScr). PEI/siRNA (w/w 1.5) polyplexes were used as controls.

As shown **in Figure 43**, Chol17-PCX and Chol25-PCX exhibited significantly higher NCOA3 knock-down (78% and 52% respectively) than other PCX polyplexes (PCX-1 = 21%, PCX-2 = 9.6%, PEG-PCX = 3.5%). PEI displayed second high NCOA3 gene silencing with 59%, however, it caused significant off-target effects as indicated by decreased NCOA3 levels observed with PEI/siScr [296]. Chol17-PCX was chosen to form dual-function polyplexes with siNCOA3 to treat PC *in vivo*, due to the highest NCOA3 gene silencing and effective inhibition of cell migration.

4.4.9 Inhibition of primary pancreatic tumor growth by PCX/siNCOA3 polyplexes

CXCR4 and its ligand CXCL12 promote metastatic and invasive process of PC, fostered by the expression of matrix-metalloproteinase including MMP-2 and MMP-9 [297-300]. Except the role of CXCR4/SDF-1 axis in PC metastasis, it also extensively involved in tumor proliferation [122, 289, 290]. NCOA3 is a chromatin remodelling enzyme, which plays a vital role in mucins regulation, creates pro-inflammatory conditions and modulates tumor microenvironment to promote growth and dissemination of PC cells [85]. Therefore, both CXCR4 and NCOA3 are involved in the proliferation of PC cells and in maintenance of tumor microenvironment that promotes metastatic spread.

First, we tested whether combining inhibition of CXCR4 and NCOA3 affects the growth of the primary PC tumors. The antitumor activity of Chol17-PCX^{G1}/siNCOA3 polyplexes was evaluated in orthotopic pancreatic cancer animal model. CD18/HPAF.luc cells were implanted into the pancreas of female nude mice and allowed to grow for 10 days. As shown in **Figure 44**, the body weight of mice decreased less than 10% after tumor implantation. However, all of the mice recovered after 7 days.

10 days after orthotopic implantation of CD18/HPAF.luc cells, the presence of the tumors was established by whole-body bioluminescence imaging and mice were randomized into three experimental groups (saline, Chol17-PCX^{G1}/siScr, and Chol17-PCX ^{G1}/siNCOA3). Polyplexes were prepared at a polycation/siRNA w/w ratio of 2 and administrated by tail vein injections with 40 µg siRNA/mouse, 3 times per week and 13 courses in total. None of the treatments caused any significant effect or lose on the body weight, indicating the nontoxicity of the injected PCX/siNCOA3 polyplexes.

Mice were sacrificed on day 39 post-implantation. Treatments with both PCX/siScr and PCX/siNCOA3 slowed down the progresses of primary pancreatic tumor (**Figure 45 a-b**). However, the combination of CXCR4 inhibition and NCOA3 silencing showed significantly better effect on slowing down the growth of primary PC than PCX/siScr, suggesting the superior activity of combination treatment. As shown in **Figure 45c,** the NCOA3 gene silencing in primary PC tumors was confirmed by qRT-PCR. PCX/siNCOA3 induced 30% NCOA3 gene silencing compared with saline group, which had significantly statistical difference ($P<0.01$).

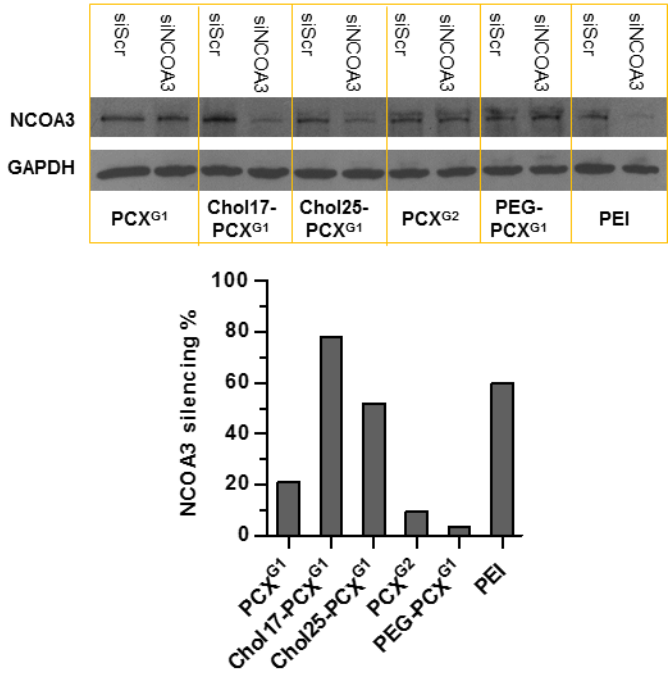

Figure 43. NCOA3 gene silencing by PCX/siNCOA3 polyplexes in CD18/HPAF.luc PC cells. NCOA3 silencing was determined by Western blot (top) using polyplexes prepared at w/w ratio of 2 and used at 200 nM siRNA. The percent of NCOA3 silencing (bottom) was calculated from NCOA3 band intensity of PCX/siNCOA3 relative to the corresponding PCX/siScr control. PEI polyplexes were prepared at w/w 1.5.

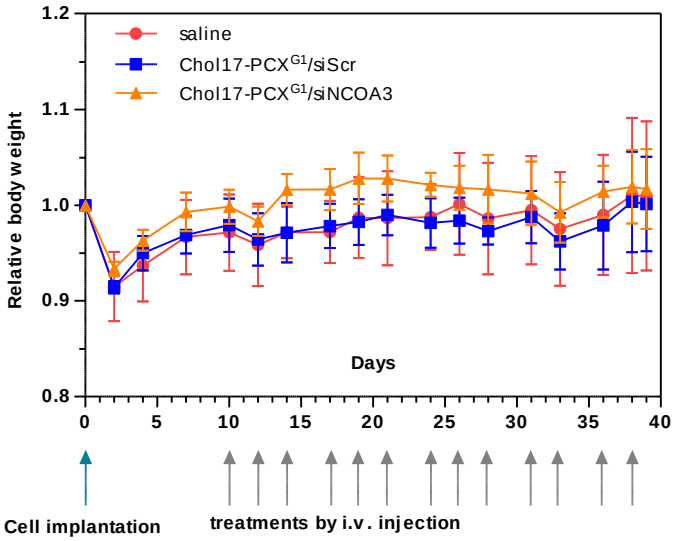

Figure 44. Average body weight after orthotopic implantation of CD18/HPAF.luc cells and during treatment with Chol17-PCX^{G1}/siNCOA3 (n=6), Chol17-PCX^{G1}/siScr (n=7), and saline (n=7). The results were expressed as average of relative body weights ± SD values.

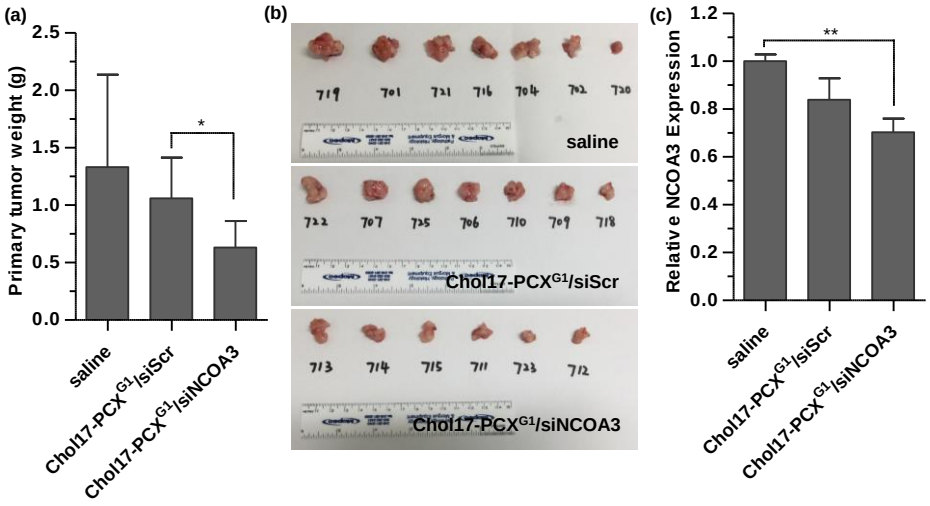

Figure 45. Effect of systemic treatment with Chol17-PCX^{G1}/siNCOA3 (w/w 2) on the growth of primary pancreatic tumor. (a) Primary tumor weights were measured after necropsy. (b) Photograph of resected primary PC tumors. (c) Silencing of NCOA3 expression in the primary PC tumors by RT-PCR (results shown as ratio of mean relative NCOA3 expression compared with saline treated mice ± SD (n=3)). Statistical comparisons by unpaired t-test (***p<0.001, **p<0.01, *p<0.05).

4.4.10 Antimetastatic effect of PCX/siNCOA3 polyplexes

One of the significant reasons for low survival rate in PC is early metastasis. PC metastasize to a broad range of organs, such as pericardium, stomach, spleen diaphragm, small and large intestines, gallbladder, and ovaries [301, 302]. However, the most common metastatic site is liver. As shown in **Figure 46**, the mice from saline group had metastasis in a wide range of organs on day 39. All saline treated mice displayed metastasis in the ovary and stomach, six out seven showed tumor spread to in small intestine and diaphragm, five out seven had metastasis in liver, spleen and lymph node. Furthermore, they also showed metastasis in kidney and large intestine. Treatment with PCX/siScr, which inhibited CXCR4 in PC, reduced the metastasis in all of the organs except spleen. Specifically, the incidence of stomach metastasis was much lower in the PCX/siScr group compared with the saline group, which had statistically significant in Fisher's exact test ($p=0.0047$). Combination treatment with PCX/siNCOA3 greatly resulted in much lower incidence of metastasis in all of the organs. Statistically significant differences were observed in the incidences of metastases in liver, ovary and stomach between PCX/siNCOA3 and saline groups. And PCX/siNCOA3 showed better effect on preventing metastasis in liver, diaphragm, ovary, lymph node and stomach than PCX/siScr, indicating that both CXCR4 inhibition and NCOA3 knock-down contributed to the overall antimetastatic activity of the polyplexes for PC therapy.

4.4.11 Regulation of mucin expression and hypoxic environment by PCX/siNCOA3 polyplexes

Mucins are critical of PC progression, metastasis and chemoresistance. NCOA3 regulates mucin expression at both transcriptional and post-translational levels [85]. As confirmed by the immunohistochemistry analysis in **Figure 47a**, NCOA3 silencing reduced the expression of Muc4 significantly in PC primary tumors. Down-regulation of NCOA3

also has shown to cause significant decrease in the expression of LOXL2, which participates in fibroblast activation and hardening of desmoplasia [85]. Multiple chemokines in PC microenvironment are enhanced by NCOA3 overexpression and involves in the activation of pancreatic stellate cells, recruitment of immune cells as well as maintenance of pro-inflammatory conditions. Pancreatic stellate cells secret large amount of collagens and extracellular matrix proteins, which are crosslinked by LOXL2, leading to the formation of desmoplasia, poor tumor perfusion and severe hypoxia in PC microenvironment. As shown in **Figure 47a**, the H&E staining revealed the inner structure of primary PC tumors. The less purple (pink) part corresponded to the tumor necrosis, which was induced by the hypoxia in tumor microenvironment. **Figure 47b** revealed that treatment with PCX/siNCOA3 significantly decreased the necrotic area in PC primary tumors from about 17% to 2.5% in comparison with PCX/siScr and saline group.

4.4.12 Tumor perfusion enhanced by PCX/siNCOA3 polyplexes

Desmoplasia subsequently caused collapse of the blood vessels, poor tumor perfusion, increased interstitial pressure, extreme hypoxia, and poor delivery of therapeutics. If the tumor perfusion is enhanced, more chemotherapeutics can be delivered into PC tissues and improve the chemosensitivity. It was reported that inhibition of LOXL2 reduced extracellular matrix and desmoplasia [303, 304]. In order to investigate whether tumor perfusion can be improved by PCX/siNCOA3 treatment, tumor perfusion was evaluated by magnetic resonance imaging. As shown in **Figure 48**, PC tumor perfusion was enhanced after NCOA3 silencing, which was due to its role in desmoplastic reaction. After treatment with PCX/siNCOA3, the tumor perfusion increased from 44.3 to 62.5 mL/100 g/min. The enhanced tumor perfusion will facilitate drug delivery, regulate PC microenvironment, ameliorate hypoxia condition, improve the chemosensitivity and decrease the aggressiveness in PC.

4.4.13 Conclusion

We have designed dual-function polyplexes to simultaneously deliver siNCOA3 and inhibit CXCR4 chemokine receptor to treat pancreatic cancer. Our study tested a series of PCX formed polyplexes and screened formulations that can effectively knock down NCOA3 expression at protein level. Cholesterol modification of PCX provided the most optimized set of properties to achieve CXCR4 antagonism, siRNA delivery and efficient gene silencing in PC. Our results demonstrates that combining the tumor microenvironment regulation by NCOA3 silencing and antimetastatic effect of CXCR4 antagonism led to slow-down of pancreatic tumor progress, prevention of tumor metastasis to distant organs, decrease of Muc4 expression in primary tumors and enhancement of perfusion in PC microenvironment. Since desmoplasia and CXCR4 overexpression are characteristic features of both primary and metastatic PC tumors, the developed PCX polyplexes are suitable for delivery to both primary and metastatic PC sites [305]. Furthermore, regulation of tumor microenvironment led to enhanced tumor perfusion, however, may also facilitate cancer cell metastasis out of primary site. Therefore, combining tumor-microenvironment modulating strategies with simultaneous antimetastatic ability of CXCR4-inhibiting polymers has the potential to minimize any side effects. Future development of these dual-function systems will focus on optimization of NCOA3 silencing *in vivo* to decrease the treatment courses and improve overall antitumor effects with combination of chemodrugs.

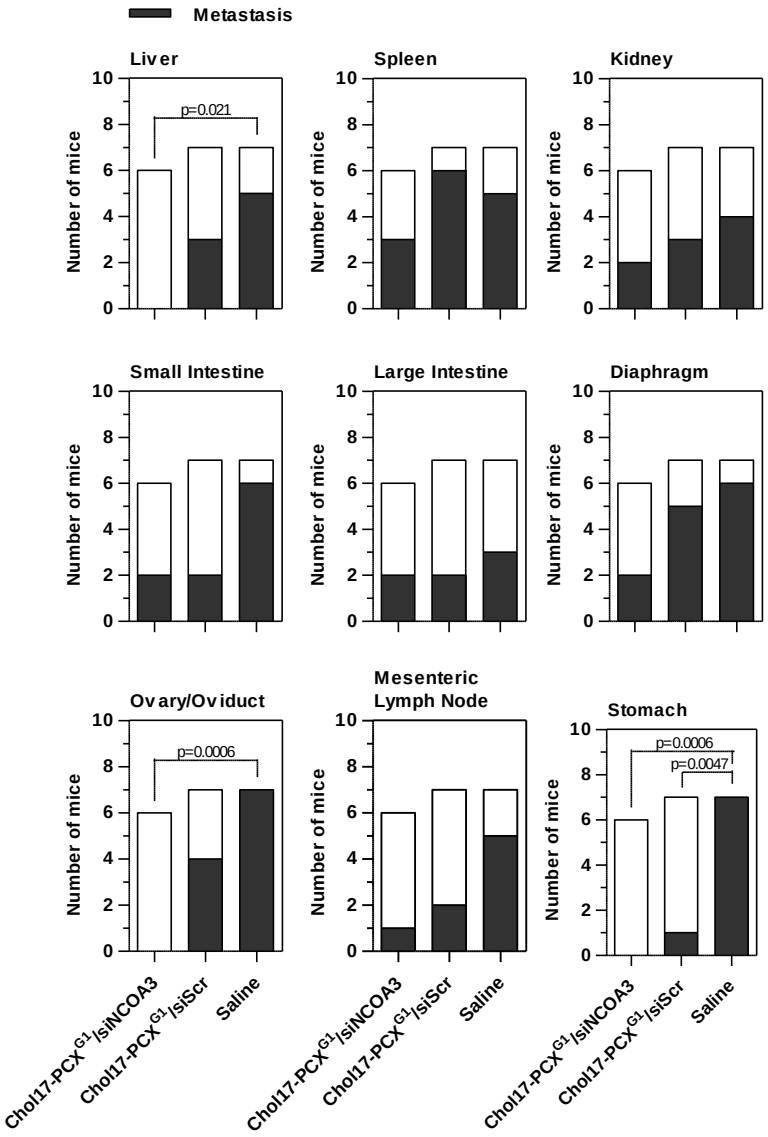

Figure 46. Effect of PCX/siNCOA3 treatment on the incidence of PC metastasis in the orthotopic CD18/HPAF.luc PC model. The presence of metastasis in major organs and tissues was determined on day 39 following implantation of the PC cells in mice. Fisher's exact test was used to compare the incidence of metastasis between groups and $p<0.05$ was considered to be statistically significant.

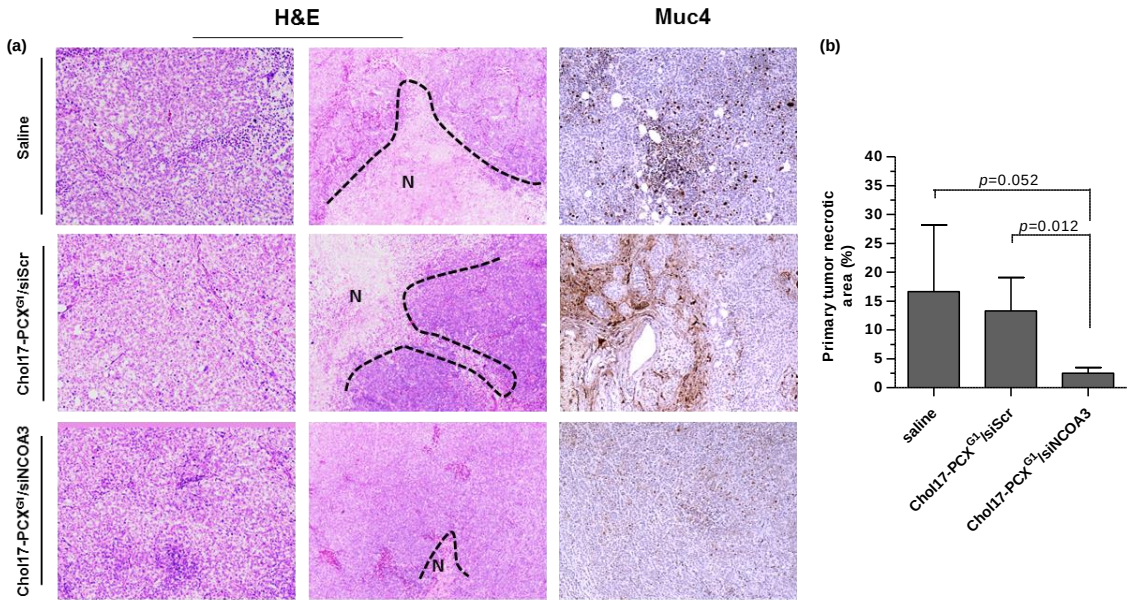

Figure 47. Analysis of primary pancreatic tumors after treatment with Chol17-PCX^{G1}/siNCOA3 polyplexes. (a) H&E staining and MUC4 immunohistochemistry analysis (magnification 40x). (b) Extent of necrosis in primary tumor determined from the H&E staining.

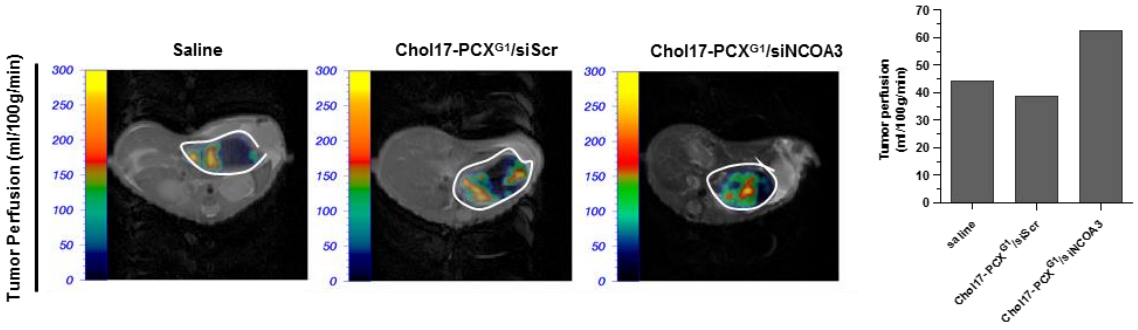

Figure 48. Primary tumor perfusion on day 39 determined from magnetic resonance imaging.

Chapter 5 – Overall Conclusions, Significance and Future Studies

Metastasis is the main cause of cancer mortality and morbidity, resulting in several million deaths annually. Unfortunately, existing therapeutic approaches rarely reverse or stop metastatic progression. For PC, less than 20% of patients are candidates for surgery due to spread beyond the pancreas. Gemcitabine is the first-line treatment for metastatic pancreatic cancer. However, the objective response rate is less than 10%. The emergence of desmoplasia in PC is becoming a problem which presents substantial barriers to perfusion, diffusion, and convection of antitumor therapeutics into the PC tissues. It results in collapse of the blood vessels, increases interstitial pressure, extreme hypoxia, poor tumor perfusion, and poor delivery of therapeutics. Thus, there is very urgent need to develop therapies that focus on regulating tumor microenvironment, chemosensitizing tumor to therapeutics and preventing metastasis.

Small interfering RNA (siRNA) has rapidly emerged as one of the most promising new therapeutic agents for the treatment of many diseases. The capacity of siRNA to selectively destroy any mRNA sequences offers the possibility to alter the behavior of pathological cells. siRNA has shown great potential for therapeutic benefits even in complex diseases like cancer [306]. PLK1 is a key mitotic regulator in mammalian cells, which is an attractive target in cancer treatment [269, 270]. PLK1 expression is elevated in multiple types of human cancers and it has a prognostic value for predicting aggressiveness of cancer [271]. Inhibition of PLK1 by using gene silencing with siRNA results in cell apoptosis and inhibition of tumor growth. NCOA3 is a master regulator of musin expression in PC both at the transcriptional and post-translational levels [307]. The NCOA3 expression is significantly elevated in primary PC tumors and in metastatic lung, lymph and liver lesions. NCOA3 also upregulates the expression of chemokines to impact tumor microenvironment. NCOA3 silencing by siRNA leads to downregulate the

expression of mucins and diminish desmoplasia to enhance treatment. A major obstacle that currently prevents the clinical use of siRNA therapy is a lack of reliable methods to deliver siRNA to target cells. The short half-life of siRNA in blood circulation and the need for intracellular cytoplasmic delivery represent major challenges for clinical translation [308]. Therefore, the effective delivery system should be developed.

CXCR4 and its chemokine ligand SDF-1 play a crucial role in the crosstalk between cancer cells and their microenvironment, and are involved in tumor progression, angiogenesis, metastasis and survival. Many clinical studies show that CXCR4 expression in various cancers (e.g. PC) is associated with more aggressive disease, more metastases, and shorter overall patient survival. This dissertation addresses the need for such therapies by exploiting the decisive role of CXCR4 chemokine receptor in the metastatic spread of PC as a target for development of combination treatments based on dual-function nanoparticles. There is growing evidence that inhibition of CXCR4 has the potential to prevent metastasis and limit tumor growth. Metastasis is a systemic disease and therefore, effective methods of systemic delivery of the treatments are necessary. By developing nanoparticles capable of simultaneous CXCR4 inhibition and delivery of antitumor therapeutic siRNA, we are able to prevent metastasis and improve overall anticancer activity.

We have successfully synthesized CXCR4-inhibiting polycations (PCX) using Michael polyaddition. The PCX could self-assemble into nanosized particles with nucleic acids through electrostatic interaction and function as efficient transfection agent while exhibiting effective CXCR4 antagonism. To enhance the CXCR4 antagonism, we reported synthesis of novel monocyclam monomers and their polymerization to PCX. The CXCR4 inhibitory activity of the synthesized monocyclam monomers increased significantly following incorporation into the polymers. Furthermore, the CXCR4 inhibitory activity of

second generation of PCX was higher compared with the previously reported polymers based on commercial CXCR4 antagonist AMD3100, confirming the importance of a proper presentation of the ligands within synthetic polymers. To improve the physical properties and safety of PCX, it was modified by PEGylation. Our results demonstrated that modification of PCX with PEG decreased toxicity of the polymers, while preserving their CXCR4 antagonism. Polyplexes prepared with PEG-PCX inhibited invasion of cancer cells to an extent similar to the commercial CXCR4 antagonist Plerixafor. Negative effect of PEG on transfection activity of PEG-PCX polyplexes could be overcome by using polyplexes formulated with a mixture of PCX and PEG-PCX. Although efficient in DNA delivery, the original PCX exhibited poor siRNA delivery activity. Therefore, we developed PCX as siRNA delivery vectors to achieve combined antimetastatic and antitumor effect. PCX was modified with cholesterol, which led to increased overall stability, cell uptake as well as intracellular trafficking of siRNA polyplexes. After obtaining a series of dual-function PCX polymers with the conceptually new approach to deliver therapeutic nucleic acids and preventing cancer metastasis, NCOA3 siRNA was chosen to form nanoparticles with PCX to address unresolved problems of chemoresistance and provide an immediate therapeutic opportunity for the lethal PC. We tested a series of PCX formed polyplexes and screened formulations that can effectively knock down NCOA3 expression at protein level. Our results demonstrate that in the combination of the tumor microenvironment regulation by NCOA3 silencing with antimetastatic effect of CXCR4 antagonism, slow-down of the pancreatic tumor progress, prevention of tumor metastasis to distant organs, decrease of mucin expression in primary tumors and enhancement of perfusion in tumor microenvironment were achieved.

Despite tremendous promise in anticancer therapies, siRNA is nearly certainly to be used in combination with other treatments. Our study supports the use of

PCX/siNCOA3 as a promising neoadjuvant or adjuvant treatment with conventional chemotherapeutics such as gemcitabine. Our future studies will focus on improving the polyplex formulations and on the anticancer and antimetastatic effect of these polyplexes in combination with gemcitabine. We predict that increased tumor perfusion observed here, together with chemosensitizing effect of NCOA3 knockdown and related mucin downregulation will improve activity. Further, given the well-established fact that gemcitabine treatment upregulates CXCR4 expression in pancreatic cancer, the use of PCX in the siNCOA3 delivery is an ideal choice. However, the NCOA3 silencing of dual-function systems will be optimized *in vivo* to decrease the treatment courses and improve overall antitumor effects.

Bibliography

[1] Y. Wang, Y. Xie, D. Oupicky, Potential of CXCR4/CXCL12 Chemokine Axis in Cancer Drug Delivery, Current pharmacology reports, 2 (2016) 1-10.

[2] Y. Zhang, P. Yang, X.F. Wang, Microenvironmental regulation of cancer metastasis by miRNAs, Trends in cell biology, 24 (2014) 153-160.

[3] D. Hanahan, Robert A. Weinberg, Hallmarks of Cancer: The Next Generation, Cell, 144 (2011) 646-674.

[4] D.X. Nguyen, P.D. Bos, J. Massague, Metastasis: from dissemination to organ-specific colonization, Nature reviews. Cancer, 9 (2009) 274-284.

[5] T. Oskarsson, E. Batlle, J. Massague, Metastatic stem cells: sources, niches, and vital pathways, Cell stem cell, 14 (2014) 306-321.

[6] D.F. Quail, J.A. Joyce, Microenvironmental regulation of tumor progression and metastasis, Nature medicine, 19 (2013) 1423-1437.

[7] J.A. Joyce, J.W. Pollard, Microenvironmental regulation of metastasis, Nature reviews. Cancer, 9 (2009) 239-252.

[8] N. Navin, J. Kendall, J. Troge, P. Andrews, L. Rodgers, J. McIndoo, K. Cook, A. Stepansky, D. Levy, D. Esposito, L. Muthuswamy, A. Krasnitz, W.R. McCombie, J. Hicks, M. Wigler, Tumour evolution inferred by single-cell sequencing, Nature, 472 (2011) 90-94.

[9] L. Ding, M.J. Ellis, S. Li, D.E. Larson, K. Chen, J.W. Wallis, C.C. Harris, M.D. McLellan, R.S. Fulton, L.L. Fulton, R.M. Abbott, J. Hoog, D.J. Dooling, D.C. Koboldt, H. Schmidt, J. Kalicki, Q. Zhang, L. Chen, L. Lin, M.C. Wendl, J.F. McMichael, V.J. Magrini, L. Cook, S.D. McGrath, T.L. Vickery, E. Appelbaum, K. Deschryver, S. Davies, T. Guintoli, L. Lin, R. Crowder, Y. Tao, J.E. Snider, S.M. Smith, A.F. Dukes, G.E. Sanderson, C.S. Pohl, K.D.

Delehaunty, C.C. Fronick, K.A. Pape, J.S. Reed, J.S. Robinson, J.S. Hodges, W. Schierding, N.D. Dees, D. Shen, D.P. Locke, M.E. Wiechert, J.M. Eldred, J.B. Peck, B.J. Oberkfell, J.T. Lolofie, F. Du, A.E. Hawkins, M.D. O'Laughlin, K.E. Bernard, M. Cunningham, G. Elliott, M.D. Mason, D.M. Thompson, Jr., J.L. Ivanovich, P.J. Goodfellow, C.M. Perou, G.M. Weinstock, R. Aft, M. Watson, T.J. Ley, R.K. Wilson, E.R. Mardis, Genome remodelling in a basal-like breast cancer metastasis and xenograft, Nature, 464 (2010) 999-1005.

[10] S. Yachida, S. Jones, I. Bozic, T. Antal, R. Leary, B. Fu, M. Kamiyama, R.H. Hruban, J.R. Eshleman, M.A. Nowak, V.E. Velculescu, K.W. Kinzler, B. Vogelstein, C.A. Iacobuzio-Donahue, Distant metastasis occurs late during the genetic evolution of pancreatic cancer, Nature, 467 (2010) 1114-1117.

[11] S.A. Mani, W. Guo, M.J. Liao, E.N. Eaton, A. Ayyanan, A.Y. Zhou, M. Brooks, F. Reinhard, C.C. Zhang, M. Shipitsin, L.L. Campbell, K. Polyak, C. Brisken, J. Yang, R.A. Weinberg, The epithelial-mesenchymal transition generates cells with properties of stem cells, Cell, 133 (2008) 704-715.

[12] J.P. Thiery, H. Acloque, R.Y. Huang, M.A. Nieto, Epithelial-mesenchymal transitions in development and disease, Cell, 139 (2009) 871-890.

[13] M. Labelle, S. Begum, R.O. Hynes, Direct signaling between platelets and cancer cells induces an epithelial-mesenchymal-like transition and promotes metastasis, Cancer cell, 20 (2011) 576-590.

[14] A.K. Bonde, V. Tischler, S. Kumar, A. Soltermann, R.A. Schwendener, Intratumoral macrophages contribute to epithelial-mesenchymal transition in solid tumors, BMC cancer, 12 (2012) 35.

[15] J. Condeelis, J.W. Pollard, Macrophages: obligate partners for tumor cell migration, invasion, and metastasis, Cell, 124 (2006) 263-266.

[16] D.I. Gabrilovich, S. Ostrand-Rosenberg, V. Bronte, Coordinated regulation of myeloid cells by tumours, Nature reviews. Immunology, 12 (2012) 253-268.

[17] F. van Zijl, M. Mair, A. Csiszar, D. Schneller, G. Zulehner, H. Huber, R. Eferl, H. Beug, H. Dolznig, W. Mikulits, Hepatic tumor-stroma crosstalk guides epithelial to mesenchymal transition at the tumor edge, Oncogene, 28 (2009) 4022-4033.

[18] R. Kalluri, M. Zeisberg, Fibroblasts in cancer, Nature reviews. Cancer, 6 (2006) 392-401.

[19] G.S. Karagiannis, T. Poutahidis, S.E. Erdman, R. Kirsch, R.H. Riddell, E.P. Diamandis, Cancer-associated fibroblasts drive the progression of metastasis through both paracrine and mechanical pressure on cancer tissue, Molecular cancer research : MCR, 10 (2012) 1403-1418.

[20] A. Orimo, P.B. Gupta, D.C. Sgroi, F. Arenzana-Seisdedos, T. Delaunay, R. Naeem, V.J. Carey, A.L. Richardson, R.A. Weinberg, Stromal fibroblasts present in invasive human breast carcinomas promote tumor growth and angiogenesis through elevated SDF-1/CXCL12 secretion, Cell, 121 (2005) 335-348.

[21] E.I. Deryugina, J.P. Quigley, Matrix metalloproteinases and tumor metastasis, Cancer metastasis reviews, 25 (2006) 9-34.

[22] C. Dayer, I. Stamenkovic, Recruitment of Matrix Metalloproteinase-9 (MMP-9) to the Fibroblast Cell Surface by Lysyl Hydroxylase 3 (LH3) Triggers Transforming Growth Factor-beta (TGF-beta) Activation and Fibroblast Differentiation, The Journal of biological chemistry, 290 (2015) 13763-13778.

[23] G.L. Semenza, Hypoxia-inducible factors in physiology and medicine, Cell, 148 (2012) 399-408.

[24] S. Chouaib, Y. Messai, S. Couve, B. Escudier, M. Hasmim, M.Z. Noman, Hypoxia promotes tumor growth in linking angiogenesis to immune escape, Frontiers in immunology, 3 (2012) 21.

[25] M. Sidani, J. Wyckoff, C. Xue, J.E. Segall, J. Condeelis, Probing the microenvironment of mammary tumors using multiphoton microscopy, Journal of mammary gland biology and neoplasia, 11 (2006) 151-163.

[26] L.J. Gay, B. Felding-Habermann, Contribution of platelets to tumour metastasis, Nature reviews. Cancer, 11 (2011) 123-134.

[27] A.F. Chambers, G.N. Naumov, H.J. Varghese, K.V. Nadkarni, I.C. MacDonald, A.C. Groom, Critical steps in hematogenous metastasis: an overview, Surgical oncology clinics of North America, 10 (2001) 243-255, vii.

[28] M. Pein, T. Oskarsson, Microenvironment in metastasis: roadblocks and supportive niches, American journal of physiology. Cell physiology, 309 (2015) C627-638.

[29] L. Rahib, B.D. Smith, R. Aizenberg, A.B. Rosenzweig, J.M. Fleshman, L.M. Matrisian, Projecting cancer incidence and deaths to 2030: the unexpected burden of thyroid, liver, and pancreas cancers in the United States, Cancer research, 74 (2014) 2913-2921.

[30] S. Kaur, S. Kumar, N. Momi, A.R. Sasson, S.K. Batra, Mucins in pancreatic cancer and its microenvironment, Nature reviews. Gastroenterology & hepatology, 10 (2013) 607-620.

[31] N. Le, M. Sund, A. Vinci, G.c.g.o. Pancreas, Prognostic and predictive markers in pancreatic adenocarcinoma, Digestive and liver disease : official journal of the Italian

Society of Gastroenterology and the Italian Association for the Study of the Liver, 48 (2016) 223-230.

[32] C. Feig, A. Gopinathan, A. Neesse, D.S. Chan, N. Cook, D.A. Tuveson, The pancreas cancer microenvironment, Clinical cancer research : an official journal of the American Association for Cancer Research, 18 (2012) 4266-4276.

[33] L. Rahib, B.D. Smith, R. Aizenberg, A.B. Rosenzweig, J.M. Fleshman, L.M. Matrisian, Projecting Cancer Incidence and Deaths to 2030: The Unexpected Burden of Thyroid, Liver, and Pancreas Cancers in the United States, Cancer Res., 74 (2014) 2913-2921.

[34] C.J. Whatcott, H. Han, R.G. Posner, G. Hostetter, D.D. Von Hoff, Targeting the tumor microenvironment in cancer: why hyaluronidase deserves a second look, Cancer discovery, 1 (2011) 291-296.

[35] S. Pandol, M. Edderkaoui, I. Gukovsky, A. Lugea, A. Gukovskaya, Desmoplasia of pancreatic ductal adenocarcinoma, Clinical gastroenterology and hepatology : the official clinical practice journal of the American Gastroenterological Association, 7 (2009) S44-47.

[36] I. Watanabe, T. Hasebe, S. Sasaki, M. Konishi, K. Inoue, T. Nakagohri, T. Oda, K. Mukai, T. Kinoshita, Advanced pancreatic ductal cancer: fibrotic focus and beta-catenin expression correlate with outcome, Pancreas, 26 (2003) 326-333.

[37] A. Vonlaufen, P.A. Phillips, Z. Xu, D. Goldstein, R.C. Pirola, J.S. Wilson, M.V. Apte, Pancreatic stellate cells and pancreatic cancer cells: an unholy alliance, Cancer research, 68 (2008) 7707-7710.

[38] L.A. Liotta, E.C. Kohn, The microenvironment of the tumour-host interface, Nature, 411 (2001) 375-379.

[39] J.M. Bailey, B.J. Swanson, T. Hamada, J.P. Eggers, P.K. Singh, T. Caffery, M.M. Ouellette, M.A. Hollingsworth, Sonic hedgehog promotes desmoplasia in pancreatic

cancer, Clinical cancer research : an official journal of the American Association for Cancer Research, 14 (2008) 5995-6004.

[40] G.C. Chu, A.C. Kimmelman, A.F. Hezel, R.A. DePinho, Stromal biology of pancreatic cancer, Journal of cellular biochemistry, 101 (2007) 887-907.

[41] M. Pasca di Magliano, S. Sekine, A. Ermilov, J. Ferris, A.A. Dlugosz, M. Hebrok, Hedgehog/Ras interactions regulate early stages of pancreatic cancer, Genes & development, 20 (2006) 3161-3173.

[42] B.P. Toole, M.G. Slomiany, Hyaluronan: a constitutive regulator of chemoresistance and malignancy in cancer cells, Seminars in cancer biology, 18 (2008) 244-250.

[43] J. Ringel, R. Jesnowski, C. Schmidt, J. Ringel, H.J. Kohler, J. Rychly, S.K. Batra, M. Lohr, CD44 in normal human pancreas and pancreatic carcinoma cell lines, Teratogenesis, carcinogenesis, and mutagenesis, 21 (2001) 97-106.

[44] M. Edward, C. Gillan, D. Micha, R.H. Tammi, Tumour regulation of fibroblast hyaluronan expression: a mechanism to facilitate tumour growth and invasion, Carcinogenesis, 26 (2005) 1215-1223.

[45] P.P. Provenzano, C. Cuevas, A.E. Chang, V.K. Goel, D.D. Von Hoff, S.R. Hingorani, Enzymatic targeting of the stroma ablates physical barriers to treatment of pancreatic ductal adenocarcinoma, Cancer cell, 21 (2012) 418-429.

[46] M. Edward, J.A. Quinn, S.M. Pasonen-Seppanen, B.A. McCann, R.H. Tammi, 4-Methylumbelliferone inhibits tumour cell growth and the activation of stromal hyaluronan synthesis by melanoma cell-derived factors, The British journal of dermatology, 162 (2010) 1224-1232.

[47] M. Hajime, Y. Shuichi, N. Makoto, Y. Masanori, K. Ikuko, K. Atsushi, S. Mutsuo, T. Keiichi, Inhibitory effect of 4-methylesculetin on hyaluronan synthesis slows the

development of human pancreatic cancer in vitro and in nude mice, International journal of cancer. Journal international du cancer, 120 (2007) 2704-2709.

[48] H. Nakazawa, S. Yoshihara, D. Kudo, H. Morohashi, I. Kakizaki, A. Kon, K. Takagaki, M. Sasaki, 4-methylumbelliferone, a hyaluronan synthase suppressor, enhances the anticancer activity of gemcitabine in human pancreatic cancer cells, Cancer chemotherapy and pharmacology, 57 (2006) 165-170.

[49] B. Diop-Frimpong, V.P. Chauhan, S. Krane, Y. Boucher, R.K. Jain, Losartan inhibits collagen I synthesis and improves the distribution and efficacy of nanotherapeutics in tumors, Proceedings of the National Academy of Sciences of the United States of America, 108 (2011) 2909-2914.

[50] E.E. Merika, K.N. Syrigos, M.W. Saif, Desmoplasia in pancreatic cancer. Can we fight it?, Gastroenterology research and practice, 2012 (2012) 781765.

[51] M. Hidalgo, A. Maitra, The hedgehog pathway and pancreatic cancer, The New England journal of medicine, 361 (2009) 2094-2096.

[52] S. Hamada, A. Masamune, T. Shimosegawa, Novel therapeutic strategies targeting tumor-stromal interactions in pancreatic cancer, Frontiers in physiology, 4 (2013) 331.

[53] X. Li, Q. Ma, W. Duan, H. Liu, H. Xu, E. Wu, Paracrine sonic hedgehog signaling derived from tumor epithelial cells: a key regulator in the pancreatic tumor microenvironment, Critical reviews in eukaryotic gene expression, 22 (2012) 97-108.

[54] H. Cheng, E. Merika, K.N. Syrigos, M.W. Saif, Novel agents for the treatment of pancreatic adenocarcinoma. Highlights from the "2011 ASCO Annual Meeting". Chicago, IL, USA; June 3-7, 2011, JOP : Journal of the pancreas, 12 (2011) 334-338.

[55] K.P. Olive, M.A. Jacobetz, C.J. Davidson, A. Gopinathan, D. McIntyre, D. Honess, B. Madhu, M.A. Goldgraben, M.E. Caldwell, D. Allard, K.K. Frese, G. Denicola, C. Feig, C.

Combs, S.P. Winter, H. Ireland-Zecchini, S. Reichelt, W.J. Howat, A. Chang, M. Dhara, L. Wang, F. Ruckert, R. Grutzmann, C. Pilarsky, K. Izeradjene, S.R. Hingorani, P. Huang, S.E. Davies, W. Plunkett, M. Egorin, R.H. Hruban, N. Whitebread, K. McGovern, J. Adams, C. Iacobuzio-Donahue, J. Griffiths, D.A. Tuveson, Inhibition of Hedgehog signaling enhances delivery of chemotherapy in a mouse model of pancreatic cancer, Science, 324 (2009) 1457-1461.

[56] V. Kumar, G. Mondal, P. Slavik, S. Rachagani, S.K. Batra, R.I. Mahato, Codelivery of small molecule hedgehog inhibitor and miRNA for treating pancreatic cancer, Molecular pharmaceutics, 12 (2015) 1289-1298.

[57] G. Feldmann, V. Fendrich, K. McGovern, D. Bedja, S. Bisht, H. Alvarez, J.B. Koorstra, N. Habbe, C. Karikari, M. Mullendore, K.L. Gabrielson, R. Sharma, W. Matsui, A. Maitra, An orally bioavailable small-molecule inhibitor of Hedgehog signaling inhibits tumor initiation and metastasis in pancreatic cancer, Molecular cancer therapeutics, 7 (2008) 2725-2735.

[58] S.X. Liu, Z.S. Xia, Y.Q. Zhong, Gene therapy in pancreatic cancer, World journal of gastroenterology, 20 (2014) 13343-13368.

[59] S.A. Rosenberg, P. Aebersold, K. Cornetta, A. Kasid, R.A. Morgan, R. Moen, E.M. Karson, M.T. Lotze, J.C. Yang, S.L. Topalian, et al., Gene transfer into humans--immunotherapy of patients with advanced melanoma, using tumor-infiltrating lymphocytes modified by retroviral gene transduction, The New England journal of medicine, 323 (1990) 570-578.

[60] S.L. Ginn, I.E. Alexander, M.L. Edelstein, M.R. Abedi, J. Wixon, Gene therapy clinical trials worldwide to 2012 - an update, The journal of gene medicine, 15 (2013) 65-77.

[61] S. Jones, X. Zhang, D.W. Parsons, J.C. Lin, R.J. Leary, P. Angenendt, P. Mankoo, H. Carter, H. Kamiyama, A. Jimeno, S.M. Hong, B. Fu, M.T. Lin, E.S. Calhoun, M. Kamiyama, K. Walter, T. Nikolskaya, Y. Nikolsky, J. Hartigan, D.R. Smith, M. Hidalgo, S.D. Leach, A.P. Klein, E.M. Jaffee, M. Goggins, A. Maitra, C. Iacobuzio-Donahue, J.R. Eshleman, S.E. Kern, R.H. Hruban, R. Karchin, N. Papadopoulos, G. Parmigiani, B. Vogelstein, V.E. Velculescu, K.W. Kinzler, Core signaling pathways in human pancreatic cancers revealed by global genomic analyses, Science, 321 (2008) 1801-1806.

[62] W. Wang, W. Li, N. Ma, G. Steinhoff, Non-viral gene delivery methods, Current pharmaceutical biotechnology, 14 (2013) 46-60.

[63] N. Nayerossadat, T. Maedeh, P.A. Ali, Viral and nonviral delivery systems for gene delivery, Advanced biomedical research, 1 (2012) 27.

[64] K.C. Soares, L. Zheng, B. Edil, E.M. Jaffee, Vaccines for pancreatic cancer, Cancer journal, 18 (2012) 642-652.

[65] J.A. Williams, A.E. Carnes, C.P. Hodgson, Plasmid DNA vaccine vector design: impact on efficacy, safety and upstream production, Biotechnology advances, 27 (2009) 353-370.

[66] K.R. Noss, S.A. Wolfe, S.R. Grimes, Upregulation of prostate specific membrane antigen/folate hydrolase transcription by an enhancer, Gene, 285 (2002) 247-256.

[67] N.M. Dean, C.F. Bennett, Antisense oligonucleotide-based therapeutics for cancer, Oncogene, 22 (2003) 9087-9096.

[68] J.H. Chan, S. Lim, W.S. Wong, Antisense oligonucleotides: from design to therapeutic application, Clinical and experimental pharmacology & physiology, 33 (2006) 533-540.

[69] D.L. Lewis, J.A. Wolff, Systemic siRNA delivery via hydrodynamic intravascular injection, Advanced drug delivery reviews, 59 (2007) 115-123.

[70] F. Petrocca, J. Lieberman, Promise and challenge of RNA interference-based therapy for cancer, Journal of clinical oncology : official journal of the American Society of Clinical Oncology, 29 (2011) 747-754.

[71] C. Yang, R. Hu, T. Anderson, Y. Wang, G. Lin, W.-C. Law, W.-J. Lin, Q.T. Nguyen, H.T. Toh, H.S. Yoon, C.-K. Chen, K.-T. Yong, Biodegradable nanoparticle-mediated K-ras down regulation for pancreatic cancer gene therapy, Journal of Materials Chemistry B, 3 (2015) 2163-2172.

[72] X. Zhao, F. Li, Y. Li, H. Wang, H. Ren, J. Chen, G. Nie, J. Hao, Co-delivery of HIF1alpha siRNA and gemcitabine via biocompatible lipid-polymer hybrid nanoparticles for effective treatment of pancreatic cancer, Biomaterials, 46 (2015) 13-25.

[73] F. Pittella, H. Cabral, Y. Maeda, P. Mi, S. Watanabe, H. Takemoto, H.J. Kim, N. Nishiyama, K. Miyata, K. Kataoka, Systemic siRNA delivery to a spontaneous pancreatic tumor model in transgenic mice by PEGylated calcium phosphate hybrid micelles, Journal of controlled release : official journal of the Controlled Release Society, 178 (2014) 18-24.

[74] S.A. Onate, S.Y. Tsai, M.J. Tsai, B.W. O'Malley, Sequence and characterization of a coactivator for the steroid hormone receptor superfamily, Science, 270 (1995) 1354-1357.

[75] J.J. Voegel, M.J. Heine, C. Zechel, P. Chambon, H. Gronemeyer, TIF2, a 160 kDa transcriptional mediator for the ligand-dependent activation function AF-2 of nuclear receptors, The EMBO journal, 15 (1996) 3667-3675.

[76] H. Chen, R.J. Lin, R.L. Schiltz, D. Chakravarti, A. Nash, L. Nagy, M.L. Privalsky, Y. Nakatani, R.M. Evans, Nuclear receptor coactivator ACTR is a novel histone acetyltransferase and forms a multimeric activation complex with P/CAF and CBP/p300, Cell, 90 (1997) 569-580.

[77] C.S. Suen, T.J. Berrodin, R. Mastroeni, B.J. Cheskis, C.R. Lyttle, D.E. Frail, A transcriptional coactivator, steroid receptor coactivator-3, selectively augments steroid receptor transcriptional activity, The Journal of biological chemistry, 273 (1998) 27645-27653.

[78] S.L. Anzick, J. Kononen, R.L. Walker, D.O. Azorsa, M.M. Tanner, X.Y. Guan, G. Sauter, O.P. Kallioniemi, J.M. Trent, P.S. Meltzer, AIB1, a steroid receptor coactivator amplified in breast and ovarian cancer, Science, 277 (1997) 965-968.

[79] R.S. Carroll, M. Brown, J. Zhang, J. DiRenzo, J. Font De Mora, P.M. Black, Expression of a subset of steroid receptor cofactors is associated with progesterone receptor expression in meningiomas, Clinical cancer research : an official journal of the American Association for Cancer Research, 6 (2000) 3570-3575.

[80] V.J. Gnanapragasam, H.Y. Leung, A.S. Pulimood, D.E. Neal, C.N. Robson, Expression of RAC 3, a steroid hormone receptor co-activator in prostate cancer, British journal of cancer, 85 (2001) 1928-1936.

[81] R. Reiter, A. Wellstein, A.T. Riegel, An isoform of the coactivator AIB1 that increases hormone and growth factor sensitivity is overexpressed in breast cancer, The Journal of biological chemistry, 276 (2001) 39736-39741.

[82] B. Holcomb, M.T. Yip-Schneider, J.M. Matos, J. Dixon, J. Kennard, J. Mahomed, R. Shanmugam, J. Sebolt-Leopold, C.M. Schmidt, Pancreatic cancer cell genetics and signaling response to treatment correlate with efficacy of gemcitabine-based molecular targeting strategies, Journal of gastrointestinal surgery : official journal of the Society for Surgery of the Alimentary Tract, 12 (2008) 288-296.

[83] B.M. Ghadimi, E. Schrock, R.L. Walker, D. Wangsa, A. Jauho, P.S. Meltzer, T. Ried, Specific chromosomal aberrations and amplification of the AIB1 nuclear receptor

coactivator gene in pancreatic carcinomas, The American journal of pathology, 154 (1999) 525-536.

[84] R.T. Henke, B.R. Haddad, S.E. Kim, J.D. Rone, A. Mani, J.M. Jessup, A. Wellstein, A. Maitra, A.T. Riegel, Overexpression of the nuclear receptor coactivator AIB1 (SRC-3) during progression of pancreatic adenocarcinoma, Clinical cancer research : an official journal of the American Association for Cancer Research, 10 (2004) 6134-6142.

[85] S. Kumar, S. Das, S. Rachagani, S. Kaur, S. Joshi, S.L. Johansson, M.P. Ponnusamy, M. Jain, S.K. Batra, NCOA3-mediated upregulation of mucin expression via transcriptional and post-translational changes during the development of pancreatic cancer, Oncogene, 34 (2015) 4879-4889.

[86] Y.-P. Hu, B. Haq, K.L. Carraway, N. Savaraj, T.J. Lampidis, Multidrug resistance correlates with overexpression of Muc4 but inversely with P-glycoprotein and multidrug resistance related protein in transfected human melanoma cells, Biochem. Pharmacol., 65 (2003) 1419-1425.

[87] L. Huang, J. Ren, D. Chen, Y. Li, S. Kharbanda, D. Kufe, MUC1 cytoplasmic domain coactivates Wnt target gene transcription and confers transformation, Cancer Biol. Ther., 2 (2003) 702-706.

[88] T. Kawano, R. Ahmad, H. Nogi, N. Agata, K. Anderson, D. Kufe, MUC1 oncoprotein promotes growth and survival of human multiple myeloma cells, Int J Oncol, 33 (2008) 153.

[89] M. Saitou, M. Goto, M. Horinouchi, S. Tamada, K. Nagata, T. Hamada, M. Osako, S. Takao, S. Batra, T. Aikou, MUC4 expression is a novel prognostic factor in patients with invasive ductal carcinoma of the pancreas, J. Clin. Pathol., 58 (2005) 845-852.

[90] P. Chaturvedi, A.P. Singh, S. Chakraborty, S.C. Chauhan, S. Bafna, J.L. Meza, P.K. Singh, M.A. Hollingsworth, P.P. Mehta, S.K. Batra, MUC4 mucin interacts with and stabilizes the HER2 oncoprotein in human pancreatic cancer cells, Cancer Res., 68 (2008) 2065-2070.

[91] M. Andrianifahanana, A. Agrawal, A.P. Singh, N. Moniaux, I. van Seuningen, J.P. Aubert, J. Meza, S.K. Batra, Synergistic induction of the MUC4 mucin gene by interferon-gamma and retinoic acid in human pancreatic tumour cells involves a reprogramming of signalling pathways, Oncogene, 24 (2005) 6143-6154.

[92] S. Bafna, S. Kaur, N. Momi, S. Batra, Pancreatic cancer cells resistance to gemcitabine: the role of MUC4 mucin, Br. J. Cancer, 101 (2009) 1155-1161.

[93] M. Andrianifahanana, N. Moniaux, B.M. Schmied, J. Ringel, H. Friess, M.A. Hollingsworth, M.W. Büchler, J.-P. Aubert, S.K. Batra, Mucin (MUC) gene expression in human pancreatic adenocarcinoma and chronic pancreatitis a potential role of MUC4 as a tumor marker of diagnostic significance, Clin. Cancer Res., 7 (2001) 4033-4040.

[94] M.A. Hollingsworth, J.M. Strawhecker, T.C. Caffrey, D.R. Mack, Expression of MUC1, MUC2, MUC3 and MUC4 mucin mRNAs in human pancreatic and intestinal tumor cell lines, Int. J. Cancer, 57 (1994) 198-203.

[95] S. Kaur, S. Kumar, N. Momi, A.R. Sasson, S.K. Batra, Mucins in pancreatic cancer and its microenvironment, Nature Reviews Gastroenterology and Hepatology, 10 (2013) 607-620.

[96] H.-U. Park, J.-W. Kim, G.E. Kim, H.-I. Bae, S.C. Crawley, S.C. Yang, J.R. Gum, S.K. Batra, K. Rousseau, D.M. Swallow, Aberrant expression of MUC3 and MUC4 membrane-associated mucins and sialyl lex antigen in pancreatic intraepithelial neoplasia, Pancreas, 26 (2003) e48-e54.

[97] X. Wei, H. Xu, D. Kufe, Human MUC1 oncoprotein regulates p53-responsive gene transcription in the genotoxic stress response, Cancer Cell, 7 (2005) 167-178.

[98] J. Xu, R.C. Wu, B.W. O'Malley, Normal and cancer-related functions of the p160 steroid receptor co-activator (SRC) family, Nature reviews. Cancer, 9 (2009) 615-630.

[99] V. Barry-Hamilton, R. Spangler, D. Marshall, S. McCauley, H.M. Rodriguez, M. Oyasu, A. Mikels, M. Vaysberg, H. Ghermazien, C. Wai, C.A. Garcia, A.C. Velayo, B. Jorgensen, D. Biermann, D. Tsai, J. Green, S. Zaffryar-Eilot, A. Holzer, S. Ogg, D. Thai, G. Neufeld, P. Van Vlasselaer, V. Smith, Allosteric inhibition of lysyl oxidase-like-2 impedes the development of a pathologic microenvironment, Nature medicine, 16 (2010) 1009-1017.

[100] H. Smith, C. Whittall, B. Weksler, J. Middleton, Chemokines stimulate bidirectional migration of human mesenchymal stem cells across bone marrow endothelial cells, Stem cells and development, 21 (2012) 476-486.

[101] Y. Le, Y. Zhou, P. Iribarren, J. Wang, Chemokines and chemokine receptors: their manifold roles in homeostasis and disease, Cellular & molecular immunology, 1 (2004) 95-104.

[102] F.R. Balkwill, The chemokine system and cancer, The Journal of pathology, 226 (2012) 148-157.

[103] R.K. Ganju, S.A. Brubaker, J. Meyer, P. Dutt, Y. Yang, S. Qin, W. Newman, J.E. Groopman, The alpha-chemokine, stromal cell-derived factor-1alpha, binds to the transmembrane G-protein-coupled CXCR-4 receptor and activates multiple signal transduction pathways, The Journal of biological chemistry, 273 (1998) 23169-23175.

[104] Z.G. Goldsmith, D.N. Dhanasekaran, G protein regulation of MAPK networks, Oncogene, 26 (2007) 3122-3142.

[105] L.J. Bendall, R. Baraz, J. Juarez, W. Shen, K.F. Bradstock, Defective p38 mitogen-activated protein kinase signaling impairs chemotaxic but not proliferative responses to stromal-derived factor-1alpha in acute lymphoblastic leukemia, Cancer research, 65 (2005) 3290-3298.

[106] J.F. Wang, I.W. Park, J.E. Groopman, Stromal cell-derived factor-1alpha stimulates tyrosine phosphorylation of multiple focal adhesion proteins and induces migration of hematopoietic progenitor cells: roles of phosphoinositide-3 kinase and protein kinase C, Blood, 95 (2000) 2505-2513.

[107] S.R. Vlahakis, A. Villasis-Keever, T. Gomez, M. Vanegas, N. Vlahakis, C.V. Paya, G protein-coupled chemokine receptors induce both survival and apoptotic signaling pathways, Journal of immunology, 169 (2002) 5546-5554.

[108] M. Mellado, A.J. Vila-Coro, C. Martinez, J.M. Rodriguez-Frade, Receptor dimerization: a key step in chemokine signaling, Cellular and molecular biology, 47 (2001) 575-582.

[109] U.M. Domanska, R.C. Kruizinga, W.B. Nagengast, H. Timmer-Bosscha, G. Huls, E.G. de Vries, A.M. Walenkamp, A review on CXCR4/CXCL12 axis in oncology: no place to hide, European journal of cancer, 49 (2013) 219-230.

[110] T. Ishikawa, K. Nakashiro, S.K. Klosek, H. Goda, S. Hara, D. Uchida, H. Hamakawa, Hypoxia enhances CXCR4 expression by activating HIF-1 in oral squamous cell carcinoma, Oncology reports, 21 (2009) 707-712.

[111] R.J. Phillips, J. Mestas, M. Gharaee-Kermani, M.D. Burdick, A. Sica, J.A. Belperio, M.P. Keane, R.M. Strieter, Epidermal growth factor and hypoxia-induced expression of CXC chemokine receptor 4 on non-small cell lung cancer cells is regulated by the phosphatidylinositol 3-kinase/PTEN/AKT/mammalian target of rapamycin signaling

pathway and activation of hypoxia inducible factor-1alpha, The Journal of biological chemistry, 280 (2005) 22473-22481.

[112] J.D. Kubic, J.W. Lui, E.C. Little, A.E. Ludvik, S. Konda, R. Salgia, A.E. Aplin, D. Lang, PAX3 and FOXD3 Promote CXCR4 Expression in Melanoma, The Journal of biological chemistry, 290 (2015) 21901-21914.

[113] O. Salvucci, A. Bouchard, A. Baccarelli, J. Deschenes, G. Sauter, R. Simon, R. Bianchi, M. Basik, The role of CXCR4 receptor expression in breast cancer: a large tissue microarray study, Breast cancer research and treatment, 97 (2006) 275-283.

[114] F. Andre, W. Xia, R. Conforti, Y. Wei, T. Boulet, G. Tomasic, M. Spielmann, M. Zoubir, N. Berrada, R. Arriagada, G.N. Hortobagyi, M.C. Hung, L. Pusztai, S. Delaloge, S. Michiels, M. Cristofanilli, CXCR4 expression in early breast cancer and risk of distant recurrence, The oncologist, 14 (2009) 1182-1188.

[115] M. Kato, J. Kitayama, S. Kazama, H. Nagawa, Expression pattern of CXC chemokine receptor-4 is correlated with lymph node metastasis in human invasive ductal carcinoma, Breast cancer research : BCR, 5 (2003) R144-150.

[116] Q.D. Chu, N.T. Holm, P. Madumere, L.W. Johnson, F. Abreo, B.D.L. Li, Chemokine receptor CXCR4 overexpression predicts recurrence for hormone receptor-positive, node-negative breast cancer patients, Surgery, 149 (2011) 193-199.

[117] L. Chang, M. Karin, Mammalian MAP kinase signalling cascades, Nature, 410 (2001) 37-40.

[118] T.N. Hartmann, J.A. Burger, A. Glodek, N. Fujii, M. Burger, CXCR4 chemokine receptor and integrin signaling co-operate in mediating adhesion and chemoresistance in small cell lung cancer (SCLC) cells, Oncogene, 24 (2005) 4462-4471.

[119] A.Z. Fernandis, A. Prasad, H. Band, R. Klosel, R.K. Ganju, Regulation of CXCR4-mediated chemotaxis and chemoinvasion of breast cancer cells, Oncogene, 23 (2004) 157-167.

[120] K.E. Luker, G.D. Luker, Functions of CXCL12 and CXCR4 in breast cancer, Cancer letters, 238 (2006) 30-41.

[121] X. Sun, G. Cheng, M. Hao, J. Zheng, X. Zhou, J. Zhang, R.S. Taichman, K.J. Pienta, J. Wang, CXCL12 / CXCR4 / CXCR7 chemokine axis and cancer progression, Cancer metastasis reviews, 29 (2010) 709-722.

[122] K. Cui, W. Zhao, C. Wang, A. Wang, B. Zhang, W. Zhou, J. Yu, Z. Sun, S. Li, The CXCR4-CXCL12 Pathway Facilitates the Progression of Pancreatic Cancer< i> Via</i> Induction of Angiogenesis and Lymphangiogenesis, J. Surg. Res., 171 (2011) 143-150.

[123] X. Li, Q. Ma, Q. Xu, H. Liu, J. Lei, W. Duan, K. Bhat, F. Wang, E. Wu, Z. Wang, SDF-1/CXCR4 signaling induces pancreatic cancer cell invasion and epithelial-mesenchymal transition in vitro through non-canonical activation of Hedgehog pathway, Cancer letters, 322 (2012) 169-176.

[124] F. Marchesi, P. Monti, B.E. Leone, A. Zerbi, A. Vecchi, L. Piemonti, A. Mantovani, P. Allavena, Increased survival, proliferation, and migration in metastatic human pancreatic tumor cells expressing functional CXCR4, Cancer research, 64 (2004) 8420-8427.

[125] Y. Matsuo, N. Ochi, H. Sawai, A. Yasuda, H. Takahashi, H. Funahashi, H. Takeyama, Z. Tong, S. Guha, CXCL8/IL-8 and CXCL12/SDF-1alpha co-operatively promote invasiveness and angiogenesis in pancreatic cancer, International journal of cancer. Journal international du cancer, 124 (2009) 853-861.

[126] A.P. Singh, S. Arora, A. Bhardwaj, S.K. Srivastava, M.P. Kadakia, B. Wang, W.E. Grizzle, L.B. Owen, S. Singh, CXCL12/CXCR4 Protein Signaling Axis Induces Sonic

Hedgehog Expression in Pancreatic Cancer Cells via Extracellular Regulated Kinase- and Akt Kinase-mediated Activation of Nuclear Factor κB: Implications for bidirectional tumor-stromal interactions, J. Biol. Chem., 287 (2012) 39115-39124.

[127] R. Marechal, P. Demetter, N. Nagy, A. Berton, C. Decaestecker, M. Polus, J. Closset, J. Devière, I. Salmon, J.-L. Van Laethem, High expression of CXCR4 may predict poor survival in resected pancreatic adenocarcinoma, Br. J. Cancer, 100 (2009) 1444-1451.

[128] T. Welsch, S. Keleg, F. Bergmann, L. Degrate, S. Bauer, J. Schmidt, Comparative analysis of tumorbiology and CD133 positivity in primary and recurrent pancreatic ductal adenocarcinoma, Clin Exp Metastasis, 26 (2009) 701-711.

[129] P. Guo, J.-O. You, J. Yang, D. Jia, M.A. Moses, D.T. Auguste, Inhibiting Metastatic Breast Cancer Cell Migration via the Synergy of Targeted, pH-triggered siRNA Delivery and Chemokine Axis Blockade, Mol. Pharm., (2014).

[130] A. Egorova, A. Kiselev, M. Hakli, M. Ruponen, V. Baranov, A. Urtti, Chemokine-derived peptides as carriers for gene delivery to CXCR4 expressing cells, The Journal of Gene Medicine, 11 (2009) 772-781.

[131] U. Unzueta, M.V. Cespedes, N. Ferrer-Miralles, I. Casanova, J. Cedano, J.L. Corchero, J. Domingo-Espin, A. Villaverde, R. Mangues, E. Vazquez, Intracellular CXCR4(+) cell targeting with T22-empowered protein-only nanoparticles, International journal of nanomedicine, 7 (2012) 4533-4544.

[132] C. Chittasupho, K. Lirdprapamongkol, P. Kewsuwan, N. Sarisuta, Targeted delivery of doxorubicin to A549 lung cancer cells by CXCR4 antagonist conjugated PLGA nanoparticles, European journal of pharmaceutics and biopharmaceutics : official journal of Arbeitsgemeinschaft fur Pharmazeutische Verfahrenstechnik e.V, 88 (2014) 529-538.

[133] R.T. Wang, X.Y. Zhi, S.Y. Yao, Y. Zhang, LFC131 peptide-conjugated polymeric nanoparticles for the effective delivery of docetaxel in CXCR4 overexpressed lung cancer cells, Colloid Surf. B-Biointerfaces, 133 (2015) 43-50.

[134] E.L. Snyder, C.C. Saenz, C. Denicourt, B.R. Meade, X.S. Cui, I.M. Kaplan, S.F. Dowdy, Enhanced targeting and killing of tumor cells expressing the CXC chemokine receptor 4 by transducible anticancer peptides, Cancer research, 65 (2005) 10646-10650.

[135] C. de la Torre, I. Casanova, G. Acosta, C. Coll, M.J. Moreno, F. Albericio, E. Aznar, R. Mangues, M. Royo, F. Sancenón, R. Martínez-Máñez, Gated Mesoporous Silica Nanoparticles Using a Double-Role Circular Peptide for the Controlled and Target-Preferential Release of Doxorubicin in CXCR4-Expresing Lymphoma Cells, Advanced Functional Materials, 25 (2015) 687-695.

[136] A. Egorova, A. Kiselev, M. Hakli, M. Ruponen, V. Baranov, A. Urtti, Chemokine-derived peptides as carriers for gene delivery to CXCR4 expressing cells, The journal of gene medicine, 11 (2009) 772-781.

[137] A. Egorova, M. Bogacheva, A. Shubina, V. Baranov, A. Kiselev, Development of a receptor-targeted gene delivery system using CXCR4 ligand-conjugated cross-linking peptides, The journal of gene medicine, 16 (2014) 336-351.

[138] W.H. Driessen, N. Fujii, H. Tamamura, S.M. Sullivan, Development of peptide-targeted lipoplexes to CXCR4-expressing rat glioma cells and rat proliferating endothelial cells, Molecular therapy : the journal of the American Society of Gene Therapy, 16 (2008) 516-524.

[139] H. Hanaoka, T. Mukai, H. Tamamura, T. Mori, S. Ishino, K. Ogawa, Y. Iida, R. Doi, N. Fujii, H. Saji, Development of a 111In-labeled peptide derivative targeting a chemokine receptor, CXCR4, for imaging tumors, Nuclear medicine and biology, 33 (2006) 489-494.

[140] J. Kuil, T. Buckle, J. Oldenburg, H. Yuan, A.D. Borowsky, L. Josephson, F.W. van Leeuwen, Hybrid peptide dendrimers for imaging of chemokine receptor 4 (CXCR4) expression, Molecular pharmaceutics, 8 (2011) 2444-2453.

[141] J. Kuil, T. Buckle, H. Yuan, N.S. van den Berg, S. Oishi, N. Fujii, L. Josephson, F.W. van Leeuwen, Synthesis and evaluation of a bimodal CXCR4 antagonistic peptide, Bioconjugate chemistry, 22 (2011) 859-864.

[142] S.G. Tarasov, V. Gaponenko, O.M. Howard, Y. Chen, J.J. Oppenheim, M.A. Dyba, S. Subramaniam, Y. Lee, C. Michejda, N.I. Tarasova, Structural plasticity of a transmembrane peptide allows self-assembly into biologically active nanoparticles, Proceedings of the National Academy of Sciences of the United States of America, 108 (2011) 9798-9803.

[143] P. Guo, J.O. You, J. Yang, M.A. Moses, D.T. Auguste, Using breast cancer cell CXCR4 surface expression to predict liposome binding and cytotoxicity, Biomaterials, 33 (2012) 8104-8110.

[144] P. Guo, J.O. You, J. Yang, D. Jia, M.A. Moses, D.T. Auguste, Inhibiting metastatic breast cancer cell migration via the synergy of targeted, pH-triggered siRNA delivery and chemokine axis blockade, Molecular pharmaceutics, 11 (2014) 755-765.

[145] S. Nimmagadda, M. Pullambhatla, M.G. Pomper, Immunoimaging of CXCR4 expression in brain tumor xenografts using SPECT/CT, Journal of nuclear medicine : official publication, Society of Nuclear Medicine, 50 (2009) 1124-1130.

[146] B. Le Bon, N. Van Craynest, J.M. Daoudi, C. Di Giorgio, A.J. Domb, P. Vierling, AMD3100 conjugates as components of targeted nonviral gene delivery systems: synthesis and in vitro transfection efficiency of CXCR4-expressing cells, Bioconjugate chemistry, 15 (2004) 413-423.

[147] A.C. Misra, K.E. Luker, H. Durmaz, G.D. Luker, J. Lahann, CXCR4-Targeted Nanocarriers for Triple Negative Breast Cancers, Biomacromolecules, 16 (2015) 2412-2417.

[148] D.Y. Gao, T. Lin Ts, Y.C. Sung, Y.C. Liu, W.H. Chiang, C.C. Chang, J.Y. Liu, Y. Chen, CXCR4-targeted lipid-coated PLGA nanoparticles deliver sorafenib and overcome acquired drug resistance in liver cancer, Biomaterials, 67 (2015) 194-203.

[149] J. Li, Y. Zhu, S.T. Hazeldine, C. Li, D. Oupicky, Dual-function CXCR4 antagonist polyplexes to deliver gene therapy and inhibit cancer cell invasion, Angew. Chem. Int. Ed. Engl., 51 (2012) 8740-8743.

[150] J. Li, D. Oupicky, Effect of biodegradability on CXCR4 antagonism, transfection efficacy and antimetastatic activity of polymeric Plerixafor, Biomaterials, 35 (2014) 5572-5579.

[151] Y. Wang, J. Li, D. Oupicky, Polymeric Plerixafor: Effect of PEGylation on CXCR4 Antagonism, Cancer Cell Invasion, and DNA Transfection, Pharm. Res., 31 (2014) 3538-3548.

[152] Y. Wang, J. Li, Y. Chen, D. Oupicky, Balancing polymer hydrophobicity for ligand presentation and siRNA delivery in dual function CXCR4 inhibiting polyplexes, Biomater Sci, 3 (2015) 1114-1123.

[153] Y. Wang, S.T. Hazeldine, J. Li, D. Oupicky, Development of Functional Poly(amido amine) CXCR4 Antagonists with the Ability to Mobilize Leukocytes and Deliver Nucleic Acids, Advanced healthcare materials, 4 (2015) 729-738.

[154] J. Li, A.M. Lepadatu, Y. Zhu, M. Ciobanu, Y. Wang, S.C. Asaftei, D. Oupicky, Examination of structure-activity relationship of viologen-based dendrimers as CXCR4 antagonists and gene carriers, Bioconjugate chemistry, 25 (2014) 907-917.

[155] S. Nimmagadda, M. Pullambhatla, K. Stone, G. Green, Z.M. Bhujwalla, M.G. Pomper, Molecular imaging of CXCR4 receptor expression in human cancer xenografts with [64Cu]AMD3100 positron emission tomography, Cancer research, 70 (2010) 3935-3944.

[156] R.A. De Silva, K. Peyre, M. Pullambhatla, J.J. Fox, M.G. Pomper, S. Nimmagadda, Imaging CXCR4 expression in human cancer xenografts: evaluation of monocyclam 64Cu-AMD3465, Journal of nuclear medicine : official publication, Society of Nuclear Medicine, 52 (2011) 986-993.

[157] M.C. Smith, K.E. Luker, J.R. Garbow, J.L. Prior, E. Jackson, D. Piwnica-Worms, G.D. Luker, CXCR4 regulates growth of both primary and metastatic breast cancer, Cancer research, 64 (2004) 8604-8612.

[158] E. De Clercq, The bicyclam AMD3100 story, Nature reviews. Drug discovery, 2 (2003) 581-587.

[159] T. Engl, B. Relja, D. Marian, C. Blumenberg, I. Muller, W.D. Beecken, J. Jones, E.M. Ringel, J. Bereiter-Hahn, D. Jonas, R.A. Blaheta, CXCR4 chemokine receptor mediates prostate tumor cell adhesion through alpha5 and beta3 integrins, Neoplasia, 8 (2006) 290-301.

[160] M.R. Kuhne, T. Mulvey, B. Belanger, S. Chen, C. Pan, C. Chong, F. Cao, W. Niekro, T. Kempe, K.A. Henning, L.J. Cohen, A.J. Korman, P.M. Cardarelli, BMS-936564/MDX-1338: a fully human anti-CXCR4 antibody induces apoptosis in vitro and shows antitumor activity in vivo in hematologic malignancies, Clinical cancer research : an official journal of the American Association for Cancer Research, 19 (2013) 357-366.

[161] F. Abedini, H. Hosseinkhani, M. Ismail, A.J. Domb, A.R. Omar, P.P. Chong, P.D. Hong, D.S. Yu, I.Y. Farber, Cationized dextran nanoparticle-encapsulated CXCR4-siRNA enhanced correlation between CXCR4 expression and serum alkaline phosphatase in a

mouse model of colorectal cancer, International journal of nanomedicine, 7 (2012) 4159-4168.

[162] F. Abedini, M. Ismail, H. Hosseinkhani, T.A. Ibrahim, A.R. Omar, P.P. Chong, M.H. Bejo, A.J. Domb, Effects of CXCR4 siRNA/dextran-spermine nanoparticles on CXCR4 expression and serum LDH levels in a mouse model of colorectal cancer metastasis to the liver, Cancer management and research, 3 (2011) 301-309.

[163] K. Jiang, J. Li, J.P. Yin, Q. Ma, B. Yan, X. Zhang, L. Wang, L.F. Wang, T. Liu, Y.L. Zhang, Q.Y. Fan, A.G. Yang, X.C. Qiu, B.A. Ma, Targeted delivery of CXCR4-siRNA by scFv for HER2(+) breast cancer therapy, Biomaterials, 59 (2015) 77-87.

[164] P. Vaupel, D.K. Kelleher, M. Hockel, Oxygen status of malignant tumors: pathogenesis of hypoxia and significance for tumor therapy, Seminars in oncology, 28 (2001) 29-35.

[165] A.L. Harris, Hypoxia--a key regulatory factor in tumour growth, Nature reviews. Cancer, 2 (2002) 38-47.

[166] B. Romain, M. Hachet-Haas, S. Rohr, C. Brigand, J.L. Galzi, M.P. Gaub, E. Pencreach, D. Guenot, Hypoxia differentially regulated CXCR4 and CXCR7 signaling in colon cancer, Molecular cancer, 13 (2014) 58.

[167] Y. Lee, Y. Chen, N.I. Tarasova, V. Gaponenko, The structure of monomeric components of self-assembling CXCR4 antagonists determines the architecture of resulting nanostructures, Nanotechnology, 22 (2011) 505101.

[168] S. Asaftei, D. Huskens, D. Schols, HIV-1 X4 Activities of Polycationic “Viologen” Based Dendrimers by Interaction with the Chemokine Receptor CXCR4: Study of Structure–Activity Relationship, J. Med. Chem., 55 (2012) 10405-10413.

[169] R.K. Jain, Normalizing tumor microenvironment to treat cancer: bench to bedside to biomarkers, Journal of clinical oncology : official journal of the American Society of Clinical Oncology, 31 (2013) 2205-2218.

[170] P. Carmeliet, R.K. Jain, Molecular mechanisms and clinical applications of angiogenesis, Nature, 473 (2011) 298-307.

[171] Y. Chen, Y. Huang, T. Reiberger, A.M. Duyverman, P. Huang, R. Samuel, L. Hiddingh, S. Roberge, C. Koppel, G.Y. Lauwers, A.X. Zhu, R.K. Jain, D.G. Duda, Differential effects of sorafenib on liver versus tumor fibrosis mediated by stromal-derived factor 1 alpha/C-X-C receptor type 4 axis and myeloid differentiation antigen-positive myeloid cell infiltration in mice, Hepatology, 59 (2014) 1435-1447.

[172] R. Marechal, P. Demetter, N. Nagy, A. Berton, C. Decaestecker, M. Polus, J. Closset, J. Deviere, I. Salmon, J.L. Van Laethem, High expression of CXCR4 may predict poor survival in resected pancreatic adenocarcinoma, British journal of cancer, 100 (2009) 1444-1451.

[173] R.M. Thomas, J. Kim, M.P. Revelo-Penafiel, R. Angel, D.W. Dawson, A.M. Lowy, The chemokine receptor CXCR4 is expressed in pancreatic intraepithelial neoplasia, Gut, 57 (2008) 1555-1560.

[174] T. Mori, R. Doi, M. Koizumi, E. Toyoda, D. Ito, K. Kami, T. Masui, K. Fujimoto, H. Tamamura, K. Hiramatsu, N. Fujii, M. Imamura, CXCR4 antagonist inhibits stromal cell-derived factor 1-induced migration and invasion of human pancreatic cancer, Molecular cancer therapeutics, 3 (2004) 29-37.

[175] S. Singh, S.K. Srivastava, A. Bhardwaj, L.B. Owen, A.P. Singh, CXCL12-CXCR4 signalling axis confers gemcitabine resistance to pancreatic cancer cells: a novel target for therapy, British journal of cancer, 103 (2010) 1671-1679.

[176] A.P. Singh, S. Arora, A. Bhardwaj, S.K. Srivastava, M.P. Kadakia, B. Wang, W.E. Grizzle, L.B. Owen, S. Singh, CXCL12/CXCR4 protein signaling axis induces sonic hedgehog expression in pancreatic cancer cells via extracellular regulated kinase- and Akt kinase-mediated activation of nuclear factor kappaB: implications for bidirectional tumor-stromal interactions, The Journal of biological chemistry, 287 (2012) 39115-39124.

[177] R. Siegel, D. Naishadham, A. Jemal, Cancer statistics, 2013, CA. Cancer J. Clin., 63 (2013) 11-30.

[178] N. Moniaux, G.C. Varshney, S.C. Chauhan, M.C. Copin, M. Jain, U.A. Wittel, M. Andrianifahanana, J.P. Aubert, S.K. Batra, Generation and characterization of anti-MUC4 monoclonal antibodies reactive with normal and cancer cells in humans, The journal of histochemistry and cytochemistry : official journal of the Histochemistry Society, 52 (2004) 253-261.

[179] Y. Wang, S. Gao, W.H. Ye, H.S. Yoon, Y.Y. Yang, Co-delivery of drugs and DNA from cationic core-shell nanoparticles self-assembled from a biodegradable copolymer, Nature materials, 5 (2006) 791-796.

[180] Y.W. Kim, H.F. Kern, T.D. Mullins, M.J. Koriwchak, R.S. Metzgar, Characterization of clones of a human pancreatic adenocarcinoma cell line representing different stages of differentiation, Pancreas, 4 (1989) 353-362.

[181] M.P. Torres, S. Rachagani, V. Purohit, P. Pandey, S. Joshi, E.D. Moore, S.L. Johansson, P.K. Singh, A.K. Ganti, S.K. Batra, Graviola: a novel promising natural-derived drug that inhibits tumorigenicity and metastasis of pancreatic cancer cells in vitro and in vivo through altering cell metabolism, Cancer letters, 323 (2012) 29-40.

[182] P. Seshacharyulu, M.P. Ponnusamy, S. Rachagani, I. Lakshmanan, D. Haridas, Y. Yan, A.K. Ganti, S.K. Batra, Targeting EGF-receptor(s) - STAT1 axis attenuates tumor

growth and metastasis through downregulation of MUC4 mucin in human pancreatic cancer, Oncotarget, 6 (2015) 5164-5181.

[183] S.G. Kim, N.V. Tsekos, Perfusion imaging by a flow-sensitive alternating inversion recovery (FAIR) technique: Application to functional brain imaging, Magn Reson Med, 37 (1997) 425-435.

[184] H. Maeda, G.Y. Bharate, J. Daruwalla, Polymeric drugs for efficient tumor-targeted drug delivery based on EPR-effect, European journal of pharmaceutics and biopharmaceutics : official journal of Arbeitsgemeinschaft fur Pharmazeutische Verfahrenstechnik e.V, 71 (2009) 409-419.

[185] R. Haag, F. Kratz, Polymer therapeutics: concepts and applications, Angewandte Chemie, 45 (2006) 1198-1215.

[186] R. Duncan, Polymer conjugates as anticancer nanomedicines, Nature reviews. Cancer, 6 (2006) 688-701.

[187] F. Yuan, M. Dellian, D. Fukumura, M. Leunig, D.A. Berk, V.P. Torchilin, R.K. Jain, Vascular permeability in a human tumor xenograft: molecular size dependence and cutoff size, Cancer research, 55 (1995) 3752-3756.

[188] M. Dellian, F. Yuan, V.S. Trubetskoy, V.P. Torchilin, R.K. Jain, Vascular permeability in a human tumour xenograft: molecular charge dependence, British journal of cancer, 82 (2000) 1513-1518.

[189] K. Greish, J. Fang, T. Inutsuka, A. Nagamitsu, H. Maeda, Macromolecular therapeutics: advantages and prospects with special emphasis on solid tumour targeting, Clinical pharmacokinetics, 42 (2003) 1089-1105.

[190] H. Maeda, J. Fang, T. Inutsuka, Y. Kitamoto, Vascular permeability enhancement in solid tumor: various factors, mechanisms involved and its implications, International immunopharmacology, 3 (2003) 319-328.

[191] H. Varkony, V. Weinstein, E. Klinger, J. Sterling, H. Cooperman, T. Komlosh, D. Ladkani, R. Schwartz, The glatiramoid class of immunomodulator drugs, Expert opinion on pharmacotherapy, 10 (2009) 657-668.

[192] P. Raggi, S. Vukicevic, R.M. Moyses, K. Wesseling, D.M. Spiegel, Ten-year experience with sevelamer and calcium salts as phosphate binders, Clinical journal of the American Society of Nephrology : CJASN, 5 Suppl 1 (2010) S31-40.

[193] F.R. Balkwill, The chemokine system and cancer, The Journal of Pathology, 226 (2012) 148-157.

[194] A. Zlotnik, A.M. Burkhardt, B. Homey, Homeostatic chemokine receptors and organ-specific metastasis, Nat. Rev. Immunol., 11 (2011) 597-606.

[195] M. Brave, A. Farrell, S.C. Lin, T. Ocheltree, S.P. Miksinski, S.L. Lee, H. Saber, J. Fourie, C. Tornoe, B. Booth, W.S. Yuan, K. He, R. Justice, R. Pazdur, FDA Review Summary: Mozobil in Combination with Granulocyte Colony-Stimulating Factor to Mobilize Hematopoietic Stem Cells to the Peripheral Blood for Collection and Subsequent Autologous Transplantation, Oncology, 78 (2010) 282-288.

[196] Y. Wang, J. Li, D. Oupicky, Polymeric Plerixafor: Effect of PEGylation on CXCR4 Antagonism, Cancer Cell Invasion, and DNA Transfection, Pharmaceutical research, (2014).

[197] G.J. Bridger, R.T. Skerlj, P.E. Hernandez-Abad, D.E. Bogucki, Z. Wang, Y. Zhou, S. Nan, E.M. Boehringer, T. Wilson, J. Crawford, M. Metz, S. Hatse, K. Princen, E. De Clercq, D. Schols, Synthesis and structure-activity relationships of azamacrocyclic C-X-C

chemokine receptor 4 antagonists: analogues containing a single azamacrocyclic ring are potent inhibitors of T-cell tropic (X4) HIV-1 replication, Journal of medicinal chemistry, 53 (2010) 1250-1260.

[198] L. Parhamifar, A.K. Larsen, A.C. Hunter, T.L. Andresen, S.M. Moghimi, Polycation cytotoxicity: a delicate matter for nucleic acid therapy-focus on polyethylenimine, Soft Matter, 6 (2010) 4001-4009.

[199] V. Mersch-Sundermann, S. Knasmuller, X.J. Wu, F. Darroudi, F. Kassie, Use of a human-derived liver cell line for the detection of cytoprotective, antigenotoxic and cogenotoxic agents, Toxicology, 198 (2004) 329-340.

[200] S. Hatse, K. Princen, G. Bridger, E. De Clercq, D. Schols, Chemokine receptor inhibition by AMD3100 is strictly confined to CXCR4, FEBS Lett., 527 (2002) 255-262.

[201] H.E. Broxmeyer, C.M. Orschell, D.W. Clapp, G. Hangoc, S. Cooper, P.A. Plett, W.C. Liles, X. Li, B. Graham-Evans, T.B. Campbell, G. Calandra, G. Bridger, D.C. Dale, E.F. Srour, Rapid mobilization of murine and human hematopoietic stem and progenitor cells with AMD3100, a CXCR4 antagonist, J. Exp. Med., 201 (2005) 1307-1318.

[202] P. Vader, L.J. van der Aa, J.F. Engbersen, G. Storm, R.M. Schiffelers, Disulfide-based poly(amido amine)s for siRNA delivery: effects of structure on siRNA complexation, cellular uptake, gene silencing and toxicity, Pharmaceutical research, 28 (2011) 1013-1022.

[203] C. Lin, Z. Zhong, M.C. Lok, X. Jiang, W.E. Hennink, J. Feijen, J.F. Engbersen, Novel bioreducible poly(amido amine)s for highly efficient gene delivery, Bioconjugate chemistry, 18 (2007) 138-145.

[204] J. Li, Y. Wang, Y. Zhu, D. Oupicky, Recent advances in delivery of drug-nucleic acid combinations for cancer treatment, J. Controlled Rel., 172 (2013) 589-600.

[205] C.E. Thomas, A. Ehrhardt, M.A. Kay, Progress and problems with the use of viral vectors for gene therapy, Nature reviews. Genetics, 4 (2003) 346-358.

[206] D.W. Pack, A.S. Hoffman, S. Pun, P.S. Stayton, Design and development of polymers for gene delivery, Nature reviews. Drug discovery, 4 (2005) 581-593.

[207] C.K. Payne, S.A. Jones, C. Chen, X. Zhuang, Internalization and Trafficking of Cell Surface Proteoglycans and Proteoglycan-Binding Ligands, Traffic, 8 (2007) 389-401.

[208] O. Boussif, F. Lezoualc'h, M.A. Zanta, M.D. Mergny, D. Scherman, B. Demeneix, J.P. Behr, A versatile vector for gene and oligonucleotide transfer into cells in culture and in vivo: polyethylenimine, Proceedings of the National Academy of Sciences of the United States of America, 92 (1995) 7297-7301.

[209] A.C. Hunter, Molecular hurdles in polyfectin design and mechanistic background to polycation induced cytotoxicity, Advanced drug delivery reviews, 58 (2006) 1523-1531.

[210] Q. Zhou, C. Wu, D.S. Manickam, D. Oupicky, Evaluation of pharmacokinetics of bioreducible gene delivery vectors by real-time PCR, Pharm. Res., 26 (2009) 1581-1589.

[211] R.S. Burke, S.H. Pun, Extracellular barriers to in vivo PEI and PEGylated PEI polyplex-mediated gene delivery to the liver, Bioconjugate Chem., 19 (2008) 693-704.

[212] A.E. Smith, A. Sizovs, G. Grandinetti, L. Xue, T.M. Reineke, Diblock glycopolymers promote colloidal stability of polyplexes and effective pDNA and siRNA delivery under physiological salt and serum conditions, Biomacromolecules, 12 (2011) 3015-3022.

[213] T. Merdan, K. Kunath, H. Petersen, U. Bakowsky, K.H. Voigt, J. Kopecek, T. Kissel, PEGylation of poly(ethylene imine) affects stability of complexes with plasmid DNA under in vivo conditions in a dose-dependent manner after intravenous injection into mice, Bioconjugate Chem., 16 (2005) 785-792.

[214] O.M. Merkel, D. Librizzi, A. Pfestroff, T. Schurrat, K. Buyens, N.N. Sanders, S.C. De Smedt, M. Béhé, T. Kissel, Stability of siRNA polyplexes from poly(ethylenimine) and poly(ethylenimine)-g-poly(ethylene glycol) under in vivo conditions: Effects on pharmacokinetics and biodistribution measured by Fluorescence Fluctuation Spectroscopy and Single Photon Emission Computed Tomography (SPECT) imaging, J. Controlled Rel., 138 (2009) 148-159.

[215] D. Oupicky, M. Ogris, K.A. Howard, P.R. Dash, K. Ulbrich, L.W. Seymour, Importance of lateral and steric stabilization of polyelectrolyte gene delivery vectors for extended systemic circulation, Mol. Ther., 5 (2002) 463-472.

[216] D. Oupicky, R.C. Carlisle, L.W. Seymour, Triggered intracellular activation of disulfide crosslinked polyelectrolyte gene delivery complexes with extended systemic circulation in vivo., Gene Ther., 8 (2001) 713-724.

[217] R. Kircheis, L. Wightman, E. Wagner, Design and gene delivery activity of modified polyethylenimines, Advanced drug delivery reviews, 53 (2001) 341-358.

[218] T. Merdan, K. Kunath, H. Petersen, U. Bakowsky, K.H. Voigt, J. Kopecek, T. Kissel, PEGylation of poly(ethylene imine) affects stability of complexes with plasmid DNA under in vivo conditions in a dose-dependent manner after intravenous injection into mice, Bioconjugate chemistry, 16 (2005) 785-792.

[219] S.J. Sung, S.H. Min, K.Y. Cho, S. Lee, Y.J. Min, Y.I. Yeom, J.K. Park, Effect of polyethylene glycol on gene delivery of polyethylenimine, Biological & pharmaceutical bulletin, 26 (2003) 492-500.

[220] A. Malek, F. Czubayko, A. Aigner, PEG grafting of polyethylenimine (PEI) exerts different effects on DNA transfection and siRNA-induced gene targeting efficacy, Journal of drug targeting, 16 (2008) 124-139.

[221] J. Li, Y. Zhu, S.T. Hazeldine, S.M. Firestine, D. Oupicky, Cyclam-based polymeric copper chelators for gene delivery and potential PET imaging, Biomacromolecules, 13 (2012) 3220-3227.

[222] C.Y. Hong, Y.Z. You, D.C. Wu, Y. Liu, C.Y. Pan, Thermal control over the topology of cleavable polymers: From linear to hyperbranched structures, J. Am. Chem. Soc., 129 (2007) 5354-+.

[223] R.E. Fitzsimmons, H. Uludağ, Specific effects of PEGylation on gene delivery efficacy of polyethylenimine: interplay between PEG substitution and N/P ratio, Acta biomaterialia, 8 (2012) 3941-3955.

[224] J.H. Brumbach, C. Lin, J. Yockman, W.J. Kim, K.S. Blevins, J.F. Engbersen, J. Feijen, S.W. Kim, Mixtures of poly(triethylenetetramine/cystamine bisacrylamide) and poly(triethylenetetramine/cystamine bisacrylamide)-g-poly(ethylene glycol) for improved gene delivery, Bioconjugate chemistry, 21 (2010) 1753-1761.

[225] G. Maurstad, B.T. Stokke, K.M. Varum, S.P. Strand, PEGylated chitosan complexes DNA while improving polyplex colloidal stability and gene transfection efficiency, Carbohydrate polymers, 94 (2013) 436-443.

[226] B.J. Rackstraw, S. Stolnik, S.S. Davis, F. Bignotti, M.C. Garnett, Development of multicomponent DNA delivery systems based upon poly(amidoamine)-PEG co-polymers, Biochimica et biophysica acta, 1576 (2002) 269-286.

[227] S.H. Pun, M.E. Davis, Development of a nonviral gene delivery vehicle for systemic application, Bioconjugate chemistry, 13 (2002) 630-639.

[228] H. Petersen, P.M. Fechner, A.L. Martin, K. Kunath, S. Stolnik, C.J. Roberts, D. Fischer, M.C. Davies, T. Kissel, Polyethylenimine-graft-poly(ethylene glycol) copolymers:

influence of copolymer block structure on DNA complexation and biological activities as gene delivery system, Bioconjugate chemistry, 13 (2002) 845-854.

[229] S. Mishra, P. Webster, M.E. Davis, PEGylation significantly affects cellular uptake and intracellular trafficking of non-viral gene delivery particles, Eur. J. Cell Biol., 83 (2004) 97-111.

[230] S. Mishra, P. Webster, M.E. Davis, PEGylation significantly affects cellular uptake and intracellular trafficking of non-viral gene delivery particles, European journal of cell biology, 83 (2004) 97-111.

[231] G.A. Rao, R. Tsai, D. Roura, J.A. Hughes, Evaluation of the transfection property of a peptide ligand for the fibroblast growth factor receptor as part of PEGylated polyethylenimine polyplex, Journal of drug targeting, 16 (2008) 79-89.

[232] L. Casettari, D. Vllasaliu, G. Mantovani, S.M. Howdle, S. Stolnik, L. Illum, Effect of PEGylation on the Toxicity and Permeability Enhancement of Chitosan, Biomacromolecules, (2010).

[233] L.O. Gerlach, R.T. Skerlj, G.J. Bridger, T.W. Schwartz, Molecular interactions of cyclam and bicyclam non-peptide antagonists with the CXCR4 chemokine receptor, The Journal of biological chemistry, 276 (2001) 14153-14160.

[234] M.M. Rosenkilde, L.O. Gerlach, J.S. Jakobsen, R.T. Skerlj, G.J. Bridger, T.W. Schwartz, Molecular mechanism of AMD3100 antagonism in the CXCR4 receptor: transfer of binding site to the CXCR3 receptor, The Journal of biological chemistry, 279 (2004) 3033-3041.

[235] Y. Feng, C.C. Broder, P.E. Kennedy, E.A. Berger, HIV-1 entry cofactor: functional cDNA cloning of a seven-transmembrane, G protein-coupled receptor, Science, 272 (1996) 872-877.

[236] M. Kucia, K. Jankowski, R. Reca, M. Wysoczynski, L. Bandura, D.J. Allendorf, J. Zhang, J. Ratajczak, M.Z. Ratajczak, CXCR4-SDF-1 signalling, locomotion, chemotaxis and adhesion, Journal of molecular histology, 35 (2004) 233-245.

[237] K. Tachibana, S. Hirota, H. Iizasa, H. Yoshida, K. Kawabata, Y. Kataoka, Y. Kitamura, K. Matsushima, N. Yoshida, S. Nishikawa, T. Kishimoto, T. Nagasawa, The chemokine receptor CXCR4 is essential for vascularization of the gastrointestinal tract, Nature, 393 (1998) 591-594.

[238] J. Floege, B. Smeets, M.J. Moeller, The SDF-1/CXCR4 axis is a novel driver of vascular development of the glomerulus, Journal of the American Society of Nephrology : JASN, 20 (2009) 1659-1661.

[239] T. Murakami, K. Kawada, M. Iwamoto, M. Akagami, K. Hida, Y. Nakanishi, K. Kanda, M. Kawada, H. Seno, M.M. Taketo, Y. Sakai, The role of CXCR3 and CXCR4 in colorectal cancer metastasis, International journal of cancer. Journal international du cancer, 132 (2013) 276-287.

[240] B.C. Zhao, Z.J. Wang, W.Z. Mao, H.C. Ma, J.G. Han, B. Zhao, H.M. Xu, CXCR4/SDF-1 axis is involved in lymph node metastasis of gastric carcinoma, World journal of gastroenterology : WJG, 17 (2011) 2389-2396.

[241] M. Burger, A. Glodek, T. Hartmann, A. Schmitt-Graff, L.E. Silberstein, N. Fujii, T.J. Kipps, J.A. Burger, Functional expression of CXCR4 (CD184) on small-cell lung cancer cells mediates migration, integrin activation, and adhesion to stromal cells, Oncogene, 22 (2003) 8093-8101.

[242] S. Uchida, K. Itaka, Q. Chen, K. Osada, T. Ishii, M.-A. Shibata, M. Harada-Shiba, K. Kataoka, PEGylated polyplex with optimized PEG shielding enhances gene introduction in lungs by minimizing inflammatory responses, Mol. Ther., 20 (2012) 1196-1203.

[243] J.H. Brumbach, C. Lin, J. Yockman, W.J. Kim, K.S. Blevins, J.F.J. Engbersen, J. Feijen, S.W. Kim, Mixtures of Poly(triethylenetetramine/cystamine bisacrylamide) and Poly(triethylenetetramine/cystamine bisacrylamide)-g-poly(ethylene glycol) for Improved Gene Delivery, Bioconjugate Chem., 21 (2010) 1753-1761.

[244] T. Blessing, M. Kursa, R. Holzhauser, R. Kircheis, E. Wagner, Different strategies for formation of PEGylated EGF-conjugated PEI/DNA complexes for targeted gene delivery, Bioconjugate Chem., 12 (2001) 529-537.

[245] A. Reynolds, D. Leake, Q. Boese, S. Scaringe, W.S. Marshall, A. Khvorova, Rational siRNA design for RNA interference, Nature biotechnology, 22 (2004) 326-330.

[246] S.J. Tebes, P.A. Kruk, The genesis of RNA interference, its potential clinical applications, and implications in gynecologic cancer, Gynecologic oncology, 99 (2005) 736-741.

[247] D.H. Kim, J.J. Rossi, Strategies for silencing human disease using RNA interference, Nature reviews. Genetics, 8 (2007) 173-184.

[248] M. Dominska, D.M. Dykxhoorn, Breaking down the barriers: siRNA delivery and endosome escape, Journal of cell science, 123 (2010) 1183-1189.

[249] K.A. Whitehead, R. Langer, D.G. Anderson, Knocking down barriers: advances in siRNA delivery, Nature reviews. Drug discovery, 8 (2009) 129-138.

[250] R.M. Schiffelers, A. Ansari, J. Xu, Q. Zhou, Q. Tang, G. Storm, G. Molema, P.Y. Lu, P.V. Scaria, M.C. Woodle, Cancer siRNA therapy by tumor selective delivery with ligand-targeted sterically stabilized nanoparticle, Nucleic acids research, 32 (2004) e149.

[251] M. Zheng, G.M. Pavan, M. Neeb, A.K. Schaper, A. Danani, G. Klebe, O.M. Merkel, T. Kissel, Targeting the Blind Spot of Polycationic Nanocarrier-Based siRNA Delivery, ACS Nano, 6 (2012) 9447-9454.

[252] M. Cavazzana-Calvo, A. Thrasher, F. Mavilio, The future of gene therapy, Nature, 427 (2004) 779-781.

[253] M. Cavazzana-Calvo, S. Hacein-Bey, G. de Saint Basile, F. Gross, E. Yvon, P. Nusbaum, F. Selz, C. Hue, S. Certain, J.L. Casanova, P. Bousso, F.L. Deist, A. Fischer, Gene therapy of human severe combined immunodeficiency (SCID)-X1 disease, Science, 288 (2000) 669-672.

[254] C.E. Nelson, J.R. Kintzing, A. Hanna, J.M. Shannon, M.K. Gupta, C.L. Duvall, Balancing Cationic and Hydrophobic Content of PEGylated siRNA Polyplexes Enhances Endosome Escape, Stability, Blood Circulation Time, and Bioactivity in Vivo, ACS Nano, 7 (2013) 8870-8880.

[255] Z. Liu, Z. Zhang, C. Zhou, Y. Jiao, Hydrophobic modifications of cationic polymers for gene delivery, Prog. Polym. Sci., 35 (2010) 1144-1162.

[256] E. Ranucci, M.A. Suardi, R. Annunziata, P. Ferruti, F. Chiellini, C. Bartoli, Poly(amidoamine) conjugates with disulfide-linked cholesterol pendants self-assembling into redox-sensitive nanoparticles, Biomacromolecules, 9 (2008) 2693-2704.

[257] A. Bajaj, P. Kondaiah, S. Bhattacharya, Synthesis and gene transfection efficacies of PEI-cholesterol-based lipopolymers, Bioconjugate chemistry, 19 (2008) 1640-1651.

[258] W.J. Kim, C.W. Chang, M. Lee, S.W. Kim, Efficient siRNA delivery using water soluble lipopolymer for anti-angiogenic gene therapy, Journal of controlled release : official journal of the Controlled Release Society, 118 (2007) 357-363.

[259] D.A. Wang, A.S. Narang, M. Kotb, A.O. Gaber, D.D. Miller, S.W. Kim, R.I. Mahato, Novel branched poly(ethylenimine)-cholesterol water-soluble lipopolymers for gene delivery, Biomacromolecules, 3 (2002) 1197-1207.

[260] C.J. Chen, J.C. Wang, E.Y. Zhao, L.Y. Gao, Q. Feng, X.Y. Liu, Z.X. Zhao, X.F. Ma, W.J. Hou, L.R. Zhang, W.L. Lu, Q. Zhang, Self-assembly cationic nanoparticles based on cholesterol-grafted bioreducible poly(amidoamine) for siRNA delivery, Biomaterials, 34 (2013) 5303-5316.

[261] D. Wen, D. Chitkara, H. Wu, M. Danquah, R. Patil, D.D. Miller, R.I. Mahato, LHRH-Conjugated Micelles for Targeted Delivery of Antiandrogen to Treat Advanced Prostate Cancer, Pharmaceutical research, 31 (2014) 2784-2795.

[262] X. Zhang, J. Lu, Y. Huang, W. Zhao, Y. Chen, J. Li, X. Gao, R. Venkataramanan, M. Sun, D.B. Stolz, L. Zhang, S. Li, PEG-farnesylthiosalicylate conjugate as a nanomicellar carrier for delivery of paclitaxel, Bioconjugate chemistry, 24 (2013) 464-472.

[263] T. Reschel, C. Konak, D. Oupicky, L.W. Seymour, K. Ulbrich, Physical properties and in vitro transfection efficiency of gene delivery vectors based on complexes of DNA with synthetic polycations, J. Controlled Rel., 81 (2002) 201-217.

[264] S.K. Filippov, C. Konak, P. Kopeckova, L. Starovoytova, M. Spirkova, P. Stepanek, Effect of Hydrophobic Interactions on Properties and Stability of DNA-Polyelectrolyte Complexes, Langmuir, 26 (2010) 4999-5006.

[265] D. Fischer, Y. Li, B. Ahlemeyer, J. Krieglstein, T. Kissel, In vitro cytotoxicity testing of polycations: influence of polymer structure on cell viability and hemolysis, Biomaterials, 24 (2003) 1121-1131.

[266] L. Parhamifar, A.K. Larsen, A.C. Hunter, T.L. Andresen, S.M. Moghimi, Polycation cytotoxicity: a delicate matter for nucleic acid therapy—focus on polyethylenimine, Soft Matter, 6 (2010) 4001-4009.

[267] C. Wu, J. Li, Y. Zhu, J. Chen, D. Oupicky, Opposing influence of intracellular and membrane thiols on the toxicity of reducible polycations, Biomaterials, 34 (2013) 8843-8850.

[268] A. Neamnark, O. Suwantong, R.K. Bahadur, C.Y. Hsu, P. Supaphol, H. Uludag, Aliphatic lipid substitution on 2 kDa polyethylenimine improves plasmid delivery and transgene expression, Mol. Pharm., 6 (2009) 1798-1815.

[269] Y. Degenhardt, T. Lampkin, Targeting Polo-like kinase in cancer therapy, Clin. Cancer Res., 16 (2010) 384-389.

[270] C. McInnes, M.D. Wyatt, PLK1 as an oncology target: current status and future potential, Drug Discov Today, 16 (2011) 619-625.

[271] K. Strebhardt, Multifaceted polo-like kinases: drug targets and antitargets for cancer therapy, Nat. Rev. Drug Discovery, 9 (2010) 643-660.

[272] Y.D. Yao, T.M. Sun, S.Y. Huang, S. Dou, L. Lin, J.N. Chen, J.B. Ruan, C.Q. Mao, F.Y. Yu, M.S. Zeng, J.Y. Zang, Q. Liu, F.X. Su, P. Zhang, J. Lieberman, J. Wang, E. Song, Targeted delivery of PLK1-siRNA by ScFv suppresses Her2+ breast cancer growth and metastasis, Sci Transl Med, 4 (2012) 130ra148.

[273] X. Liu, M. Lei, R.L. Erikson, Normal Cells, but Not Cancer Cells, Survive Severe Plk1 Depletion, Mol. Cell. Biol., 26 (2006) 2093-2108.

[274] S. Seth, Y. Matsui, K. Fosnaugh, Y. Liu, N. Vaish, R. Adami, P. Harvie, R. Johns, G. Severson, T. Brown, A. Takagi, S. Bell, Y. Chen, F. Chen, T. Zhu, R. Fam, I. Maciagiewicz, E. Kwang, M. McCutcheon, K. Farber, P. Charmley, M.E. Houston Jr, A. So, M.V. Templin, B. Polisky, RNAi-based Therapeutics Targeting Survivin and PLK1 for Treatment of Bladder Cancer, Mol. Ther., (2011).

[275] M. Thomas, A.M. Klibanov, Enhancing polyethylenimine's delivery of plasmid DNA into mammalian cells, Proc. Natl. Acad. Sci. U. S. A., 99 (2002) 14640-14645.

[276] A. Bajaj, P. Kondaiah, S. Bhattacharya, Synthesis and gene transfection efficacies of PEI− cholesterol-based lipopolymers, Bioconjug. Chem., 19 (2008) 1640-1651.

[277] H. Eliyahu, A. Makovitzki, T. Azzam, A. Zlotkin, A. Joseph, D. Gazit, Y. Barenholz, A. Domb, Novel dextran–spermine conjugates as transfecting agents: comparing water-soluble and micellar polymers, Gene Ther., 12 (2004) 494-503.

[278] M. Kurisawa, M. Yokoyama, T. Okano, Transfection efficiency increases by incorporating hydrophobic monomer units into polymeric gene carriers, J. Controlled Release, 68 (2000) 1-8.

[279] N.P. Gabrielson, D.W. Pack, Acetylation of polyethylenimine enhances gene delivery via weakened polymer/DNA interactions, Biomacromolecules, 7 (2006) 2427-2435.

[280] Y. Wang, S. Kumar, S. Rachagani, B.R. Sajja, Y. Xie, Y. Hang, M. Jain, J. Li, M.D. Boska, S.K. Batra, D. Oupicky, Polyplex-mediated inhibition of chemokine receptor CXCR4 and chromatin-remodeling enzyme NCOA3 impedes pancreatic cancer progression and metastasis, Biomaterials, 101 (2016) 108-120.

[281] R.L. Siegel, K.D. Miller, A. Jemal, Cancer statistics, 2016, CA: a cancer journal for clinicians, 66 (2016) 7-30.

[282] D.D. Carson, The cytoplasmic tail of MUC1: a very busy place, Science signaling, 1 (2008) pe35.

[283] A. Choudhury, N. Moniaux, J.P. Winpenny, M.A. Hollingsworth, J.-P. Aubert, S.K. Batra, Human MUC4 mucin cDNA and its variants in pancreatic carcinoma, J. Biochem. (Tokyo), 128 (2000) 233-243.

[284] D. Haridas, S. Chakraborty, M.P. Ponnusamy, I. Lakshmanan, S. Rachagani, E. Cruz, S. Kumar, S. Das, S.M. Lele, J.M. Anderson, Pathobiological implications of MUC16 expression in pancreatic cancer, PLoS One, 6 (2011) e26839.

[285] S. Trehoux, B. Duchene, N. Jonckheere, I. Van Seuningen, The MUC1 oncomucin regulates pancreatic cancer cell biological properties and chemoresistance. Implication of p42-44 MAPK, Akt, Bcl-2 and MMP13 pathways, Biochemical and biophysical research communications, 456 (2015) 757-762.

[286] R. Mejias-Luque, S.K. Linden, M. Garrido, H. Tye, M. Najdovska, B.J. Jenkins, M. Iglesias, M. Ernst, C. de Bolos, Inflammation modulates the expression of the intestinal mucins MUC2 and MUC4 in gastric tumors, Oncogene, 29 (2010) 1753-1762.

[287] Y. Wang, S.T. Hazeldine, J. Li, D. Oupicky, Development of Functional Poly(amido amine) CXCR4 Antagonists with the Ability to Mobilize Leukocytes and Deliver Nucleic Acids, Adv Healthc Mater, 4 (2015) 729-738.

[288] O.M. Merkel, D. Librizzi, A. Pfestroff, T. Schurrat, K. Buyens, N.N. Sanders, S.C. De Smedt, M. Behe, T. Kissel, Stability of siRNA polyplexes from poly(ethylenimine) and poly(ethylenimine)-g-poly(ethylene glycol) under in vivo conditions: effects on pharmacokinetics and biodistribution measured by Fluorescence Fluctuation Spectroscopy and Single Photon Emission Computed Tomography (SPECT) imaging, Journal of controlled release : official journal of the Controlled Release Society, 138 (2009) 148-159.

[289] Z. Wang, Q. Ma, Q. Liu, H. Yu, L. Zhao, S. Shen, J. Yao, Blockade of SDF-1/CXCR4 signalling inhibits pancreatic cancer progression in vitro via inactivation of canonical Wnt pathway, Br. J. Cancer, 99 (2008) 1695-1703.

[290] W. Zhong, W. Chen, D. Zhang, J. Sun, Y. Li, J. Zhang, Y. Gao, W. Zhou, S. Li, CXCL12/CXCR4 axis plays pivotal roles in the organ-specific metastasis of pancreatic adenocarcinoma: A clinical study, Experimental and therapeutic medicine, 4 (2012) 363-369.

[291] L. Xu, D.G. Duda, E. di Tomaso, M. Ancukiewicz, D.C. Chung, G.Y. Lauwers, R. Samuel, P. Shellito, B.G. Czito, P.C. Lin, M. Poleski, R. Bentley, J.W. Clark, C.G. Willett, R.K. Jain, Direct evidence that bevacizumab, an anti-VEGF antibody, up-regulates SDF1alpha, CXCR4, CXCL6, and neuropilin 1 in tumors from patients with rectal cancer, Cancer research, 69 (2009) 7905-7910.

[292] T.T. Batchelor, D.G. Duda, E. di Tomaso, M. Ancukiewicz, S.R. Plotkin, E. Gerstner, A.F. Eichler, J. Drappatz, F.H. Hochberg, T. Benner, D.N. Louis, K.S. Cohen, H. Chea, A. Exarhopoulos, J.S. Loeffler, M.A. Moses, P. Ivy, A.G. Sorensen, P.Y. Wen, R.K. Jain, Phase II study of cediranib, an oral pan-vascular endothelial growth factor receptor tyrosine kinase inhibitor, in patients with recurrent glioblastoma, Journal of clinical oncology, 28 (2010) 2817-2823.

[293] S. Hiratsuka, D.G. Duda, Y. Huang, S. Goel, T. Sugiyama, T. Nagasawa, D. Fukumura, R.K. Jain, C-X-C receptor type 4 promotes metastasis by activating p38 mitogen-activated protein kinase in myeloid differentiation antigen (Gr-1)-positive cells, Proceedings of the National Academy of Sciences of the United States of America, 108 (2011) 302-307.

[294] S. Arora, A. Bhardwaj, S. Singh, S.K. Srivastava, S. McClellan, C.S. Nirodi, G.A. Piazza, W.E. Grizzle, L.B. Owen, A.P. Singh, An undesired effect of chemotherapy: gemcitabine promotes pancreatic cancer cell invasiveness through reactive oxygen species-dependent, nuclear factor kappaB- and hypoxia-inducible factor 1alpha-mediated up-regulation of CXCR4, The Journal of biological chemistry, 288 (2013) 21197-21207.

[295] Y. Xie, C.J. Wehrkamp, J. Li, Y. Wang, Y. Wang, J.L. Mott, D. Oupicky, Delivery of miR-200c Mimic with Poly(amido amine) CXCR4 Antagonists for Combined Inhibition of Cholangiocarcinoma Cell Invasiveness, Mol. Pharm., 13 (2016) 1073-1080.

[296] O.M. Merkel, A. Beyerle, B.M. Beckmann, M. Zheng, R.K. Hartmann, T. Stöger, T.H. Kissel, Polymer-related off-target effects in non-viral siRNA delivery, Biomaterials, 32 (2011) 2388-2398.

[297] F. Balkwill, The significance of cancer cell expression of the chemokine receptor CXCR4, in: Semin Cancer Biol, Elsevier, 2004, pp. 171-179.

[298] D.D. Billadeau, S. Chatterjee, P. Bramati, R. Sreekumar, V. Shah, K. Hedin, R. Urrutia, Characterization of the CXCR4 signaling in pancreatic cancer cells, Journal of Gastrointestinal Cancer, 37 (2006) 110-119.

[299] F. Pan, S. Ma, W. Cao, H. Liu, F. Chen, X. Chen, R. Shi, SDF-1alpha upregulation of MMP-2 is mediated by p38 MAPK signaling in pancreatic cancer cell lines, Mol Biol Rep, 40 (2013) 4139-4146.

[300] J. Zhang, S. Sarkar, V.W. Yong, The chemokine stromal cell derived factor-1 (CXCL12) promotes glioma invasiveness through MT2-matrix metalloproteinase, Carcinogenesis, 26 (2005) 2069-2077.

[301] S. Yachida, C.A. Iacobuzio-Donahue, The pathology and genetics of metastatic pancreatic cancer, Arch Pathol Lab Med, 133 (2009) 413-422.

[302] S. Yachida, S. Jones, I. Bozic, T. Antal, R. Leary, B. Fu, M. Kamiyama, R.H. Hruban, J.R. Eshleman, M.A. Nowak, Distant metastasis occurs late during the genetic evolution of pancreatic cancer, Nature, 467 (2010) 1114-1117.

[303] F. Rückert, P. Joensson, H.-D. Saeger, R. Grützmann, C. Pilarsky, Functional analysis of LOXL2 in pancreatic carcinoma, Int J Colorectal Dis, 25 (2010) 303-311.

[304] V. Barry-Hamilton, R. Spangler, D. Marshall, S. McCauley, H.M. Rodriguez, M. Oyasu, A. Mikels, M. Vaysberg, H. Ghermazien, C. Wai, Allosteric inhibition of lysyl oxidase-like-2 impedes the development of a pathologic microenvironment, Nat. Med., 16 (2010) 1009-1017.

[305] C.J. Whatcott, C.H. Diep, P. Jiang, A. Watanabe, J. LoBello, C. Sima, G. Hostetter, H.M. Shepard, D.D. Von Hoff, H. Han, Desmoplasia in primary tumors and metastatic lesions of pancreatic cancer, Clin. Cancer Res., 21 (2015) 3561-3568.

[306] G.R. Devi, siRNA-based approaches in cancer therapy, Cancer gene therapy, 13 (2006) 819-829.

[307] S. Kumar, S. Das, S. Rachagani, S. Kaur, S. Joshi, S.L. Johansson, M.P. Ponnusamy, M. Jain, S.K. Batra, NCOA3 mediated upregulation of mucin expression via transcriptional and post-translational changes during the development of pancreatic cancer., Oncogene, doi: 10.1038/onc.2014.409 (2014).

[308] D.V. Morrissey, J.A. Lockridge, L. Shaw, K. Blanchard, K. Jensen, W. Breen, K. Hartsough, L. Machemer, S. Radka, V. Jadhav, N. Vaish, S. Zinnen, C. Vargeese, K. Bowman, C.S. Shaffer, L.B. Jeffs, A. Judge, I. MacLachlan, B. Polisky, Potent and persistent in vivo anti-HBV activity of chemically modified siRNAs, Nature biotechnology, 23 (2005) 1002-1007.